Evolution of the Cryogenian Port Askaig Formation in Scotland

Dilshad Omer Ali

Declaration

These doctoral studies were conducted under the supervision of Professor Daniel Paul Le Heron. This thesis and the work presented in it, unless otherwise acknowledged, is the result of original studies carried out by myself, in collaboration with others, while enrolled at Royal Holloway University of London. No part of this work have been submitted for a degree to any other university.

Dilshad Omer Ali
20.12.2017

Abstract

The Port Askaig Formation (PAF) represents an exceptionally well preserved archive of the Cryogenian (Sturtian) glaciation in NW Scotland. Evidence for compelling glacial features in diamictites of the PAF was established in the 1960s, but during the 1970s the prospect of mis-interpreting mass flow deposits as glacial was raised. The "glacial school" emphasised that these rocks were deposited from grounded-ice and/or floating-ice, whereas the "mass-flow school" suggested that these sediments were formed as a result of mass-flow processes in a tectonically active basin. There continues to be debate as to how "glacial" the diamictites really are, and if they are glacial, how many glaciations / ice sheet oscillations are recorded, in the context of the snowball Earth hypothesis.

In this context, this thesis provides a detailed perspective of the PAF from island exposures on the Garvellachs archipelago, supplemented by an additional study on Islay. Individual diamictite beds, numbered as D1-D47 by early workers, are re-examined, with thorough description of the lower levels of the succession is provided for the first time. Based on a traditional, well-proven lithofacies approach, this thesis present the results of the author's six months fieldwork on the archipelago. A total of about 2100 m of newly measured, highly detailed sedimentary logs and correlation panels are presented, supplemented by 16 "contact sheets" (i.e. plan view facies distributions at the outcrop scale), > 100 palaeocurrent measurements, clast counts and thin section data. This substantial bank of data permits a detailed lithofacies approach to be taken to the PAF for the first time, allowing a robust depositional model for the evolution of the diamictite-dominated succession to be developed. Throughout the whole succession, the thesis evaluates the origin of diamictites at each level in the stratigraphy, testing multiple models (e.g. grounded-ice, floating-ice, and mass-flow as depositional mechanisms). Massive, stratified, and deformed diamictites are recorded: several are found in association with dropstone horizons in thinly laminated mudrocks. Some of these also contain tidal laminates and tidal ripples. Some diamictites exhibit classic polygonal structures on their upper surface, interpreted as patterned ground formed in a periglacial context. Correlation panels identify some substantial and abrupt thickness changes interpreted to result from syn-sedimentary fault activity. Collectively, therefore, the PAT contains clear evidence that many of the diamictites are glacially-related, if not of direct glacial origin, deposited in settings ranging from shallow glaciomarine to terrestrial, together with some evidence for re-sedimentation as mass flows (e.g. the so-called Great Breccia in the middle of the succession). The author thus recognises: (i) multiple phases of ice-oscillation (ii) postulates that syn-depositional faults influenced sedimentation patterns, (iii) the presence of glaciotectonic structures at some levels, (iv) microbial carbonate deposition and (v) tidal sandstones within the succession. Given this, it is proposed that the PAF provides a highly unusual and relatively complete record of Sturtian climate events that is probably unrivalled in comparable deposits elsewhere.

Contents

List of Figures

6

7

9

10

14

List of Table

On the Physical Geology of the Bone-caves of the Wye.
By the Rev. W. S. SYMONDS, M.A., F.G.S.

Fossil bones of the exinct mammalia have been discovered in "King Arthur's Cave," situate in Great Doward Wood, on the right bank of the Wye, between Whitechurch, near Ross, and Monmouth. They were forwarded to Prof. Owen, and were determined by him to be molar teeth of *E. primigenius*, molar teeth of *Rhinoceros tichorhinus*, gnawed astragalus and bones of *R. tichorhinus*, molar teeth and bones of *Equus fossilis*, upper molar and astragalus of *Bos primigenius*, shed antler of Reindeer (*Cervus tarandus*), right upper canine of *Hyæna spelæa*.

These fossil bones are from a cavern in a locality rich in caves in the mountain limestone, now elevated to a considerable height above the river Wye, but in which fossil bones of the extinct mammalia had not hitherto been found.

Arthur's Cave has evidently been the den of the great Cave Hyæna, as evinced by the gnawed state of many of the bones, and the remains of that animal itself. The physical geology of the district was described by the author of the paper.

On the Occurrence of Seams of Hard Sandstone in Middle Drift of East Anglia.
By J. E. TAYLOR.

A Census of the Marine Invertebrate Fauna of the Lias.
By RALPH TATE, F.G.S.

On the Diamonds of South Africa. By J. TENNANT, F.G.S.

On the Occurrence of Pebbles and Boulders of Granite in Schistose Rocks in Islay, Scotland. By JAMES THOMSON, F.G.S.

The author described the different rocks exhibited in a section across Islay, from Port Nahaven on the west to Port Askaig on the east, which principally consist of gneiss, chlorite and mica-schist, quartzites and limestone. There is a diversity of opinion as to the proper position of these rocks; some consider them of Laurentian, while others think they are of Cambrian age. The author was inclined to think they belonged to the latter period. At Port Askaig there is a precipitous cliff of quartzite about 70 feet in height, made up of about one hundred thin bands varying from 1 to 20 inches in thickness. Underlying this quartzite there is a mass of arenaceous talcose schist, showing faint traces of stratification, containing fragments, some angular but mostly rounded, of all sizes, from mere particles to great boulders of granite, resembling the granite of the Island of Mull. Similar rocks do not occur in the Island of Islay; and Mull being at a considerable distance to the north, with a deep sea between the two islands, he suggested the probability of the granite having been transported by the agency of ice.

These deposits resemble the boulder drifts of more recent times, in the following respects:—first, in the absence of stratification in one part of the section, which in another shows signs of regular deposition; secondly, in the close proximity of fragments of far transported rock, varying in size from minute fragments to large boulders; the origin he ascribed to the mass having been deposited in a tranquil sea of mud, sand, and blocks from melting drift-ice. The absence of stratification in one part of the section while it is present in another, may be accounted for by the disturbing action of icebergs, when stranded in the soft plastic mass, in parts of the sea of limited depth. He also stated that pebbles of granite had long been sought for in the conglomerates of the Old Red Sandstone; but in no part of Scotland had it been found in rocks of that age, consequently it was inferred that the granite of Scotland was posterior to the deposition of the rocks belonging to that period. The discovery of fragments and boulders of granite imbedded in these deposits, furnish adequate proof that the age of granite cannot be restricted, and that glacial action was not limited to any special geological period.

Thomson, J. 1871. _ _ _ _ _ .
40th Meeting British Association,
Liverpool Transactions, p. 88 only.

To the good memory of my wife and sons,

Rand, Adam and Anas

Acknowledgements

Chapter 1 : Introduction

1.1. Introduction

This study focusses on the Port Askaig Formation (PAF) in Argyll, Scotland (Fig.1.1). The PAF lies above the Appin Group and occupies the base of the Islay Subgroup, which is the oldest part of the Argyll Group. The rocks of these groups were mostly deposited on, or close to, an extensive continental shelf, and form laterally connected and traceable units throughout the entire Dalradian Supergroup outcrop from Scotland to Ireland (Spencer, 1971; Anderton, 1985; Stephenson and Gould, 1995; Arnaud et al., 2011). The PAF was laid down under glacial conditions. Because of its special lithological character it is an important stratigraphic marker, not only in Scotland but throughout the Caledonides (Stephenson and Gould, 1995).

This study provides a high resolution sedimentological analysis of the PAF, recording lateral and vertical stratigraphic variation and facies changes. The objective is to interpret the full range of lithofacies to reconstruct depositional environments and to attempt a sequence stratigraphic model. This will lead to a better understanding of the evolution of the PAF and the climatically-related depositional episodes it contains.

This study is important because a comparison of the PAF with other thick, relatively complete Phanerozoic and Cryogenian glacial successions suggests that the PAF is exceptional in its combination of formation thickness (~1100 m), the number of climatically-related stratigraphic episodes and the considerable thickness of its Dalradian Supergroup host.
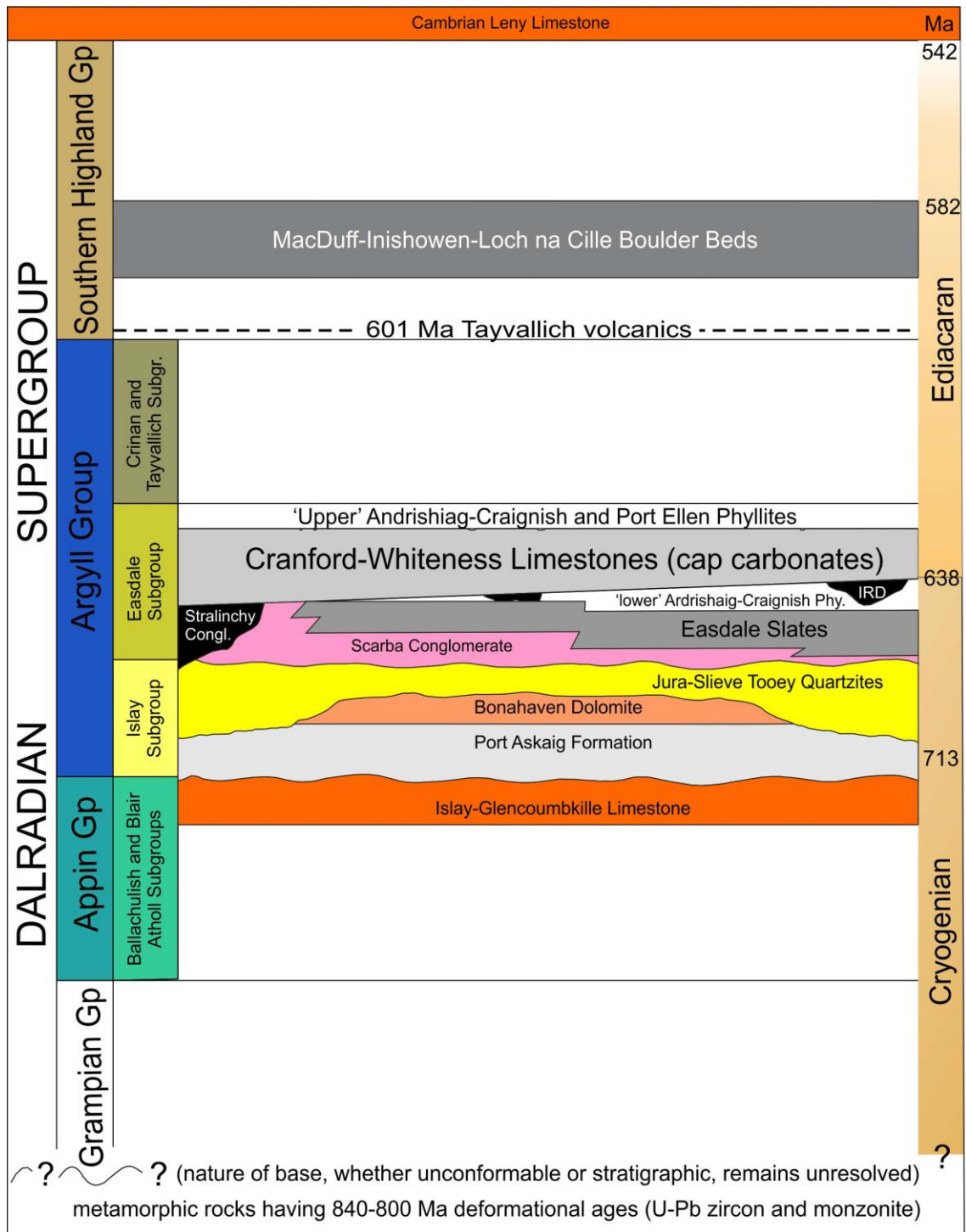
Figure 1.1: Stratified framework of the Dalradian supergroup (Prave and Fallick 2011)

1.2. Structure of the thesis

This thesis consists of nine chapters as follows:

i) Chapter one: This introduces the reader to the thesis structure and gives information about the geographical, geological, and tectonic locations of the study area. Former studies on the PAF are mentioned and disagreements between authors discussed. The chapter lists the aims of the current study and the author's opinion about disputed matters.

ii) Chapter two: This chapter discussed methodologies used to study the rocks in the Port Askaig Formation (PAF), showing the degree of detail and amount of effort spent on collecting data.

iii) Chapter three: This chapter describes, analyses, and interprets the possible depositional environments responsible for Member 1 of the PAF in the Garvellachs.

iv) Chapter four: This chapter describes, and analyses the rocks in members 2 and 3 of the PAF in the Garvellachs; and interprets their possible depositional environments.

v) Chapter five: This chapter describes stratigraphy of the PAF on Islay, from the base to the top of the formation and compares the PAF succession on the Garvellachs and Islay.

vi) Chapter six: This chapter assesses the stratigraphic boundaries in the PAF based on the data in previous chapters.

vii) Chapter seven: This chapter examines the detailed event stratigraphy seen at five selected horizons in the Garvellachs comparing sedimentary logs in various locations so as to reveal the detail preserved

viii) Chapter eight: This chapter is the heart of the thesis. Generally, it talks about glacial sequence stratigraphy in the PAF. Also, it suggests how this science could change for future study.

ix) Chapter nine: This chapter includes summary and perspective of the thesis. Then, it ends by some recommendations for future work.

The author has tried to avoid repetition as much as possible. However, there is some repetition, especially in chapters four and five, due to the similar depositional environments of lithofacies associations at different stratigraphic levels.

1.3. Geological Setting

1.3.1. The Port Askaig Formation in the context of Neoproterozoic glaciations

There is an ongoing controversial discussion between authors about climate fluctuation during late Neoproterozoic Earth history (Hoffman et al., 1998). Brasier and Shields (2000) and Kaufman et al. (1997) identified four glacial periods (Sturtian, Maikhan Uul, Ice Brook and Marinoan), none of which were global, while Kennedy et al. (1998) accept only two global glaciations (Sturtian and Marinoan). Allen and Etienne (2008) emphasised poor age control and proposed a long record of diachronous glaciation. The present consensus is that there were three glacial events in the Neoproterozoic based on tillite deposits and a cap carbonate that is commonly found above the lower two glacial succession (Arnaud and Eyles, 2006; Rooney et al., 2011; Rooney et al., 2014). Two of these events are in the Cryogenian and one in the Ediacaran. The Sturtian event is the first Cryogenian glacial event, considered to span from 717-662 Ma (Rooney et al., 2014), and the second is Marinoan, which lasted from 650-635 Ma (Arnaud et al., 2011). The third glacial event is the Gaskiers glaciation, which is less geographically extensive and shorter than former events, and placed at approximately 582 Ma (Prave et al., 2009). The palaeogeographical setting for these glaciations, suggest a strong bias to low palaeolatitudes (Fig.1.2).

The PAF is thought to be an example of an older Cryogenian, possibly Sturtian-age succession. At 720 Ma, Scotland was a part of the Laurentian craton (Benn and Prave, 2006). According to Prave et al. (2009) the age of the formation is 713 Ma, suggesting a Sturtian age. Other estimates are approximately 700 Ma (McCay et al., 2006), but no absolute age dates have been found. As a result, most authors agree with a Sturtian age for the PAF.
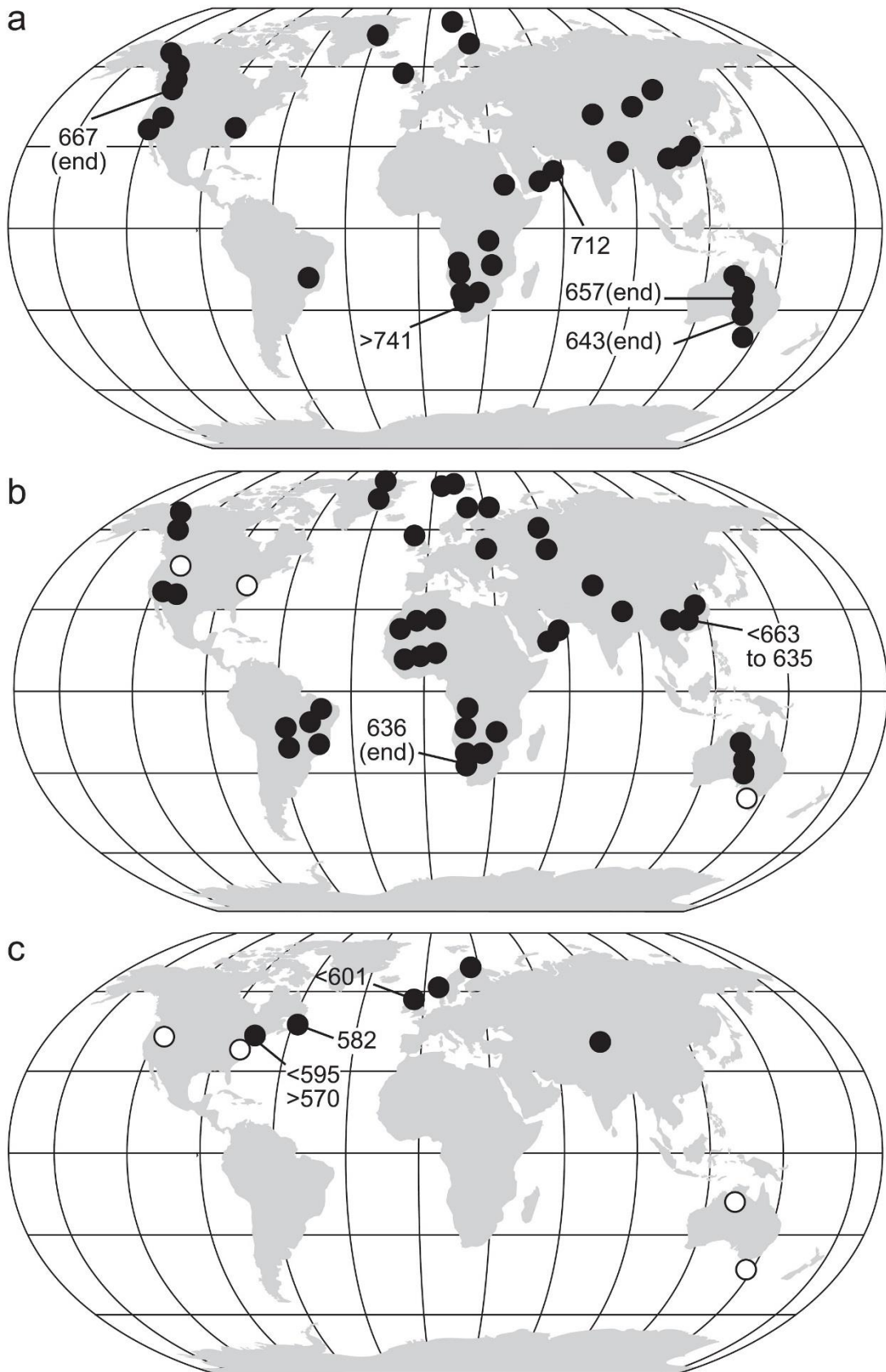
Figure 1.2: (a) Geographical distribution of Sturtian (717 – 662 Ma) glacial deposits. (b) Geographical distribution of Marinoan (650 – 635 Ma) glacial deposits. (c) Geographical distribution of Gaskiers (~582 Ma) glacial deposits. Open circles represent uncertain assignments (Fairchild and Kennedy, 2007).

1.3.2. Continental configurations during the Neoproterozoic Era

Based on palaeomagnetic evidence Li et al. (2013) proposed that the supercontinent Rodinia, with northern Scotland and Ireland on the eastern margin, assembled at approximately 900 Ma at mid-low latitudes (Fig.1.3). The continent was comparatively short-lived: oceanic crust sunk into the mantle, with development of a mantle superplume, resulting in mass rifting and the break-up (Fig.1.4) of the supercontinent at around 720 Ma (Li et al., 2013). This resulted in dispersion of the present-day continents, which then drifted towards high southern latitudes. The break-up of Rodinia was complete by 580 Ma (Li et al., 2013). Re-convergence of southern continents let to the assembly of Gondwana (Fig.1.5).
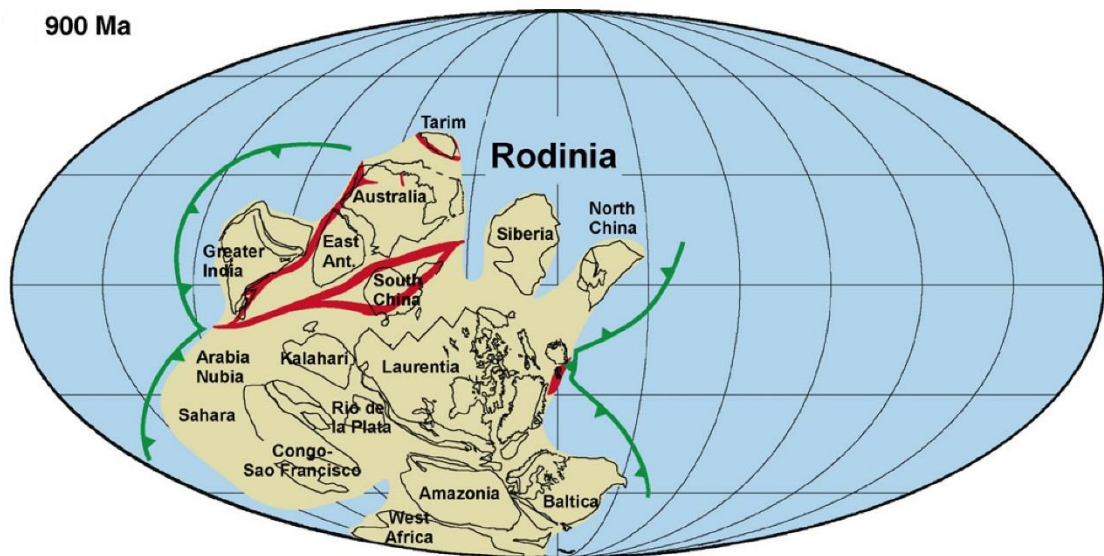
Figure 1.3: The continental configuration of the supercontinent Rodinia (Li et al., 2008)
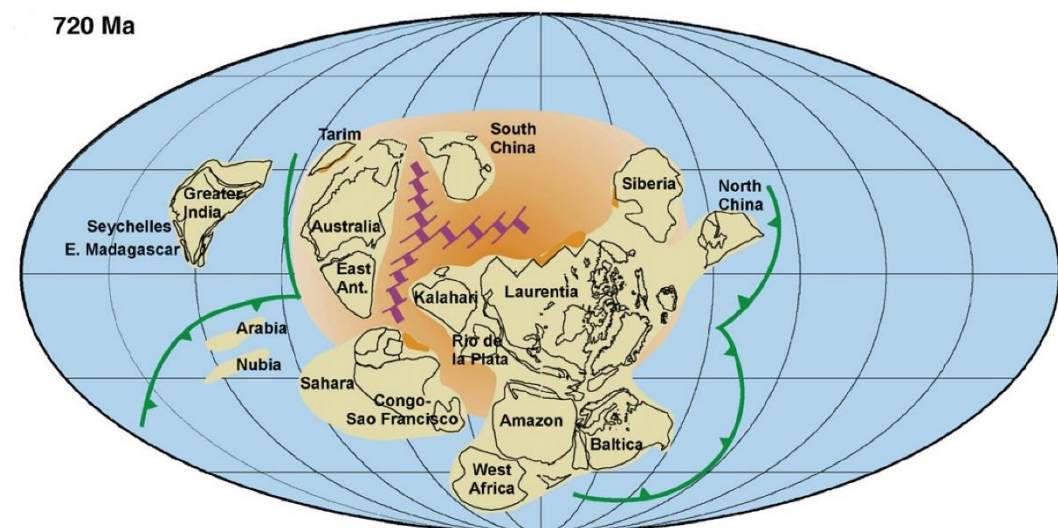
Figure 1.4: Onset of the breakup of Rodinia induced by a mantle superplume (from Li et al., 2008).

This supercontinent of Gondwana (Fig.1.6) was assembled by approximately 550 Ma (Scotese, 2009; Li et al., 2013). There are contrasting views concerning continental configuration during the

Neoproterozoic. The agreement is the acceptance of two supercontinents; the disagreements lie in the configuration of the constituents of Rodinia and the chronology of their assembly (Li et al., 2008).

Figure 1.5: Drift and re-convergence of the continents towards the South Pole (from Li et al. 2008).

The Dalradian Supergroup is a 25 km thick clastic sedimentary succession intercalated with a substantial volume of carbonate and volcanic rocks, extending in age from mid-Neoproterozoic to Early Palaeozoic. Geographically, the supergroup extends from the NE of Scotland to the SW coast of Ireland. During the Mid Ordovician Grampian phase of the Caledonian orogeny, the strata experienced variable degrees of metamorphism. The supergroup comprises the Grampian, Appin, Argyll and Southern Highland groups in ascending order. The Argyll Group can be subdivided into four sub-groups, namely the Islay, Easdale, Crinan and Tayvallich subgroups (Fig.1.1). The Port Askaig Formation (PAF) occupies the lower part of the Islay Subgroup. This 1100 m thick metasediment succession consists of diamictite interbedded with sandstone, mudstone and conglomerate. The PAF and associated strata in the Grampian Terrain comprise a series of exposures that are bounded by the Great Glen Fault to the north and the Highland Boundary Fault to the south. This thesis concentrates on the PAF with a field-based study that attempts, for the first time, to propose an event and sequence stratigraphic framework for these deposits.

The structurally complex and commonly high-grade metamorphic rocks within the Caledonian Orogenic belt of Scotland are divided into the Northern Highland and Grampian terrains (Fig.1.7). Two Tonian to Cryogenian units crop out in the northern Highland part of the orogen, namely the Moine Supergroup of the Northern Highlands and the Dava succession of the Grampian terrane. Both were deposited between 1000 Ma and 870 Ma. The younger sequence in the Grampian terrane is the Dalradian Supergroup which accumulated between 800 Ma and Ediacaran times leading on to the opening of the Iapetus Ocean and the break-up of Rodinia (Trewin, 2002). Fragments of the Laurentian continental basement on which the Moine and Dalradian succession accumulated are now represented by inliers of Archaean to Palaeoproterozoic orthogneisses (Trewin, 2002).
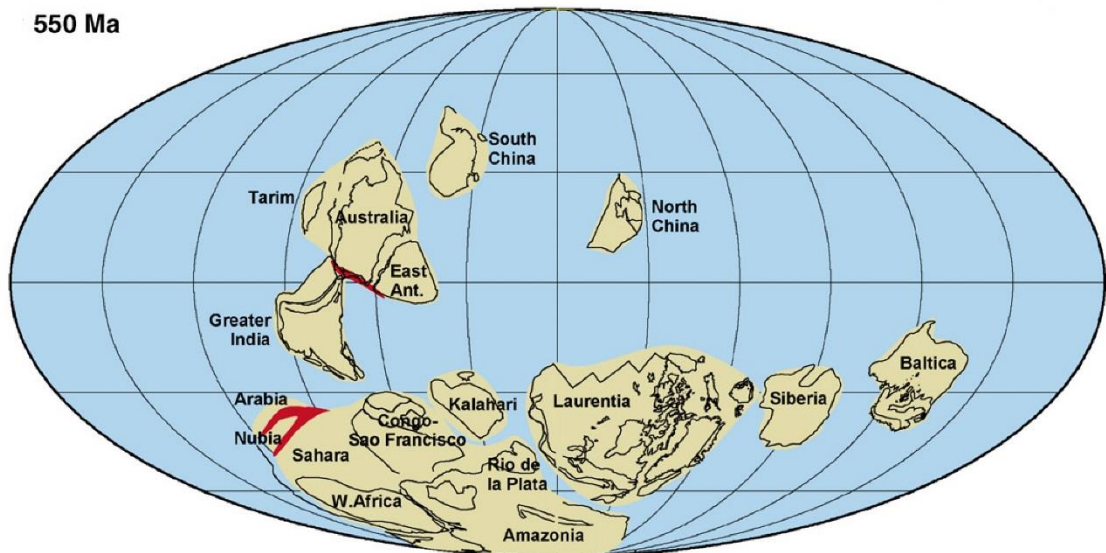
Figure 1.6: Formation of the supercontinent Gondwana in the Southern hemisphere (Li et al. 2008)

Sedimentological research in the Dalradian progressed from recognition of sedimentary structures in the 1930s, to sedimentary facies identification and merging of sedimentological data with stratigraphy, tectonics, and volcanism in the 1970s (Anderton, 1985). Most of our modern understanding of the pre-orogenic evolution of the Dalradian's Grampian terrane comes from this phase of work, in terms of progressive lithostratigraphic stretching associated with the break-up of Rodinia. Dalradian lithostratigraphical equivalents have also received attention in different parts of the Caledonian-Appalachian belt (Graham and Bradbury, 1981). In most orogenic zones variably altered metamorphic and deformed igneous rocks are common. The Argyll Group of the Scottish Dalradian is affected by low grades of metamorphism. Based on Downie (1971), metamorphosed basaltic rocks are widespread in the green schist and lower amphibolite facies terrains.

This study focusses on the PAF, which sits above the Appin Group and occupies the base of the Islay Subgroup, which is the oldest part of the Argyll Group. The rocks of this group were mostly deposited on, or close to, an extensive continental shelf, and form laterally connected and traceable units throughout the entire Dalradian Supergroup from Scotland to Ireland (Spencer, 1971; Anderton, 1985; Stephenson and Gould, 1995; Arnaud et al., 2011). The PAF, broadly laid down under a glacial influence, is an important chronostratigraphic marker, not only in Scotland but throughout the Caledonides (Stephenson and Gould, 1995).
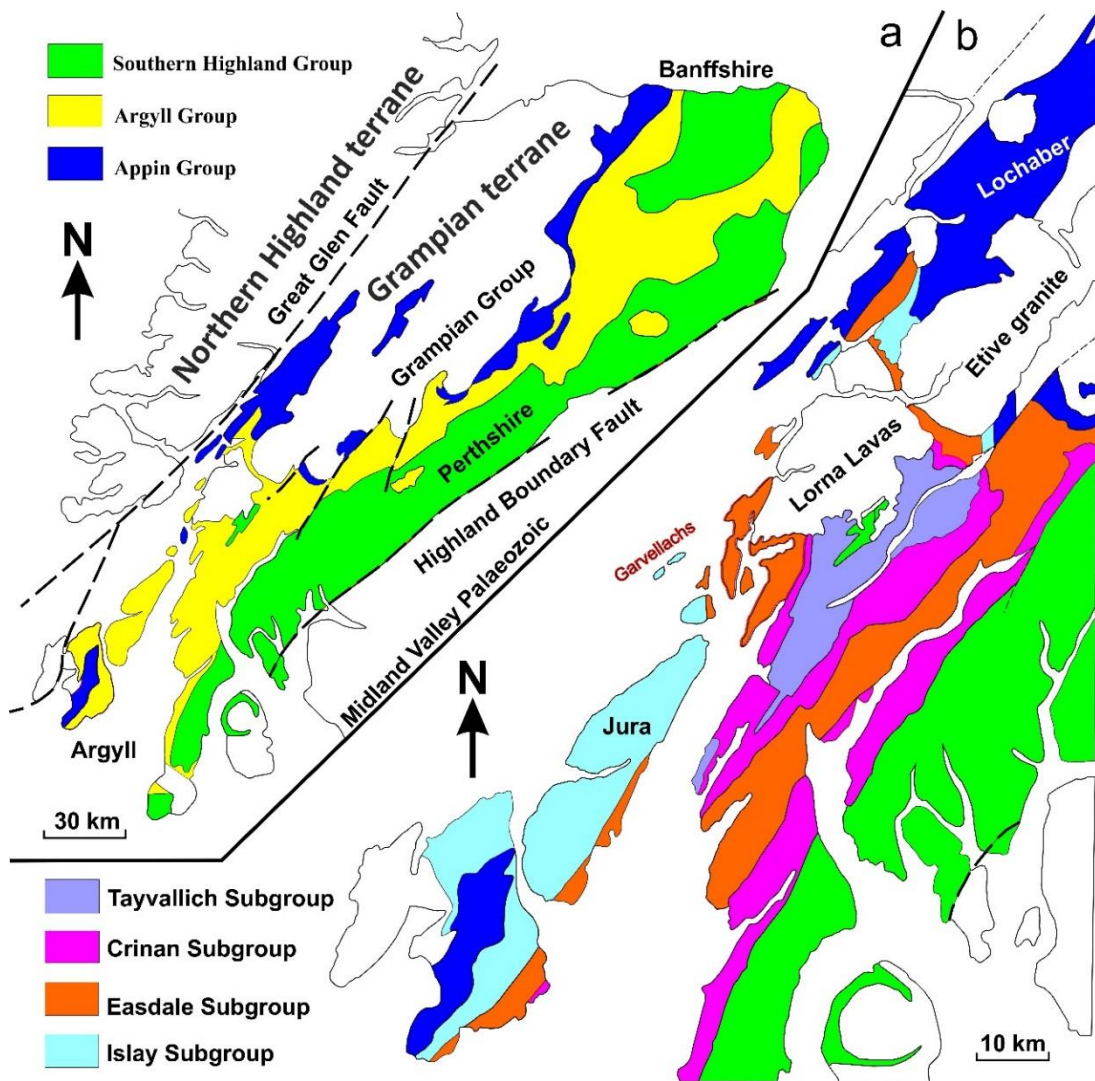
Figure 1.7: Dalradian outcrop in Scotland (excluding Shetland). a) Dalradian subdivided into groups. (b) More detailed map showing Argyll Group rocks in the SW Highlands (Anderton 1985).

Anderton (1985, 1988) discussed the nature of subsidence in the Dalradian basin of the Appin Group and the lower part of the Argyll Group, and proposed a series of up-warps in the Caledonian foreland, with major subsidence in the basin tracking the opening of Iapetus Ocean (Eyles and Eyles, 1983). A case for a major phase of subsidence, or constantly rising sea level (or both) can be made from Argyll Group times onwards, on account of the thickness of successions such as the PAF (more than 900 m thick) and the Jura Quartzite (more than 5000 m thick), demanding major accommodation availability to preserve this huge thickness of sediment. Some of the Dalradian quartzite deposits appeared to have lenticular shapes (Harris and Mendum, 1975). A deltaic environment was proposed for these lenticular bodies and Anderton (1979) suggested that they formed as a result of syndepositional faulting. A significant change in environment followed the deposition of the Jura Quartzite, with deep marine conditions accompanying the transition to an unstable tectonic environment and with growth-faulting. This phase is proposed to have commenced in Appin Group times (Anderton, 1988; Wright, 1988).

1.4. Previous work on the PAF

1.4.1. Stratigraphic and sedimentological studies

Macculloch (1819) was the first to describe what is now recognised as the PAF sediments on Islay and the Garvellach islands. He correlated a 'boulder bed' (Fig.1.9) between the mainland (Schiehallion area), Islay and the Garvellach islands (Fig.1.8). Kilburn et al. (1965) described the PAF as a uniform succession divided into 38 individual boulder beds separated by stratified conglomerate, sandstone, mudstone, and dolomite beds. This succession was interpreted as glacial in origin. The boulder beds were considered to represent the deposits of grounded ice-sheets, whereas the stratified beds were interpreted as interglacial deposits.
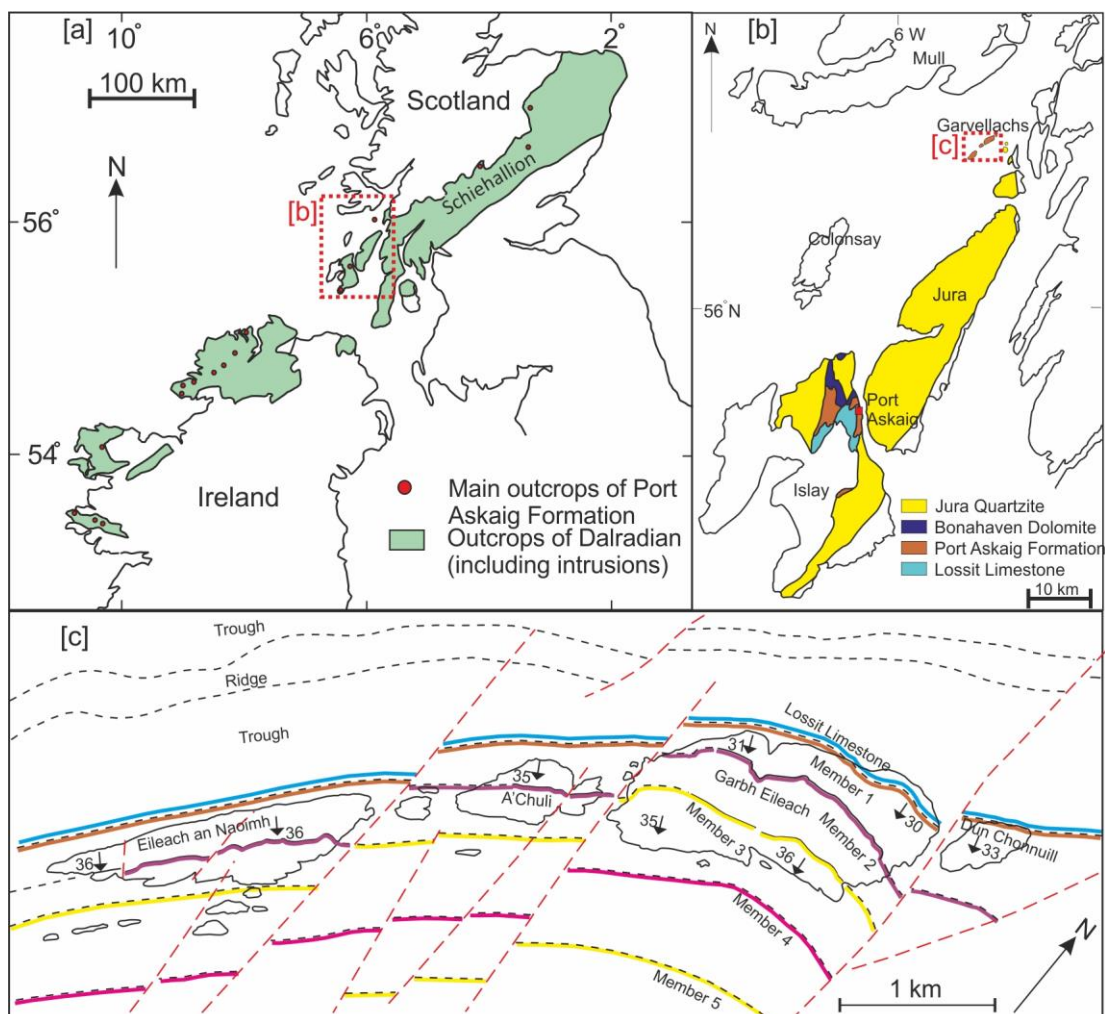
Figure 1.8: Location maps. (a) Outcrop of the Dalradian Supergroup and main localities of the Port Askaig Formation. (b) Main outcrops of the Lossit Limestone, Port Askaig, Bonahaven Dolomite and Jura Quartzite formations from Islay to the Garvellachs. (c) Port Askaig Formation members in the Garvellachs; sea-floor geology inferred from marine bathymetry data.

Figure 1.9: Diamictite (boulder) bed no.38 in the PAF, W coast of the Garbh Eileach.

Spencer (1971) logged and made a detailed map of the PAF on the Garvellach islands. He concurred with the overall glacial origin for the boulder beds proposed by Kilburn et al. (1965), meanwhile adopting a stricter description for these as diamictites (then referred to as 'mixtites') to account for the poorly sorted nature of many beds. Spencer (1971) interpreted the diamictites as tillites (i.e. of direct glacial derivation). The study revealed 47 diamictite beds interbedded with stratified conglomerate, sandstone, mudstone, and carbonate rocks. Thirty-eight diamictite beds are exposed on the Garvellach islands and nine beds crop out on the Isle of Islay. An overall interpretation of deposition from grounded ice and ice-rafting was proposed. Up to 17 advance-retreat cycles were suggested. A large antiform (Fig.1.10) in one horizon known as the Great Breccia was interpreted to result from glaciotectonic deformation. In addition, he divided the formation into five members depending on dominant facies type and changes in clast lithology. Member I is characterised by a block-bearing breccia, with clasts > 100m diameter in the diamictite, and intervals of soft-sediment deformation known locally as the "Disrupted Beds". Member II contains diamictites interbedded with stratified siliciclastic sediments, and yields extrabasinal clasts. In the Garvellachs, Member III caps the succession and contains a thick succession of sandstone beds > 80 m in thickness with interbedded diamictites and conglomerates. The upper two units (Members IV and V) are absent in the Garvellachs but crop out on Islay. These latter two members are respectively dominated by diamictite and interbedded sandstone and diamictite.

Figure 1.10: Antiform clast in magabreccia, NW of EaN. Red dashed-curves represent a stratified beds inside the clast while the white dashed-line represent stratification.

According to Spencer (1985), the depositional mechanism for the diamictites must account for the following five basic observations:

1) Irregular / unconformable basal contacts. These were viewed as more supportive of erosive, grounded ice. By contrast, conformable contacts between beds were more supportive of subaqueous deposition, e.g. ice-rafting.

2) Evidence for glaciotectonic deformation preserved in the deposits.

3) The lenticular shape of conglomerates, sandstones, and siltstones within diamictite beds which appear abruptly in stratigraphic section. These were viewed as evidence of channelized deposition by subglacial or englacial meltwaters in a grounded ice sheet.

4) The clear distinction between the massive diamictites and laminated siltstones, including dropstones.

5) The different palaeogeographical environments for non-diamictite strata in the PAF.

Comparing the PAF with stratigraphically equivalent diamictites in Greenland, Spencer (1985) concluded that each was deposited by the melting of a grounded ice sheet, with conglomerate, sandstone, siltstone and carbonate intervals deposited during ice-free periods.

An alternative view has been offered for these rocks by Eyles and Eyles (1983), involving mass movement in a glaciomarine environment. Eyles et al. (1985) studied an assemblage of deformation structures (sandstone downfolds, clastic dykes, and polygonal networks of sandstone wedges) of the PAF. They argued that the sandstone downfolds were formed as a result of subaqueous gravitational

loading aided by seismic shock. They explained that sandstone penetration wedges were formed by reverse density gradients during sedimentation.

Eyles (1988) argued that, in the context of a tectonically active basin during Dalradian times, the Great Breccia and the Disrupted Beds were produced through downslope resedimentation. Furthermore, large-scale cross-bedding in sandstone were interpreted to represent tidal influence in a shallow marine shelf deposits, thereby also implying that the diamictites were glaciomarine.

A further phase of work from one of C.H. Eyles' research students (Emmanuelle Arnaud) included mapping and logging of the Great Breccia from the cliffs and shoreline exposures on the Garvellachs (Arnaud and Eyles, 2002). It was proposed that these rocks were formed by various subaqueous sediment gravity flow processes consisting of matrix-rich debris flows and turbidities. It was suggested that the Great Breccia is not a simple megabreccia: on the basis of clast size and lithology it was divided into three units. The first unit includes clasts up to 100 m diameter, and was explained as a catastrophic collapse and failure of local calcareous and siliciclastic deposits. The second unit consists of interbedded diamictites and dolomitic conglomerate, sandstone and mudstone. The conglomerate was interpreted to be deposited from high-concentration turbulent flows with sandstones and fine-grained rocks deposited. The third and final unit is a diamictite with metre-size clasts that was interpreted as a debrite. Arnaud and Eyles (2002) also considered that the basin was tectonically active during the deposition of the Great Breccia, largely on account of the major difference between the thickness of these rocks in the Garvellach and on Islay.

Arnaud and Eyles (2006) interpreted the PAF on the Garvellach islands to have accumulated through the following three main stages:

1) First stage: primarily tectonically-controlled and dominated by sediment gravity flow processes.
2) Second stage: transitional phase, wherein extension and tectonic instability delivered sand at a high sedimentation rate to the basin with preservation of current generated facies.
3) Third stage: interbedded units of diamictite and sandstone, deposited through ice margin fluctuation and the accumulation of sandy bedforms in a tectonically stable marine setting.

Arnaud (2012) noted that the analysis of soft-sediment deformation structures in the PAF can be used to determine palaeostress on the sediment during or shortly after deposition. In recent glacial deposits, and in non-glacial basins, downslope instability may produce a series of basin-ward verging folds, if the deformation is coherent, or a partly fluidized and chaotic slump package if it is not. However, it is clearly recognised that shear and compressional stress may be gravitationally induced where melting of buried ice occurs (e.g. Harris and Murton (2005)). Deformation may also be accomplished through ice grounding or bulldozing (Ber, 2007), or simply through the effects of high sedimentation rates and compaction in glacial environments. Arnaud (2012) analysed the deformation structures of the PAF, and proposed they formed in a tectonically active basin. She noticed similarities between the Great Breccia of the PAF and carbonate megabreccias formed by subaqueous slope processes. These results

motivated Arnaud (2012) to interpret deposition of the Great Breccia as down-slope mass flow from an an active fault.

Large-scale cross-stratification, or "giant cross-beds" forming sets about 350 m thick have also been described from Member 3 of the PAF by Arnaud (2004). The cross-bedded sandstone is interbedded with diamictite and conglomerate. The cross-bed sets include up to 11 m thick foresets, exhibiting both simple and compound internal structure and mainly tangential foreset laminae with an average depositional dip of 14°. The complex, compound nature of the bedforms, in concert with the scale of the structures, led Arnaud (2004) to propose that they represent the migration of large subaqueous dunes, probably as a result of tidal and geostrophic currents in the marine environment.

Reverting to Spencer's original view, Benn and Prave (2006) found that the Disrupted Beds contained deformation structures extending from laminated siltstone into overlying diamictite beds, implying that both facies were affected by the same shearing event. There is certainly a great similarity between the micromorphology of the modern subglacial deformation till and diamictites of the PAF. Both of them exhibit localised brittle shear. Also, increasing upward strain is more compatible with subglacial, rather than mass-movement - derived deformation structures. For instance, Busfield and Le Heron (2013) concluded that the glacial re-advance produces a deformation profile that increases in intensity, and this character is compatible with subglacial shearing. This character occurs in some horizons within the PAF succession. The components of the laminated siltstone and diamictite beds, such as silty matrix, fragmented dolostone rafts, and extrabasinal clasts were found to be similar, but the degree of fragmentation and homogenization was found to be higher in diamictite. On the basis of the above, Benn and Prave (2006) concluded that the Disrupted Beds were subglacial in origin. They also concurred with Spencer (1971) that the Great Breccia is of glaciotectonic origin, dismissing the idea of gravitational mass-movement deformation. From the above discussion it is apparent there are two main opposing views concerning the origin of the PAF. All authors agree that the formation is an ice-influenced deposit. But it is controversial whether the diamictites were deposited by grounded-ice or ice-rafting or as mass-flow down submarine slopes. Evaluating depositional environments is important for building a sequence stratigraphy model. This study will concentrate on evaluating these three depositional mechanism: subaqueous mass-flow, floating-ice, or grounded-ice.

1.4.2. Province geochemical studies

There are two methods for age determination, relative age by fossils or stable isotope data, or absolute age by radiogenic isotope analysis. The Neoproterozoic succession in Scotland could contain Ediacaran fauna, but the rocks are typically too metamorphosed to contain fossils.

Turning to stable isotope data, C and Sr isotopes have been used for correlation previously. On the basis of ^{13}C data, a glacial event (Stralinchy-Reelan Formations) has been described between two previous episodes, Port Askaig and Inishowen-Loch na Cille (McCay et al., 2006). The Stralinchy-Reelan comprises diamictite and ice-rafted debris. McCay et al. (2006) interpreted the PAF, Stralinchy-Reelan and the

Inishowen-Loch na Cille as formations equivalent to the 700 Ma Sturtian, 635 Ma Marinoan and 580 Ma Gaskiers glaciations respectively.

Using trace element geochemistry, Panahi and Young (1997) proposed a provenance for the PAF. They suggested that the formation was derived from a cratonic-type shale developed on a crystalline basement. They emphasized a post-Archean shale source according to (La/Yb)$_N$ ratios. The provenance of the PAF is not accurately determined because the geochemical data was insufficient to assign a specific source. Thus, a full paleogeographic perspective was not possible.

Sawaki et al. (2010) presented a Sr^{87}/Sr^{86} analysis of the Islay Limestone Formation (i.e. the carbonate rocks immediately underlying the PAF). Similar values were present in the Ballygrant and Islay Formation on Islay, but Sr^{87}/Sr^{86} was lower than those in previous studies of the Islay Formation on Garbh Eileach (GE). The contact between the Islay and the overlying PAF has been assumed to be a major erosion surface on Islay, even though on GE the contact between them does not show a major gap. Low Sr isotope value have been found globally, and such low value are only recorded before the Sturtian glaciation in the Neoproterozoic. This supports the idea that the older Cryogenian glaciation was accompanied by extreme global silicate weathering due to the splitting of the Rodinia supercontinent and by a consequent reduction of atmospheric CO_2, so that the reconstructed Sr isotope variation from the Tonian to the earliest Cambrian demonstrates a decline of Sr^{87}/Sr^{86} values just before the Sturtian glaciation.

Based on Rhenium-Osmium (Re-Os) geochronology of the Ballachulish slate Formation, Rooney et al. (2011) interpret a depositional age of 659.6 ± 9.6 Ma for the overlying glaciogenic PAF. On this basis, they suggest that the PAF is much younger than previously thought.

Prave and Fallick (2011) agreed with McCay et al. (2006) that some Dalradian carbonate units are lithologically and C-isotopically harmonious with Neoproterozoic cap carbonates. They suggested that the Dalradian contains evidence of three distinct glaciations using C-isotope chemostratigraphy and placed the base of the Ediacaran in the Easdale subgroup and the underlying Dalradian units in the Cryogenian.

1.4.3 Port Askaig Formation and the 'Snowball Earth' hypothesis

The detailed investigation of Precambrian ice-age successions goes back at least to Kulling (1934). Further ideas about Neoproterozoic glaciations comes from the work of Mawson (1949a, 1949b). Harland (1964) considered the tillites in the context of continental drift and introduced the concept that global ice ages would provide a means to stratigraphically subdivide the later Precambrian. Dunn et al. (1971) suggested that the glacial strata could be a global Neoproterozoic time marker.

A global consideration with respect to the Neoproterozoic glacial record is whether the Earth went through a deep-frozen state and the ice-age period was 'normal' or was 'cold-based' during the Snowball Earth' theory (Kirschvink, 1992; Hoffman et al., 1998; Hoffman and Schrag, 2002; Spence et al., 2016). Also, there is controversy whether in the panglacial period Earth went through a deep-frozen

state and the hydrologic cycle shut down or there was a narrow zone of melt water in the equatorial region (Benn et al., 2015; Spence et al., 2016). All scientists are agreed that the first and longer ice-age which represents a panglacial in the Cryogenian, is Sturtian and that the later Marinoan ice age was shorter and less extensive (Kaufman et al., 1997; Kennedy et al., 1998; Brasier and Shields, 2000; Allen and Etienne, 2008).

Should a deep frozen ice-age during Sturtian times give rise to a sedimentary record? This was a puzzling issue for scientists until Busfield and Le Heron (2013) interpreted the soft-sediment shear zone within an ironstone, underlying diamictite beds, as the product of subglacial deformation in Namibia. Thus, Spence et al. (2016) propose that not all ironstones record terminal deglaciation, but a link to glaciation can still apply if oxidants were delivered either by meltwater plumes (Cox et al., 2016) or from brines expelled during sea ice formation (Lechte and Wallace, 2015).

Most supporters of the 'Snowball Earth' hypothesis emphasize that the Sturtian period was a panglacial (Kirschvink, 1992; Hoffman et al., 1998; Hoffman and Schrag, 2002; Fairchild and Kennedy, 2007; Halverson et al., 2007; Macdonald et al., 2010; Calver et al., 2013; Rooney et al., 2014; Rooney et al., 2015; Le Heron and Busfield, 2016; Spence et al., 2016). Pierrehumbert (2005) and Pierrehumbert et al. (2011) proposed that in the original 'hard' Snowball, a universal thick, ice cover existed on the oceans, composed of an upper zone of frozen sea-water. Fairchild et al. (2016) argued that if this scenario is true, then sea level must have been greatly lowered, and marine ice margins should have been located far below the shallow-water proglacial sediments. Evidence for this hypothesis can be seen in Namibia; where glaciogenic deposits are rare on platform tops, while some hundreds of metres topographically lower there are platform margin tidewater-glacial grounding-line phenomena (Domack and Hoffman, 2011). By contrast, other scientists suggest that the Sturtian 'Snowball Earth' was not a prolonged period, but there was some ice oscillation with open water especially near the equator. For instance, Le Heron (2015) recognized ice-free intervals within glacial successions in Death Valley, Namibia, and South Australia, and built a sequence stratigraphy context for these glacial rocks. Also, Spence et al. (2016) argued that significant alkalinity generation would have resulted from continental weathering if the Sturtian was of prolonged duration and would give rise to marine carbonate deposition, unless there was a hydrological shutdown, as envisaged in the Snowball model.

1.5. Aims of this thesis

This study is provides high resolution sedimentological analysis of the PAF recording lateral and vertical stratigraphic variation and facies changes. The objective is to interpret the full range of lithofacies to reconstruct depositional environments and to attempt a sequence stratigraphic model. In so doing, I evaluate the genesis of continuous intervals such as the Great Breccia and the Disrupted Beds, establishing whether they formed by glaciotectonic deformation or slope failure. I also assess the formation mechanism of polygonal sandstone wedges that appear at several stratigraphic levels and penetrate the diamictites. In addition, interpretation of the 12m thick conglomerate that locate on Sgeir Leth a Chuain and the 3m discontinuous granitic conglomerate on the same island, those two beds not

appear on the other islands of the Garvellachs. The overall aim is to propose an event and sequence stratigraphy framework for the PAF.

Chapter 2 : Methodology

This chapter describes the methods and techniques used for analysing the rocks in the PAF. Data collection was fieldwork oriented, with considerable time spent on logging, facies description, and examining stratigraphic boundaries. Throughout this project, the author has taken care to produce data of consistent quality throughout the formation and between different outcrops.

2.1. Field work

The main field area for this research was the Garvellachs archipelago in NW Scotland, supplemented by work in Islay. This has resulted in a major paper that this author has submitted to *Precambrian Research* (Ali et al., 2018: in press). This thesis is the core of the work, with the results fully laid out in chapters' four to nine. In addition, to consider the PAF diamictites in wider context, comparative work was undertaken on the Kingston Peak Formation (a probable age-equivalent of the PAF).
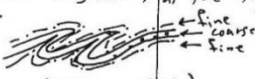
In Scotland, the author spent about 22 weeks in the field. In May 2014, in the first visit to the Garvellachs about 8 weeks was spent examining the PAF with Dr. Anthony Spencer (whole season), Professor Ian Fairchild (3 days), Professor Michael Hambrey (5 days), Dr. Ken Chew (2 days), and Hamid Daleq (5 days).

In February 2015, I visited The USA to examine the Kingston Peak Formation (KPF) in the Silurian Hills and the Kingston Range locations and spent 4 weeks in the field with Professor Dr. Dan Le Heron (Supervisor) and Saeed Al-Tofaif in the Death Valley area (California). The Death Valley work was a subsidiary part of this project, but has resulted in three co-authored papers either published or in review (Le Heron et al., 2017; Le Heron et al., in review a, b). In the same year, immediately after the USA trip, I spent 3 weeks on Islay-Scotland to examine the PAF with Dr. Anthony Spencer (whole season) and Professor Michael Hambrey (5 days); then another 5 weeks on Garvellachs were spent in the field with Dr. Anthony Spencer (whole season), Professor Ian Fairchild (3 days), Dr. Rosemary Titterton (3 days), Gunnar Knag (3 days), and Dr. Ken Chew (1 day).

To supplement the analysis of Precambrian diamictites, the author also undertook short trips to examine Quaternary outcrops around the UK of well-established glacial origin. This included: (i) a one day trip with Dr. Anthony Spencer to the coast of the North Sea at Dimlington near Hull-upon which Humber showed Quaternary diamictites; and (ii) a two day trip to North Norfolk following the Geological Society of London's Glaciated Margin Meeting in 2016, with particular focus on glaciotectonic deformation.

(a) Stratigraphic logs and charts

In total more than 5000 m of strata were logged in both the PAF (Fig.2.1) and the KP (Fig.2.2) in various localities. For the PAF, 1527 m of strata were logged on the Garvellachs in year 2014 (Fig.2.3); and 557 m logged in Islay and more than 500 m on the Garvellachs in year 2015 (Fig.2.3). Also, more than 2500 m were logged in year 2015 from the KPF (Le Heron et al., 2016; Le Heron et al., 2017). The scale for logging the PAF is 1:20; while the scale used for logging the KP is 1:100. This is because sedimentological insight is the main aim for the PAF, while the KPF sections show much less stratigraphic detail.

Unit/ m | gravel/diamict / sand / mud | Sedimentary structures | Percent gravel | Sample no. | Facies | Description | Interpretation

72

150cm 71

80cm 70

10-30cm

69

120cm

40cm 68

50 cm

Description:

gritty
Pebbly sst. with fault, include ripple marks, ripple load casts, downflow (load cast), contourtion? boulders (few), sharp & planar upper contact. pebbles are angular and sub-angular, at the top has ripple marks.

← fine
← coarse
← fine

(490 – 501)

laminated siltst. gradational upper contact.

f. gr. dolomitic sst. sharp & planar upper contact. laterally change its thickness. include some sst laminae (looks like dyke).

f. gr. sst , very few stones (1 per /3m) poorly laminated, sharp upper contact and basin

dolomitic pebble bed. sharp upper contact and planar.

D26⁻ , diam. with silty matrix, few stones. sharp upper contact and planar.

Sheet no. 5

Sedimentary logging sheet
Location E coast of A'chuli
Date 30 May 2014

MJH98

65

Figure 2.1: An example of a scanned page of the sedimentary log from the field work on the PAF on the Garvellachs-Scotland. The section is above D26 on the E coast of A'C.
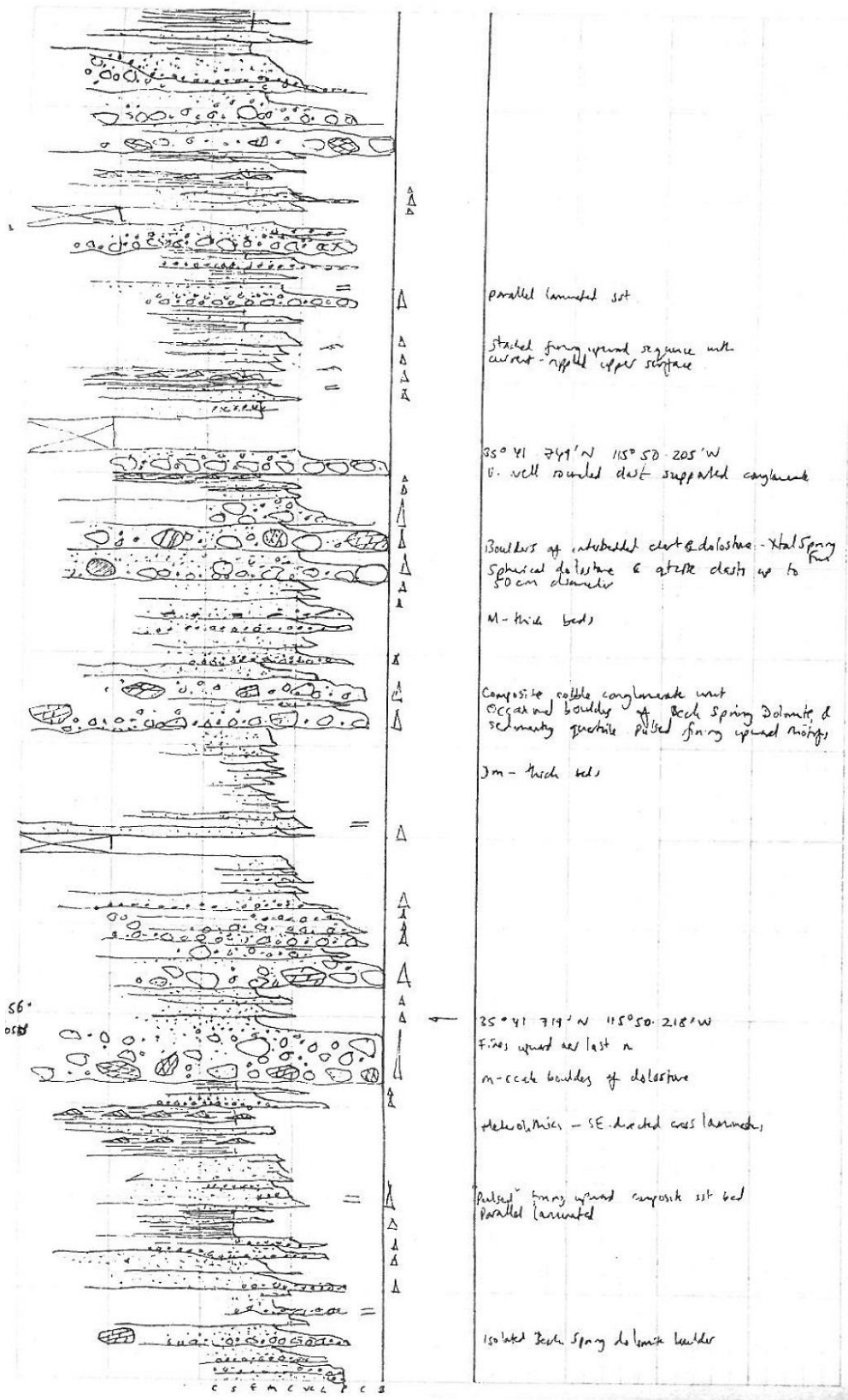
Figure 2.2: An example of a scanned page of a sedimentary log of the KP Formation in Silurian Hill-California.
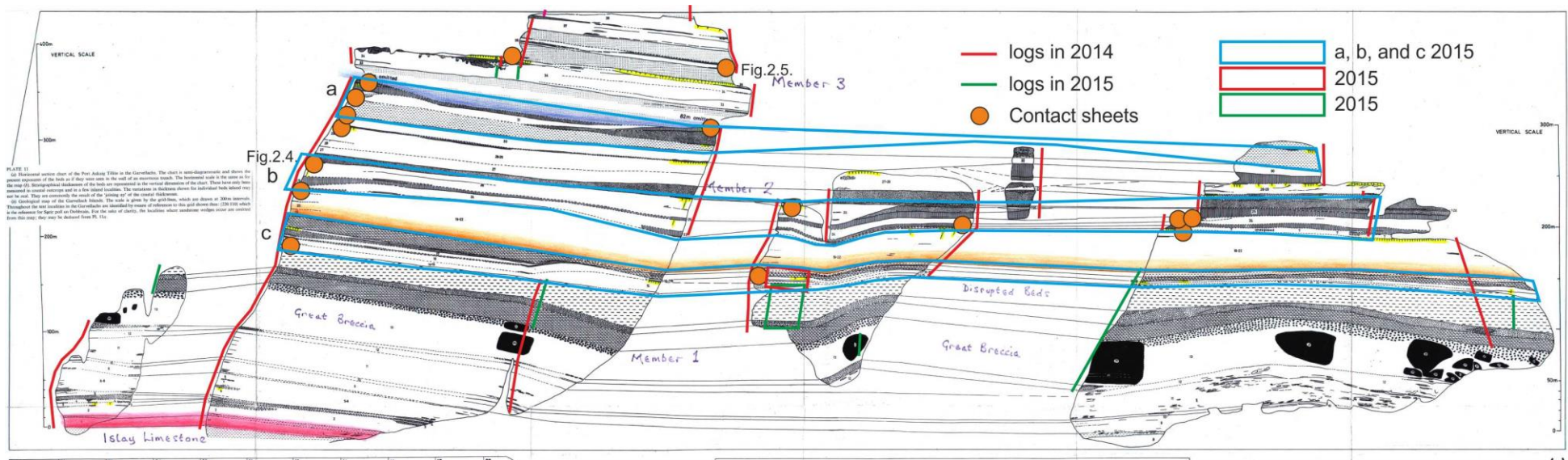
Figure 2.3: Horizontal section chart of the PAF in the Garvellachs-Scotland (Spencer, 1971). The red lines represent sections logged by author in year 2014; and the green lines are the log sections measured in year 2015. The orange circles are locations at which contact sheets have been made. The green rectangle (or rhombic) shape is the sketch (Fig.3.31); while the red rectangle is a field sketch (Fig.3.52B). 'Fig.2.4 and Fig.2.5' are locations of the two examples of the contact sheets. The blue irregular rectangle shapes a, b, and c are the detailed correlation diagrams shown in Fig.6.17, 4.1, 6.16 respectively.

42

(b) Contact sheets

The top contacts of some diamictite beds are complicated, and show as many as 15 events in just 2 m of strata, these cannot be recorded by normal logging. For recording the complete events at these contacts and/or complicated lateral changes of the beds, field sketches and 'contact sheets' have been drawn, respectively (Fig,2.4 and 2.5). The field sketches were drawn by gridding the outcrops in identical squares, checking the strata, and then drawing carefully.
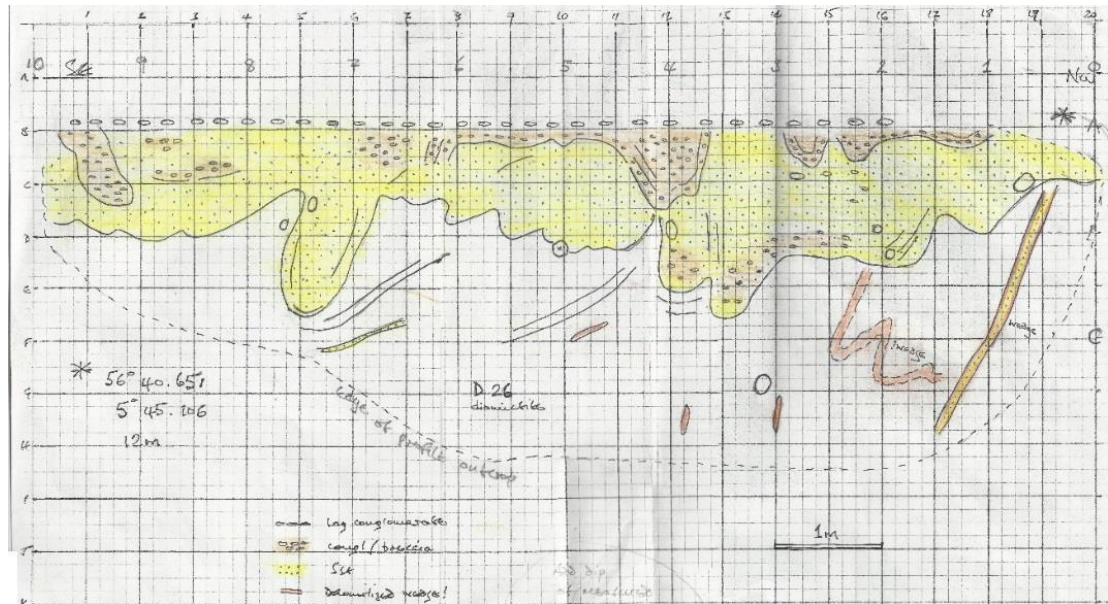
Figure 2.4: An example of the scanned copy of the field sketch made by Dr. Anthony Spencer, author and Hamid Daleq at the top of D26 on the E coast of GE. For location look at 'Fig.2.3' and final diagram see 'Fig.6.14'
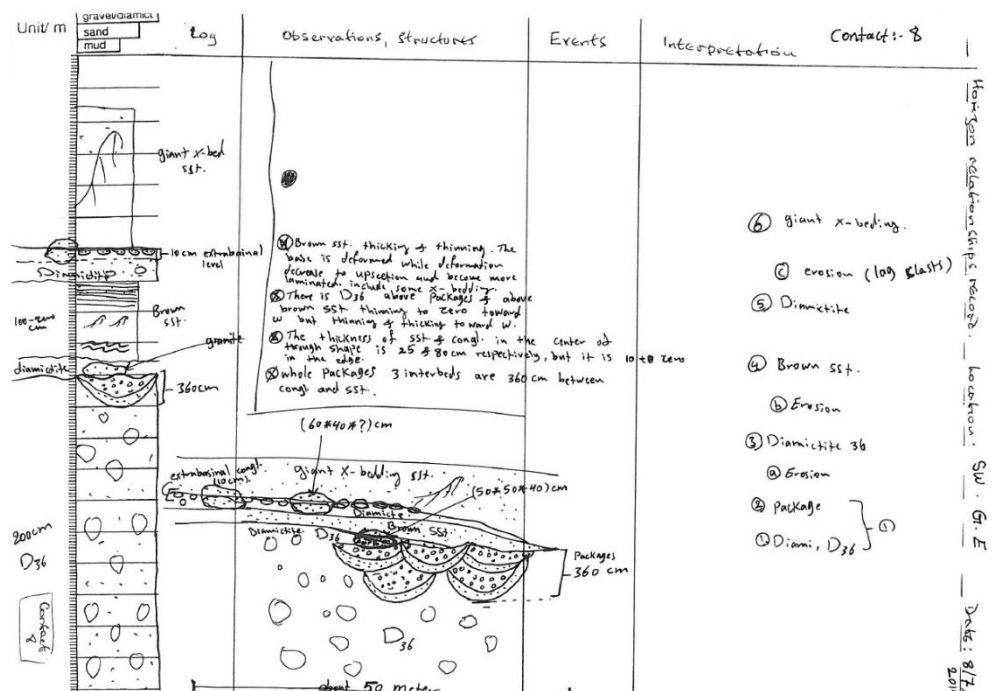
Figure 2.5: An example of the scanned copy of a contact sheet made by author at the top of D36 on the E coast of GE. For location look at 'Fig.2.3'

(c) Sampling

The author and Dr. Anthony Spencer helped Professor Ian Fairchild in the field to collect samples of intrabasinal clasts (dolomite and limestone) from D1 to D12 for stable isotope geochemical analysis. These data will help to compare with the carbonate of the *Garbh Eileach Formation (GEF)*: previously those bedded carbonates had been studied by (Jonathan Evans, 2013) one of the MSc students of Professor Ian Fairchild in Birmingham University. Sampling was done for each individual diamictite bed. In each bed 5 dolomite and 5 limestone clasts were sampled. These samples are used for a stable isotope analysis and the results were used for two accepted papers. The author is leading one of these articles and the other is led by Professor Ian Fairchild.

The author took seven samples for thin section analysis. One from the matrix of D15, and one from the sandstone wedge which penetrates D15 to compare between them whether there are similarities or differences. Two samples were taken from the rhythmically laminated beds below D31 on the west coast and inland behind the house on GE to investigate evidence for ice-rafted debris (IRD). However, samples from fine laminated siltstone must be chosen carefully because the rocks are affected by Caledonian cleavage which can give a false impression of ice-rafting (pseudo ice-rafting Fig.2.6).

Figure 2.6: D38 showing strong Caledonian cleavage (yellow lines). This structure is <u>not</u> an example of ice rafted clasts-the matrix of the diamictite is massive, not laminated.

(d) Palaeocurrent measurements

Many new palaeocurrent measurements were collected in the field from ripple marks and cross-stratifications. These data were supplemented by data collected by A. M. Spencer in the 1960's. Plotting all these data helps understanding the current movements during deposition of the PAF and hopefully gives clues about the topography/bathymetry.

Spencer (1971, Fig.13 and 15) plotted all palaeocurrent data, throughout PAF succession on the Garvellachs and Islay, from cross-beds and ripple marks. The result was a radial shape of the rose diagram. Based on that diagram Spencer (1971) suggested there was no palaeoslope during PAF deposition. However, these data are coming from different stratigraphic horizons (levels) which represent different periods of deposition during PAF succession. Thus, in this study the author has re-plotted these data for each member separately adding data collected by himself. This will be discussed in chapter eight.

(e) Clast counting

The diamictite beds of the PAF are mostly massive, structureless, and homogeneous and so look similar from place to place throughout the islands. The correlation of these beds depends on clast percentages, matrix lithology, the nature of the interbeds, and other features that extend for long distances, such as horizons bearing sandstone wedges and cryoturbations structures. The methodology of clast counting involved finding a clean and flat surface in the field, about 50X50 cm (Fig.2.7), then placing a tracing film on the surface (50X50cm) and drawing every clast bigger than 1cm and recording the lithology of every clast. A total of 184 measurements were made in 2013-2017; the author took part of these measurements in the Garvellachs and Islay.
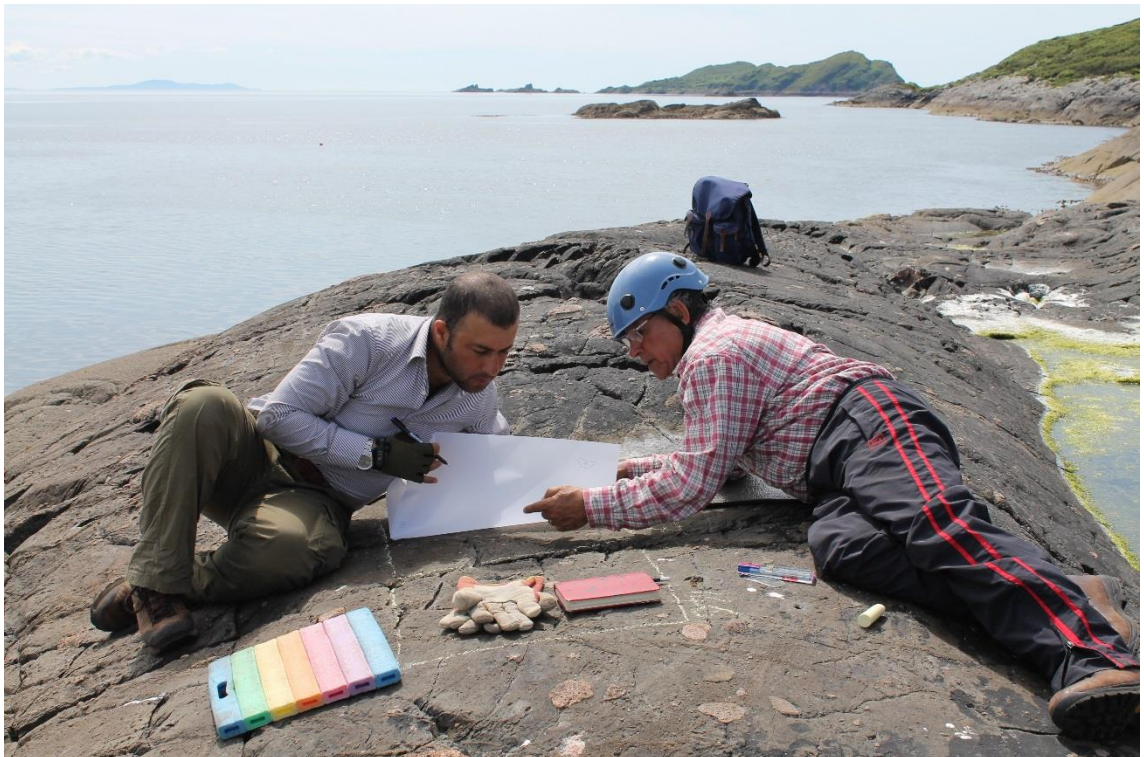
Figure 2.7: The author and geologist Hamid Daleq, clast counting on the SC of GE close the harbour in D38.

2.2. Laboratory work

(a) Petrography study

About 200 thin sections were made available for study by Dr. Spencer, derived from his study in the 1960's. Also, the author prepared seven thin sections for this study form the samples mentioned in section '2.1.C'.

(b) Naming conventions in the thesis

There are several abbreviations throughout the thesis which are used frequently. To avoid repeating these words, the author uses abbreviations. The table below shows those abbreviations:

Table 2.1: List of the abbreviations used in this thesis

Abbreviation	Meaning	Abbreviation	Meaning
N	North	M1 to M5	Member 1 to Member 5
S	South	PAF	Port Askaig Formation
E	East	GEF	Garbh Eileach Formation
W	West	DC	Dun Chonnuill
SE	Southeast	A'C	A'Chuli
NW	Northwest	EaN	Eileach an Naoimh
SC	South-centre	SLaC	Sgeir Leth a Chuain
GE	Garbh Eileach	SnM	Sgeir nam Marag
DB	Disrupted Beds	GB	Great Breccia
MD	Main Dolomite	UD	Upper Dolomite
LF	Lithofacies	LFA	Lithofacies association

Also, most of the figures and logs within this thesis have been drawn in a uniform style that use the same legend (Fig.2.14):
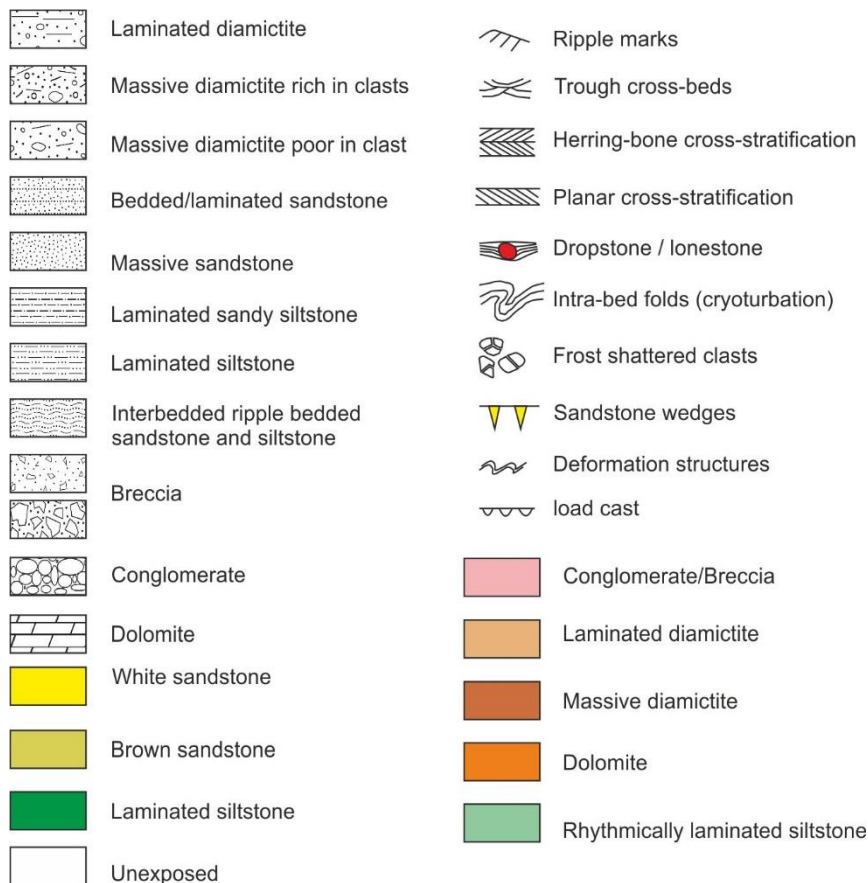
Figure 2.8: Symbols for logs and figures in the thesis.

Chapter 3 : Member 1

3.1 Dolomitic diamictite LFA (D1-D12)

This chapter aims to provide: (i) an ultra-high-resolution description of the Dolomitic diamictite lithofacies association (D1-D12); and (ii) a detailed account of depositional mechanisms. Great attention is placed on bed-by-bed description because there are significant changes in bedding contacts from sharp to gradational across the area, and this study tries to understand the significance of these changes. Owing to the locally exceptional outcrop quality, the level of detail in this chapter is necessarily very high.

As the name suggests, these rocks comprise diamictites that are enriched in dolomitic clasts. These traits alone make this facies association, whilst superficially similar to other diamictites in the PAT, worthy of detailed description and interpretation. Whilst carbonate rich diamictites are very common from other Neoproterozoic records around the world (e.g. Domack and Hoffman, 2011), the low carbonate content of most levels of the PAT begs the question as to why certain intervals should be preferentially enriched in dolomite. Detailed description of the dolomitic diamictite lithofacies association is important because they have received little attention previously, with the exception of Spencer (1971), who examined individual stratigraphic levels. The author has not visited all of the localities, as a result, the data used in this study are based on Spencer (1966) and Spencer (1971) for those outcrops.

Stratigraphically, this lithofacies association is represented by diamictites 1 to 12 (D1-D12) of Kilburn et al. (1965). Two constituent lithofacies are recognised: (i) dolomitic diamictite and (ii) interbeds of dolomite breccia, sandstone, and siltstone. In general, the dolomitic diamictite lithofacies association is distinguished by: (i) the dolomitic matrix of the beds, and (ii) the low proportion of extrabasinal clasts, which only become common in D12. Intrabasinal clasts are predominant.

(a) Dolomitic diamictite lithofacies:

The beds of the lithofacies have mostly been studied in coastal outcrops; because they are poorly exposed inland and most of the cliff outcrops are inaccessible. The lithofacies occurs in five bed-sets: D1-D2, D3-D4, D5-D8, D9-D10, and D11-D12, based on: (a) stratigraphic level, (b) relationship with the diamictite beds or interbeds above and below, (iii) lateral extension of the diamictite beds, and (iv) the nature of the interbeds that separate diamictite beds.

i. Stratigraphic position and Outcrops

D1-D4 are exposed only on DC, and the E and N coasts of GE. Exposures of D5-D8 extend to BaT, but on the E coast of DC, these units are probably represented by three large sandstone lenses lying in a homogeneous diamictite bed. On EaN, D5-D8 is continuously exposed for 250 m along strike, and contains a structure that resembles large-scale cross-stratification (Fig.3.1e). It is mostly composed of poorly bedded siltstones which contain occasional pebbles. At the NE coast of EaN (Fig.3.1e) the siltstone interfingers with D9, suggesting that the diamictite 'beds' belong to large-scale cross-strata. D9-12 are exposed throughout the whole of the Garvellachs outcrop (Table 3.1).

Table 3.1: Diamictite beds throughout the Garvellachs outcrops. D= Diamictite; E=East; DC= Dun Chonnuil; GE=Garbh Eileach; BaT=Bealach an Tarabairt; W=West; A'C=A'Chuli; EaN=Eileach an Naoimh; P=Exposed; and N=Not exposed. The green shading corresponds to outcrops that have been visited and the blue shading represents outcrops using data from others.

D. No.	E DC	W DC	E GE	N GE	BaT	W GE	E A'C	W A'C	N corner of EaN	NW EaN	W EaN
D9-D12	P	P	P	P	P	P	P	P	P	P	P
D5-D8	P	P	P	P	N	N	N	N	P	P	N
D1-D4	P	P	P	P	N	N	N	N	N	N	N

ii. Contacts

Almost all lower contacts of the diamictite beds within this lithofacies association are sharp with the interbedded rocks. However, some of the beds have a gradational contact in places and sharp contact in other places. For instance, the base of D1 on both DC and on the E coast of GE. The base of D1 on DC is gradational with the underlying GEF (Fig.3.2a). On the E coast of GE, the base is again conformable and gradational. The underlying bed 47 of the GEF is similar in general lithology to the matrix of D1, but is planar, thinly bedded, and pebble free. Spencer (1971) chose the base of D1 at a 10 cm thick gritty limestone which is recumbently folded (Fig.3.2b). On the N coast, D1 thins and is replaced laterally by bedded sediment and in the W of that outcrop the lowest diamictite bed is D2.

At the E of the outcrops on the N coast of GE, the conglomerate between D2 and D3 disappears. D2 and D3 merge and are only separated by some lenticular breccia beds (Fig.3.1b). The upper contact of D3 is sharp with the overlying siltstones or sandstones. On the N coast of GE, D3 rests on dolomite breccia with a sharp contact and has a sharp contact with the sandstone above. In the W of this outcrop, D3 is interbedded with dolomite breccia and is replaced eventually by 6 m of dolomite breccia.
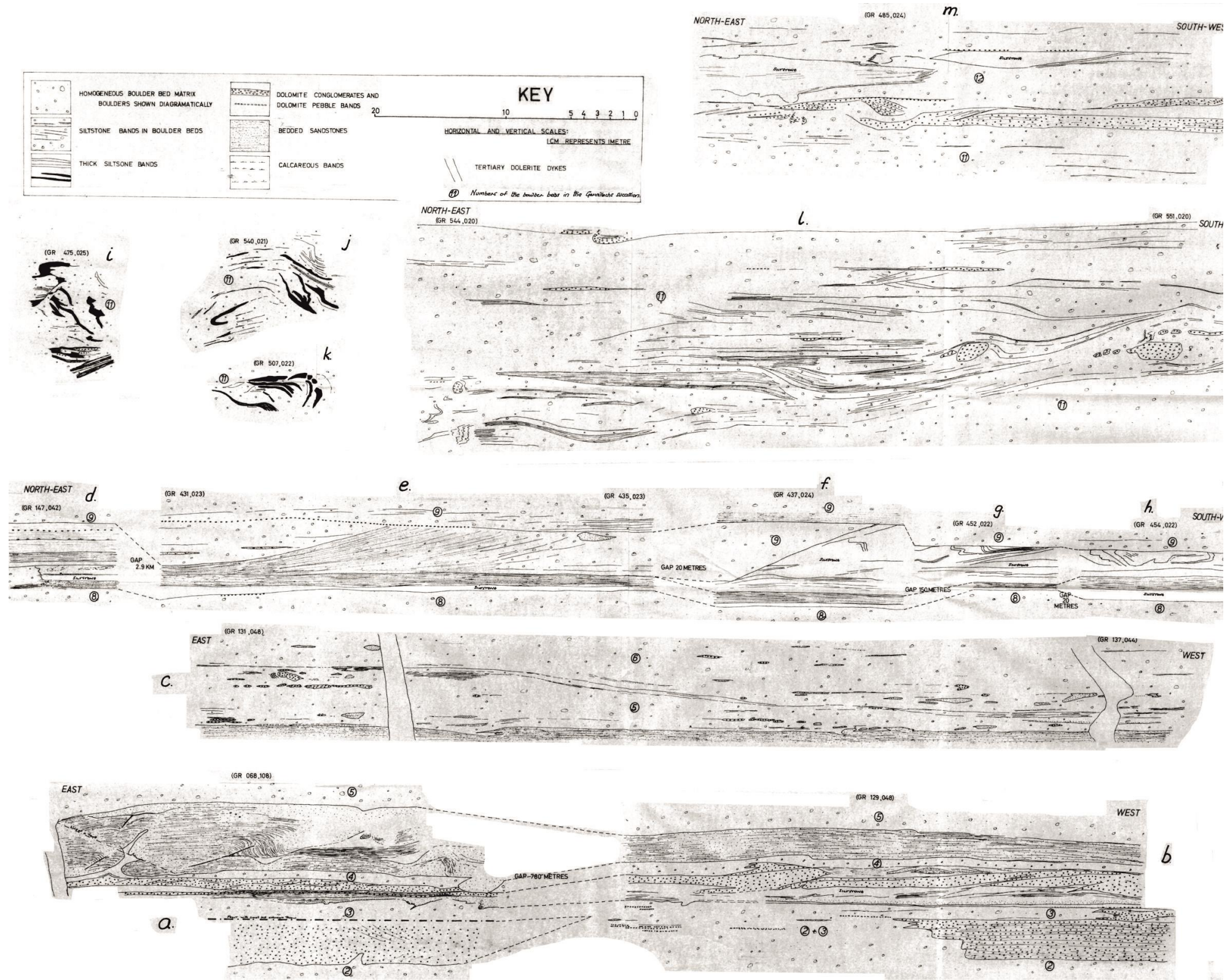
Figure 3.1: Scale drawings showing the geometry of the sedimentary structures in D1-D12 (Spencer, 1966; Fig.37)
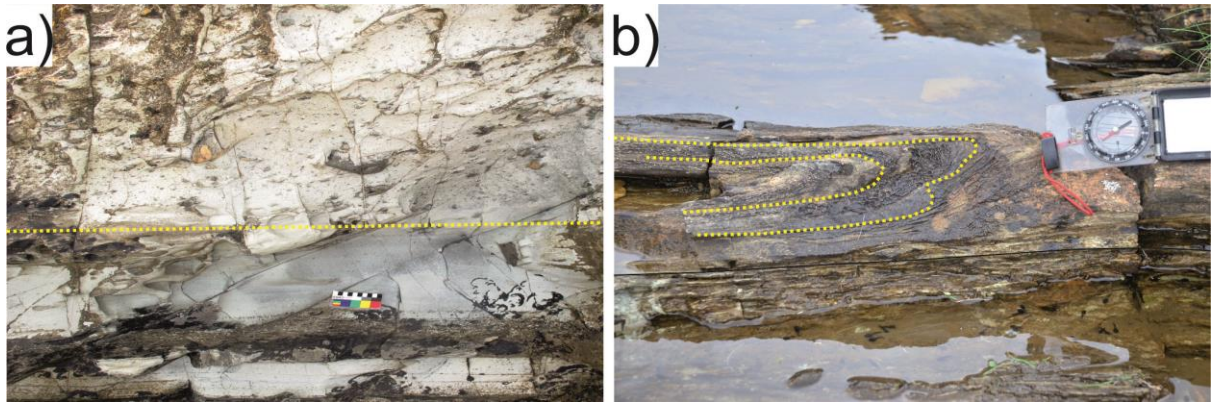
Figure 3.2: (a) dashed-line is a gradational contact between GEF and PAF, on the NE coast of DC. (b) Recumbent fold close to the base of the D1 on the E coast of GE.

On the E coast of GE, D3 rests on a dolomite breccia with a sharp contact, while the sandstone overlying D3 shows loading and interfingering with the matrix of D3 (Fig.3.1a). On this outcrop, the lower and upper contact of D4 is sharp with underlying dolomite breccia and overlying sandstone respectively. About 12 m towards the W D4 is cross-cut by sandstone with a channel-like geometry (Fig.3.1a). In this place, D4 disappears for 1 m and the sandstone above it has a contact with the dolomite breccia below D4 (Fig.3.1a). The top of this breccia interfingers with D4 above (Fig.3.1b).

On the E coast of GE, the lower contact of D5 changes abruptly with the underlying rocks, except in two places, which are gradationally interdigitated with the underlying sandstone.

The top of D7 is complicated because of lenticular grit bands within this diamictite, especially on the N coast of GE, where the top is taken at a horizon of lenticular grit bands up to 1 m in thickness. These can be seen to lie parallel to the bedding at three different stratigraphic levels. Most of the interbeds that separate the diamictite beds in this group are lenticular and of short lateral extent. When they are missing, the diamictite beds merge and cannot be distinguished.

On the E coast of DC and GE D9 rests on a sandstone and on a graded sandstone to pebbly bed, respectively (Fig.3.3); both beds die out after tens of meters (Fig.3.4). The upper contact of D9 changes abruptly to lenticular dolomite breccia beds; on the E coast of GE and the NW corner of EaN, the upper contact of D9 is overlain by siltstone (Fig.3.3).

The lower and upper contacts of D10 are sharp. It is underlain by a laminated siltstone, except on the E and W coasts of DC, where D10 rest on a lenticular dolomite breccia. In places where these beds are missing, it is difficult to separate D9 and D10. The top of D10 is overlain by laminated siltstone, on the W coast of DC, W coast of BaT, and NW coast of EaN or by D11 (E coast of DC).
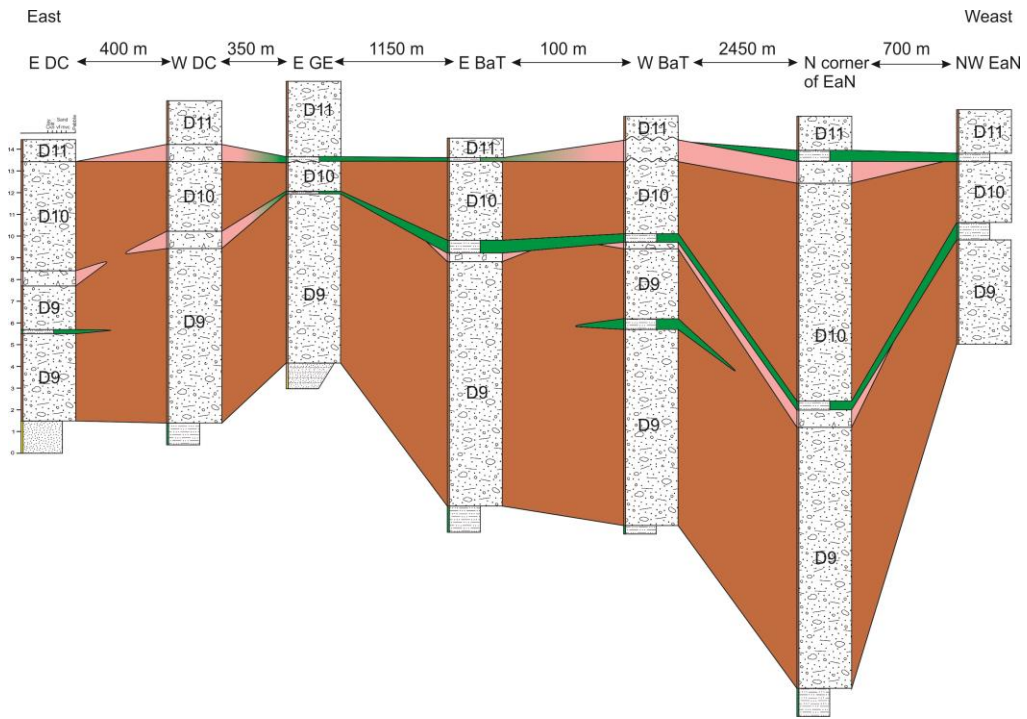
Figure 3.3: Correlation logs between D9 to the base of D11.
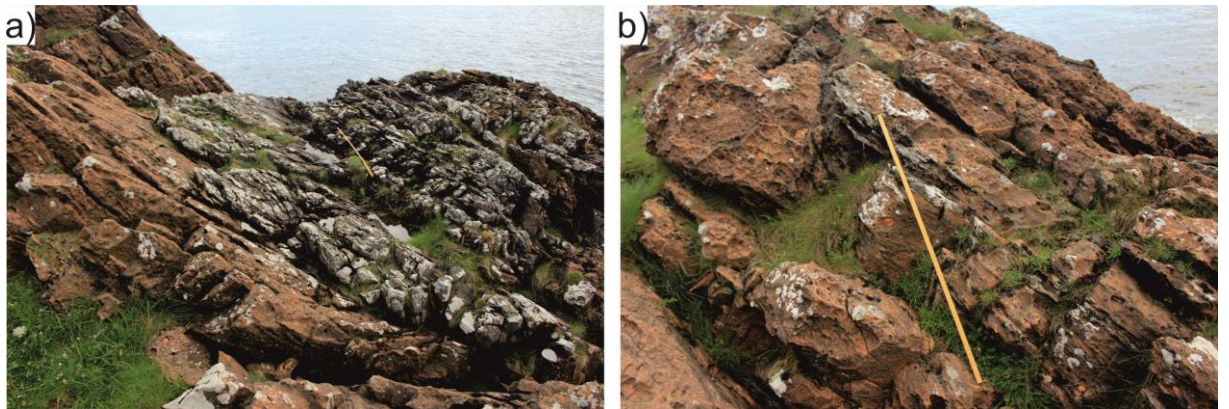
Figure 3.4: Sandstone bed dies out, on DC; (a) A 2 metres thick sandstone bed dies out laterally after tens of metres (b). Ruler is 1 m scale

iii. Lithology

In general, the diamictite beds typically weathered into honeycomb on coastal outcrops (Fig.3.5A). They are composed of dolomitic fawn colour matrix at lower stratigraphic levels, which gradually changes to more arenaceous light grey colour matrix at higher levels (Fig.3.5B, C, and D). The matrix contains intra- and extra-basinal clasts. The intra-basinal clasts are dark brown dolomite (Fig.3.5D), more common and replaced gradually with extra-basinal, and grey or orange coloured quartzite, clasts in higher stratigraphic level.
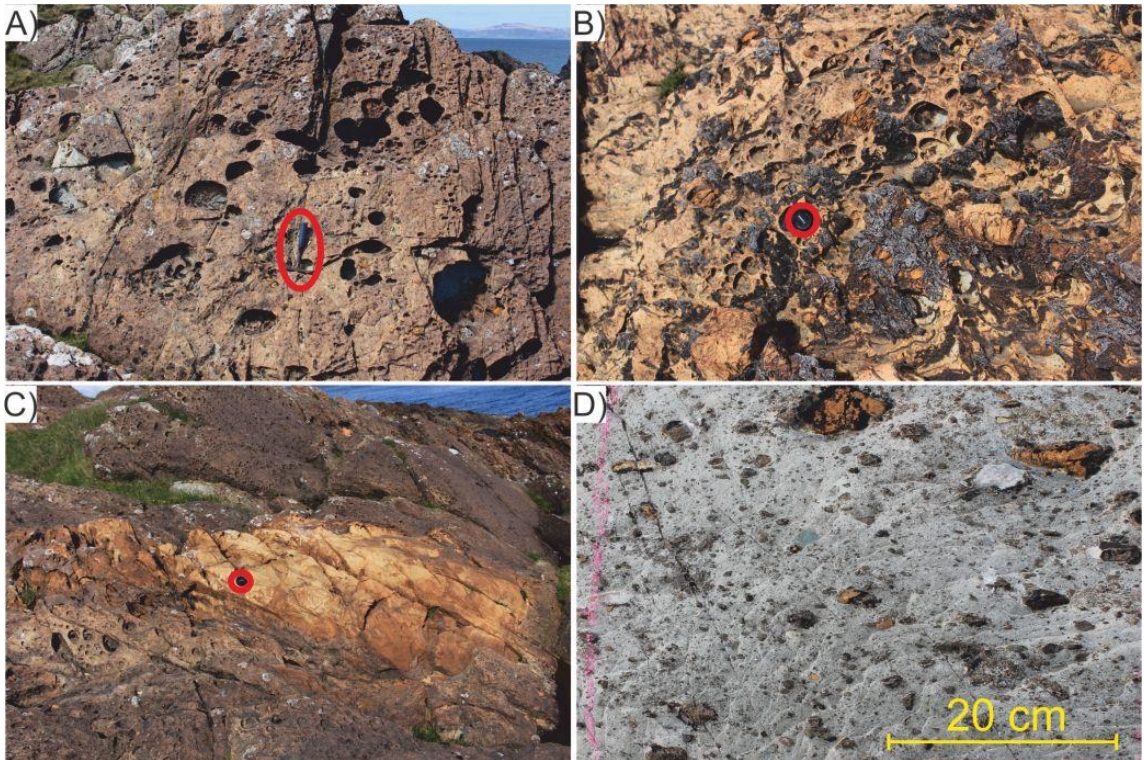
Figure 3.5: (A) Honey comb weathering structure in D11, NE coast of EaN. **(B-D)** Gradational change in the diamictite matrix from dolomitic siltstone (B) in D1-D2 to dolomitic arenaceous (C) in D5-6 to more arenaceous (D) in D7. Geological hammer, camera lens cap (58 mm) are for scale, respectively, in A, B, and C.

D1 and D2 have a well cleaved dolomitic siltstone matrix containing scattered intra-basinal clasts. No extra-basinal clasts are recorded except one quartzite clast in the N coast of GE (Fig.3.6a). D2 is perfectly homogeneous, does not include lenticular bedded sediment, and is 8 m to 14 m thick.

In the N outcrop on GE, folds affect three horizons just below D1; the middle beds of the folded horizons (Fig.3.6c and d) are cross-cut by a narrow, planar sandstone dyke (Fig.3.6b). The folds are tight and sharp with axes striking E-W to NE-SW, which are overturned toward the N and NW and with amplitudes of up to 1 m (Fig.3.6c, d and 3.7). The sandstone dyke is planar and undeformed by the folds.

Figure 3.6: Pitted line is a (a) quartzite clast at the base of the D1, (b) arrows are sandstone dyke, and (c and d) folded beds in the middle horizon below D1.
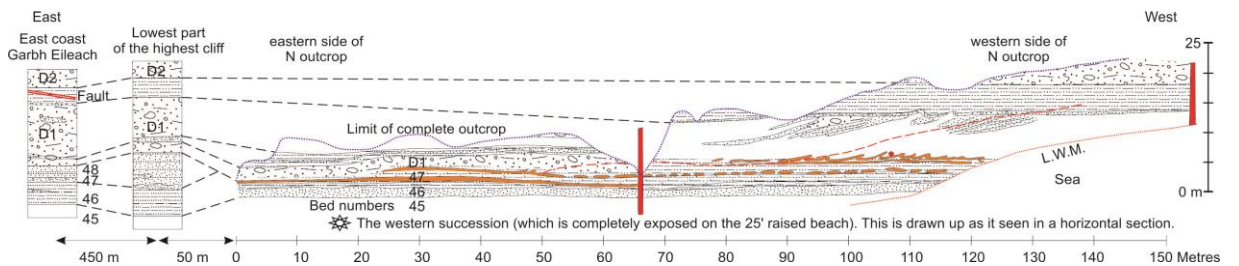
Figure 3.7: Diamictite beds nos. 1 and 2 in E and N outcrops of the Garb Eileach. D1 pinches out in the western side of the N outcrop (Spencer, 1966).

On the E coast of GE, D3 is homogeneous and poor in clast content with clasts no larger than pebble size. A small channel, 50 cm wide and 30 cm deep, infilled with fine-grained sandstone, occurs in the top of the diamictite bed in this outcrop. On the N coast of GE, D4 is like D3, contains only a few dolomite pebbles. But in the E of its outcrop here it becomes almost free of pebbles and extends upward, as a narrow tongue, some 3.5 m into the overlying sandstone.

On the N coast of GE, D5-D8 have a sandy siltstone matrix containing orange coloured intra-basinal clasts. Extra-basinal clasts are not recorded. The clasts size within D7 is bigger compare with the other diamictite beds. On DC, D6 shows a few extrabasinal clasts.

D9 and D10 are very similar; when the interbeds are missing they are homogeneous and undivided. The matrix is siltstone or sandy siltstone and contains intra-basinal and extra-basinal clasts. The intra-basinal clasts are predominant and extra-basinal clasts are rare, but their proportion is more than in previous

diamictite bed-setss. The thickness of D9 varies from 4.8 in NW coast of EaN to more than 12 m in E coast of BaT (Fig.3.3). Also, D10 thickness is 1.5 to 10 m.

iv. Sedimentary structures

These diamictite beds include different sedimentary structures such as bedding, discontinuous bands of siltstone, ripple marks, cross-stratification, and soft sediment deformation. These structures occur at different stratigraphic levels.

D1 includes some lenticular bedded horizons, one of dolomitic siltstone and the other a lenticular bed of dolomitic breccia/conglomerate, both up to 1m thick. On the E coast of DC, a block of dolomite breccia/conglomerate '2.1X1.2X0.6' m occurs floating in D4 close to its base. The bedding within the block is perpendicular to the normal stratigraphic bedding. Furthermore, D4 contains lenses of dolomite conglomerate and sandstone which make the diamictite bed more complicated here than on the E coast of GE.

The top of the D5, on the E coast of GE, is drawn at a 15cm thick pebbly dolomitic sandstone band which has a winnowed dolomite conglomerate beneath it in two places. These bands thin and die out and D5 and D6 merge insensibly at the western edge of this outcrop. However, in this outcrop, there are at least seven bands of siltstone and sandstones and one sandstone lens in the lowest 50 cm of D5. Also, five discontinuous siltstone and sandstone laminae occur, in the lowest 2 m of D7 in the same locality, lying parallel to the bedding. In this place D8 contains dark weathering siltstone laminae with some sandstone lenses. The siltstone laminae merge and divide when traced along the outcrop but generally keep parallel to the bedding.

On the N coast of GE, different levels of sandstone, dolomitic breccia, and siltstone lenses lie parallel to the bedding through the whole bed-sets of D5-8. They are especially common in the lowest 7 m of the bed-sets. Above 7 m from the base, these lenticular beds are still present but they are not frequent compared with the lower part. An intrabasinal clast inside D6-D8 on the N coast of GE about 200 m from E of BaT contains interbedded layers of siltstone, sandstone and diamictite bed; the layers within the clast are folded about an axis which plunges at 20˚ towards 071˚; the clast has a sharp contact with the host rocks.

On the E coast of DC, there is no distinct bedded horizon comparable to lenticular grit bands of the E coast of GE, except one lens of sandstone. One sandstone lens is present in D6-D8 on the E coast of DC. This lens lies 3 m below the top of the D8. This is rather high in stratigraphic level to be correlated with the lenticular grit bands which separate D7 and D8 on the E coast of GE.

In the upper part of D9, there is a discontinuous siltstone bed. On EaN, a dolomite breccia and siltstone horizon forms the top of D10. At the NE corner of EaN, the dolomite breccia and D10 interfinger with each other, and conglomerate occupies channels, up to 30 cm deep in the top of the diamictite bed. Sandy siltstone with alternating coarse and fine laminae occur in one such channel.

Whilst some diamictite beds amalgamate, making it impossible to differentiate individual beds, most are laterally continuous, and can be traced over long distances laterally. For instance, D9-10 are present along the whole outcrop of the Garvellachs, but some of the diamictite beds die out laterally after hundreds of metres. At the W of the N outcrop of GE, the lowest part of D1 wedges out and cross-cuts the underlying bedded sediments which are equivalent to part of beds 47 and 48 of the GEF in the E coast succession (Fig.3.7). The upper part of D1 is poorly represented here, though the bedded sediments beneath D2 are the same here as in the E.

The interbeds are usually discontinuous and die out laterally; for example, the discontinuous beds between D5-8. There are examples that are continuous for a long distance parallel to the strike; such as, the siltstone beds that separate D9 and D10.

(b) Interbed lithofacies

In this thesis, the author follows Spencer (1971) in referring to the lenticular beds that separate diamictite beds D1-D12 from each other as 'interbeds'. In the present study, this particular terminology is re-used for this special facies association to avoid repetition of the facies or sub-facies description; because the bedded sediments within dolomitic diamictite facies association have complicated relationships with each other and with the diamictite beds. The word 'interbed or interbeds' here refers to the strata between diamictite beds without pointing to individual lithofacies or sub-lithofacies.

The interbeds that separate D1 to D12 consist of three sub-lithofacies: dolomite breccia, sandstone and siltstone. In general, the dolomite breccia is composed of angular to sub-rounded clasts within dolomitic siltstone to dolomitic arenaceous matrix. The sandstone beds are mostly discontinuous or lenticular and are well sorted, dark to light grey colour, and fine to medium-grained sandstone.

i. Stratigraphic position, outcrops and lithology

Bed-set between D1 and D2: Interbeds between D1-D2 are exposed only in DC and GE. On DC, there are a group of beds-sandstone, siltstone, and dolomite-which separate these two diamictite beds. The dolomite is punctuated by ribbons of sandstone (Fig.3.8b and c) and some deformation. On the E coast of GE, a dolomite breccia bed occurs about 1 m below the base of D1 (Fig.3.8a); the fragments of this breccia are from the underlying dolomite bed. Also, D1 and D2 are separated by a group of bedded sediments: a thin discontinuous breccia bed, dolomitic sandstone and siltstone. The bedded sediments beneath D2 are the same in N and E coasts of GE. On the N coast, the base of the bed-sets is occupied by a conglomerate (largest clast seen, 24X11X5 cm) like the conglomerate at the top of D1 in the E.
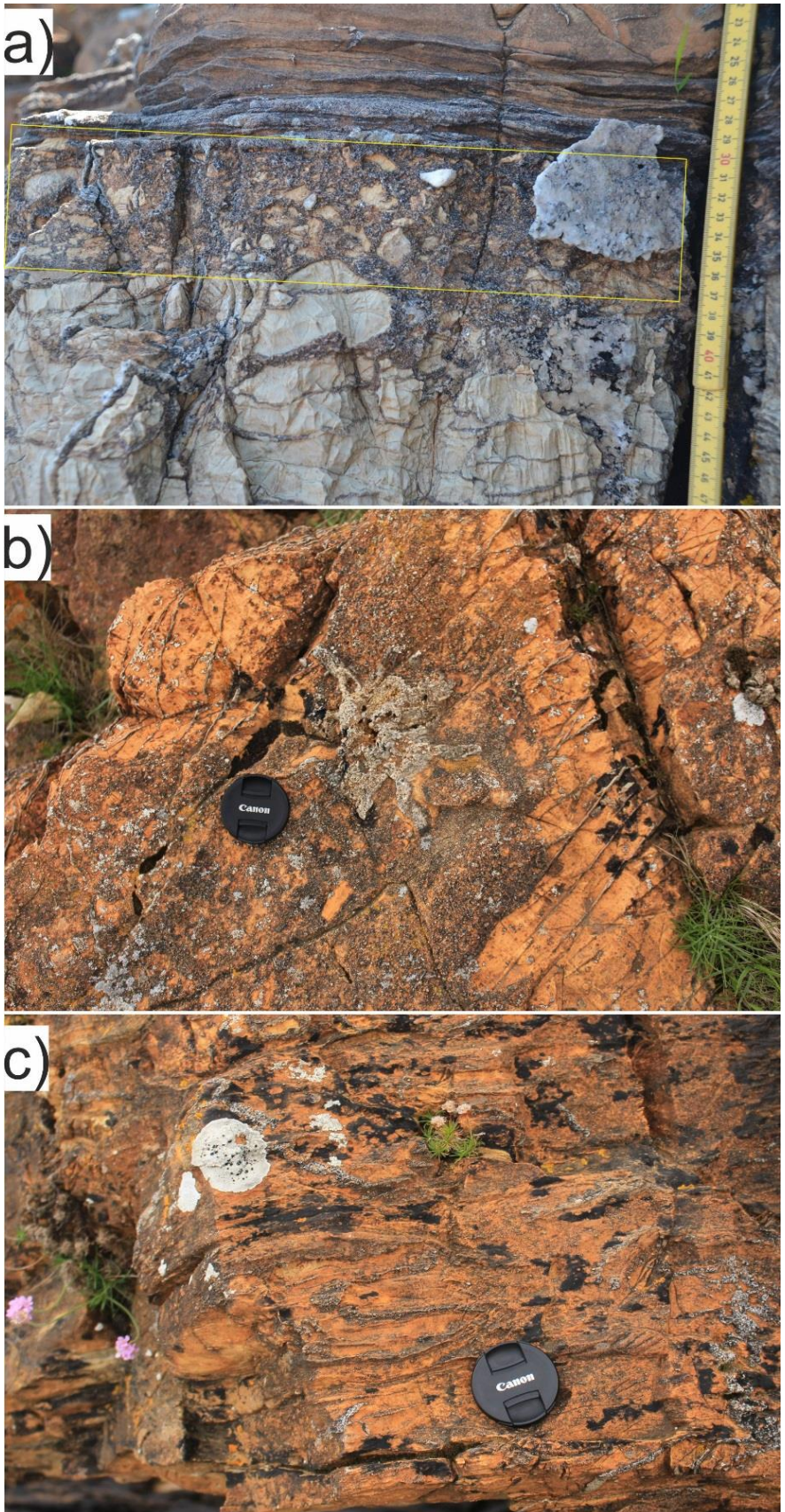
Figure 3.8: (a) An active layer, brecciated top (yellow rectangle) dolomite bed, about 1 m underneath the base of D1, E coast of GE. Ruler for scale. **(b)** Pulses of sandy, dark brown, material within dolomite that separate D1 and D2 on DC. **(c)** Deformation within dolomite that separates D1 and D2 on DC, lens cap is 58 mm for scale.

Beneath lies a series of unbedded dolomitic siltstone with sandstones occuring as large scale cross-stratification foresets. At two places these siltstones are exchanged by pebbly sandstones beds, and the latter resemble a diamictite bed in appearance (Fig.3.7). Because of this, and of the breccia above, the siltstones are equivalent to the upper part of D1. This is supported by the occurrence of an ovoid granitic cobble (20X11 cm in cross-section) at their base (red circle on Fig.3.7).

Bed-sets between D2 and D3: On the E coast of GE a 4m dolomite breccia (Fig.3.10 a-b) has a sandy dolomite matrix and contains white dolomite pebbles (Fig.3.10b). The clasts are plate like and up to 15 cm across. Moreover, within this breccia two cross-stratification units occur, one with a 2m bed-form height records a current towards 307˚ and the other a current generally from the NW. On DC, the succession is similar to the E coast of GE, but the breccia bed on D2 is thinner (Fig.3.9). There, a 10cm thick sandy conglomerate sits on the top of a breccia bed.

Figure 3.9: Breccia bed at the top D2, E coast of DC. Geologist (Ian Fairchild) for scale.
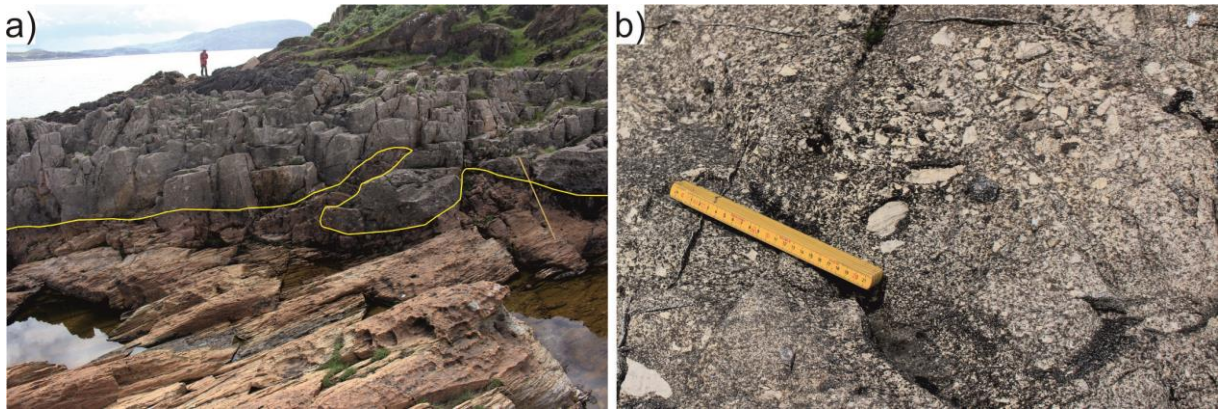
Figure 3.10: Dolomite breccia bed on top of D2, on the E coast of GE. (a) The yellow line represents the contact between D2 and the dolomite breccia bed on top. There is a fold about 1 m amplitude. Ruler is 100 cm for scale. (b) Angular clasts within the dolomite breccia bed.

On the N coast of GE, the dolomite conglomerate between D2 and D3 ends towards the E with a sharp contact against normal diamictite (Fig.3.1b); to the E lenses of dolomite pebbles and sandstone lie parallel to bedding in otherwise homogeneous diamictite, so that D2 and D3 merge into each other. Twenty metres to the E of the eastern edge of the area represented by (Fig.3.1b) there are no bedded horizons within D2 and D3. At the western edge of the outcrop (Fig.3.1b) D3 is replaced over a lateral distance of 6 m by a bedded dolomite. The overlying bedded sandstone, siltstone and breccia/conglomerate of D3 are here similar to those on the E coast of GE. The dolomite conglomerate is cross-stratified in two places, with current flows towards 129˚ and 149˚.

Bed-sets between D4 and D8: On the N coast of GE, D4 and D5 are separated by a sandstone bed, 5.5 m thick (Fig.3.1a), which is medium grained, well bedded, and contains only few dolomite pebbles, all less than 4 cm in diameter. To the W of this outcrop the base of the sandstone lies in a channel which cuts right through D4. Within the sandstone occur four soft sediment fold structures, three of which are associated with narrow veins of siltstone. The largest siltstone vein, is not associated with any folds in the sandstone, however, D6 is overlain by a dolomite conglomerate up to 1 m thick. Above the conglomerate comes a well bedded, 2.1m thick, pink sandstone. The base of the sandstone is undulatory and one upfold strikes at 037 degrees. The sandstone is well sorted and pebble free, and appears to belong to a single cross-stratification unit deposited by a current flowing towards 321˚.

On the E coast of DC, several siltstone, sandstone and dolomite breccia lenses occur in the lower parts of D7 and D8. These have no equivalents on the E coast of GE. The only continuous horizon in this bed-set of diamictite beds which is not lenticular is the siltstone, which lies from 1.5m to 4m above the sandstone at the base of the group (Fig.3.1c). This may be correlated with the sandstone which separates D5 and D6 on the E coast of GE. Sandstone lenses are common in the lowest 2m of D6 in the area of 'Fig.3.1c'. The contacts of these lenses with the surrounding sediments are sharp.

Bed-sets between D8 and D10: On the E coast of GE, D8 and D9 are separated by beds of fine-laminated siltstone and pebbly grit with faint bedding. On the NE coast of GE, these strata become thicker; and on EaN, the total thickness of these bed-sets is up to 8 m, comprising siltstone, sandstone lenses, and

dolomitic conglomerate beds. The bed-sets that separate D9 from D10 consist of siltstone; this interval is distinctive because it is constant and continuous from the W of DC to EaN, a distance of 5 km.

ii. Contacts

The lower and upper contacts of the interbeds are usually sharp. One special case is at the base of the dolomitic breccia between D1 and D2 where there is a single fold structure. The amplitude of the fold, at the base of the dolomitic breccia bed between D2 and D3, is 1 m and its strike is 045˚. This is very close to the trend of the folds which affect the dolomite conglomerate in the N coast outcrop of D1 (Fig.3.7)

iii. Sedimentary structures

On the E coast of GE just underneath D7, lenses of grit occur. The three-dimension shape of the lenses cannot be determined, which is unfortunate, because if these lenses are channel infillings their strike might give the prevailing current flow direction. However, one of the grits is cross-stratified and gives a current direction from 262˚.

On EaN, the interbeds between D8 and D9 include interesting large cross-stratification (Fig.3.1e). It is mostly composed of poorly bedded siltstone which contains occasional pebbles. At the E coast of EaN (Fig.3.1e) the siltstone interfingers with D9, showing that layers of diamictite are involved in the cross-stratification. The eastern contact of the siltstone with D9 is sharp and the diamictite bed contains sandstone and siltstone lenses, mostly flat lying. A thin pebble bed with some siltstone overlies both the eastern and western areas of diamictite bed and the siltstone (Fig.3.1e and f).

The sandy siltstones within the bedded sediments between D8 and D9 are commonly current ripple bedded. Two groups of ripple marks were recorded: (i) those on the E coast of GE which strike NE-SW and; (ii) all the other measured ripple marks which strike almost at right angles to previous one (Spencer, 1971). The ripple marks recorded from DC are symmetrical. In addition to ripple marks, cross-stratification is present. On the E coast of GE, a cross-bedding unit with ripple height of 40cm records a current towards 320˚, but in one case from N-E. The 15 available current indicators from this bed-sets show no overall preferred orientation.

In Fig.3.1g and h, the interbedded sediment is much thinner than further E and the bedding in the siltstone shows intrabed-folds. These folds are truncated by the same stratigraphic level the cross-stratification structure of Fig.3.1e and f; above that horizon comes a normal diamictite bed.

(c) Depositional environment of the dolomitic diamictite LFA

The controversy about the PAF depositional environments between authors relates to three hypotheses: (i) grounded-ice/floating-ice; (ii) mass-flow; or (iii) a combination between these if the formation was deposited in marginal environments. Based on the new field data and previous works, the author will focus on these hypotheses to test the setting of this lithofacies associations within the PAF. The main features to be interpreted are listed in Table 3.2.

Mass-flow settings

Stratigraphically, the presence of the dome-shaped stromatolites close to the base of PAF (Fig.3.11), within the upper part of the GE Formation (previously Islay), does not fit with a mass flow hypothesis, because stromatolite sediments appear to have been laid down in very shallow water (Spencer, 1971). However, suggesting that the diamictite beds mostly formed by mudflows or mass flows derived from a nearby mountain slope and deposited in shallow water is a more likely scenario. These diamictite beds (D1-D12), in general, do not show evidence of shear deformation typical of subglacial till; also, the lack of outwash deposits was brought up by Arnaud and Eyles (2006). Also, Arnaud and Eyles (2006) noted that striated clasts have not been founded in the diamictite beds of the succession, and generally, suggested that the diamictite beds in the PAF accumulated by various process in a tectonically active and glacially influenced marine setting.

Glacial settings

This chapter is highly cross referenced to Spencer (1971) because he is the only person who gave a simple interpretation and discussion about D1-D12.

Features such as the brecciated top of a dolomite bed (Fig.3.8a), cross-stratified sandstone, patches of diamictite inside the sandstone, and the lateral changes of the diamictites suggest deposition on a glaciated margin. Spencer (1971) interpreted D1 and D2 as formed at the edge of an ice-sheet without further details, for instance, whether it is a lateral moraine or proglacial deposits.

Figure 3.11: Microbial sedimentary structure (stromatolite) in the upper part of the Garbh Eileach Formation, on the NE corner of the GE.

Spencer (1971) suggested that the cross-cutting base of D1, on the N coast outcrop of GE was a result of either erosion beneath the diamictite bed by the agent which transported the diamictite bed material, or non-deposition of parts of beds 47 and 48 of the GEF. In this model, both D1 and D2 formed from one event. The lateral dying out of D1, on the N coast of GE, is replaced by bedded dolomites and unbedded siltstone with large scale sandstone cross-stratifications and two diamictite patches.

The breccia bed separating D2 and D3 on the N coast of GE terminates abruptly against a diamictite bed. Spencer (1971) suggested this relationship is difficult to form if diamictite beds were produced by mudflow deposits, because the geometry of the beds, and abrupt and lateral changes cannot easily be explained by this hypothesis. The easier interpretation for producing this type of the relationship is in a sub-glacial environment. It could be formed in a channel below a grounded-ice sheet.

Combination settings

Features recorded within D1-D12 are inconsistent: some of them indicate water-lain features and others show grounded-ice deposition. For instance, features like stromatolites (Fig.3.11), outsized extrabasinal clasts (ice-raft?) (Fairchild et al., 2017, in press), laminated sediments, patches of diamictite inside the sandstone, and the gradational contact of the base of the PAF on DC (Fig.3.2a) all support a water lain hypothesis. By contrast, syn-sedimentary folds beneath the diamictite bed (Fig.3.6C-D, 3.2b) that have similar trends with the glaciotectonic folds in higher stratigraphic levels, the brecciated top of the dolomite bed (Fig.3.8a) which can be fitted back like a jigsaw, and the cross-cutting base of D1 on the N coast (Fig.3.7) all support a grounded-ice hypothesis.

The present author agrees with Arnaud and Eyles (2006) that striated clasts have not been found in the PAF, but that does not mean the PAF is a non-glacial deposit for the following reasons. Globally, striated clast surfaces are more typical on fine-grained sandstone and siltstone pebbles (Le Heron, 2015), and these lithologies are rare in the PAF. In the PAF, clasts are predominantly carbonate in the lower part of the formation, and replaced by granite and quartzite upward the succession. Following a similar argument, striation are generally rare on carbonate clasts in Sturtian age due to '(1) metamorphic overprint that may contribute to eradication of striae, or (2) on carbonate clasts any striation is likely to be a locus for weathering and microkarst development, so their preservation in such ancient strata is made more unlikely' (Le Heron, 2015). Furthermore, the brecciated top of a dolomitic bed (Fig.3.8a), on the E of GE, is likely to have formed as an active layer cryoturbation in situ in a periglacial environment (subaerial exposure). Both brecciated tops - the dolomite at the E coast of GE and the folded dolomites at the N coast of GE - are at the same stratigraphic level. This level of subaerial exposure implies that the overlying diamictite (D1) was probably formed by grounded-ice.

The cross-cutting beds on the N coast (Fig.3.7) of GE can be explained by ice oscillation (Fig.3.12B). Moreover, the cross-stratified sandstone (in Fig.3.7) might represent water currents flowing from the W, while the patches of the diamictite material within sandstone may represent debris from small icebergs, or frozen lumps inside the sandstone in small fluvioglacial channel in a periglacial environment.
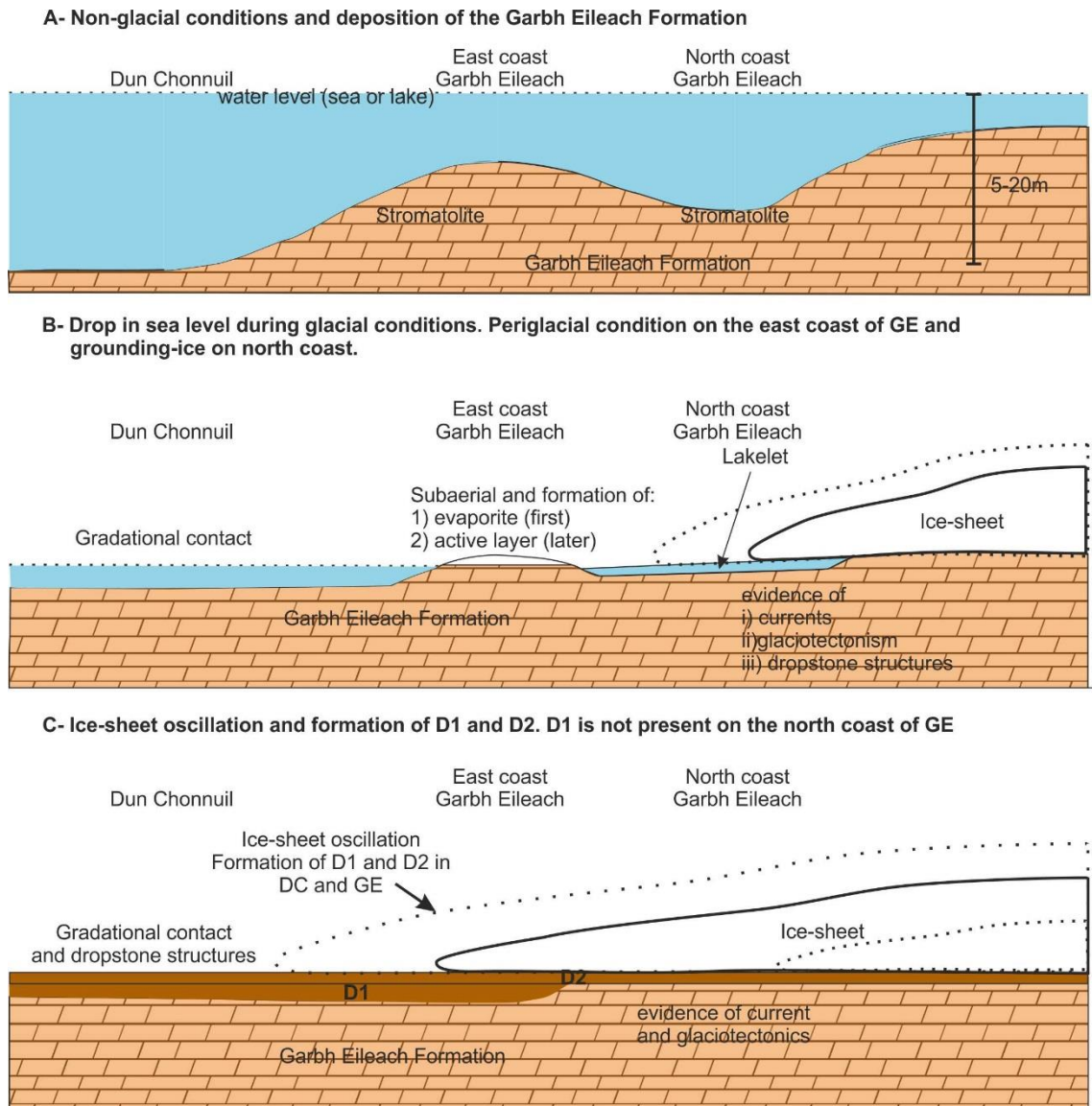
Figure 3.12: A cartoon showing the depositional mechanism of D1 and D2 in DC and the E and N coasts of GE.

Discussion of environmental interpretation of D1-D12

The following section now discusses the beds of D1-D12 LFA in term of the three hypotheses: mass-flow, grounded-ice and combination. The gradational contact of the base of the PAF on DC may indicate ice-rafted debris in very shallow water (Fig.3.12). Also, the size of the clast supports this idea, because the clast size is small not more than few centimetres across (Fig.3.2a). The presence of stromatolites does not automatically mean that the water depth was shallow, because there are prokaryotic populations in sediments as deep as 800 m below the seafloor (D'hondt et al., 2004). However, the microbial structure that is close to the base of the PAF is dome shaped (Fig.3.11), and inclined. This geometry is typical of very shallow environments (e.g. subtidal to tidal flat environments) because they take this shape in response to wave and water agitation (Le Ber et al., 2013). Upward growth and competition probably explains the inclined domes shown in Fig.3.11.

Folds, at the western cliff of N outcrop of GE (Fig.3.6C-D), could be produced by syn-sedimentary glacial, mass-flow, or later tectonic mechanisms. A tectonic mechanism can be ruled out because the folds are cross-cut by an undeformed sandstone dyke (Fig.3.6B). In subglacial or englacial environments such a fold can be produced by shearing. Spencer (1971) interpreted this fold to reflect glacial shearing, without pointing whether it is subglacial, proglacial or englacial. Comparison was drawn to folds in the Quaternary Cromer Till on the N Norfolk coast. However, these folds in the PAF may be developed by downslope gravitational movement (slumping). The folds in the western exposure are developed in dolomite. They are uniformly overturned towards the N and NW showing that they are not loading structures, because they are not convolute laminations.

Lenses of sandstone and conglomerate at the top of D2 and D3, in the eastern part of the N coast (Fig.3.1b), are difficult to explain if D2 and D3 are mudflow deposits. Their formation was separated by an interval of dolomitic breccia in four outcrops, stretching from the N coast of GE to the eastern coast of DC. The conglomerate represents a different environment because: (i) the clasts of the conglomerate are angular to subangular (Fig.3.10b), suggesting localised short distance transport; and (ii) the large size of the clasts means powerful current velocity. It is remarkable therefore that the conglomerate is absent in the eastern part of the N coast (Fig.3.1b). High energy currents would be expected to leave a record such as an erosional surface, conglomerate bed, or pebble lag: instead D2 and D3 merge into each other. On the N coast of GE, the glacial hypothesis can easily explain the D2-conglomerate-D3 succession.

Moreover, this conglomerate between D2 and D3 (Fig.3.1b) is not a megaclast, sensu Terry and Goff (2014), or series of clasts floating in the diamictite matrix for it has a similar thickness and stratigraphic position in three other outcrops, up to a maximum distance of 1.5 km stretching from N coast of GE to eastern coast of DC. In addition, it is not produced by the breaking or tearing off of eastward continuation of the bed, either by ice or mass flow action, because there is no dolomitic conglomerate clast recorded at this stratigraphic level which is continuously exposed for 80 m to the E of the conglomerate margin. However, such an action might be the reason to produce the blocks of conglomerate in higher stratigraphic level: such as, in D4 on the E of DC.

The glacial hypothesis can explain both the sharp margin to the conglomerate and the bedded lenses in D2 and D3. The sharp edge of the conglomerate can be interpreted as the edge of a stream channel beneath the ice. The lenticular beds on the eastern side of the N outcrop (Fig.3.1b) might be formed by frozen blocks within the ice or as small channelway. The latter hypothesis explains their sharp margins, but occasionally, the area to which water currents had access beneath the ice increased and the pebble and sandstone bands lying within the diamictite bed were deposited. The water currents did not spread very far from the channelway as only 45m to the E of its edge all the bedded lenses disappear and the diamictite becomes homogeneous. Both, frozen blocks and channelway, can be form within the ice or underneath the ice.

In addition, there are other features that support the glacial hypothesis. D3 is replaced laterally by dolomitic breccia in the western part of the N coast outcrop of the GE (Fig.3.1b). Also, in the E coast, D4 is replaced by dolomite breccia (Fig.3.10). Neither of these relationships seems to be due to contemporaneous folding.

The well sorted lithology of the interbeds: there are interbedded sediments between diamictite beds such as conglomerate and well sorted pebble free sandstone. The conglomerate is a remarkably uniform lithology, and very even-grained. This purity of the bedded sediments might be thought remarkable in a sub-glacial environment, produced by winnowing of the till-like material.

There are two hypotheses to explain the sharp contact of the lenses underneath D7 and within D5-D8 bed-sets with the surrounding rock:

First, they could be transported clasts and deposited inside diamictite beds. Based on the size of the lenses and unsorted diamictite beds, two settings could form such clasts are possible: (a) grounded-ice; and (b) mass-flow or ice-rafting. An ice-rafting mechanism is unlikely owing to the absence of punctured laminae and no any signs for striated surfaces. Also, there is no evidence of deformation underneath the lenses. Based on lack of such evidence ice-rafting can be ruled out. The lenses could be formed subaqueously by mass flow. However, stratification in the lenses is the same as normal stratigraphy. If they had been transported by mass flow then some 'clasts' would have been notated. The same would be true if the lenses were clasts transported by grounded-ice. So, the clast hypothesis can be ruled out.

Second, they could be formed contemporaneously with the diamictite. The different grain size with the host rock and the sharp contacts rule out the mass flow hypothesis. These lenses can be formed in a subglacial environment as product of varying amount of water transport by glacial streams. The sharp contacts might be expected and the size range of lenses would be expected on the glacial hypothesis.

Diamictites D6-8 can be distinguished only on the E coast of GE. The bedded horizons that separate these diamictite beds are thicker than the discontinuous lenses seen in the area of 'Fig.3.1c'. This suggests that the D6-D7 and D7-D8 interbeds must thin and die out laterally. The easiest interpretation for all the horizons which separate D5-8 is that they formed as a result of subglacial streams which were only active in certain areas.

There are some facts that must be taken in consideration when interpreting the cross-stratification seen in Fig.3.1e and f: (i) on the western side of the structure, the laminated siltstone of the foresets is interbedded with the D9 matrix; (ii) the three dimensional structure cannot be seen; and (iii) E and W of the structure, the diamictite bed does not show stratification. Based on (i), one can decide that the cross-stratification formed during the deposition of the diamictite bed. Because of (ii), there are two possibilities to form foresets with such a cross-stratification: *first*, as the margin of a channel filled with diamictite with a current flow N-S (Fig.3.1e); *second,* as a low relief channel filled by diamictite with a current flow toward NE. The present author agree with Spencer (1971) that this structure possibly formed in subglacial deposits. In this model, the diamictite bed forms through ice-melting whereas

siltstone forms by a water current flowing in, e.g. subglacial channel ways. Similar structures can be seen in Quaternary deposit at Cromer, N of Norfolk, but it is smaller scale (Fig.3.13). In this analogue, there is an important observation; the siltstone does not include pebbles, while bounded by diamictite beds from the base and the top just like the siltstone in the PAF.

Figure 3.13: Fine-laminated siltstone without outsize clasts filling the low relief and bounded by diamictite beds from base and top; N Norfolk.

The deformation structures in siltstones (Fig.3.1g and h) may also be interpreted as large-scale slump folds, or alternatively convoluted lamination or folds produced by ice movement (Spencer, 1971; Plaziat et al., 1990; Alfaro et al., 1997; Menzies, 2000; Van der Wateren et al., 2000; Pratt, 2002; McCarroll and Rijsdijk, 2003; Nogueira et al., 2003; van der Meer et al., 2003; Menzies et al., 2016). There are several factors which produce convolute lamination structure; for example, seismic shocks (earth quake), triggers as tectonic stress, gravity flow, and storm-wave impact (Nogueira et al., 2003). Such structures affects the whole thickness of a bed along an entire outcrop (Plaziat et al., 1990; Alfaro et al., 1997; Pratt, 2002; Nogueira et al., 2003). Busfield and Le Heron (2013) noted that the intensity of ductile deformation features commonly increases upward in subglacial shear zones; by contrast, the intensity of deformation is commonly greatest at the base of a shearing submarine gravity flow (Arnaud and Eyles, 2006). Based on deformation rate (Spencer, 1966), the author tentatively supports a glaciotectonic model (Menzies, 2000; Van der Wateren et al., 2000; McCarroll and Rijsdijk, 2003; van der Meer et al., 2003; Menzies et al., 2016) because; as shown in Fig.3.1 g and h, the intensity of deformation increases upward.

In summary, the table below (Table.3.2) shows the most common features within each of the lithofacies associations described in this chapter, together with the more plausible interpretation for each. According to the table, the lithofacies mostly formed by grounded-ice. However, it is not the only environment; because there are couple levels which can be seen floating-ice and periglacial environments.

Table 3.2: Features and lithofacies that occur within the Dolomitic diamictite lithofacies association with interpretation summary.

Features/beds	Lithofacies	Subaqueous mass-flow	Floating ice	Grounded ice	More likely in this study
Diamictite beds	D1-D12	Possible	Unlikely	Possible	Grounded-ice
Massive diamictite	D1, D2, D5-D8, D9, and D12	Possible	Unlikely	Possible	Grounded-ice
Stratification structures/beds within diamictite	D11, and some other horizons like D9	Possible	Unlikely	Possible	Grounded-ice
Intense folding & thrusting	Base D1 on the EGE and within bedded strata below D2 on NWGE	Possible	Possible (by dragging ice-bergs)	Possible	Grounded-ice
Abrupt lateral termination of interbeds	D1-D2, D2-D3, and D8-D9	Unlikely	Unlikely	Possible	Grounded-ice
Sharp bases of diamictite beds	D1-D12	Possible	Unlikely	Possible	Grounded-ice
Gradational base of diamictite beds	D1 on DC	Possible	Possible	Unlikely	Floating ice-bergs
Angular (breccia) top of dolomite bed	Below D1 and on base of PAF on Islay	Unlikely	Unlikely	Possible	Periglacial
Long lateral correlation of diamictite beds	D9 and D10	Possible	Possible	Possible	Grounded-ice
Highly discontinuous laterally diamictite	D1, D3, and D4	Possible	Unlikely	Possible	Grounded-ice

3.2 Great Breccia LFA (D13):

Diamictite bed 13 or 'The Great Breccia (GB)' is a unique, highly distinctive bed-set in the PAF because it contains megaclasts whose size reaches hundreds of metres across. It overlies diamictite 12 and underlies the Main Dolomite (Fig.3.14). Based on lithology, there are three main lithofacies in the GB, which in stratigraphic order are arranged in a group as follows: the dolomitic megaclast lithofacies forms the main part of the GB, the boulder conglomerate lithofacies overlies it and, in places above, a thin lithofacies of diamictite is present below the Main Dolomite (Table.3.3).

Table 3.3: Lithofacies within GB

	Lithofacies	Description
Base overlying GBLA	Main Dolomite	Massive and/or bedded dolomite
Great Breccia Lithofacies Association (GBLA)	Diamictite	Very poorly sorted sediment with >1% clasts sandy siltstone
	Boulder conglomerate	Rounded and angular boulder size clast in a matrix
	Dolomitic megaclasts	Matrix with megaclasts.
Group of beds underlying GB	Sandstone and dolomite beds	Discontinuous beds separate the GBLA from the underlying D12
	Diamictite	
	Dolomitic conglomerate beds	

(a) Dolomitic megaclasts Lithofacies:

i. Stratigraphic positions and outcrops

These strata are well exposed along the Garvellach Islands. The main part of the GB is about 43-50 m thick. It overlies diamictite D12 and underlies the Main Dolomite facies association or the 'boulder conglomerate lithofacies'. It is remarkable in containing macro-boulders (using terminology of Terry and Goff (2014)) up to hundreds of metres in length. The lithofacies is refers to the Garvellachs. Spencer (1971) proposed that a comparable lithofacies at the same stratigraphic interval could be recognized on Islay at the base of the PAF but the dolomitic megaclast facies is thinner (4m) and contains much smaller clasts (less than 2 m diameter). The descriptions below refer to the Garvellach Islands.

ii. Contacts

The lower contact of the dolomitic megaclast unit above D12 is marked by a group of discontinuous bedded strata from 0-10 m thick and composed of three beds: sandstones, bedded dolomite, and thin diamictite and dolomitic conglomerates, in ascending order.

Sandstone and dolomite beds: The lowermost bedded sandstone and dolomite are usually less than 1 m thick. In this stratigraphic level, on A'C, there is no bedded horizon; instead, there are several large lenses of gritty dolomite which occur in the top of D12 (Fig.3.15).

Diamictite occurs in the centre of the group (Table.3.3) and reaches a maximum thickness of 5 m on the N coast of GE. In places, this diamictite bed resembles some parts of the overlying GB in the coarseness

and abundance of included fragments: for example, on the NE side of BaT and NE and NW coast of EaN (Fig.3.15). In other outcrops, the diamictite is much finer-grained and more comparable with the underlying dolomitic diamictite beds, for example on the W and S coasts of DC, the NW side of BaT and the N coast of A'C (Fig.3.15). On the E coast of GE, this diamictite bed occurs within an otherwise homogeneous dolomitic conglomerate as a very thin lenticular shape.
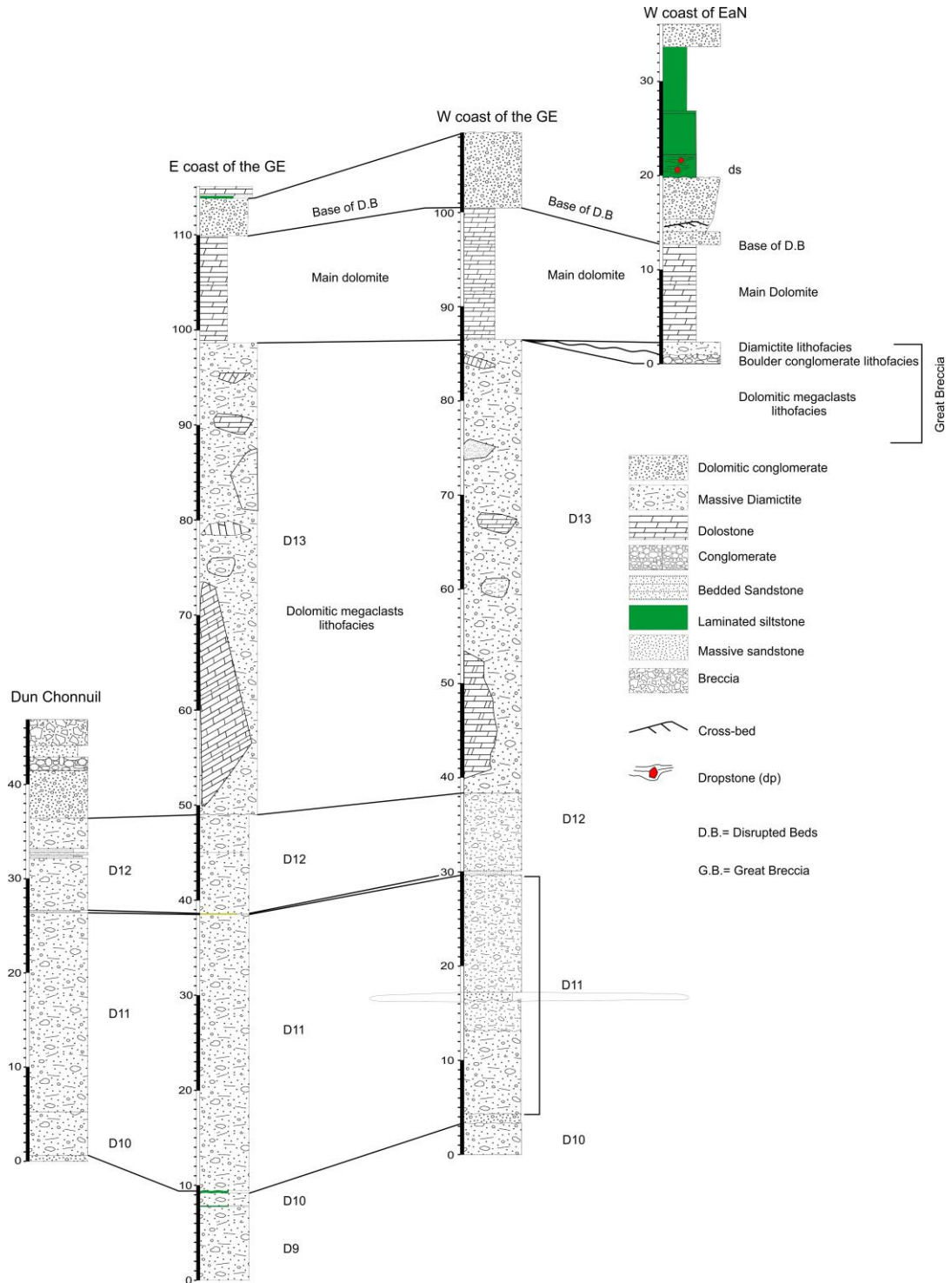
Figure 3.14: Sedimentary logs of the GB in the Garvellach Islands. The E coast section is a composite section along the E coast of the GE. The W coast section is a composite section from BaT and sections along the W coast of GE.
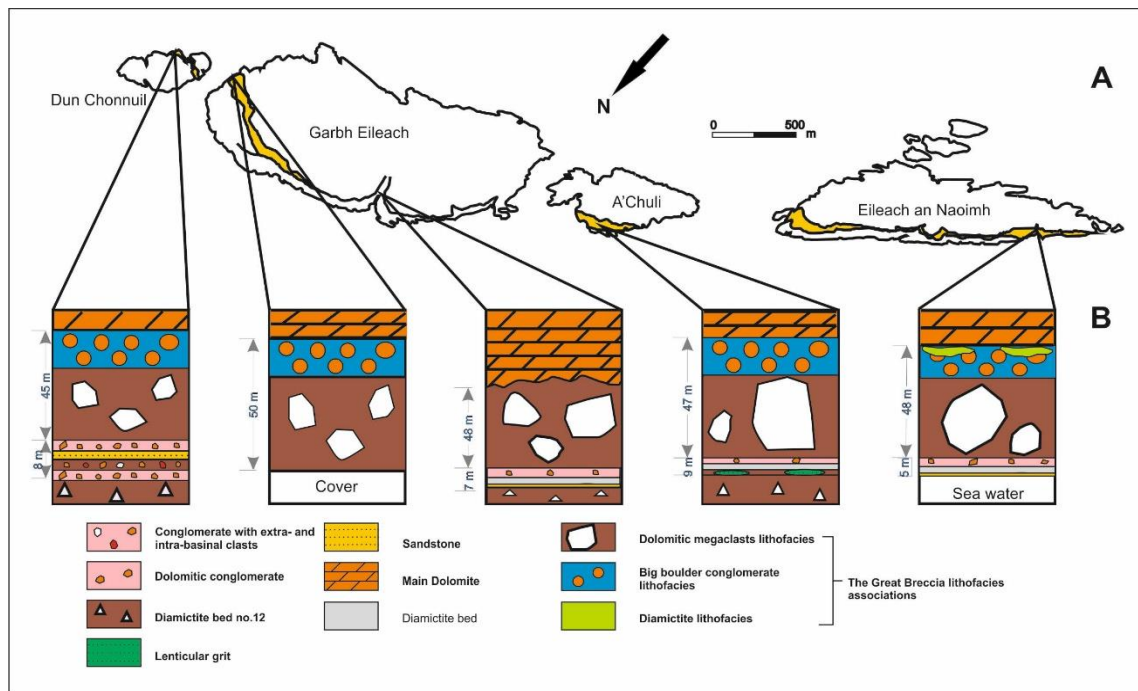
Figure 3.15: (A) Plan views of the outcrops of the GB on each of the four Garvellach Islands. **(B)** Schematic vertical section (the vertical thickness showed next to the beds) through outcrops of the GB, showing the three lithofacies.

Dolomitic conglomerate beds occur at the top of the group and although variable in thickness are more persistent laterally than the other strata. The conglomerate is absent in only one (north coast of EaN (Fig.3.15)) of the nine outcrops, in which this group is exposed. The maximum thickness of the conglomerate is up to 7.5 m on the N coast of A'C. On the NW coast of EaN, these beds have an even thickness and are quite continuous. However, in this place, the 'dolomitic conglomerate beds' are exposed in only one part of the outcrop and absent in the other parts; in this case, the 'dolomitic megaclast lithofacies' part of the GB rests directly on the middle 'diamictite' bed in this interval. In addition, on the E coast of DC and the E coast of GE, conglomerate occurs as bedding-parallel lenses. On A'C, the conglomerate is well bedded and consists of a gritty dolomitic matrix and contains fine grained, cream coloured dolomite pebbles. The clasts are tightly packed, although matrix-supported; most are sub-angular to sub-rounded. They range 2 - 23 cm in diameter. At some stratigraphic intervals, this bed is almost pebble-free.

The upper contact of the dolomitic megaclast lithofacies is often gradational with the 'boulder conglomerate lithofacies'. For instance, in the SW of EaN (Fig.3.16) the megaclast lithofacies has a gradational contact with the overlying 'boulder conglomerate'. By contrast, at BaT (Fig.3.17) the Main Dolomite rests directly on a megaclast in the GB at a sharp and undulating contact.

Figure 3.16: All three lithofacies of the GB units on the N-W coast of EaN. Geologists (circled) for scale.

Figure 3.17: (A) and (A`) the upper contact of the GB lithofacies association with the Main Dolomite lithofacies association on BaT. Geologist for scale.

iii. Lithology

There are two main components in the dolomitic megaclast unit:

The matrix is fine-grained, compositionally immature, and texturally semi-mature, dark grey on fresh surfaces, buff on weathered surfaces. Dolomite, quartz and clay minerals/mica are the main component of the matrix, while the minor components are plagioclase and potash feldspar with small amounts of rock fragments, which in a few cases may form a significant proportion of the grains. The diamictite contains sedimentary clasts of pebble, cobble, boulder and macro-boulder sizes (sensu Terry and Goff (2014)). All the clasts are derived from sedimentary rocks. Some clasts are derived from the underlying GEF (Fig.3.18A-C), for example the stromatolitic limestone (Fig.3.18D-E). The clasts in the dolomitic megaclast lithofacies are typically much larger than those in the underlying dolomitic diamictite beds (D1-D12), albeit with a similar dolomitic matrix. The lithology of the boulder and cobble size clasts within the dolomitic megaclast is commonly similar to those in the lower dolomitic diamictite facies. However, clasts >2 m across are more abundant than in the lower diamictite beds (D1-D12).

Figure 3.18: (A) Interbedded dolomite (orange coloured) and limestone (grey coloured) within GEF on the E coast of GE. Camera lens cap is 58mm. (B) and (C) Clasts within dolomitic megaclast lithofacies which is identical to (A) on the N coast of GE. The ruler is 35 cm and 17 cm for scale, respectively, in (B) and (C). (D) Bed of GEF with stromatolites on the E coast of GE. The ruler is 1m long. (E) Clast within dolomitic megaclasts which is identical to (D) on the N coast of GE. The ruler is 40 cm long.

Megaclasts: the dolomitic megaclast bed includes meso to macro-boulders of massive diamictite and of bedded strata. The outer contacts of the massive diamictite clasts are sometimes difficult to map (Fig.3.20), but can be identified because the megaclast bed 'matrix' has two or three times more clasts than the 'normal' diamictite lithology in the megaclasts. The stratified megaclasts are easier to identify due to their sharp edges and the truncation of their strata (Fig.3.20). Spencer (1971) mapped the megaclast bed in an exposure of a representative area of approximately 2000m^2 on the NE of A'C. There, 68 meso-boulders with diameters less than 20m and bigger than 1 m were mapped and comprised these lithologies: 47% were dolomites, 25% dolomitic diamictites, 9% siltstones, 6% sandstones, 12% interbeds, and 1% dolomitic conglomerates (Fig.3.19).
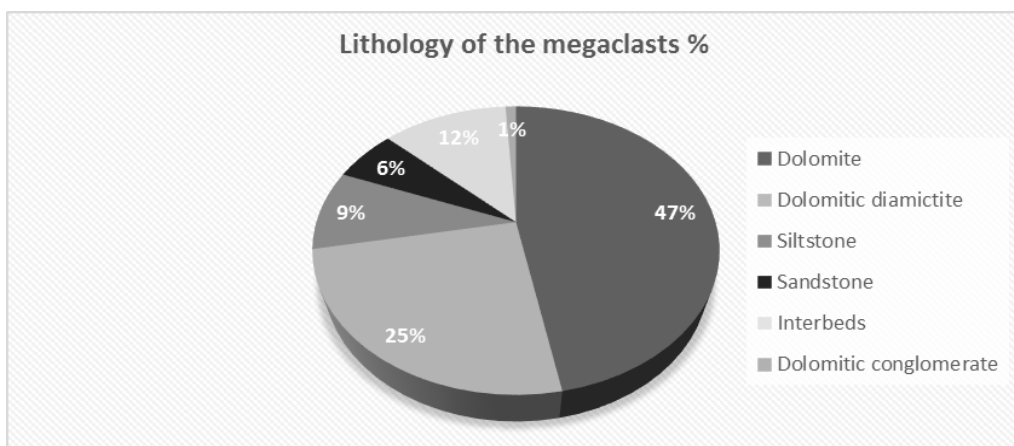
Figure 3.19: Pie diagram shows the lithology of the mesoclasts (bigger than 1 m diametre and less than 20 m diametre) percentage within dolomitic megaclast lithofacies, on the N-E coast of A'C.
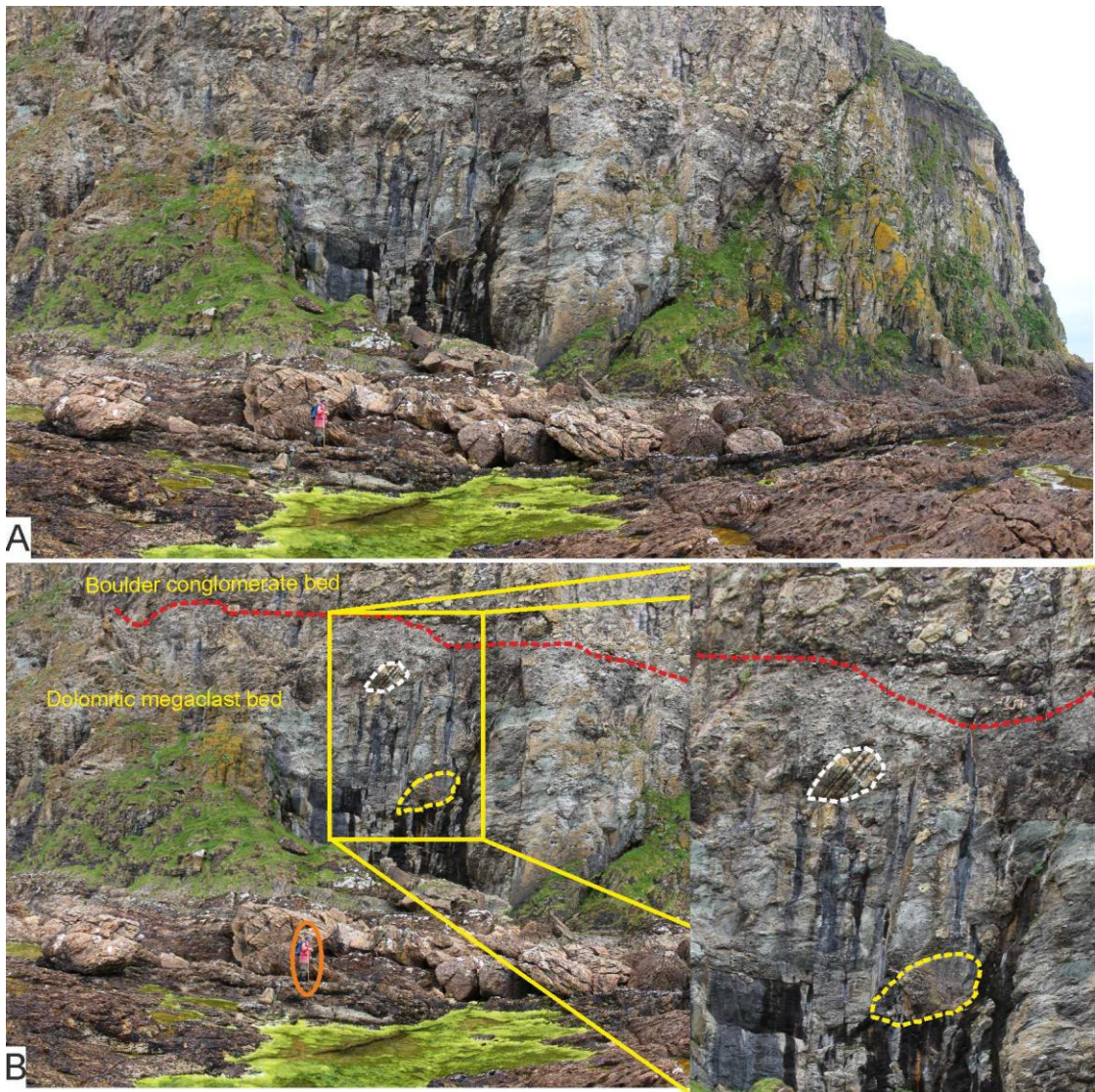
Figure 3.20: N coast of GE (A and B) massive (yellow dashed line) and bedded (white dashed line) boulders within dolomitic megaclast lithofacies, on the N coast of the GE. The red dashed line shows the gradational contact between dolomitic megaclast and boulder conglomerate facies. Geologist (orange circled) for scale.

Taking all the outcrops of the GB in the Garvellachs, 13 clasts of >20 m diameter were identified. These comprise three different lithologies – diamictite (dominant), dolomite and interbeds. The clasts of diamictite are quite comparable to the underlying diamictite beds (D1-D12) in respect of lithology, clast types, and homogeneity. For example, the large stratified clast on the N coast of A'C is identical with D1 and the topmost part of the GEF (Fig.3.21 and 3.22).
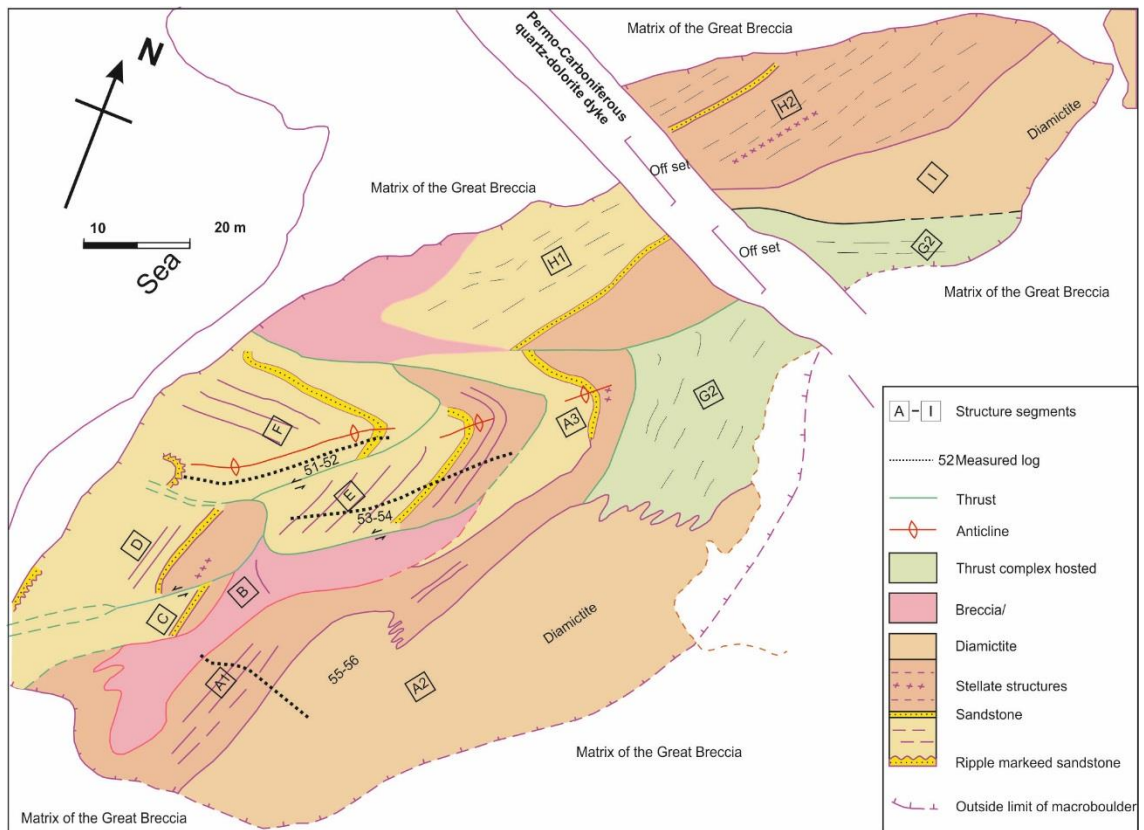
Figure 3.21: Geological map of a complex macro-boulder on the N coast of A'C, showing thrust faults and folds within the clast. The black dotted lines (three lines) show the location of the sedimentary logs (Fig.3.22) within the boulder (Mapping by Spencer, Ali (author), Fleming, Fairchild, and Chew).
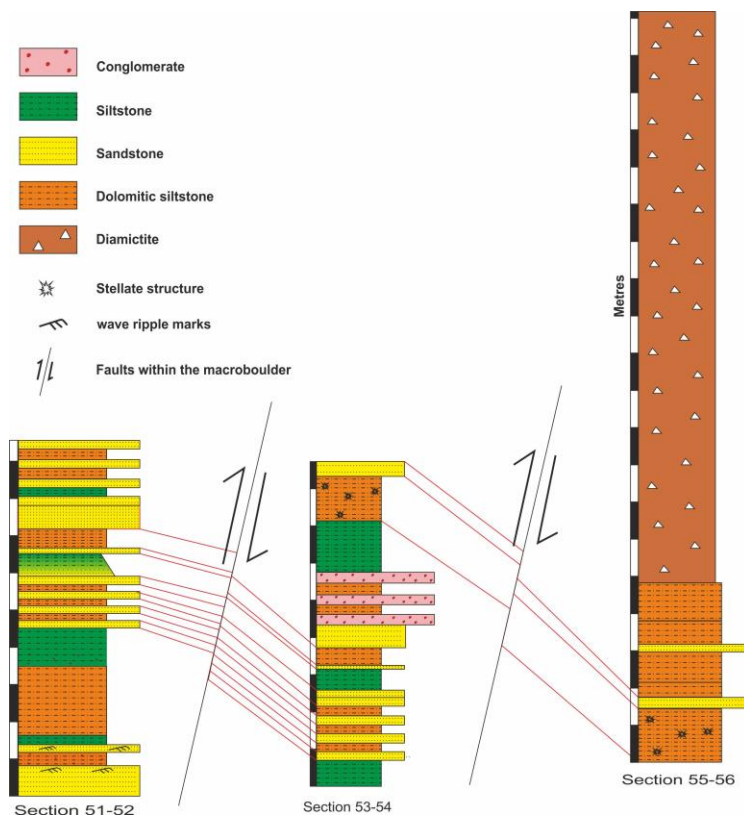
Figure 3.22: Three stratigraphic logs within the macro-boulder (Fig.3.21) which can be correlated. They give a stratigraphy identical to the topmost part of the GEF and D1-on NE GE.

iv. Sedimentary structures

On the N of A'C and at the base of the GB, there are some deformation structures (Fig.3.23). These structures are represented by sedimentary dyke (Fig.3.23a and c), sensu Pini et al. (2012), and deformed clast (Fig.Fig.3.23b and d).
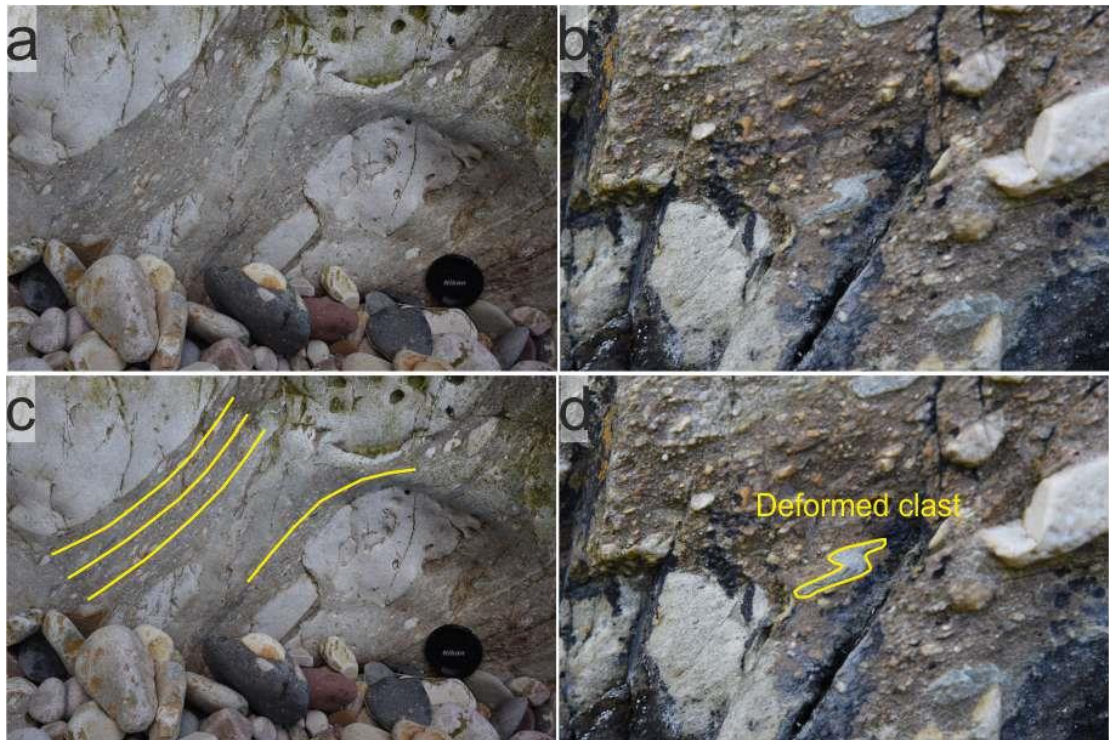
Figure 3.23: Deformation structures at the base of the GB, on the N of A'C. (a-c) lamination wrapping clasts (sedimentary dyke sensu Pini et al. 2012)

The larger sedimentary clasts are irregular to tabular bodies with highly irregular and sharply defined edges (Fig.3.20 and 3.24). However, where two diamictite megaclasts are in contact with each other (e.g. SW EaN) it is hard to distinguish the boundary. Within the bedded clasts, dislocations and fold structures have been observed.
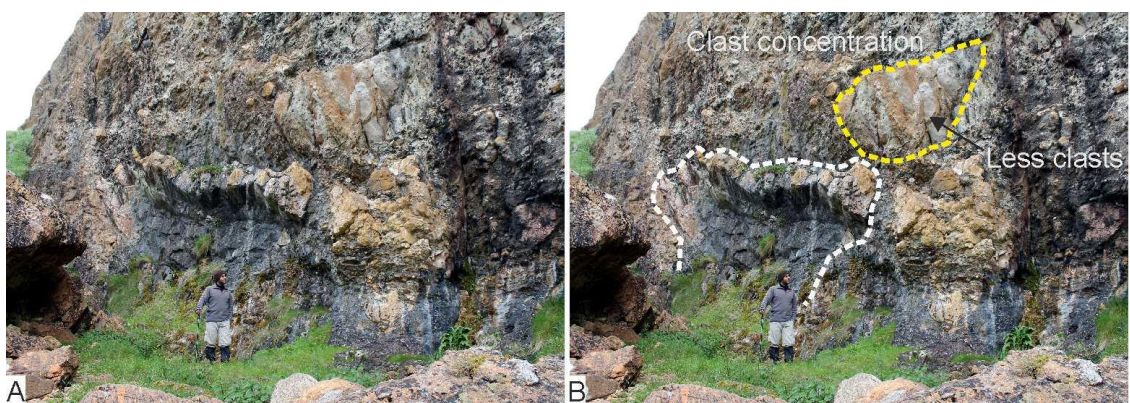
Figure 3.24: Massive (yellow dashed line) and bedded (white dashed line) boulders within dolomitic megaclast bed, on the N coast of the GE. Geologist for scale. See the clast concentration within matrix of the lithofacies and less clasts within the massive raft.

A remarkable example of a folded megaclast, colloquially 'The Bubble', is exposed on the N coast of EaN (Fig.1.10). The dimensions of this megaclast are 320X64X45 m (Fig.1.10). This megaclast comprises

deformed, laminated and massive dolostone in a large, asymmetric fold, overturned towards the NW, the axial trace of which steepens upward. The attitude of the bedding in the megaclast is steeper than that of the regional structural dip at this location. There are dislocations by a series of listric thrust faults between adjacent rocks and the fold. Some similarities have been seen between the general line of the axial trace of the fold and the uppermost part of the fold, but with some deviation and bifurcations. An anastomosing fault and zone of breccia dolostone is located in the accessible lower thrust fault. Local shear and minor folding have been observed along the bedding planes, in places where the bedding of the laminated dolostone runs parallel to the direction of the thrusting. At this site, D13 is underlain by strata that now have a dip of 40° to the SE and the original disposition of the lower thrust fault was suggested to be close to horizontal.

On the N coast of A'C (Fig.3.21 and 3.22), the best exposed megaclast shows a complicated internal succession that consists of dolomitic diamictite underlain by interbedded dolomites, dolomitic siltstone and sandstones. The entire internal succession within the megaclast exhibits folding and thrusting (Fig.3.21). The stratigraphic succession of the dolomite, sandstone and dolomitic siltstone beds are consistent with the dolomite, sandstone and dolomitic siltstone beds in the GEF. Also, a horizon with stellate structures is present in the uppermost beds of the GEF (Fig.3.25A and B), on the NE of GE and a similar stellate structure occurs within one of the dolomite beds inside this megaclast (Fig.3.25C). Also, the diamictite bed composition and abundance of clasts compare to the D1 and/or D2 of the PAF.

In the outcrops of the GB in the Garvellachs, 17 stratified megaclasts have been described, mapped, and sketched in detail. The dips of these megaclasts were measured by Ed Fleming and Tony Spencer and compared with the regional dip. The average dip of the 17 stratified clasts is 43° and their strike 050°, whilst the regional dip averages 35°. This measurement can be rotated back to palaeohorizontal and then has an overall average dip of 09° towards 140°. The measurements show that the average dip of 15 slab shaped rafts is steeper by about 10-25 degrees than regional bedding dip: they all dip towards the SE. According to these data, the clasts exhibit an imbrication towards SE.
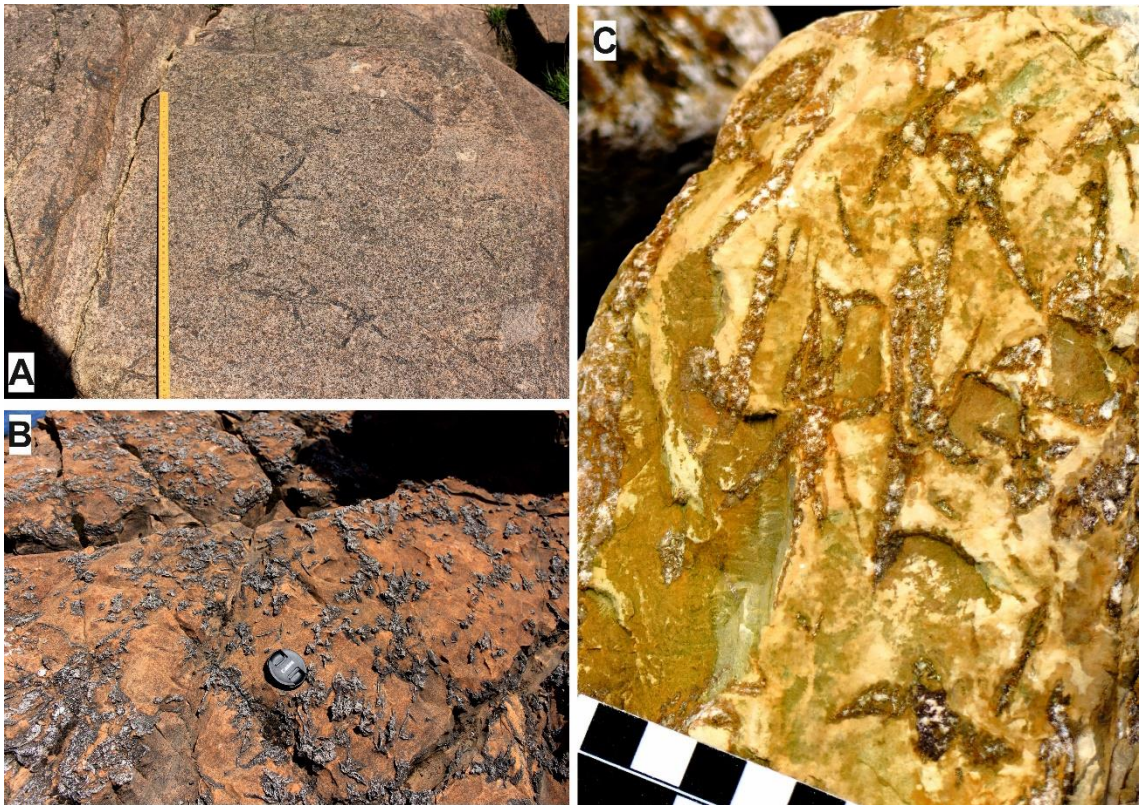
Figure 3.25: (A) and (B) Stellate structure within dolomite bed in the GEF, on the E coast of GE. Ruler is 45 cm long. **(C)** Stellate structure within one of the beds inside the bedded macro-boulder on the N coast of A'C. Ruler for scale, each square is 1 cm.

(b) Boulder conglomerate lithofacies

i. Stratigraphic position and outcrops

This lithofacies occurs on top of the dolomitic megaclasts lithofacies and is exposed along all the outcrops of the GB lithofacies association in the Garvellachs, except at BaT where the Main Dolomite rest directly on the dolomitic megaclasts facies (Fig.3.15).

ii. Contacts

The lower contact with the underlying 'dolomitic megaclasts facies' is gradational. The size, shape and amount of the clasts in the facies are different compared to the 'dolomitic megaclasts facies', but the dolomitic clasts in the boulder conglomerate have a particular size concentration and a more rounded shape.

The upper contact of the 'boulder conglomerate' with the overlying Main Dolomite is often difficult to identify in outcrop. Where a fine-grained dolomitic diamictite, up to 2m thick, overlies the conglomerate (N coast of GE, N coast of A'C, and W coast of EaN (Fig.3.15)) the two lithofacies are clearly separate. Where this thin lithofacies is absent, the closely packed dolomite clasts in the top of the conglomerate cannot be separated from the overlying Main Dolomite: an exact contact cannot be determined.

iii. Lithology

The facies is easily recognized by containing closely-packed (Fig.3.26), oval shaped 'dolomite boulders' that are commonly 1-5.5 m in diameter. The boulders have smooth outlines, rounded to angular, with a

predominance of sub-angular to sub-rounded outer surfaces and are closely packed. The yellow coloured dolomite clasts are abundant and homogeneous; other lithologies like dolomitic sandstone, siltstone and diamictite are also present. The matrix of the bed is a gritty dolomitic siltstone and the thickness of the facies varies from 0-14 m.

On the NW coast of GE, the boulder conglomerate facies is absent, and there the Main Dolomite bed rests with unconformity on one of the rafts within the dolomitic megaclasts lithofacies (Fig.3.17). Moreover, the conglomerate becomes much thinner than normal in places where the megaclasts facies contains giant megaclasts, for example, on the NE corner of EaN.

Figure 3.26: Smooth and rounded boulders, floating in a matrix with sub-angular to sub-rounded smaller clasts in the 'boulder conglomerate' lithofacies of the GB lithofacies association, on the N coast of A'C. (Photo by: Dr.Anthony Spencer).

(c) Diamictite lithofacies

In three locations, namely (i) the N coast of GE (ii) the N coast of A'C and (iii) the NW coast of EaN (Fig.3.16), a bed of diamictite lithofacies rests above the boulder conglomerate lithofacies (Fig.3.15). The diamictite is lenticular and ranges between 0-2 m thick, and has sharp basal and top contacts, with the boulder conglomerate and the Main Dolomite.

(d) Depositional environments of the GB

Any interpretation of the GB must account for (i) its uniform thickness across the Garvellachs and (ii) its tripart composition, with three lithofacies recorded in many locations, of which the dolomitic megaclast lithofacies is the dominant rock type. The absence of the boulder conglomerate and diamictite lithofacies at BaT (Fig.3.17) is interpreted to imply that these form lenticular geometries above the main dolomitic megaclast lithofacies. The latter also exhibit obvious thickening and thinning with boulder conglomerate and diamictites resting in depressions between the megaclasts.

The GB has three plausible interpretation hypotheses. First, it could be formed as a submarine mass-flow or slide breccia, an interpretation supported by one school (Eyles and Eyles, 1983; Eyles, 1988; Arnaud and Eyles, 2002, 2006). The second interpretation is as an olistostrome deposit, whereby glacially-derived material collapsed under gravity in a subaqueous slide (by analogy to the Kingston Peak Formation in Death Valley – California (e.g. Macdonald et al., 2013; Le Heron et al., 2014). Thirdly, the GB could represent a true tillite, which formed subaerially or subglacially modified by glaciotectonic processes (Spencer, 1971; Benn and Prave, 2006). An origin as a fault breccia can be ruled out: no syn-depositional fault or shearing/deformation related to fault have been seen.

i. Mass-flow settings (non-glacial)

A submarine mass-flow hypothesis was suggested by some authors (Eyles and Eyles, 1983; Arnaud and Eyles, 2002; Arnaud, 2012). The GB was interpreted, according to this hypothesis, as a submarine debris-flow initiated at the margins of a carbonate basin (Eyles and Eyles, 1983). The latter workers proposed that the debris-flow and turbidity currents re-sedimented the stratified dolomitic conglomerate, sandstone and siltstone from underlying beds (D1-D12) based on geometry, matrix and intra-basinal clasts amounts.

Arnaud and Eyles (2002), interpreted the 'dolomitic megaclasts lithofacies' (described in their paper as unit 1 and 2) as a catastrophic subaqueous landslide associated with local tectonic activity. This interpretation was based on: (i) their view of the GB as a 'composite graded sequence' comprising alternating deformed and undeformed deposits, (ii) an intimate association with undeformed submerged sediment gravity flow and traction current deposits, and (iii) a localised fault control origin for the mega clasts of the GB. This suggestion highlighted the comparatively restricted occurrence of the GB to outcrops on the Garvellachs and Islay. It is noteworthy that strata of a comparable character to those in the GB, (highly deformed clast- and matrix-supported breccia) are well known from both ancient and modern carbonate megabreccias (Spence and Tucker, 1997; Payros et al., 1999).

Arnaud (2012) emphasises the similarity to carbonate megabreccias forming along active faults, argued that the flooding surface at the base of the Disrupted Beds is better explained by the tectonic model; and that alternating deformed and undeformed intervals are more compatible with episodic slope failure, rather than ice overriding.

The submarine mass flow hypothesis is an attractive means of explaining many features within the GB. A thick and mobile mudflow, which would exert little frictional drag at its base, may account for the little disturbed base, conformable contact, thickness and homogeneity of the matrix of the Breccia. Additionally, the folds within some of the rafts could be explained as gravitational slump folds in more coherent parts of the flow, comparable with the El Gordo Megabed in Tavernas basin-Almeria (Fig.3.27). Most authors in this school combine the interpretation of the GB with the Disrupted Beds (Eyles, 1988; Arnaud and Eyles, 2002, 2006; Arnaud, 2012). However, the present author suggests that these intervals, and their corresponding lithofacies associations, differ considerably in terms of lithology, structure and mode of formation. Furthermore, the GB is separated from the Disrupted Beds by the 12m thick Main Dolomite which is highly different from them lithologically.

Figure 3.27: Thrust fault within the El Gardo megabed in the Tavernas basin-Almeria. The white line represent bedding surface, yellow line and semi-arrows shows thrust fault, and the red curves for the folding deformation within the bed. Geological hammer is scale (Photo by: Javier Hernandez-Molina)

ii. Grounded-ice settings

A glaciotectonic origin can also explain many of the features within the GB, including the size of the megabreccia clasts when compared to the thickness of the host bed, the homogeneity of the matrix, and the occurrences of folds and thrust structures within dolomitic megaclasts. The giant blocks, with associated folding and thrusting, could have been emplaced through glaciotectonism.

A subglacial setting was favoured by Spencer (1971) because the intra-basinal blocks within the GB (dolomitic megaclast lithofacies of the present author), which are up to several hundred metres in length and several tens of metres in width and thickness, could not be transported by mudflow of the same thickness. According to Spencer (1971) the transportation distance of these blocks must be at least a few kilometres to account for: (i) the complete size mixing and homogeneity of the matrix of the breccia; (ii) on the Garvellachs, the GB is separated from the source of many of the giant clasts, the underlying bedded sediment of the Lossit and GEF, by 100 m of diamictites; and (iii) the GB can also be found on Islay, about 50 km distance from the Garvellachs, where it rests directly on the Lossit Limestone (Spencer, 1971, pp. 62). Thus, the giant blocks of dolomite within the dolomitic megaclasts lithofacies must have been transported within the sedimentary basin containing previously deposited diamictites (to form resedimented, massive diamictite blocks within the GB: Fig.3.20 and 3.23) and finally deposited conformably, on a thick diamictite succession. Spencer (1971) argued that such a lateral sequence implies transport of several kilometres.

Benn and Prave (2006) found the consistent style and scale of the deformation within the GB to be closely comparable to proglacial glaciotectonic complexes in the Pleistocene of northern Europe (van der Wateren, 1985; 1987; Aber et al., 1989; Hart and Boulton, 1991; Klint and Pedersen, 1995; Pedersen, 2000).

Whilst mudflows can explain the folds within the megaclasts as deformation within gravitational slump folds, the internal deformation complexity within the macroboulder on the N coast of A'C (Fig.3.21 and 3.22) is difficult to explain with this mechanism. This is because thrust faults (Fig.3.27) and folds (Mutti et al., 2006) that formed in mass-transport complexes (MTC) occur within both the matrix and the clasts; while thrusting within the clast on A'C in the GB occurs within the clast. Another example is, the size of the 'bubble' (Fig.1.10) on EaN measuring 320X64X45 m (Spencer, 1971) where the thickness of the GB is about 50 m, almost the same thickness as the clast. The question here is: whether a 50 m thick mass-flow is capable of transporting a large clast of the same thickness as the flow.

The occurence of shallow/subaerial deposits (D1-D12) below the GB and the Main Dolomite above are not obstacles to a mass flow interpretation: Shanmugam and Wang (2015) highlighted how mass-flow processes can act everywhere, even subaerially.

Spencer (1971) suggested a glaciotectonic deformation in a subglacial or ice marginal setting, based on similarity to deformed chalk rafts in Quaternary tills of Norfolk (UK) and its correlative erosion unconformity on Islay. Moreover, he commented that the boulder conglomerate lithofacies is more puzzling and problematic than the dolomitic megaclasts lithofacies. This reason is the dolomitic boulder concentration in this stratigraphic level, and smooth and rounded to angular surface of the clasts. Spencer (1971) proposed the smooth and rounded surface cannot be formed by abrasion during transport by water current because: i) the conglomerate contains boulders up to 5.5 m across and ii) the absence of the layering. In addition, he disagreed with the explanation of this conglomerate as a storm beach deposit because of the size of the clasts and fine-grained siltstone matrix.

The boulder conglomerate has a gradational contact with the underlying 'dolomitic megaclasts lithofacies' (Fig.3.16 and 3.20). Because of this, Spencer (1971) proposed that the mechanism in the formation of the dolomitic megaclasts lithofacies also played a large part in the formation of the big boulder conglomerate. Nevertheless, the origin of the conglomerate remained unknown because: i) it is not known whether mudflow can produce such a rounded boulder or not and ii) no glacial deposit similar to this conglomerate had been described at that time.

iii. Combination settings (Glacial plus mass-flow)

Megaclast can probably be carried by a mass-flow if it has same density as that of the clast or during slope failure. The former possibility needs a high velocity current to move clasts of hundreds metres across (Pini et al., 2012); while the latter just need a slope and gravity to initiate motion. Earlier, Arnaud and Eyles (2002), interpreted the beds as catastrophic mass-flow deposit, comparable to Sturzstrom accumulations (Hsü, 1975; Williams et al., 2004; Hsü, 2013). The flows responsible for these deposits are characterized by high velocity current and high sediment load almost close to the solid state (Shanmugam and Wang, 2015). Considering, the distance between Islay and Garvellachs Islands which is

about 47 km and the thickness change of the GB between two locations which is about 45m (4 m thick on Islay and 45-50 m thick on Garvellachs), the result will be a slope of less than 1° (estimated by trigonometry) from Islay towards Garvellachs. If these huge blocks had been transported as a result of mass-flow, under high velocity, a steeper slope (more than 1°) would have been required to effectively carry out such slumping or sliding (Pini et al., 2012; Shanmugam and Wang, 2015). The existence of a slope of <1° and a corresponding distance of about 50 km is insufficient for the formation of such a bed as a mass-flow deposit. Based on Pini et al. (2012), the blocks within the 'dolomitic megaclast' lithofacies belong to Type 2 in their classification of mass-transport complex (MTC). This type is characterised by: (i) hyper concentrated suspension; (ii) generation of a complex debris-flow carrying out-size coherent blocks (metres to hundreds of metres across); (iii) usually arranged in isolated slump-like folds (blocky flow deposits by Mutti et al., 2006); (iv) has a high velocity (catastrophic); (v) has shear-zones at the base and inside the fluid; (vi) includes fragments of substratum material (both coherent or complex loose); and (vii) is characterised by the high transport velocity. Such a hyper-concentrated fluid with mega-blocks and high velocity would require a slope of more than 1°.

According to the classification by Pini et al. (2012) both the dolomitic megaclasts and the boulder conglomerate lithofacies classify as Type 2 MTC's, on account of their clast size and matrix. Type 2 MTC's are characterised by injections (sedimentary dykes); which are laminated or layered and wraps around blocks at the base of the strata or lithofacies (Pini et al., 2012; Fig.3). This feature was clearly observed at the base of the dolomitic megaclast lithofacies (Fig.3.23), while it was dominantly present within the boulder conglomerate lithofacies apart from the base (Fig.3.26). In the Pini et al. (2012) study of different MTC types, structures common to Type 2 MTCs include fluid-escape and injection-related structures, while types 1 and 3 (finer sediments like sand) are characterised by carpet action. Evidence of liquefaction such as fluidization, cyclic loading- and shear-related liquefaction (Allen, 1982) was not observed in the GB.

The "Racetrack" clasts in Death Valley-California, are a good small example to show that a thin flow layer (few centimetres of ice) can allow the transport of large blocks. After a rainfall event, the top surface of the water in the playa freezes at night, then in the early morning it melts. However, because the veneer of ice around clasts stays longer, they slide along the slippery, muddy surface to leave a track behind (Lorenz et al., 2014).

Although both the mudflow and glacial hypotheses each explain many of the features in the GB, neither of them explain all the observed features. For example, the complex thrusts within the megaclast (not matrix) on the N coast of A'C (Fig.3.21) cannot be formed by a mudflow. Although folding is produced by sliding and gravity action (Mutti et al., 2006; Pini et al., 2012), thrusting and faulting require higher stresses. Furthermore, there is not a normal gradation within the dolomitic megaclasts lithofacies. However, the gradational contact between the 'dolomitic megaclasts' and the 'boulder conglomerate' lithofacies indicate that they formed by similar mechanisms and within the same environment. The smooth and rounded to subangular surface of the clasts inside the conglomerate (Fig.3.26) suggest

transport in water rather than by ice. In addition, neither of the hypotheses address the Diamictite lithofacies in this lithofacies association (Fig.3.16), and which processes produce that comparison with the Kingston Peak Formation.

There are textural similarities between the 'dolomitic megaclasts lithofacies' in the GB and a 'megaclast facies association' in the Kingston Peak (KP) Formation in Death Valley-California. Firstly, tabular and highly irregular edges of the clasts have been observed in both (Spencer, 1971; Le Heron et al., 2014). Secondly, most of the clasts within the megaclast facies of the KP are of carbonate lithology derived from the underlying Crystal Spring Formation and Beck Spring Dolomite, but arkosic sandstone and conglomerate clasts also occur (Le Heron et al., 2014). By comparison, most of the clasts within the 'dolomitic megaclast lithofacies' of the GB are carbonate and diamictite derived from the underlying GEF (Fig.1.10, 3.18, 3.21 and 3.22) and underlying diamictite beds D1-D12 (Fairchild et al., 2017: in press), with quartzite clasts a minor proportion. Thirdly, the megaclast facies of the KP contains intensely sheared, carbonate-dominated diamictite beds and gneissic basement (Le Heron et al., 2014); similarly, the dolomitic megaclasts of the GB are also intensely sheared, e.g. the 'bubble' (Fig.1.10). Fourthly, above the 'megaclast facies' in the KP there is a 'boulder conglomerate' which compares to the 'boulder conglomerate lithofacies' in the PAF. Comparison between these two different successions reinforce the impression that they formed by the similar processes with the PAF also formed as an olistostrome deposit. By contrast, there is an abundance of gradational bedding, flaser/wavy-bedding, thickening upward sequences, rip up clasts, and erosional surfaces within the KPF succession. All of these features are absent in the GB of the PAF, with the possible exception of the gradational contact between 'dolomitic megaclast' and 'boulder conglomerate' lithofacies.

In respect of the preceding discussion, it should be noted that the rocks beneath the GB are interpreted as subglacial and the Main Dolomite at the top of the GB exhibits microbial structures (Fig.3.18E) (i.e. shallow marine indicators). If the GB is interpreted as deposited in a mass-flow (non-glacial) setting, then it is not plausible to have a deep marine environment bounded from below and above by shallow marine sediments without sufficient changes.

iv. Depositional environment of GB LFA
On the basis of data and features in Table.3.4 several observations must be explained in any interpretation of the GB: (i) massive diamictite; (ii) rounded clasts in boulder dolomitic conglomerate LF; (iii) wrapping laminae around the clasts; (iv) absence of stratification in the matrix of dolomitic megaclasts LF; (v) intense folding and thrusting within the megaclasts without matrix; (vi) megaclast size; (vii) absence of shearing structures below the dolomitic megaclasts LF; (viii) imbrication of megaclasts within the dolomitic megaclasts LF; and (ix) minor shearing and deformed clasts (Fig.3.23). Some of these features are environmentally-specific, such as, points (i), (v) and (vii) in mentioned features, which can be interpreted just by floating-ice, glaciotectonic in subglacial environment by grounded-ice, and mass-flow respectively (Table.3.4). However, there are some features, which cannot

be used to distinguish between two or more environments, for instance, features in (ii), (iv), (vi), and (viii) can be formed by either grounded-ice or mass-flow deposits (Table.3.4).

Fig.3.28 tries to integrate interpretations for the all features recorded in Table.3.4. The dolomitic megaclast LF could be formed at the edge of the ice-sheet by glaciotectonism when the ice-sheet was retreating and reworked as an olistostrome. The boulder conglomerate lithofacies is a part of the GB because of the gradational lower contact with the 'dolomitic megaclast lithofacies' everywhere and the erosional upper contact (Fig.3.17) with the Main Dolomite at BaT. The dolomite concentration reflects a carbonate-dominant source area. The smooth and rounded surface of the clasts indicate sustained transport.
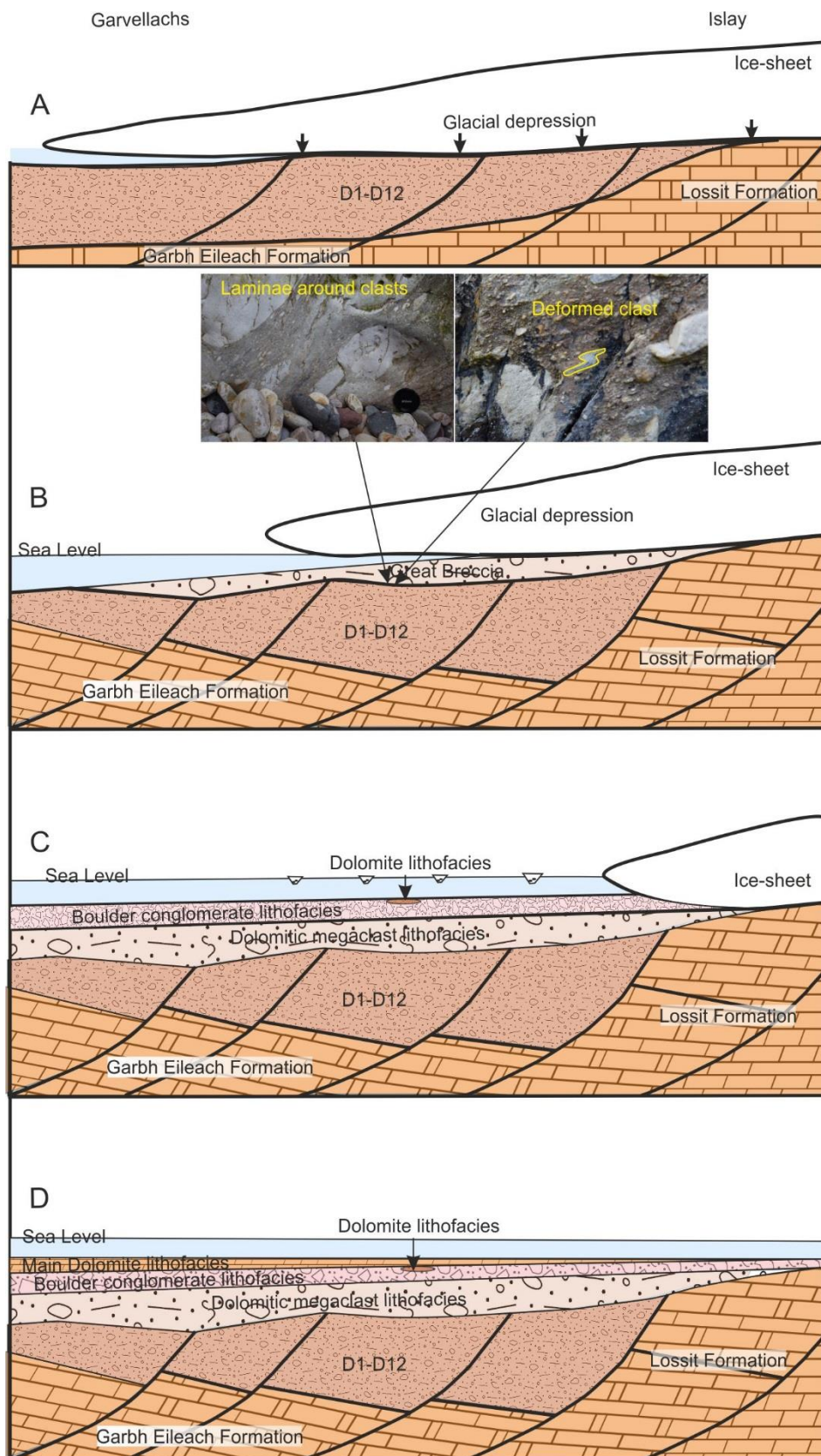
Figure 3.28: Cartoon representing the stages of the depositional mechanism of the lithofacies within GB. The two photographs are from the base of the GB on the N coast of A'C; they show small scale shearing and deformation.

In summary, the megaclasts cannot have been thrusted in a mass-flow as the thrusts occur just within

the clasts, as in the megaclast on the N of A'C; and there are not glaciotectonism without shearing and

subglacial deformation. Thus, these megaclasts probably were thrusted, plucked and transported by glaciotectonism first and then become part of a MTC (Olistostolith), when the ice retreated.

Table 3.4: Features representing the depositional environment for the GBLA.

Features	Lithofacies	Subaqueous mass-flow	Floating ice	Grounded ice	Preferred interpretation in this study
Diamictite	Diamictite LF (Lenticular beds at top of G.B.)	Possible	Possible	Possible	Ice-raft
Rounded clasts	Boulder Dolomitic conglomerate	Possible	Not possible	Possible	Mass-flow Grounded-ice
Wrapping laminae around the clasts	At the base of the dolomitic megaclast LF	Possible	Not possible	Possible	Grounded-ice Mass-flow
Wrapping laminae around the clasts	Boulder Dolomitic conglomerate	Possible	Not possible	Possible	Grounded-ice Mass-flow
Absence of stratification in the matrix of Dolomitic megaclasts LF	matrix of Dolomitic megaclast LF	Possible	Unlikely	Possible	Grounded-ice Mass-flow
Imbrication of megaclasts	Dolomitic megaclast LF	Possible	Not possible	Possible	Grounded-ice Mass-flow
Intense folding and thrusting in megaclasts	Dolomitic megaclast LF	Unlikely	Not possible	Possible	Grounded-ice
Megaclasts	Dolomitic megaclast LF	Possible	Not possible	Possible	Mass-flow Grounded-ice
Absence of shearing structure	base of G.B.	Possible	Not possible	Possible	Mass-flow
Minor shearing and clast deformation	Base of the megaclast lithofacies	Possible	Not possible	Possible	Mass-flow Grounded-ice

3.3 Main Dolomite LF (MD)

A detailed description of the Main Dolomite lithofacies is important because: (i) it has received little attention previously, with the exception of Spencer (1966, 1971); (ii) previous authors have concentrated on the Great Breccia (below) and the Disrupted Beds (above) lithofacies associations (Eyles and Eyles, 1983; Eyles, 1988; Arnaud and Eyles, 2006; Benn and Prave, 2006; Allen and Etienne, 2008). Furthermore, the occurrence of significant dolomite intervals in Neoproterozoic diamictites raises questions about the intensity of glaciation.

i. Stratigraphic position and outcrops

The Main Dolomite lithofacies is exposed along the whole Garvellachs outcrop. It lies above the Great Breccia lithofacies association.

ii. Contacts

The lower contact of the Main Dolomite lithofacies with the Great Breccia lithofacies association is sharp in some places and appears gradational in others (Fig.3.17 and 3.16). The upper contact is everywhere sharp, with the dolomite conglomerate which forms the base of the Disrupted Beds.

iii. Lithology

The Main Dolomite consists of a creamy to yellow weathering dolomite beds. It gives the appearance of being homogeneous due to its fine-grained lithology and the absence of well-marked bedding-planes. The rock does not react with the cold dilute HCl (5%) and staining (Dixon, 1965) shows that it is a dolomite. Despite the excellent and extensive outcrops of the unit, not a single extrabasinal clast has been found. Generally, the dolomite is fine-grained and homogeneous, but in places contains a large amount of detrital material. For instance, on A'C and BaT, 2 m at the base of the dolomite bed include clasts of various sizes and shapes. The dolomite clasts are commonly 1-2 mm in diameter (Fig.3.29); but in certain bands there are clasts up to 10 mm in diameter. The shape of the fragments varies from sub-angular to rounded, and they are present in about half of the thickness of the lithofacies on A'C. They occur in organised bands and follow the general bedding. On A'C, the coarsest detrital bed occurs in the lowest 1 m of the dolomite, where there is a conglomerate containing pebbles of up to 2 cm in diameter. The rest of the lithofacies is fine-grained and contains two types of lamina: white laminae and some quartzose laminae; they are irregular, fine-grained, are parallel to the bedding, and are spaced at 0.5-1 cm intervals.

Figure 3.29: The yellow line represents the contact between the lower laminated part which contains detrital clasts (yellow arrows), and the upper microbial part of the MD lithofacies at BaT.

iv. Sedimentary structures

There are no obvious sedimentary structures in this dolomite, except for faint planar bedding. Also, the fine-grained dolomite gives a massive appearance to the unit. On BaT, there are some signs of microbial (Stromatolite) material (Fig.3.30).
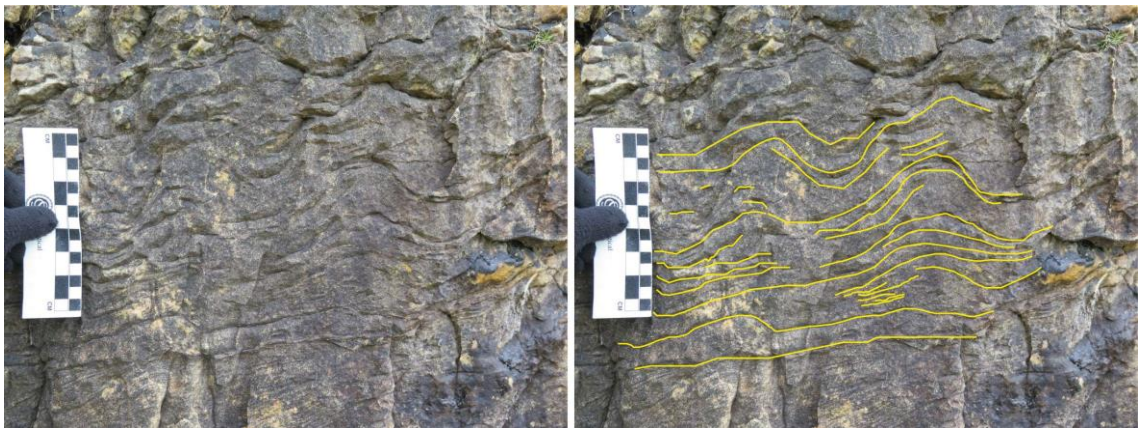
Figure 3.30: Microbial structures within the MD lithofacies at BaT.

v. Depositional environment of the MD

Interpretation of the origin of the Main Dolomite lithofacies is difficult, because of the lack of distinctive features (except microbial structures), the slight metamorphism, and the neglect of this lithofacies by previous authors. The main questions about this dolomite are: whether it is primary or secondary, lacustrine or marine. Based on the description above, the dolomites appear to be of two types; detrital and fine-grained with some postulated structures (Fig.3.29). The fine-grained dolomite could be formed by direct precipitation from solution, although it cannot be proved because of the metamorphism (Spencer, 1966). No evidence has been found to support a secondary replacement origin, although the complete penecontenporaneous dolomitization of limestone is possible. Spencer (1966) emphasized that the dolomite appears to have been deposited subaqueously, because of the absence of desiccation cracks, flake breccias, and dune cross-stratification. However, there is no definite indication of the water depth nor of whether it was marine or lacustrine.

The presence of the extrabasinal clasts in the lithofacies associations below and above the MD (respectively the GB and the DB) is evidence of their having both formed by mass-flow. The absence of extrabasinal clasts in the MD itself contrast with this and argues against a mass-flow origin for the MD. In explaining the MD, Spencer (1966) suggested two possibilities for the absence of extrabasinal clasts: (i) no ice-bergs were present to raft erratics; and (ii) ice-bergs were excluded from the Garvellachs area.

The author suggests two additional possibilities: The first is that the source of the dolomite could be different to the other sediments; and it deposited as a detrital dolomite. The second is that the dolomite was formed as a result of microbial growth, after the ice had melted and retreated far from the Garvellachs, on a carbonate platform. The latter hypotheses are more likely, especially when extrabasinal clasts are present in the overlying dolomite conglomerate. The absence of ice from the Garvellachs area, therefore implies that the Main Dolomite was deposited during a substantial interstadial or even an interglacial period. In addition, based on Le Ber et al. (2013) the presence of the postulated microbial part above the detrital part indicates deep subtidal environment.

3.4 Disrupted Beds LFA:

These rocks were described first and named 'Disrupted Beds' by Kilburn et al. (1965). Spencer (1966, 1971) recognized five such beds. Siltstone with disrupted dolomite beds occurred in Beds 2 and 4, whereas Beds 1, 3, 5 are dolomitic conglomerates with conglomerate boulders and siltstone. These sediments have also been described by Eyles et al. (1985), Eyles and Clark (1985), Eyles (1988), Arnaud and Eyles (2002), Arnaud (2004), Arnaud and Eyles (2006), Benn and Prave (2006), Allen and Etienne (2008), and Arnaud (2012). This lithofacies association has the disturbed appearance of chaotic, mixed-up, pulled apart strata. In detail, there are various lithofacies formed by different mechanisms (Fig.3.31): (i) dolomitic conglomerate lithofacies; (ii) bluish siltstone diamictite- disrupted dolomite lithofacies; (iii) rhythmically laminated siltstone, brown sandstone, and conglomeratic diamictite lithofacies; and (iv) dolomite rimmed conglomerate lithofacies. These lithofacies are mingled and change very quickly in geometry. They cannot be shown by one typical stratigraphic log and are difficult to correlate over hundreds or thousands of metres distance (Fig.3.32).

i. Stratigraphic position and outcrops

The 'Disrupted Beds' are exposed completely along the Garvellach Islands (Fig.2.3). The thickness of the association ranges from 26m to 40m. On the E coast of GE, the 'Disrupted Beds' lies 160 m above the base of the PAF; while on Islay, because of the absence of D1-12 and most of the Great Breccia's thickness, it is about 4 m from the base.

ii. Contacts

The lower contact is sharp between the lowest dolomite conglomerate bed within the 'Disrupted Beds', which can be followed through the outcrops of the Garvellach Islands, and the underlying 'Main Dolomite' bed above the Great Breccia. Furthermore, the upper boundary is sharp with D14 above.

iii. Lithologies

The lithology, thickness of the beds, and texture of the rocks in the 'Disrupted Beds' are horizontally and vertically very variable, and form a continuous range from massive dark blue-siltstone containing fragments to multi-lithology clast-rich diamictite beds with blue-siltstone matrix. The predominant clast lithology is dolostone (43-65%), but other clasts include quartz (17-22%), gneiss (4-12%), granite (4-8%), and lesser amounts of limestone, sandstone, schist, and amphibolite. The following is a detailed description of this facies association:
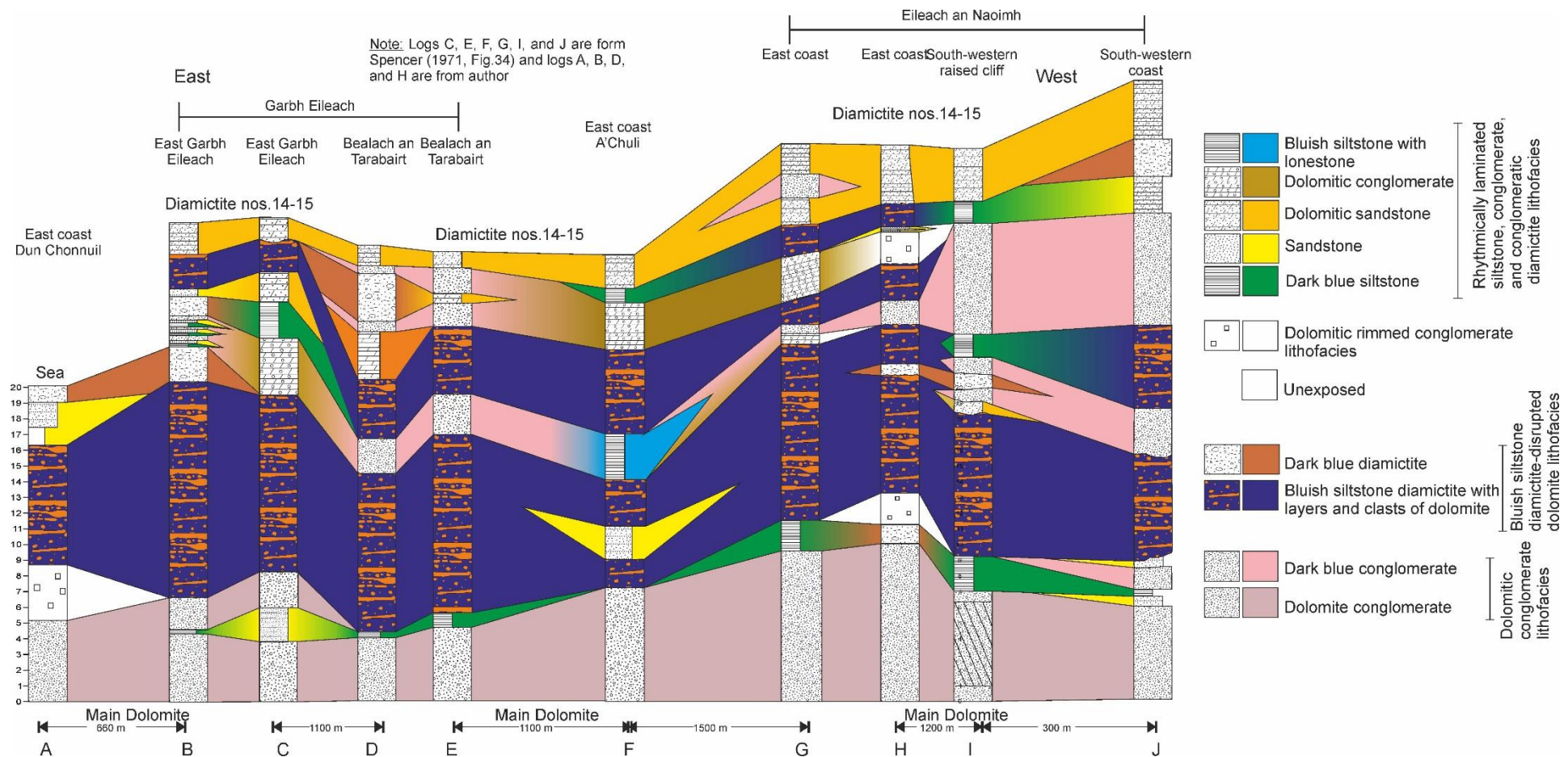
Figure 3.31: Stratigraphic correlation of the Disrupted Beds through the Garvellachs in 7 localities.
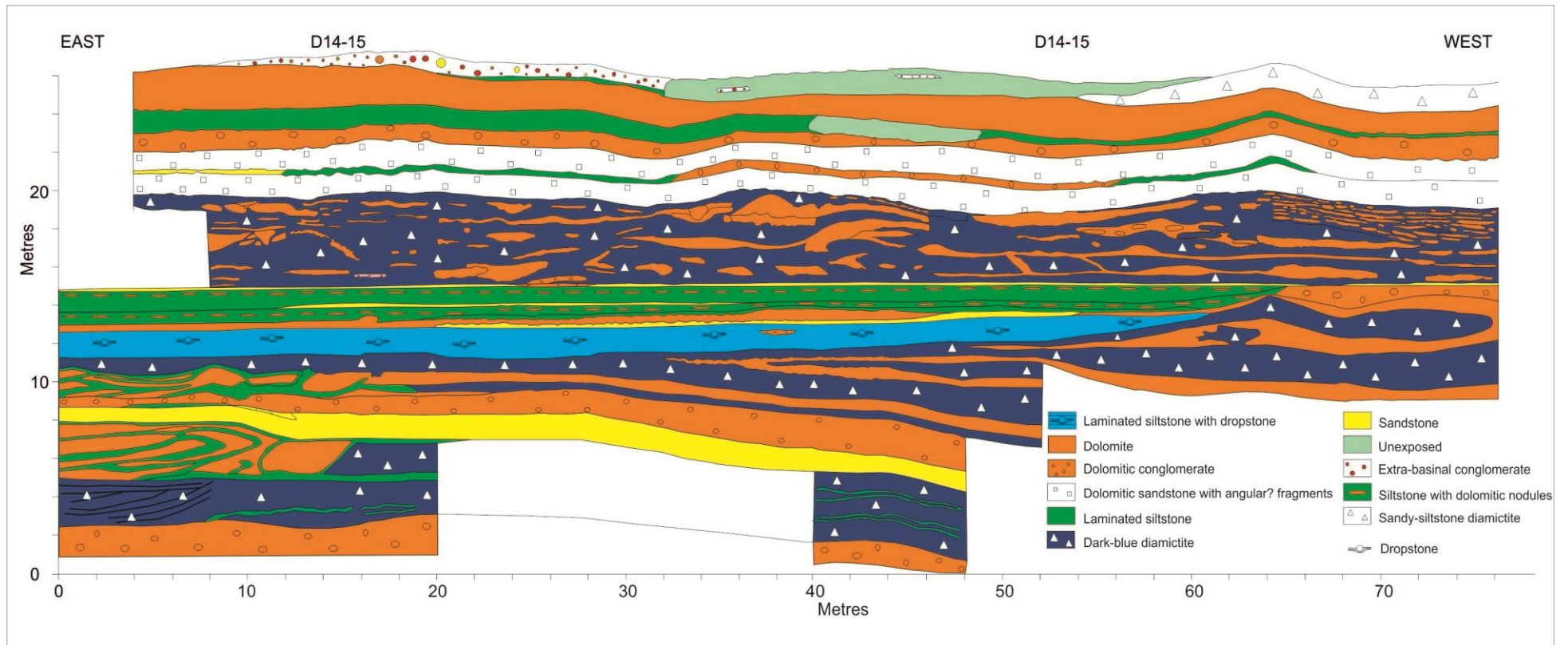
Figure 3.32: Field sketch on the E coast of A'C, represents true thickness and various lateral extensions of the beds. This sketch took 8 days of work involving 5 geologists. It represents the true thickness of the strata and lithology of the different lithofacies. The outcrop was gridded and measured then drawn carefully avoiding faults.

(a) Dolomitic conglomerate lithofacies

This is a persistent lithofacies and lies at the base of the association. It consists of sandy siltstone matrix that contains various types of clasts. The matrix is a black sandy siltstone in fresh surface, changed to cinder-like colour on weathered surfaces; and in two places the dolomitic conglomerate lithofacies contains diamictite beds with a similar dark colour matrix (Fig.3.31). Clasts are pebble sized and the average diameter is about 3 cm and maximum size which is recorded is 100X90X90 cm. The shapes and geometry of the clasts are sub-rounded to rounded, equidimensional to ovoid in cross-section, and tightly packed clasts. The dominant lithology of the clasts is dolomite identical to underlying bedded dolomite. However, some pebbles of a red quartzite are recorded; extrabasinal clasts occur rarely but usually in a large size. The average size of the extrabasinal clasts are 10 cm in diameter and the maximum size recorded is boulder.

The thickness of the lithofacies ranges from 4-7 m. It is not well-stratified, but in parts it shows cross-stratification; for instance, on the W coast of EaN there is a cross-stratification of more than 6 m thick foreset (Fig.3.33). Spencer (1966) recorded palaeocurrent directions of the dolomite conglomerate lithofacies in seven different localities and six of them record currents flowing generally towards the SE (Spencer, 1966, Fig. 64 c).

Figure 3.33: Cross-stratification, one more than 6 m thick foreset, within dolomitic conglomerate lithofacies on the W coast of EaN. The red line is 6 m scale.

The upper contact of the dolomite conglomerate lithofacies is interbedded with thinly laminated sandy siltstone. However, the lower contact is sharp with the underlying Main Dolomite.

(b) Bluish siltstone diamictite- disrupted dolomite lithofacies

On the E coast of Garbh Eileach (GE) the lithofacies appears in two stratigraphic horizons (Fig.3.31): 6.3 to 20 m and 26.3 to 28.2 m from the base of the Disrupted Beds lithofacies association (Fig.3.31); and it is equivalent to Bed nos. 2 and 4 according to Spencer (1966, 1971). The maximum thickness of the lower and the upper horizons of the lithofacies is about 13.3 and 5.3 m, respectively, on the E coast of GE and E coast of A'C (Fig.3.31). Also, the minimum thickness of the lower and upper horizons is about 2 and zero m on the E coast of A'C and SW coast of EaN (Fig.3.31).

It consists of a homogeneous and unbedded dark bluish-grey siltstone matrix which contains genetically related components: (i) disrupted boudinaged dolomite beds; (ii) dolomitic conglomerate lenses; and (iii) dolomite pebble clasts. The thickness of the lithofacies varies from zero to 13.3 m and it contains extrabasinal clasts in all lithologies, even in the disrupted dolomite. The lithofacies is beautiful and easily recognised in the field, because of the sharp contacts and colour contrast between the dark siltstone matrix and the thin beige coloured dolomite beds and levels of boulders, which follow the strike.

The dolomite beds are clearly observed due to their sharp contact with the grey-blue siltstone. The dolomite beds are very irregular in thickness and are discontinuous. None of them extend more than 100m (Fig.3.32). Many of the dolomite beds and levels of dolomite boulders are gently undulating, but all approximately parallel the overall bedding.

The dolomite conglomerates are very irregular levels and beds and often end abruptly (Fig.3.34). On A'C, at the top of the lithofacies there is a sandstone wedge which penetrates about 1 m down into the underlying siltstone (Spencer, 1966, Fig. 54c). In addition to bedded dolomite and lenticular conglomerate the bluish-grey siltstone contains many white dolomite pebbles, few sandstone pebbles and some extrabasinal clasts. The dolomite clasts have sharp contacts with the matrix and the shape is smooth and rounded, while within pebbles sized less than 5 mm in diameter angular fragments are common. Also, some of the clasts are rounded and contain fragments that look like a piece of conglomerate.

Figure 3.34: Bluish siltstone diamictite-disrupted dolomite lithofacies in BaT. The dolomite conglomerate (beige colour) are very irregular levels and beds end abruptly.

On the W coast of EaN, there are some sedimentary structures and features within the lower horizon of the bluish-grey diamictite-disrupted dolomite lithofacies: (i) deformation folds (Fig.3.35A, B); (ii) clast

clusters, a concentration of the clasts in a lenticular shape; the top of the lens shape is sometimes flat or convex while the base of the lens is flat or concave shape within fine laminated siltstone (Fig.3.36); (iii) in some cases, there are clast clusters where a large clast is surrounded by a halo of smaller clasts apparently smeared around the larger clast (Fig.3.35C, D); (iv) clast shearing (Fig.3.37A); and (v) obstacle clast (Fig.3.37B). Folds are rare, but are present on the W coast of EaN (Fig.3.35A, B). The dolomite bed is deformed and bounded from the base and the top by diamictite. In the 'Fig.3.35A, B' the outcrop face trends from 335 to 155 (i.e. NW to SE); and the right-hand limb of the anticline dips are 68° towards the right; also, the crest of the anticline plunges into the outcrop at 53° dip towards an azimuth of 100°. The anticline verges to the NW. In the same outcrop about 6 m towards the W, there are clast clusters (Fig.3.35C, D and Fig.3.36).
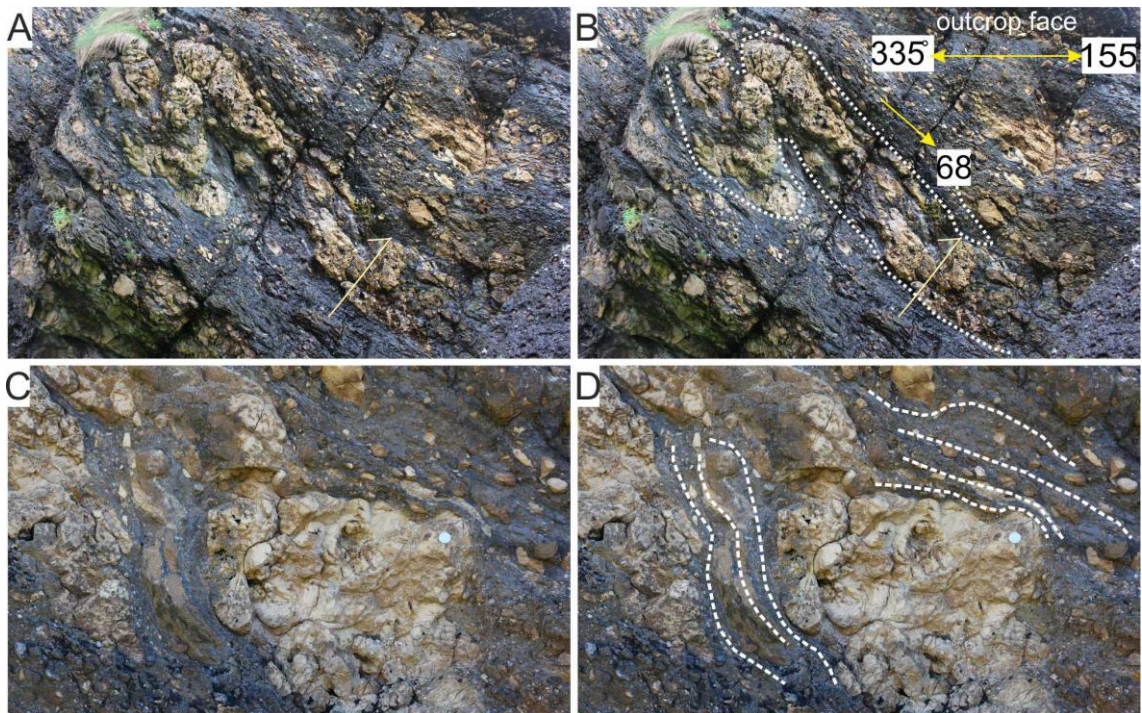
Figure 3.35: (A and B) dolomite fold within silty diamictite on the W coast of EaN. The ruler is 1 m scale and looks like an arrow pointing to younger strata. (C and D) Clast cluster (Galaxy) structure; the big dolomite clast is surrounded by laminae and smaller clasts. The coin is 1.8cm diametre.

Sometimes the siltstones include lonestones also. Clast shearing is another feature recorded just 2 m away from the dolomite fold towards the W (Fig.3.35A). The clast shearing direction is surprising, because it is exactly in the opposite direction of the fold shearing. Two bands of iron oxide occur in the lithofacies on the SW coast of EaN; they lie parallel to the bedding and are up to 15cm thick, but just one of them appears on the SW raised cliff, while both disappear on the E coast of this island and the other islands of the Garvellachs.
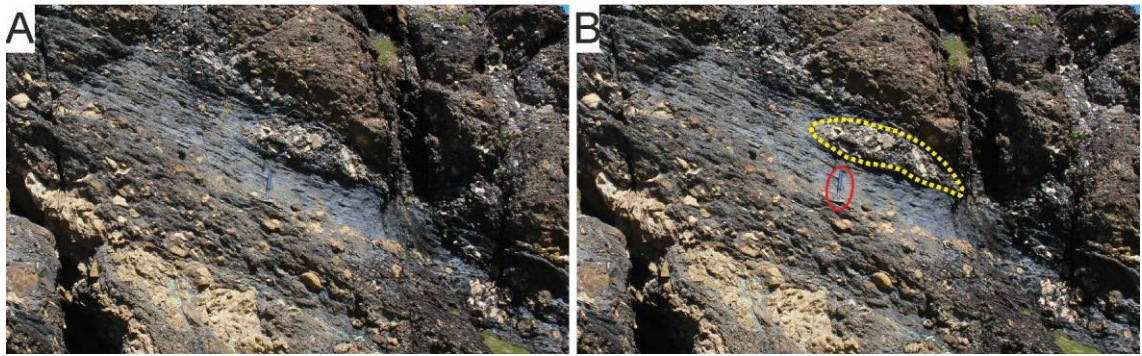
Figure 3.36: Clast cluster (dumpstone) within laminated bluish-grey siltstone lithofacies on the W coast of EaN. Also, lonestones are present within fine laminated siltstones. Geological hammer for scale.
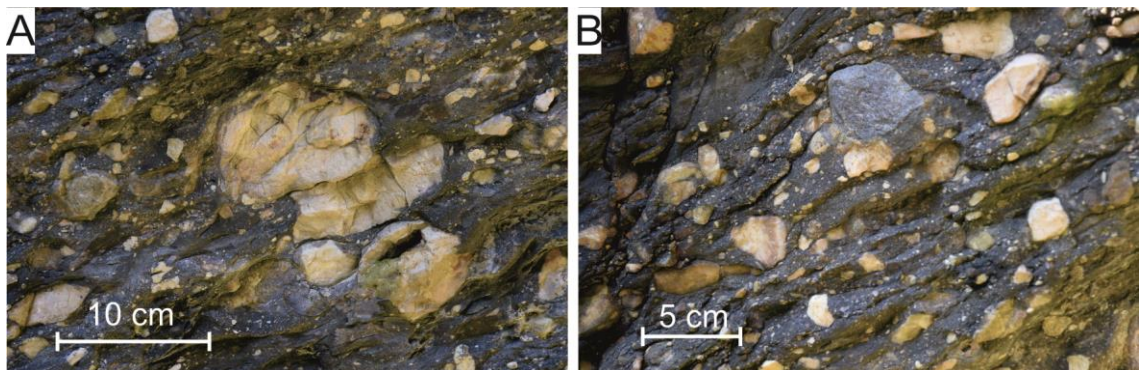
Figure 3.37: On the W coast of EaN (A) Dislocated clast as a result of shearing. (B) Obstacle clast, the big size arenaceous grey clast (compare with the surrounding clasts) supporting the smaller sized dolomite clasts that comes behind it and directed down-current.
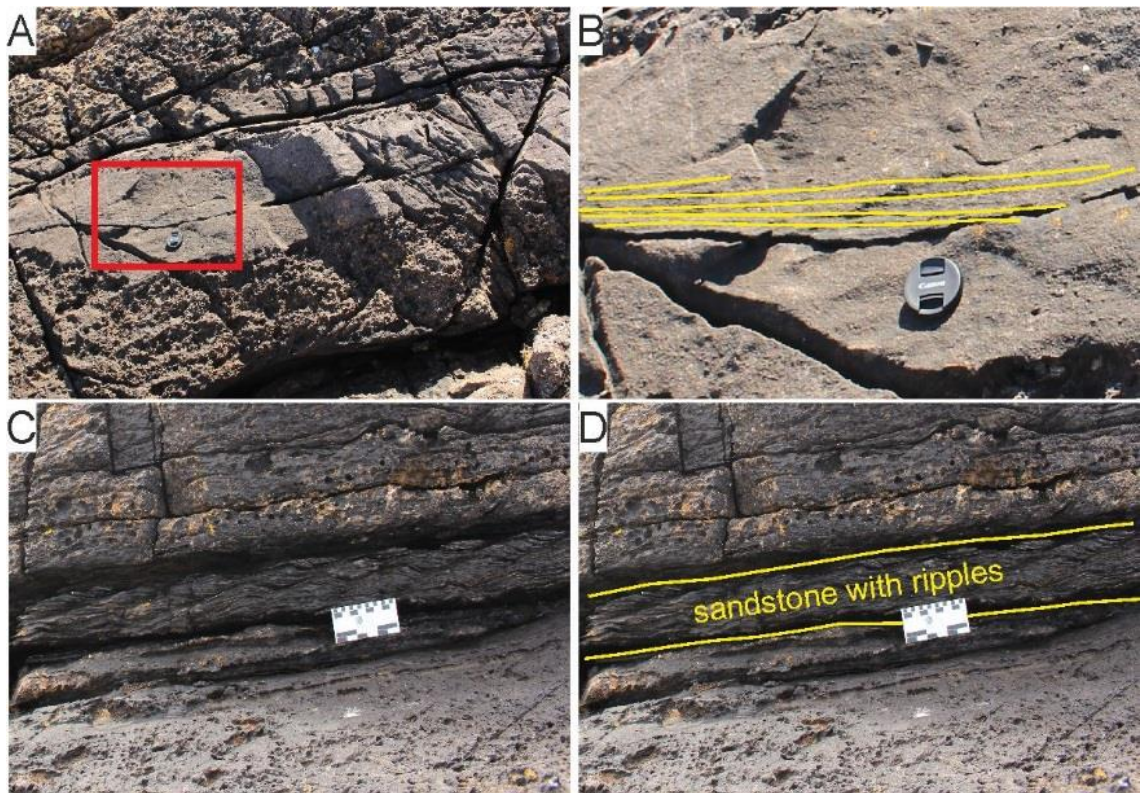
Figure 3.38: Sandstone bed within bluish siltstone diamictite-disrupted dolomite lithofacies, on the E coast of A'C. (A) sandstone bed dies out towards the E; the red box is representing figure 'B'. (B) low angle cross-stratification. (C and D) ripple marks in the sandstone bed.

The bluish-grey siltstone matrix, beside the components mentioned above, contains other bedded horizons. For instance, a laminated siltstone on the E coast of GE, the sandstone on A'C (Fig.3.31F), which shows cross-stratification and parallel ripple marks (Fig.3.38), and a level of extrabasinal cobbles.

The upper horizon of the lithofacies again has a series of disrupted white dolomites, lying in bluish pebbly diamictite. Also, extrabasinal boulders are present. On the E coast of EaN, two of the dolomite beds within this horizon are affected by folds (Fig.3.39a, b). In 'Fig.3.39a' the dolomite seems to contain a bedded horizon, but has been broken as a result of folding.
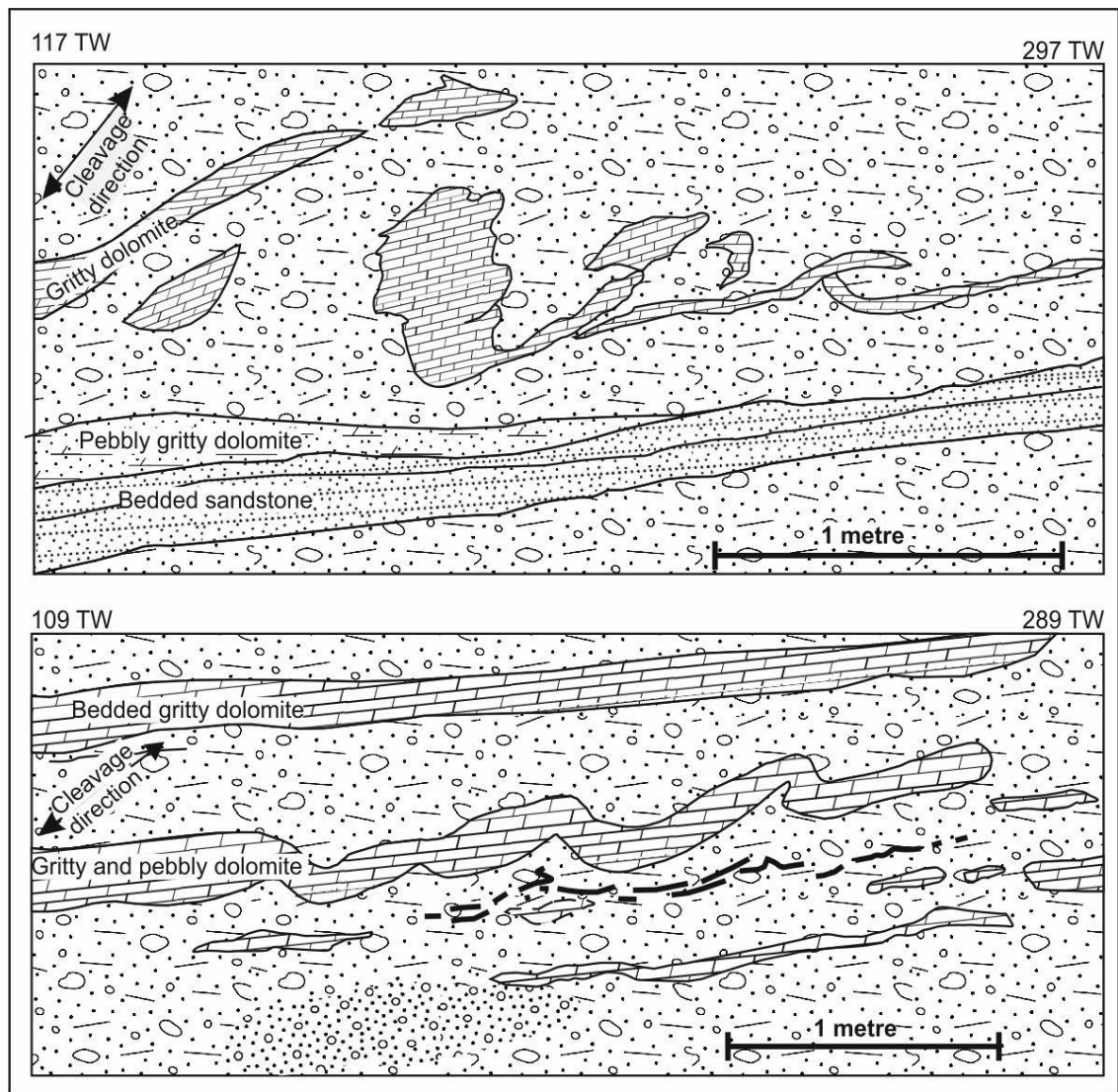
Figure 3.39: Field sketches of discontinuous dolomite bands lying in dark blue pebbly siltstones. The dolomite bands are affected by folds which in 'a' may have led to the dolomite band becoming broken, E coast of EaN (re-drawn from Spencer, 1966, Fig.58a and b).

(c) Rhythmically laminated siltstone, brown sandstone, conglomerate and conglomeratic diamictite lithofacies

This occupies the stratigraphic level between the two horizons of the 'Bluish-grey siltstone-dolomitic diamictite lithofacies' and below the lower horizon of this lithofacies (Fig.3.31); also, it is equivalent to parts of Bed nos. 2-5, according to Spencer (1966, 1971). The lithofacies consists of four sub-lithofacies: (i) rhythmically laminated siltstone, (ii) brown sandstone, (iii) lenticular conglomerate, and (iv)

97

conglomeratic diamictite. All have a dominant dark coloured matrix; although light coloured dolomitic conglomerate and brown sandstones do occur (Fig.3.31). The siltstone beds are well-laminated and contain predominant dolomite clasts and some extrabasinal clasts (Fig.3.40).

Rhythmically laminated siltstone sublithofacies: On the E coast of A'C, a 2 m thick siltstone bed thins toward the W and dies out after 60 m distance (Fig.3.31F and 3.32). It consists of rhythmically-laminated, fine-grained, grey-coloured, and lenticular shaped siltstones bed. It has sharp lower and upper contacts (Fig.3.40), with the underlying diamictite bed and the sandstone bed above. Each individual lamina is about 1-3 mm thick (Fig.3.42), represented by couples of fine-and coarse-grained sediments. The darker colour is coarser grained, more resistant to the weathering, and forms ridges; while the lighter colour shows finer sediments, is less resistant, and forms grooves (Fig.3.42).
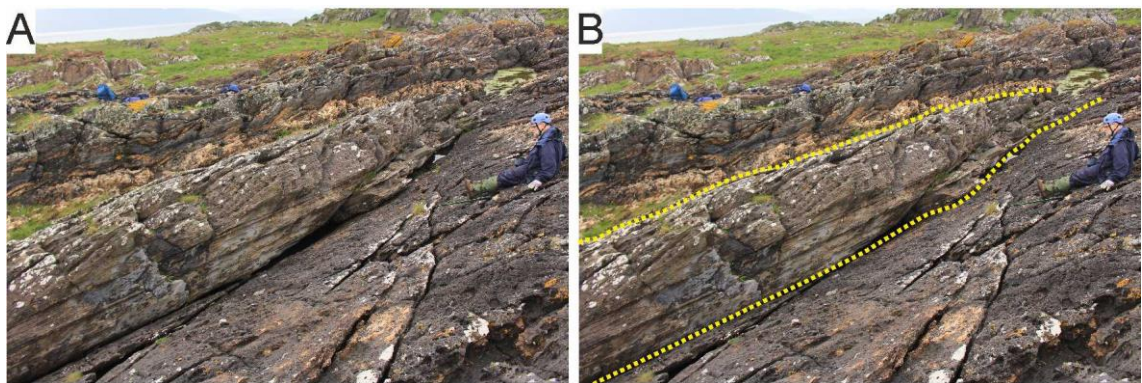
Figure 3.40: (A and B) rhythmically laminated siltstone within 'rhythmically laminated siltstone, brown sandstone, conglomerate and conglomeratic diamictite lithofacies', on the E coast of A'C. The dashed yellow line in 'B' shows the base and top of the laminated siltstone bed. Geologist (Ian Fairchild) for scale.
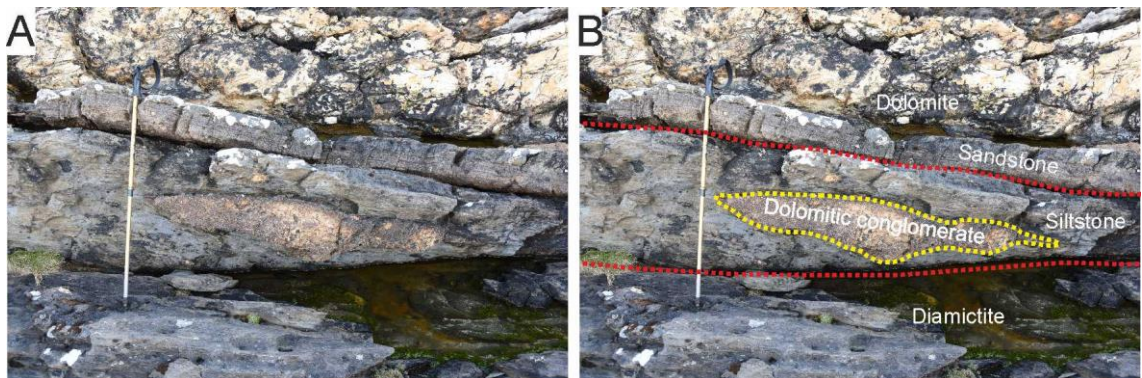
Figure 3.41: (A and B) lenticular dolomitic conglomerate within the rhythmically laminated siltstone on A'C. In 'B' the red line shows the lower and upper contact of the siltstone, and the yellow line exhibits the lenticular shape of the dolomitic conglomerate. The stick is 1m scale.
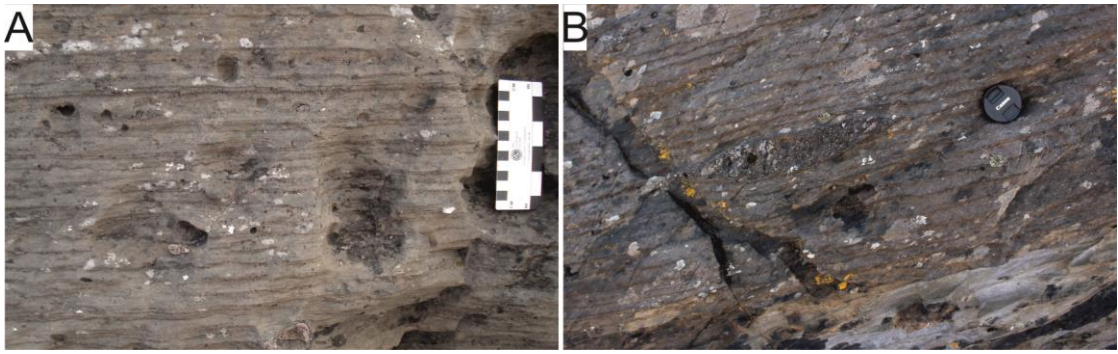
Figure 3.42: (A and B) rhythmically laminated siltstone on the E coast of A'C. (A) Few extra basinal clast within the siltstone, ruler for scale; and (B) lenticular sandstone and gritty matrix lens within laminated siltstone bed; camera cap is 58mm.

The siltstone contains clasts of dolomite and lenses of different lithologies. The dolomite clasts are rounded and the common size is about 6 cm across. The largest dolomite clasts recorded within the siltstones measures 39X9 cm in cross-section and lies parallel to the bedding. Also, lenses of conglomerate, gritty material, and sandstones occur within these siltstones (Fig.3.41 and 3.42). The sandstone and gritty lenses are small sized, not more than 30X10 cm in cross-section; while the maximum size of dolomitic conglomerate lens is about 100X30 cm in cross-section (Fig.3.41, 3.42B). The laminated structures of the siltstone are affected by the clasts and lenses. Some of the laminations are punctured by the clasts or lenses (Fig.3.43); also, laminae under the clasts or lens are typically deflected (Fig.3.41, 3.42, and 3.43).
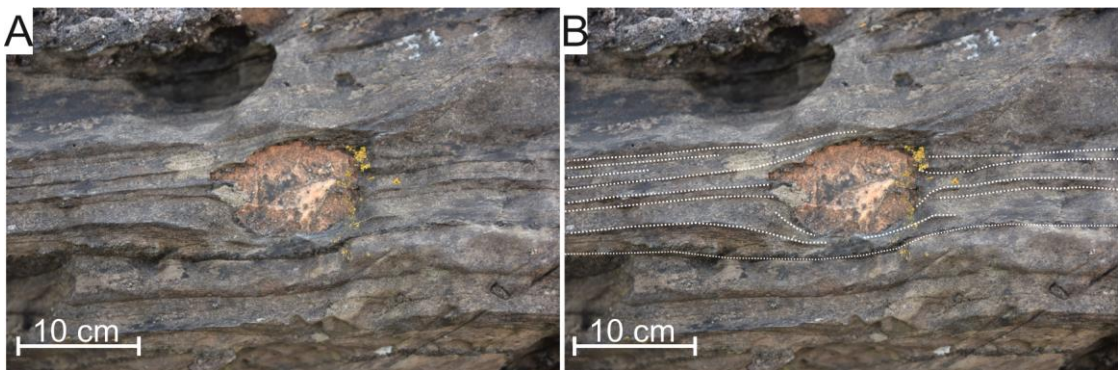
Figure 3.43: Dolomite clast within rhythmically laminated siltstone on the E coast of A'C.

On the SW coast raised beach cliff of A'C, within the diamictite beds in this lithofacies there are two dolomite bands (Fig.3.44). They are milky coloured and well recognised from the distance because of the colour contrast between them and the siltstone. The lower-band is thicker than the upper-band; while the lower-band is more deformed compared with the upper one (Fig.3.44).

Diamictite sublithofacies: On the SW raised beach cliff of A'C, the diamictite bed consist of bluish-grey colour matrix (Fig.3.45) with predominant dolomite clasts and rare extrabasinal clasts. The common size of the clasts is 3 cm across, while the largest size is less than 10 cm.
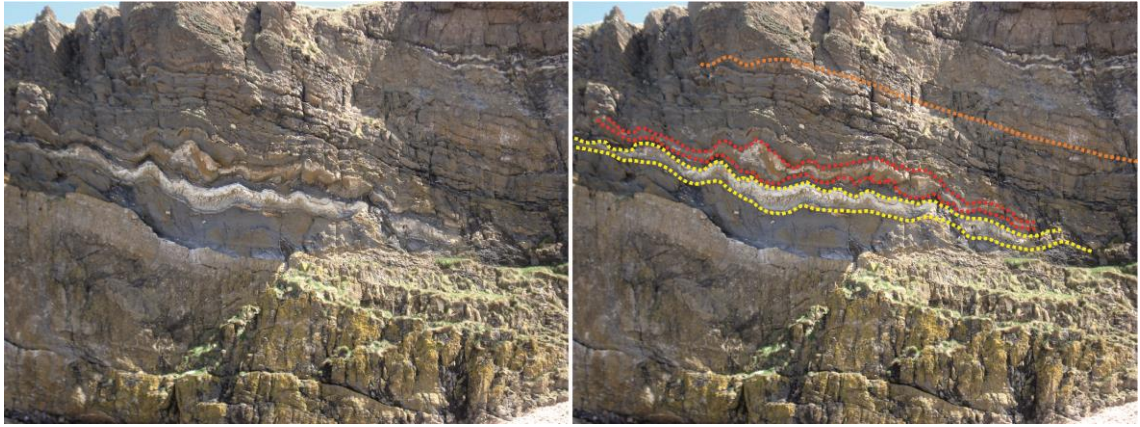
Figure 3.44: Two dolomite bands, on the W coast cliff on A'C, within diamictite bed inside 'rhythmically laminated siltstone, brown sandstone, conglomerate and conglomeratic diamictite lithofacies'. The yellow dashed line shows lower band horizon, and the red one is upper. The orange dashed line is not deformed.

Dark blue siltstone sublithofacies: The siltstone beds consist of dark blue dolomitic silt size particles and occur in different stratigraphic levels through the lithofacies (Fig.3.31). Such beds are present below the lower horizon of the 'bluish siltstone diamictite- disrupted dolomite lithofacies' in: E coast of GE, BaT, E coast of EaN, south-western raised cliff, and south-western coast of EaN (Fig.3.31B, D, E, G, I, J). Also, this siltstone appears between the upper and lower horizons of the 'bluish siltstone diamictite- disrupted dolomite lithofacies' on the E coast of GE and the south-western raised cliff of EaN (Fig.3.31C, I). In addition, it occurs on the E coast of A'C and the south-western raised cliff of EaN at the top of the upper horizon of 'bluish siltstone diamictite- disrupted dolomite lithofacies (Fig.3.31F, I).

The siltstones have sharp lower and upper contacts with the underlying and overlying sublithofacies or lithofacies. However, some gradual lateral contacts were observed into diamictite or sandstone. Sometimes the siltstones contain a few clasts, so it is difficult to decide whether it is a siltstone or a diamictite; also, in places, the grain-size gradually increases to sandstone (Fig.3.31). Moreover, in places the siltstone contains large clasts which reach more than 2 m across; for instance, on the N coast of GE.

On the SW raised cliff of EaN (Fig.3.31J), the rhythmically laminated siltstone does not show grading but exhibits couplets of fine-and coarse-grain similar to the siltstone on A'C; here they are thicker and reach 3-8 cm. Moreover, it is associated with dolomite conglomerate and pebble sized clasts are common within the siltstone.

Spencer (1966, Fig.61; 1971, Fig.36) sketched this siltstone on the N coast of GE. There, the sandstone beds are laterally replaced by a dolomitic conglomerate bed then by homogeneous massive silty diamictite bed, including dolomite clasts in an outcrop 40m long (Fig.3.46). Within the dolomite diamictite, there is a dolomite boulder in the centre part of the bed that reaches 2.3X1.8X1.0 m in size.

Figure 3.45: Diamictite sublithofacies on the SW coast of A'C. The yellow dashed line shows the upper and lower contacts of the bed. The thickness of the bed is from 0.5 to 2 m.
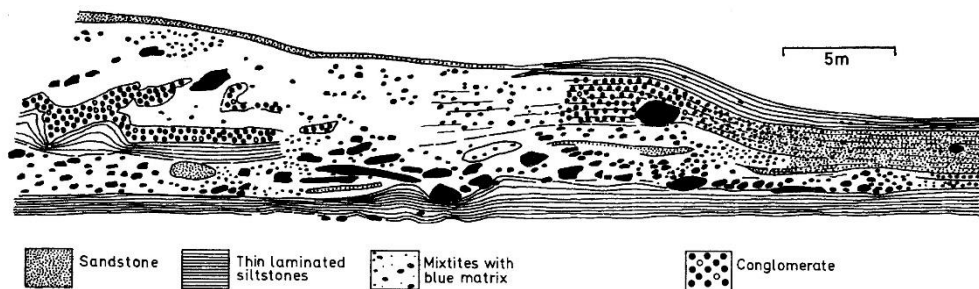
Figure 3.46: Field sketch of the Disrupted Beds outcrop on the N coast of GE; shows complex lithofacies geometries in this outcrop Spencer (1971).

Sandstone sublithofacies: The sandstone beds within the lithofacies are spread out in different stratigraphic levels (Fig.3.31) and they extend for short distances laterally. They are present as: (i) sandstone bed below, within and above lower horizon (Fig.3.31, 3.32) of the 'bluish siltstone diamictite-disrupted dolomite lithofacies'; (ii) dolomitic pebbly sandstone beds between the two horizons of the 'bluish siltstone diamictite- disrupted dolomite lithofacies'; and (iii) dolomitic sandstone above upper horizon of the 'bluish siltstone diamictite- disrupted dolomite lithofacies' (Fig.3.31, 3.32). The upper and lower contact of the beds are usually sharp with the underlying and overlying beds.

On the E coast of A'C, lenticular sandstones occur at a few stratigraphic levels within the lithofacies: (i) dolomitic pebbly sandstone above lower horizon of the bluish-grey siltstone-diamictite lithofacies (Fig.3.31); (ii) sandstone above rhythmically laminated siltstone lithofacies (Fig.3.32); and (iii) sandstone below upper horizon of bluish-grey siltstone-dolomitic diamictite lithofacies.

On the E coast of A'C, within the 'rhythmically laminated siltstone sub-lithofacies' there is a well-bedded, lenticular shaped, medium- to coarse-grained sandstone (Fig.3.31, 3.39). It contains fine laminated sandstone with ripple marks. Also, at a higher stratigraphic level 16 m from the base of the Disrupted Beds there is a sandstone bed with coarser grains and reversed graded grain size with some deformation (Fig.3.47); again, it has a short lateral extension.

Figure 3.47: A sandstone bed at the top rhythmically laminated siltstone sublithofacies on the E coast of A'C. Camera cap is 58 mm.

(d) Dolomite rimmed conglomerate lithofacies

This conglomerate consists of a brown sandy matrix with dolomite clasts. The clasts are enveloped by a sandy material identical to the matrix (Fig.3.48). The lithofacies is exposed on DC, E coast of A'C, and E coast of EaN (Fig.3.31A, H, and 3.32).

Figure 3.48: Dolomite rimmed conglomerate bed on the E coast of the A'C. The camera cap is 58 mm.

On the E coast of A'C (56°14'16''N, 05°46'48''W), about 28 m above the base of the 'Disrupted Beds lithofacies association', there are two lenticular dolomite conglomerate beds. These beds are separated

by a well laminated siltstone and a sandstone bed, respectively about 10 and 15 cm thick. The conglomerate layers are about 0-1.6 m thick, and consist of sandy matrix including clasts of various lithologies, size, and shape. Most clasts are dolomite, while extrabasinal clasts are rare. The sizes of the fragments are 1-3 cm, and most of them are angular in shape (Fig.3.48). Around them is a thin layer of coarse grained and well sorted sandy material. The actual lithology can be observed only when the outer layer is broken by a hammer. The common shape of the clasts is angular, but there are also some sub-rounded clasts. Additionally, this bed includes cross-bedded and concretion structures (Fig.3.49).

Figure 3.49: Rimmed dolomite clast within 'Dolomite rimmed conglomerate lithofacies' on the E coast of A'C.

On the E coast of EaN, similar beds of dolomite conglomerate occur in two different stratigraphic horizons. The lower horizon is about 11 m from the base of the Disrupted Beds, while the upper horizon is 28 m from the base. The clasts are commonly 1.5 and 2 cm and the maximum recorded size are 15 and 5 cm, respectively, for the lower and upper horizon.

iv. Sedimentary Structures

There are several features and sedimentary structures which can be useful for interpretation. The most common sedimentary structures are: bedding, lamination, rhythmically laminated siltstone, sedimentary deformation structures, graded-bedding, ripple marks, cross-stratification, boudinage, clast clusters, trail clasts, and lenticular bedding.

Individual laminated siltstones pinch out over tens of centimetres; they swell to include dolostone blocks and boudins, creating an augen-like structure by bifurcating around them (Fig.3.50).

Figure 3.50: Augen like structure formed by deformation of the dolomite boudins wrapping by a siltstone. Camera cap is 58 mm.

On the E coast of A'C, a discontinuous group of beds 90 cm thick occurs about 16 m from the top of the dolomitic conglomerate bed (Fig.3.32). Based on thickness of the beds and grain size, this group can be divided into lower and upper part (Fig.3.47). The former is 30 cm in thickness and shows coarsening upward interbeds between medium grain sandstone and grit materials. The individual bed is well sorted, 2-3 cm thick, show some soft deformation structures, and includes some flake shaped pebbles. The upper beds are represented coarsening upward interbeds between medium-coarse grained sandstone and gritty materials. The individual strata are well sorted, well bedded, 8-12 cm thick, and grey in colour. In both cases, there are some scattered granitic and quartzite extrabasinal clasts in a gritty lithology, the sizes of the clasts range from 0.3-2.5 cm. This group of beds is bounded by a sharp contact with the underlying well laminated siltstone and has a gradational contact with the overlying disrupted dolomitic sandstone bed.

(e) Depositional environment of the DB

The Disrupted Beds include the most complicated facies association within the succession of the PAF because: (i) the lithofacies are "entangled" with each other; (ii) most of the beds die out abruptly; and (iii) in different places, various lithofacies can be seen at the same stratigraphic horizon. To interpret these rocks and the structures within them, there are three depositional hypotheses which can be analysed: grounded ice, mass-flow and floating ice. This study depends on the data collected during fieldwork seasons and the most important to evaluate these three hypotheses for the DBFA are these features: (i) highly discontinuous laterally diamictite beds; (ii) laminated siltstone with lonestone; (iii) large scale cross-stratification within the conglomerate bed; (iv) disrupted dolomite bands/beds; (v) intense folding and thrusting; (vi) sheared clasts; (vii) clast cluster; (viii) discontinuous sandstone beds; (ix) continuous dolomite beds; (x) chaos structures (Table.3.5).

First this study briefly summarize the interpretations proposed by other authors. In addition to detailed interpretations of particular levels in the DB, Spencer (1966; 1971)concluded that his general interpretation of the DB was as a result of ice-rafting or grounded ice. By contrast, Eyles and Eyles (1983) and Eyles et al. (1985) suggested that many structures, such as conformable beds of siltstone, dolomite conglomerate and diamictite with scattered ice-rafted clasts showing faults, folds, pull-apart and boudinage structures, indicate repeated mass-movements. [Note that there is a misunderstanding on

p.59 of Eyles et al. (1985), where the Disrupted Beds refer to D14 in the first sentence of the third paragraph, rather than a lithofacies association underlying D14]. Eyles (1988)suggested that the differential cementation of interbedded carbonate and quartzo-feldspathic sediments within the DB may have promoted downslope movement and deformation by locally increasing pore pressure in uncemented layers. Arnaud & Eyles (2002) interpreted the DB as due to continuous slope instability following the deposition of the GB (Arnaud & Eyles 2006) based on: (i) the active tectonic setting; (ii) the form of the tectonic setting; (iii) the extent of the tectonic setting; and (iv) the unlikelihood of the other mechanisms. Benn & Prave (2006) rejuvenated the subglacial suggestion of Spencer and argued that the DB formed by grounded ice and represented glaciotectonism.

The author agrees with Spencer (1971) and Benn and Prave (2006) that there are features and structures (Table.3.5) that support a grounded-ice hypothesis; for instance, highly discontinuous diamictites, disrupted dolomites, intense folding and thrusting, sheared clasts, and clast clusters, where a large clast is surrounded by a halo of smaller clasts (these have been called 'galaxy structures' by van deer Meer 1993). Despite this, there are some horizons that show evidence, such as dropstones and continuous dolomite beds (Table.3.5) that support a subaqueous hypothesis (Eyles and Eyles, 1983; Eyles et al., 1985; Eyles, 1988; Arnaud and Eyles, 2002, 2006).

Based on the new field data in this study, the dolomitic conglomerate lithofacies is well-sorted, clast-supported, contains angular clasts and shows large cross-stratification (Fig.3.33) which could have formed either by grounded-ice as a high-energy meltwater stream in periglacial environment or by mass-flow processes (as a lateral channel with reworking from a local area). The shape and geometry of the cross-bed suggest progradation in a small delta at the edge of a water body.

The bluish siltstone diamictite-disrupted dolomite lithofacies could have formed subaqueously owing to fine-grained siltstone with 'clast cluster' (Fig.3.36) could be 'dumpstone' structure sensu Thomas and Connell (1983); and the presence of lenticular dolomite beds. Siltstone with the delicate laminae suggests quiescent conditions in a lake or sea. The lake vs marine issue requires study, but the evidence currently swings in favour of a lake based on the geometry and abrupt lateral changes in the lithofacies. In the other hand, structures like thrusting, folding, obstacle clasts, shear clasts, and galaxy structure are against the mass-flow hypothesis (Table.3.5). The grounded-ice interpretation explains all the features (Table.3.5). The dumpstone could be form in a lakelet (Fig.3.51) by small ice-bergs (Thomas and Connell, 1985; Benn and Evans, 2010, pp.429, and Fig.10.79c); the other structures can be formed by glaciotectonism in a subglacial environment. Both structure (subaqueous and subaerial) could be present by ice oscillation if there is a small lake in a periglacial environment close to the margin line of the ice-sheet. In addition to the bluish siltstone diamictite, there are the sandstone (Fig.3.38) within the lithofacies is more likely to be a fluvial channel because it is: (i) well-organised; (ii) fining-upward; (iii) well-sorted; (iv) includes cross-stratification and ripple marks; (v) has a channel geometry, and (vi) dies-out laterally in very short distance.

Rhythmically laminated siltstone, brown sandstone, conglomerate and conglomeratic diamictite lithofacies occur as a mixture of lithologies at similar stratigraphic horizons (Fig.3.32). Delicate laminated siltstones associated with lenticular conglomerates (Fig.3.41) and outsized clasts (Fig.3.43) indicate a subaqueous setting. Lack of 3D exposure hampers complete interpretation. So, the conglomerate lens (Fig.3.41) could be a small channel, concretion, ice-raft, or tillite pellet. Because it is not well-organised and has a sharp contact with the surrounding sediment it is not likely to be a channel or a concretion. Also, its position in rhythmically laminated siltstones makes it more likely to be due to ice-rafting than a tillite pellet. The rhythmite could result from seasonal variations in meltwater production in a lake (varve) producing a rhythmite (e.g. glacial lake Hitchcock, Massachusetts, USA (Menzies, 2002; plate 11.2), or as rhythmic couplets in a tidal cyclopel (Cowan et al., 1998; Cofaigh and Dowdeswell, 2001). Both lake and tidal interpretations are plausible, but the author prefers the latter because: (i) of the thinning upward character of the layers (Fig.3.42); and (ii) couplets of finely-laminated and coarse deposits are more compatible with the tidal rhythmites than varves.

The diamictite beds (Fig.3.45) could be reworked ice-rafted debris flows or deposited by grounded-ice within this stratigraphic horizon. There are no signs of deformation beneath the beds and the beds are massive suggesting they are more likely to be small local debris flows rather than deposits of grounded-ice. The sandstone in 'Fig.3.47' is more likely to be fluvial because it is similar to the sandstone in 'Fig.3.38'.

The dolomite rimmed conglomerate lithofacies (Fig.3.48) may be of diagenetic origin because it is similar to Fig.3.49. However, metamorphic overprinting could have had a role in modifying clast shape because they have thick rims. Thus, the possibly of metamorphic overprinting render the depositional mechanism difficult to interpret.

Based on the data herein, the depositional environment of the Disrupted Beds facies association can be summarised as marginal to an ice shelf. The ice shelf underwent some oscillation, producing glaciotectonic structures. It is suggested that this was adjacent to a tidal area.
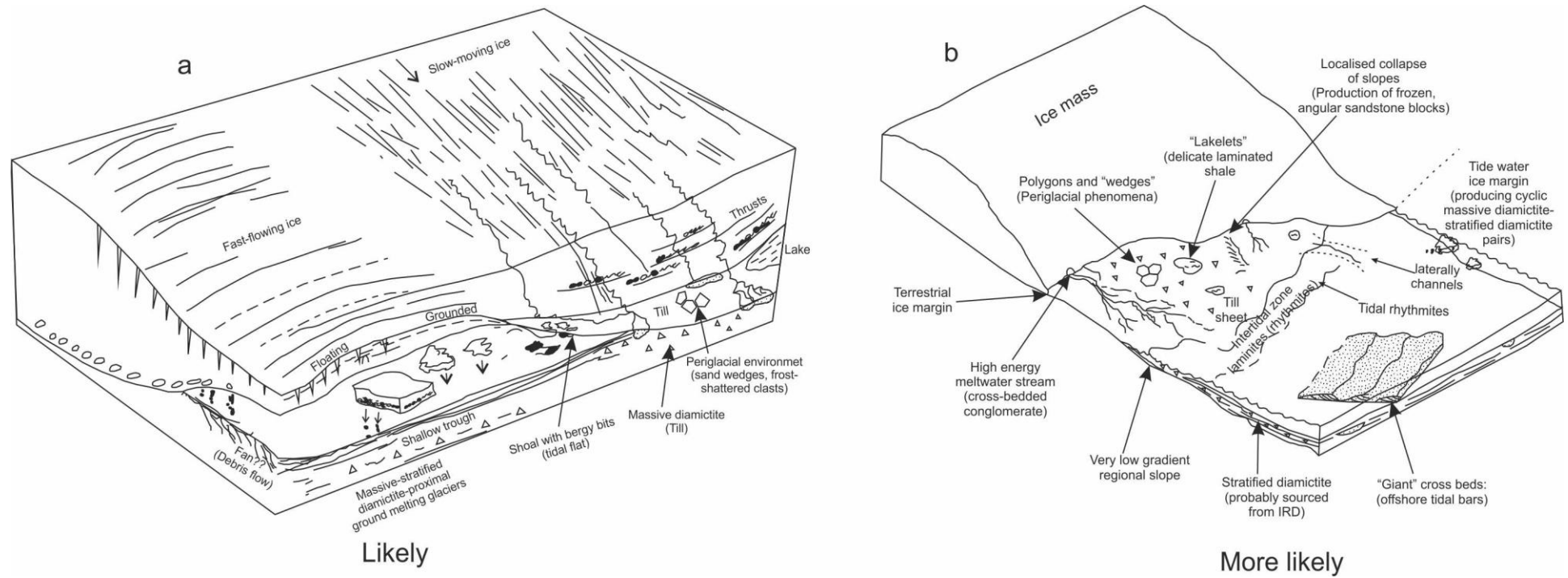
Figure 3.51: Block diagram showing ideas about the depositional environments of the Disrupted Beds lithofacies association.

Table 3.5: Features that occur within the Disrupted Beds and their interpretation.

Features/beds	Lithofacies/location	Subaqueous mass-flow	Floating ice	Grounded ice	More likely in this study
Highly discontinuous laterally diamictite	Bluish siltstone-disrupted dolomite lithofacies (Fig.3.34)	Unlikely	Unlikely	Possible	Grounded-ice
Laminated siltstone with lonestone	Rhythmically laminated Siltstone, brown sandstone, conglomerate lithofacies (Fig.3.31, 3.32)	Unlikely	possible	Unlikely	Floating-ice
Large cross-bed within conglomerate bed	Dolomitic conglomerate lithofacies on W EaN (Fig.3.33)	Possible	Possible	Possible	Non-glacial Ground ed-ice Mass-flow
Disrupted dolomite	Bluish siltstone-disrupted dolomite lithofacies	Possible	Unlikely	Possible	Concretion Ground ice Mass-flow
Intense folding and thrusting	Bluish siltstone-disrupted dolomite lithofacies (Fig.3.35A-B)	Unlikely	Unlikely	Possible	Grounded-ice
Wrapping lamina around the clasts	Bluish siltstone-disrupted dolomite lithofacies (Fig.3.35C-D)	Unlikely	Unlikely	Possible	Grounded-ice
Sheared clasts	Bluish siltstone-disrupted dolomite lithofacies (Fig.3.37A)	Unlikely	Unlikely	Possible	Grounded-ice
Galaxy structures	Bluish siltstone-disrupted dolomite lithofacies (Fig.3.35B)	Unlikely	Unlikely	Possible	Grounded-ice
Sandstone beds	EA'C (Fig.3.38)	Possible	Unlikely	Possible	Fluvioglacial
Continuous dolomite beds	Bluish siltstone-disrupted dolomite lithofacies. (Fig.3.44)	Unlikely	Unlikely	Unlikely	Marine
Chaos structures	Bluish siltstone-disrupted dolomite lithofacies (Fig.3.46)	Unlikely	Unlikely	Possible	Grounded-ice

3.5 Dolomitic diamictite- Sandstone LFA (D14-D18)

Strata belonging to this lithofacies association occur in the top of Member 1 between the Disrupted Beds and D19. They consist of three main lithofacies (dolomitic diamictite, sandstone, and Upper Dolomite) and one minor lithofacies (siltstone). These strata were studied by Kilburn et al. (1965) and Spencer (1971). Kilburn et al. (1965) numbered the diamictite beds 14 to 18. We here retain those numbers but label them: D14-D15, D16-D17, and D18. The diamictite beds are interbedded with the sandstone and siltstone and the Upper Dolomite occupies the top of this succession below D19.

(a) Stratigraphic position and outcrops

These beds of diamictite and sandstone are exposed on all of the main Garvellach Islands except DC. The thickness of the complete D14 – D18 interval varies from 3.5-24 m because not all five diamictite beds are present along the whole outcrop (Fig.3.52A). The thickest succession (25 m) is present on the E coast of the GE, where all five diamictite beds occur.

To determine the lateral extent of the five diamictites, three field studies have been made: the strata have been logged in detail across GE; detailed logging of the section on the E of A'C has been done; all other sections have been visited (except the W coast of GE). These studies have shown that the correlation depicted on Spencer (1971, plate 11A) is largely wrong.

On the E coast of GE, D18 can be followed about 370 m towards the NW (Fig.3.52A) but disappears at N 56°14'794'' and W 05°45'425''. Diamictites D16 and D17 appear to thin towards the W on GE and appear to be absent on A'C and EaN, so that on those islands only D14-15 are represented. Thus, on the E of A'C the complete interval is just 10.5 m thick and comprises four main diamictites in the E of the measured sections but as many as nine thin diamictites 50 m further towards the W (Fig.3.52B). The complete interval thins to just 6 m on the W coast of A'C and contains two diamictite beds separated by a 0.5 m thick sandstone bed (Fig.3.52A). On the E coast of EaN, just two diamictites beds occur, resembling D14 and D15 in their characters - gritty, dolomitic matrix and clast content; these beds show the minimum thickness, 3.5 m, of this unit on the Garvellachs. These strata are not well exposed in the inland of EaN, but are well exposed on the S-W where the matrix is more siliciclastic compared with the E coast, which is more dolomitic. In this part of the island the thickness of the beds reaches a maximum thickness of 8.5 m (Fig.3.52A). The stratigraphic correlation shown in Fig.3.52A shows that a major erosional unconformity exists beneath the Upper Dolomite. The complete succession of D14 to D18 is only present on the E coast of GE. Traced towards the W on GE, all four beds below are progressively truncated: Diamictite no.18, sandstone underlying D18, Diamictite nos.16-17, and sandstone underlying D16-17. Thus, on A'C and EaN only the D14-D15 interval is present
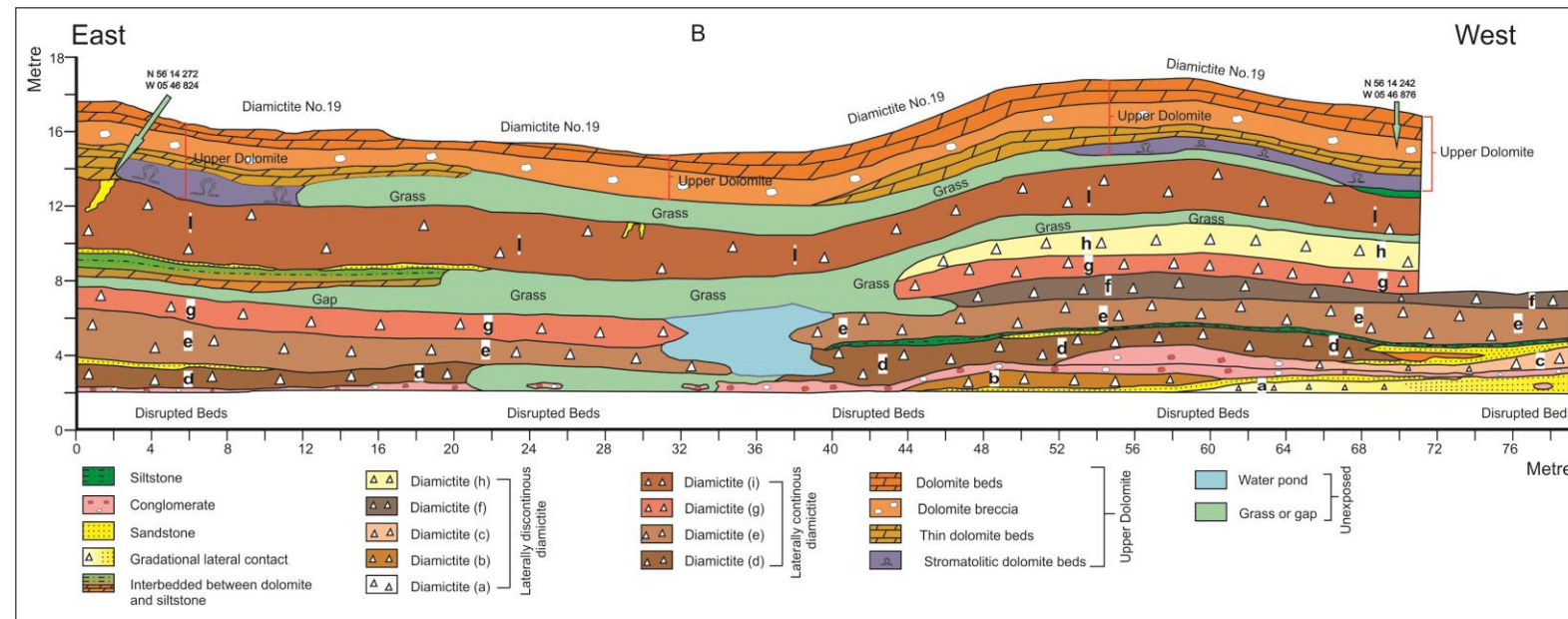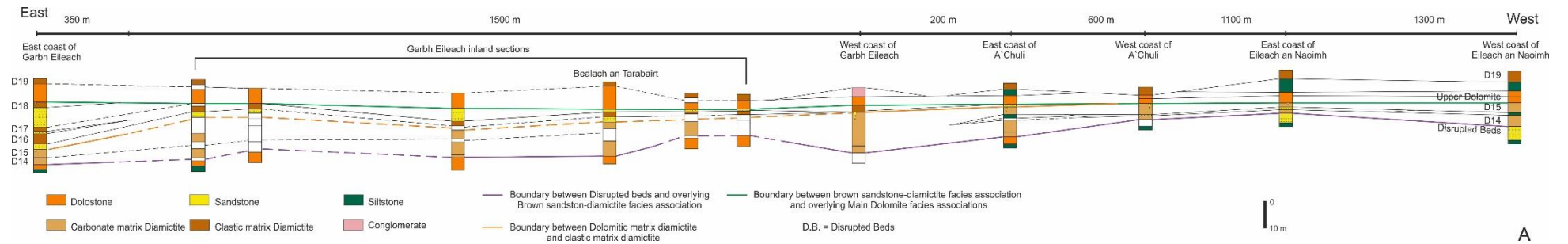
Figure 3.52: (A) Correlation sections between different localities on the Garvellach Islands. **(B)** A measured section on the E coast of A'C made by gridding the outcrop at 2m intervals. This shows high lateral variation of the diamictite beds (D14 and D15) over a 72m distance.

(b) Dolomitic diamictite lithofacies

i. Contacts

The lower boundaries of the diamictites: The basal contact of D14 is everywhere sharp above a dolomite at the top of the Disrupted Beds: it is often marked by a thin pebble bed or sandstone. Sometimes, is difficult to separate D14 and D15 because they are lithologically identical and when interbeds are absent or discontinuous it is impossible to separate them. For example, on the E cost of GE (Fig.3.52A), D14 and D15 are distinguished by clast size and abundance and the contact between them is partly gradational. At this location, D16 and D17 both rest in sharp contact with the sandstone beds below them. Finally, D18 also rest in sharp contact with the cross-bedded sandstone beneath it.

The upper boundaries: On the E coast of GE there is a gradational contact between the top of D14 and bottom of D15, whereas D15 has a sharp contact with the overlying laminated sandstone bed and is penetrated by sandstone wedges (Fig.3.53–3.56). Also, the top contacts of D16 and D17 are sharp with the overlying sandstone beds. The upper contact of D18 is sharp with the overlying Upper Dolomite; the diamictite is also penetrated by sandstone wedges from the top.
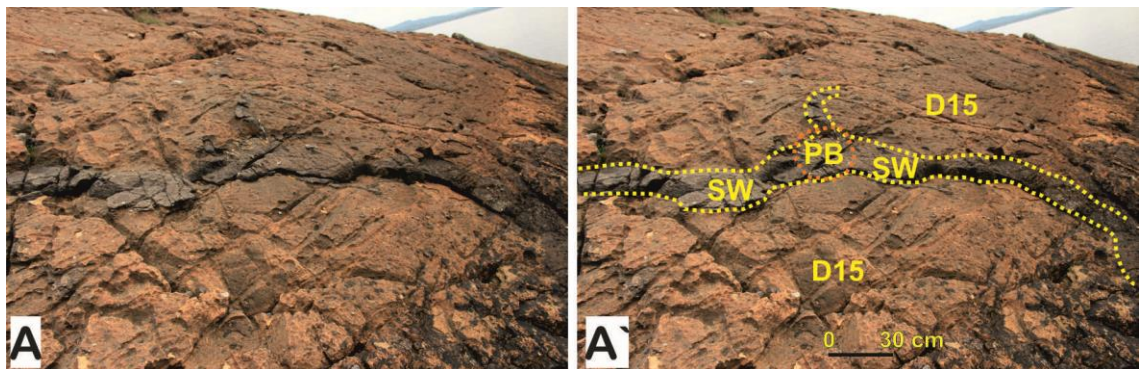
Figure 3.53: (A and A`) Sandstone wedges (SW) on the top of D15 overlain by patches of breccia (PB). E coast of GE.
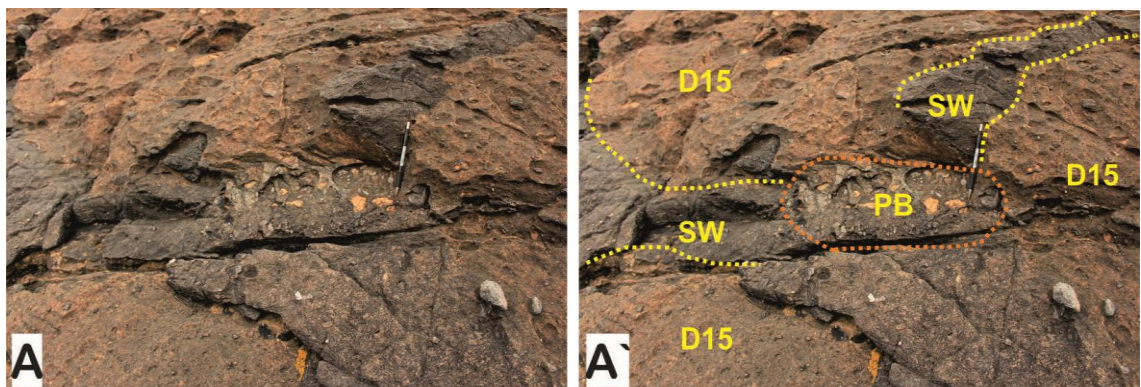
Figure 3.54: (A-A`) Close view of the patch of breccia (PB) overlying a sandstone wedge (SW) in the top of D15 from the top. E coast of GE.

ii. Lithologies

D14 and D15 are unstratified diamictites which have a gritty, dolomitic siltstone matrix and contain many clast types: in vertical succession, they are the first diamictites often to contain granitic clasts. The lower part of the matrix of D14 is more dolomitic than the upper part. Clast types are variable, some outcrops are dominated by carbonate clasts and others have a higher proportion of extra basinal clasts (Fig.3.57-3.60).
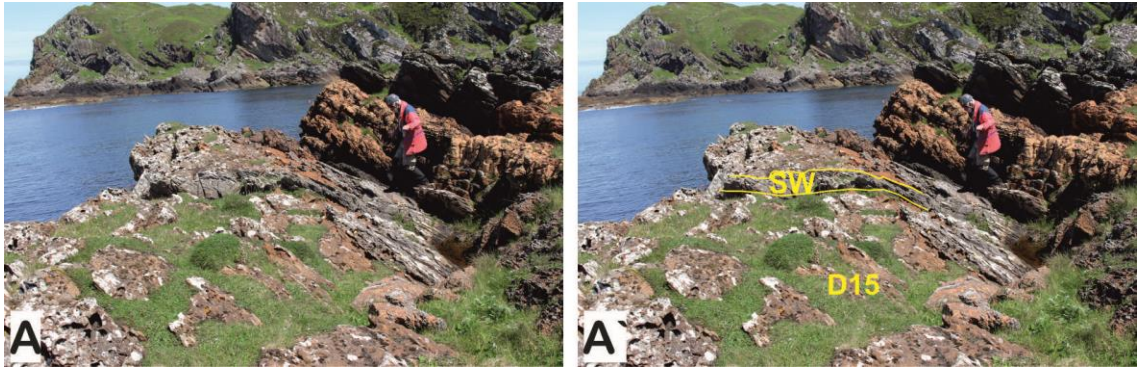
Figure 3.55: (A-A`) Sandstone wedge penetrating the top of diamictite bed D15. E coast of A'C. Geologist (Anthony M. Spencer) for scale.
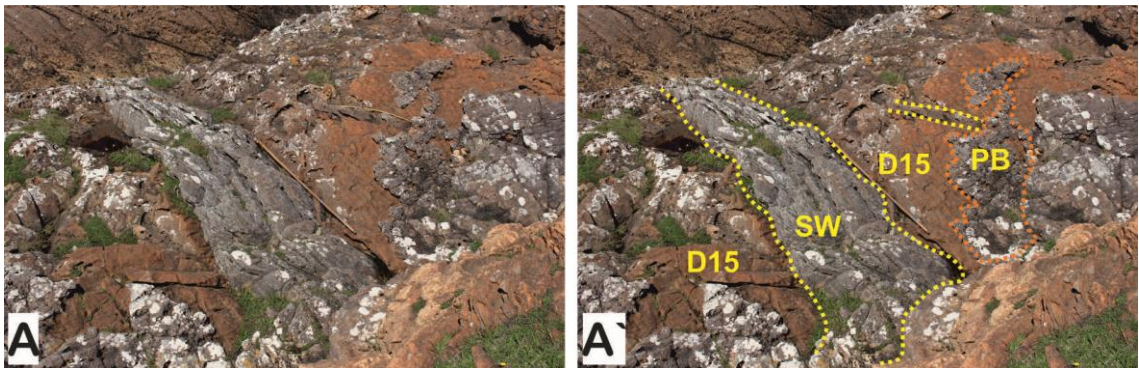
Figure 3.56: (A-A`) View looking down on sandstone wedge penetrating diamictite bed D15. Notice overlying patch of breccia (PB). E coast of A'C. Ruler is one metre scale.

The largest intra-basinal clast seen measures 155X102X30 cm, and the largest extra-basinal clast in the S-W of EaN, is 87X77X24 cm. Close to the contact between two diamictites (D14 and D15), in GE, there are some discontinuous lenticular shaped sandstones. Lithologically these two diamictites are similar to D1-D12, but differ from them in containing more than 33% extra-basinal clasts, except D15 on the W coast of EaN (Fig.3.57 – 3.60).
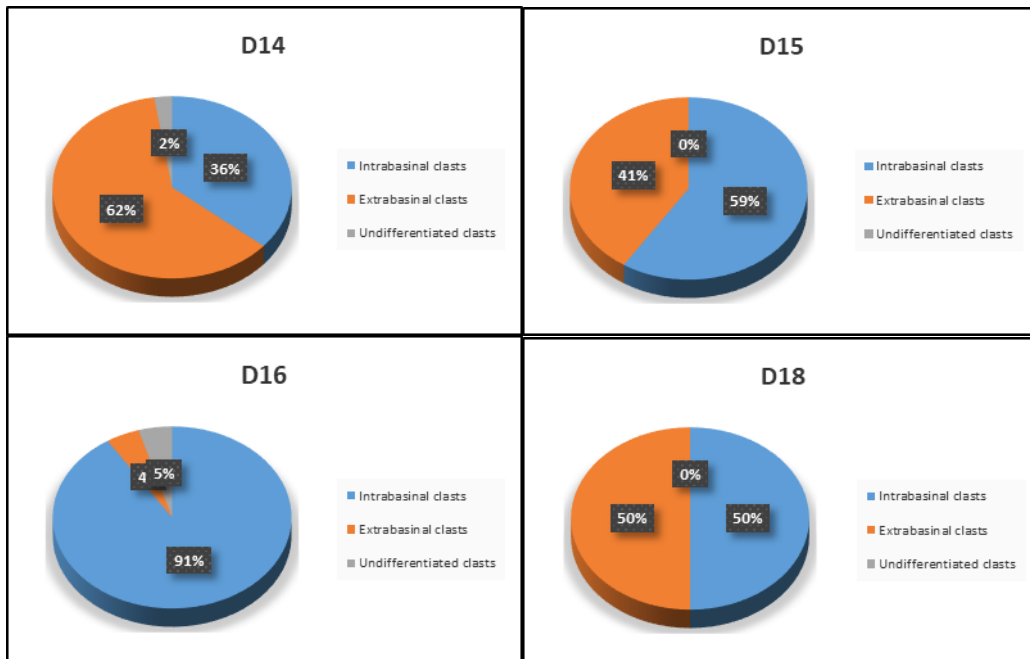
Figure 3.57: Number of clasts of different lithologies in diamictite beds D14, D15, D16 and D18, on the E coast of GE.
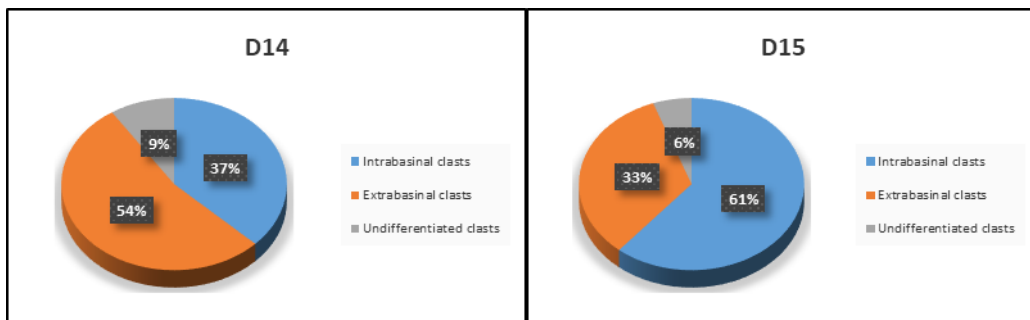
Figure 3.58: Number of clasts of different lithologies in diamictite beds D14, and D15, on the E coast of A'C.
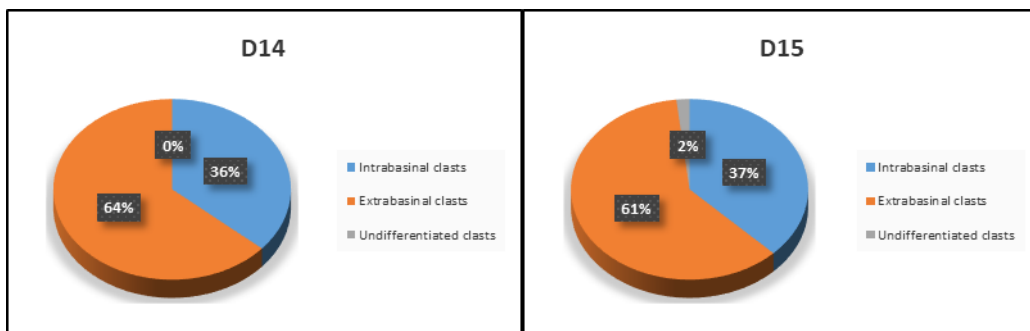
Figure 3.59: Number of clasts of different lithologies in diamictite beds D14, and D15, on the W coast of A'C.
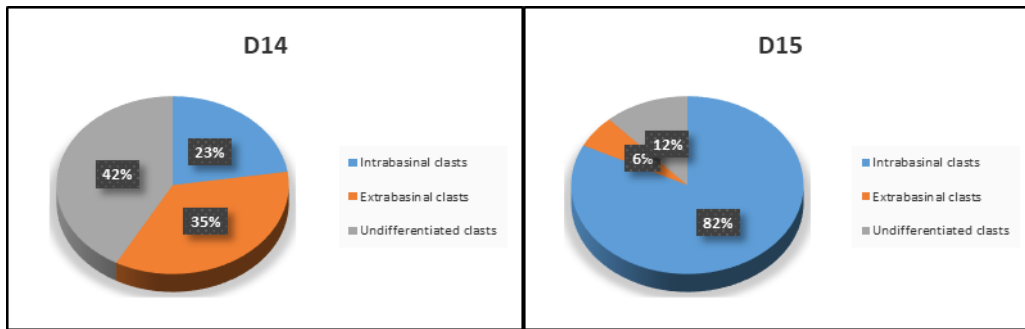
Figure 3.60: Number of clasts of different lithologies in diamictite beds D14, and D15, on the W coast of EaN.

D16-D17 are again unstratified diamictites composed of a fine-grained dolomitic siltstone matrix and including clasts of differing lithologies. These diamictite beds contain fewer clasts than D14 and D15 and the clasts are dominantly less than 5 cm in diameter. On the E coast of the GE, D17 is very poor in clasts and boulder size clasts are absent. The matrix in D16 and D17 is more siliciclastic and less dolomitic than D14-D15. D18 is different from D16 – D17: it has a sandy siltstone matrix and contains a greater number of clasts.

iii. Sedimentary Structures

On the E coasts of GE, within D14 there is a gradational coarsening upward, 20 cm thick, sandstone bed. Its shape is lenticular, and includes pebble size clasts in the upper part. This bed is located about 80 cm from the base of the diamictite layer.

On the E coast of GE and A'C, the top of D15 is penetrated about 2 m by poorly organized sandstone wedges (Fig.3.61). They are composed of fine to medium grained sandstone, are well sorted, 15-30 cm wide at the top and wedge to zero downward; they include some scattered dolomite clasts (Fig.3.62). The wedges are overlain by patches of breccia, composed of pebble sized dolomite clasts with few extra-basinal clasts surrounded by fine to medium grained sandstone matrix (Fig.3.53, 3.54, 3.56).
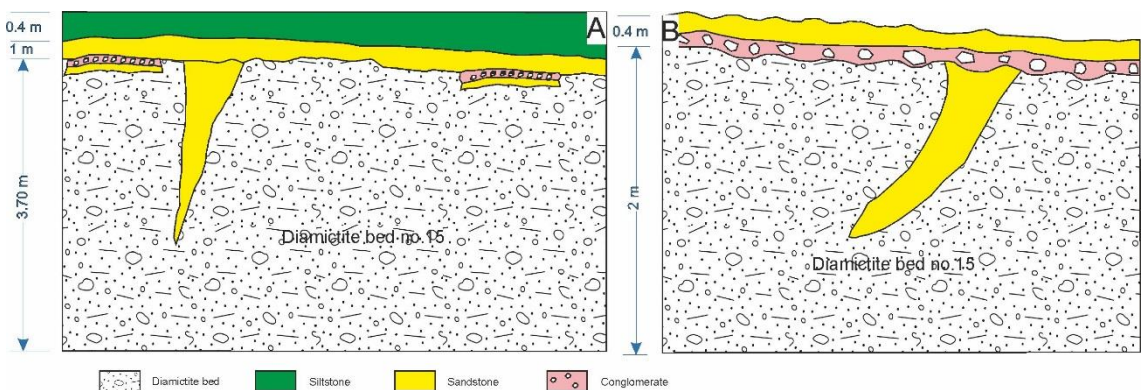
Figure 3.61: A cartoon showing the sandstone wedge in the top of diamictite bed D15. (A) On the E coast of GE; (B) on the E coast of A'C.

On the E coast of A'C, there are three sandstone wedges at the top of D14-D15 (Fig.3.61B). They consist of fine to medium-grained sandstone, well sorted, and grey in colour. The penetration depth, width, and length of the wedges in these two localities are different (Fig.3.61). The largest wedge penetrates the bed about 2m; and the width of them ranges between 20-110cm; the wedges on the E of GE are up to

10m long. The top of these wedges is overlain by patches or beds of breccia (Fig.3.61) at a sharp contact. These patches are composed of angular clasts of various lithologies enclosed by a fine to medium-grained sandstone matrix, which includes some pebbles. The size of clasts ranges from 0.5-5cm in diameter, and the dominant lithology is dolomite with lesser amounts of quartzite and granite. Similar wedges occur on the W coast of A'C and on the E coast of EaN, confirming that this stratigraphic level is the top of D14-15.
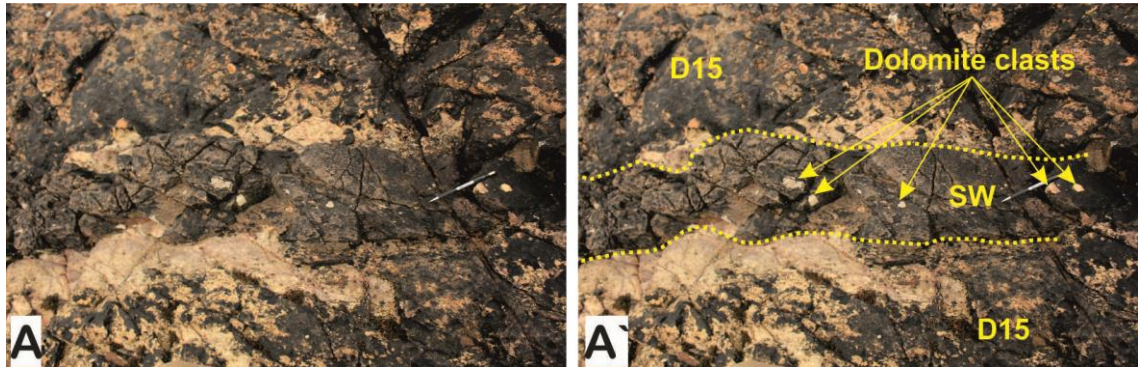
Figure 3.62: (A-A`) Scattered dolomite clasts within a sandstone wedge (SW) which penetrate diamictite no.15 (D15), on the E coast of GE. Pencil for scale.

Three sandstone wedges occur in the top of D18 on the E coast of GE. They consist of fine to medium-grained well sorted sandstone and are grey in colour; they penetrate down into D18 about 80 cm.

For the most part, as is normal for the diamictites of the PAF, in the coastal and inland outcrops visited, the diamictites appear to be homogeneous and lack internal stratification. However, where exposures are excellent, it is possible to see that this simple picture is not always true. The best exposed outcrop of D14-D15 occurs in the E of A'C and this was selected for detailed analysis. The resulting detailed section (Fig.3.52B), which took two days of fieldwork to make, shows that the internal stratification of D14-D15 here is highly complicated.

(c) Sandstone lithofacies

i. Stratigraphic position and outcrops

Four discontinuous sandstone beds separate the diamictite beds between D14 and D15, and below D16, D17 and D18. Between D14 and D15 on the W coast of A'C and the E coast of Eileach and Naoimh (Fig.3.52) is a thin (<1 m) bed of well-sorted, medium-grained sandstone. D15 and D16 on the E coast of GE are separated by a 2.5 m thick sandstone (Fig.3.52A), which thins towards the W, can be followed about one kilometre inland, but disappears on the W coast of GE. Between D16 and D17 on the E coast of GE about 2 m of sandstone is present (Fig.3.52A), but thins towards the W and dies out completely about 350 m to the W.

Between D17 and D18 on the E coast of GE, is the thickest (6.5 m) sandstone bed-sets. It is lenticular in shape and occurs below D18 on the E coast of GE or below the Upper Dolomite further W (Fig.3.52A).

ii. Lithology

The sandstone beds between or within D14 and D15 are fine-grained and well sorted. At BaT, the sandstone bed above D14-D15 and below D16 shows fining upward and can be subdivided into two: the lower part consists of breccia/conglomerate with a dolomitic matrix, sometimes the conglomerate shows thin loaded beds with a sandy matrix; the upper part is a coarse sandstone (Fig.3.52); the contact between the parts is gradational and each bed is about 20-50cm thick.

At BaT and above D14-D15, there is a group of interbedded breccia/conglomerate and sandstone beds (Fig.3.63). They have channelized geometry and are normal graded in grain-size. The clast size within the conglomerate beds is up to 15 cm across. The contact between diamictite and the conglomerate is gradational
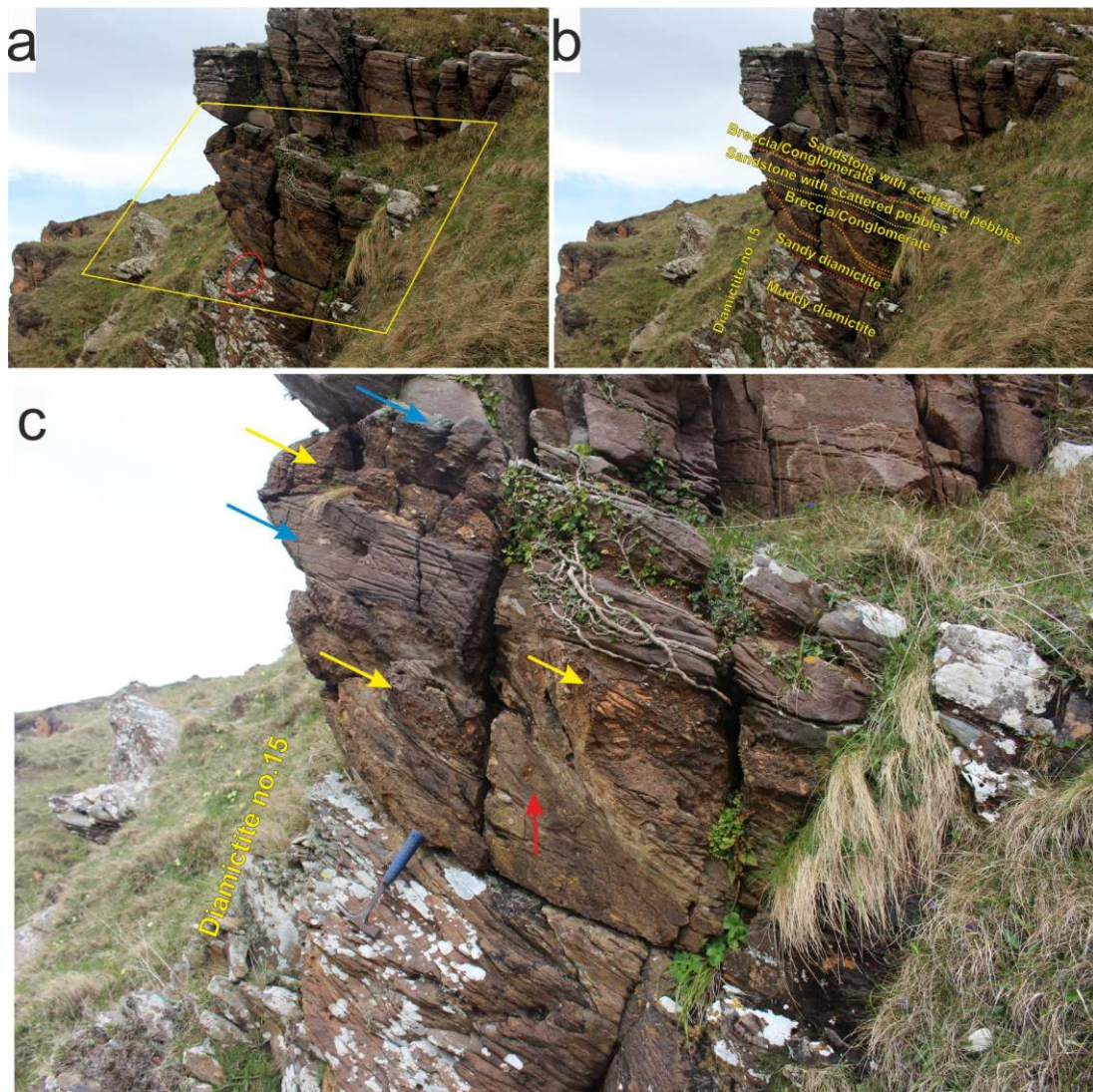
Figure 3.63: Groups of Interbedded sandstone and conglomerate/breccia beds above D14-D15 and below D16 at BaT. (a) the red circle is the hammer for scale, and the yellow rhomb is the outline of 'c'. (b) the orange dashed line shows the base of the breccia/conglomerate part; the yellow dashed line shows the base of the sandstone; and the red dashed line in D14-D15 separates muddy matrix diamictite (highly cleaved) and sandy matrix diamictite (more massive). Hammer for scale. (c) the yellow arrows shows the conglomerate/breccia beds, the blue arrows are the sandstone beds, and the red arrow shows the diamictite bed below the group.

On the E coast of GE, the sandstone below D16 is about 2 m thick (Fig.3.52A) and is fine-grained and well-sorted. The sandstone below D17 is 0.85 m (Fig.3.52A) thick there and consists of medium-grained, grey coloured sandstone. The sandstone below D18 or the Upper Dolomite is again medium-grained and well-sorted and has a maximum thickness (7.5 m) on the E coast of GE (Fig.3.52A).

iii. Sedimentary structures

The sedimentary structures that have been recorded within the beds of the sandstone lithofacies are wave ripple marks, climbing ripples, planar cross-bedding and normal graded bedding.

At BaT, the sandstone above D16 shows fining upward beds including climbing ripple marks (Fig.3.64). Also, inland at 'N 56˚14'793 and W 05˚45'893' the equivalent sandstone bed, there below the Upper Dolomite, is 4.5 m thick and exhibits gentle parallel lamination (Fig.3.65) and hummocky cross-lamination in the 50 cm from the base (Fig.3.68). The foresets are 5 to 7cm thick; while the upper part is more structureless and in places shows faint lamination. Also, 30m to the E, a 0.5m thick siltstone bed overlies the sandstone beds and underlies the Upper Dolomite (Fig.3.66); the sandstone is less than 2.5m thick there. At the top of the dolomitic siltstone, in the contact with the Upper Dolomite, pyrite cubes occur (Fig.3.67).
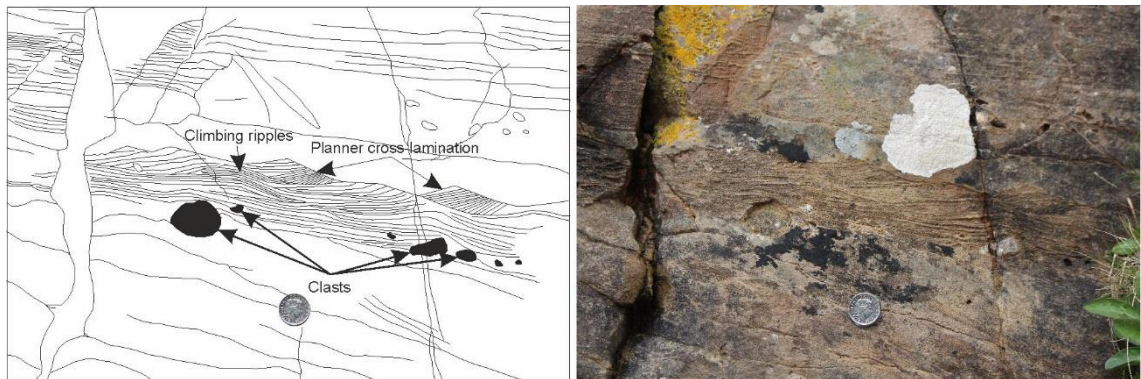
Figure 3.64: Climbing ripple marks, planar cross-lamination, and faint planar bedding within sandstone above D16 and below the Upper Dolomite at BaT. See the clasts at the base of the sandstone. Coin for scale.
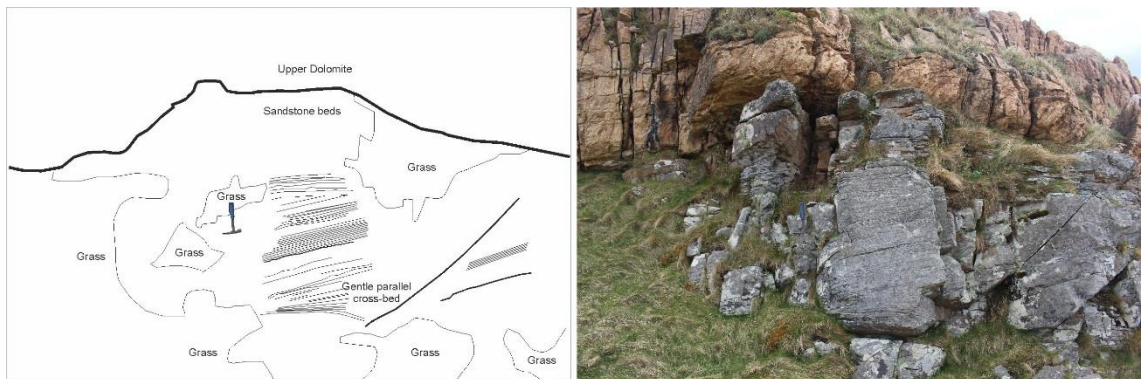
Figure 3.65: Gentle parallel cross-bedding within the sandstone above D16 and below the Upper Dolomite. Inland on GE. Hammer for scale.

Figure 3.66: Thin (0.5 m) dolomitic siltstone layer between sandstone above D16 and overlying Upper Dolomite. GE inland. Hammer is scale.

Figure 3.67: Pyrite cubes at contact between Upper Dolomite and underlying dolomitic siltstone, GE inland. Coin is scale.

Figure 3.68: Hummocky cross-stratification within the sandstone above D16 and below the Upper Dolomite. Inland on GE. Coin for scale. 30 m to the E of Fig.3.65.

(d) Dolomitic Siltstone Lithofacies:

This is a minor lithofacies within the D14-D18 interval. It is exposed in two localities: on the E coast of A'C and on the W coast of EaN. In the first place, siltstone lithofacies is exposed as a thin lenticular laminated-beds between diamictites (Fig.3.52B); and in the second place, the lithofacies occurs in the same stratigraphic level of the sandstone bed-sets between D14 and D15 (Fig.3.52A). Lithologically, it comprises fine-laminated dolomitic siltstone. It is less than 1.5 m thick and extends about 0.7 km (Fig.3.52).

(e) Depositional mechanism of the dolomitic diamictite-sandstone lithofacies association:

This LA has not previously been interpreted by others. The explanation and discussion of the depositional mechanism of this LA follows the same format for previous LA, ultimately testing

hypotheses for grounded-ice, mass-flow, and floating ice mechanisms of emplacement (Table.3.6). The correlation panel (Fig.3.52A) reveals that: (i) D16-D18 are cut-out towards the W and are only present on GE; (ii) both massive (laterally continuous) and weakly stratified diamictites (laterally discontinuous) are recognised (Fig.3.52B).

The occurrence of sandstone wedges that penetrate the top of two diamictite beds (Fig.3.53, 3.55, 3.56), is notable and demands explanation, as does the presence of breccia patches (Fig.4.54).

The main features considered (Table.3.6) in interpreting this FA are: (i) diamictite beds; (ii) highly discontinuous lateral geometry; (iii) sandstone wedges; (iv) angular clasts at the top of D15; (v) thrust fault beneath D14-D15 on the E coast of A'C, (vi) unconformity surface in Fig.3.52A beneath the Upper Dolomite (green line); and (vii) the sharp bases of D14-D18.

Sandstone wedges:

Disagreements by previous authors highlights that the origins of sandstone wedges is controversial. The author who proposed mass-flow processes of the diamictites suggested the sandstone wedges formed by subaqueous gravitational loading of sand into diamictite in a response to reverse density gradients (Eyles and Clark, 1985). By contrast, others suggested that these structures formed as a result of contraction cracks in a periglacial environment (Kilburn et al., 1965; Spencer, 1966; 1971, pp.52; Spencer, 1985; Hambrey and Alean, 2016, Fig. C.16b). Spencer (1971) interpreted the sandstone wedges as periglacial features, formed as a result of contraction cracks caused by different temperatures, for example during summer (-20˚C) and winter (-50˚C). Based on Hambrey and Alean (2016), there are two types of the clastic dykes in glacial environments: (i) subglacial dykes formed by injection of a soft sediment into a fissure extending into the beds beneath the glacier; and (ii) periglacial dyke (sandstone wedges here) that filled with sand in exposed areas in front of a glacier.

According to the new data in this study the sandstone wedges within the PAF are more likely to have formed as contraction cracks than by gravitational loading because: (i) they occur at 25 stratigraphic horizons and show similar event sequences at the top of the diamictite beds or fine-grained siltstone; (ii) they must all have formed by similar mechanisms and conditions; (iii) they consist of identical lithological composition, fine to medium-grained sandstone, in all stratigraphic horizons; except few horizons which contains fine-grained pebbles; and (iv) several of them have frost-shattered clasts within the polygonal shapes of the sandstone wedges. It is impossible to form frost-shattered clasts by loading or subaqueous processes: they need subaerial exposure, in cold and dry conditions, which is not present in the mass-flow or floating-ice environments. Thus, the only possibility which remains is periglacial.

The diamictite beds are more likely to have formed by grounded-ice and the interbeds were formed during ice-sheet oscillation or melting ice. Most observed characters (Table.3.6) favour a grounded-ice hypothesis.

Both massive and weakly laminated diamictite (a-i) in Fig.3.52B could be formed the lifting of an ice-sheet at high sea level at the edge of the ice-margin and drop it down at low sea level (Fig.3.76).

(f) Upper Dolomite lithofacies (UDL)

This lithofacies separates the 'dolomitic diamictite-sandstone lithofacies association' below and the 'arenaceous diamictite-brown sandstone lithofacies association' above. It is lacking in extrabasinal clasts, similar to the Main Dolomite at the top of the Great Breccia. However, it is different from it in thickness and is less uniform in lithology. The UDL is exposed along the whole outcrop of the Garvellach Islands, except DC.

i. Contacts

The lower contact of the UDL with the underlying D18 is sharp on the E coast of GE. To the W, after D18 and the sandstone below it are cut-out, then the contact becomes sharp and irregular with D16-D17 in GE inland (Fig.3.69). On BaT, the UDL has a sharp basal contact with fine laminated siltstone; this bed is lenticular and in less than 100m towards the W it dies out and the boundary of the UDL is sharp and irregular with the sandstone beds below. The sandstone shows some current movement recorded by ripple marks (Fig.3.64) and is continuous towards the W until it dies out before the W coast of A'C. On the W of EaN, the lower contact of the UDL is sharp and irregular with D15 (Fig.3.52A).

Figure 3.69: Lower contact of the UDL with the underlying D16-D17, GE inland.

The upper contact of the UDL with D19 is sharp and irregular everywhere, except in the E and W coast of EaN. In these two places, there are a fine-laminated siltstone between the UDL and D19 (Fig.3.70, 6.1g).

Figure 3.70: D19 overlying fine laminated siltstone, on the E coast of EaN.

ii. Lithology

The lithology of the UDL is heterogeneous vertically and horizontally, and varies in thickness from place to place. Its thickness changes between 10m to less than 3m. On the E coast of GE, the UDL consists of

structureless thick bedded dolomite and its thickness is about 6.5 m. However, on the E side of BaT it consists of cream coloured dolomite, fine-grained, relatively pure, poorly bedded and about 10m thick; while in the W side the dolomite is often a rusty yellow colour, its thickness less than 4.5m, usually arenaceous and well-bedded. In GE inland, the base of the dolomite contains sandstone clasts (Fig.3.71). The contact between the clasts and the dolomite matrix is sharp. Also, in places the dolomite includes some signs of columnar structures (Fig.3.72), similar to columnar microbial structures within the Main Dolomite lithofacies. However, nobody has recorded microbial structures before in this level. In addition, in one place of GE inland, there are lonestone at the base of the UDL coinciding with the lower contact (Fig.3.73).

On the E coast of A'C, the UDL is divided into two: (a) the lower massive dolomite; and (b) the upper bedded dolomite, separated by a sharp contact (Fig.3.74). The lower unit is discontinuous and dies out in few tens of metres and is rich in sandstone veins. Also, it shows some structures that are possibly microbial, but it is hard to say that due to metamorphism and tectonic imprint; even in thin sections the original texture is not clear. The upper unit is well bedded, fine-grained, yellow weathering and creamy on fresh surfaces.

Figure 3.71: Sandstone clast within the UDL in GE inland about 200m E of BaT. Scale bar is 15 cm.

Figure 3.72: Columnar structure within UDL in GE inland, similar to the typical columnar microbial (stromatolite) structures (Le Ber et al., 2013). Scale bar is 15 cm.

On the W coast of A'C, the lithofacies again consist of two units. However, the units here are quite different compare with the E coast. The lower unit is bedded, shows some soft sediment deformation,

about 1m thick, and there are some signs of fine laminated structure organisation; the upper unit is massive, disorganised, with an irregular top surface, is about 1-1.5m thick, and shows some brecciation at the top (Fig.3.75).

iii. Sedimentary structures

The sedimentary structures within the UDL are lonestone, massive bedding, planar bedding, and brecciation. The cut-off of D16-D18 marks an unconformity below the Upper Dolomite Lithofacies (Fig.3.52A). Owing to the presence of permafrost sandstone wedge and frost-shattered clasts at the top of D14-D15, imply subaerial exposure.
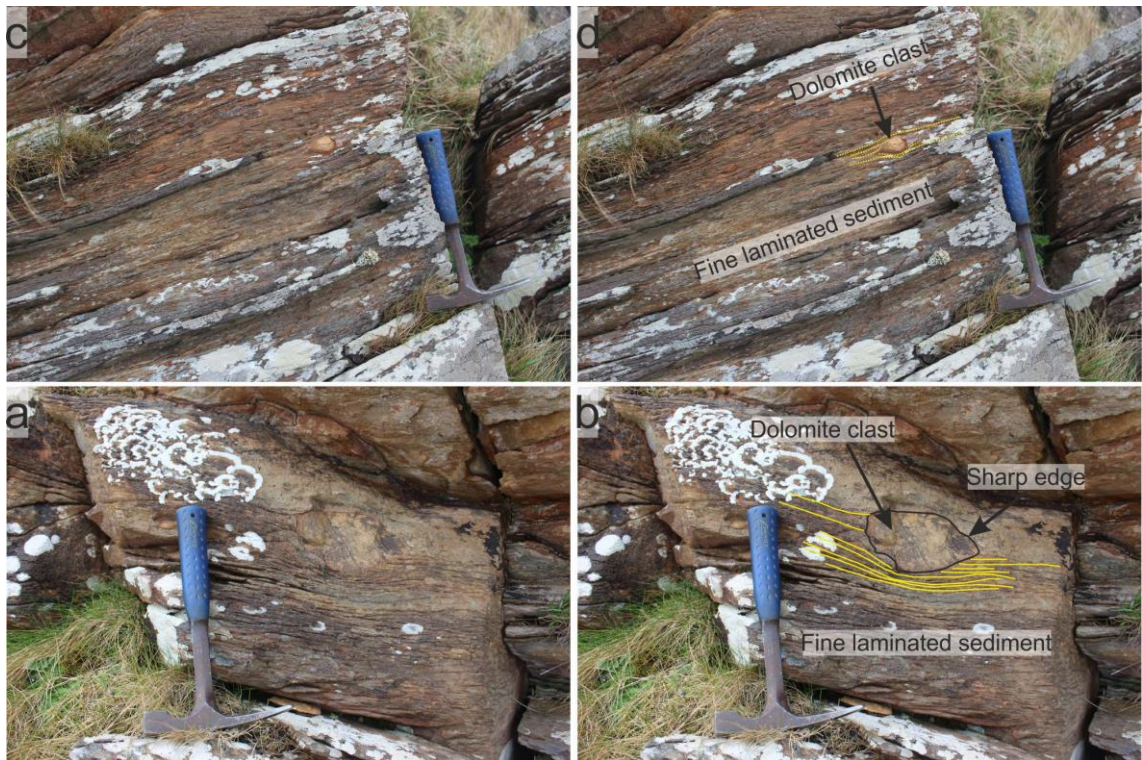
Figure 3.73: Lonestones at the base of the UDL coincide with the lower contact in GE inland, all photos are in the same horizon and in the same place.

Figure 3.74: Two separate, lower massive and upper bedded, units of the UDL on the E coast of A'C. The yellow line is the contact between units and the red line is the lower contact of the UDL with underlying sandstone bed.
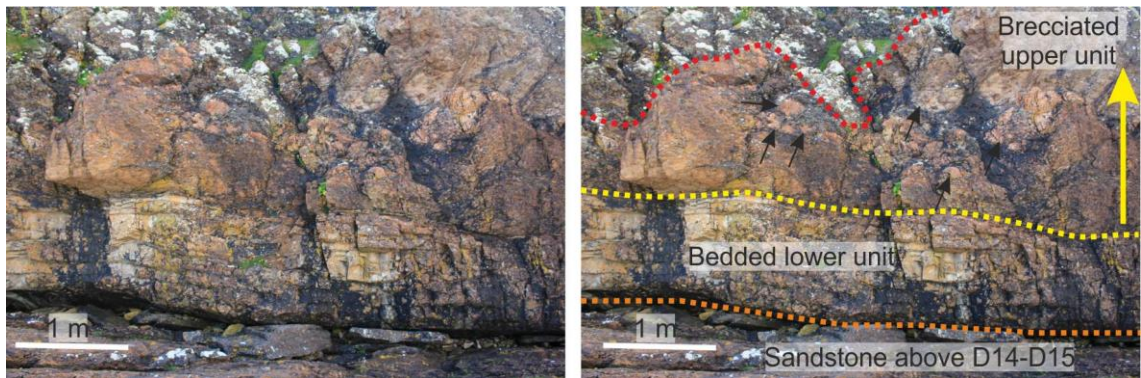
Figure 3.75: UDL on the W coast of A'C shows two units. The orange dashed line represent the lower contact between the lower bedded dolomite unit of the UDL and the underlying sandstone. The yellow line shows the contact between lower and upper units of the UDL. The red line is the upper contact of the UDL with D19. Black arrows are the brecciated clasts within the upper part of the UDL, and the yellow arrow shows the coarsening upward of the clasts.

Table 3.6: Features and lithofacies that occur within the dolomitic diamictite- Sandstone lithofacies association (D14-D18) with interpretation summary.

Features/beds	Lithofacies	Subaqueous mass-flow	Floating ice	Grounded ice	More likely in this study
Diamictite beds	D14-D18	Possible	Unlikely	Possible	Grounded-ice
Highly discontinuous laterally geometry	D14-D15 Fig.3.52B	Possible	Unlikely	Possible	Grounded-ice
Sandstone wedges	Top D15 and D18	Unlikely	Unlikely	Possible	Grounded-ice (Periglacial)
Angular clasts	Top D15	Unlikely	Unlikely	Possible	Grounded-ice (Periglacial)
Thrust structures	Base D15 on A'C	Possible	Unlikely	Possible	Grounded-ice (Glaciotectonism)
Unconformity Above LA	Correlation Fig.3.52A	Unlikely	Unlikely	Possible	Grounded-ice
Sharp bases of diamictite beds	D14-D18	Possible	Unlikely	Possible	Grounded-ice
Long lateral correlation of diamictite beds	D14-D15	Possible	Possible	Possible	Grounded-ice

(1) Stratified diamictite is deposited under a floating ice-sheet

Ice-bergs

Water level

Ice-sheet

Rain out

Stratified diamictite

Rain-out/ice rafted diamictite
(possible 'lift-up' of ice margin)
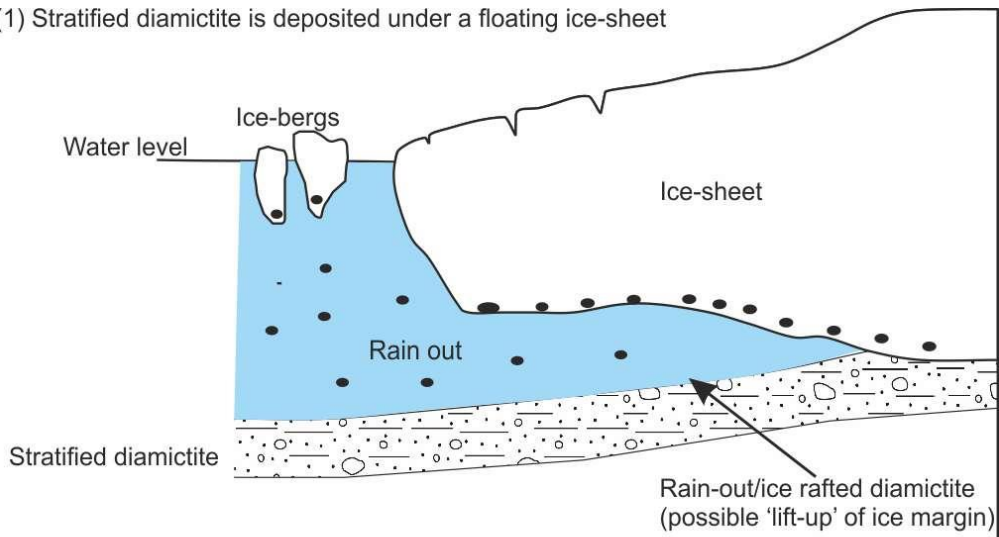
(2) Massive diamictite deposited in contact with grounded-ice

Ice-sheet

Water level

Massive diamictite
Stratified diamictite

Massive diamictite deposited
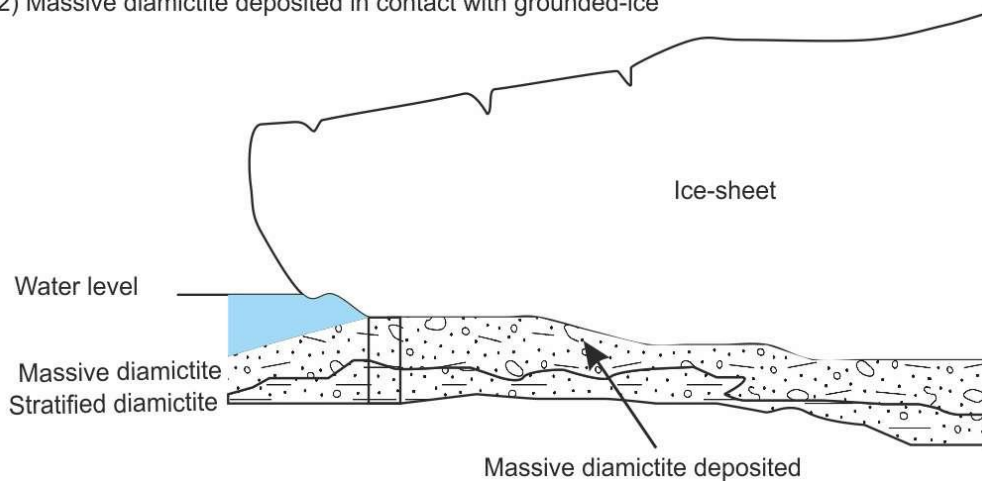
Figure 3.76: A cartoon explaining the formation of the continuous and discontinuous (massive and faint laminated) diamictite beds in Fig.3.52.

(g) Depositional environments of the UDL

The origin of the dolomite beds within the PAF is uncertain: until now nobody has provided plausible evidence about the mechanism of formation of these dolomites. In interpreting the dolomite at this stratigraphic level, the features to be considered are: (i) lack of extrabasinal clasts; (ii) presence of lonestone; (iii) presence of sandstone clasts; (iv) growing microbial structures; (v) sharp and irregular upper and lower contacts of the lithofacies; (vi) bed and unit's geometry; and (vii) brecciated clasts at the upper most part of the lithofacies on the W coast of A'C.

The main questions are whether this dolomite is primary (direct precipitation) or secondary (detrital or diagenesis), marine or lacustrine, and subaerial or subaqueous. Retallack (2011) interpreted the Nuccaleena Formation in S Australia as a loess deposit based on: (i) the presence of loess characters such as, climbing-translatent cross-stratification, linear dunes, and various types of red clay within palaeosols; (ii) lack of marine evidence such as, stromatolite, abundant sparry calcite, and crystal pseudomorphs of gypsum and barite found in other cap carbonates. However, the presence of microbial structures, lonestones, and fine-grained carbonate the Upper Dolomite rules out subaerially Loess origin. A subaqueous origin is most likely for this dolomite.

The presence of the lonestones (Fig.3.73), microbial structures (Fig.3.72) and fine laminated beds (Fig.3.73) indicate a subaqueous environment (Le Ber et al., 2013; Le Heron, 2015). There are four hypotheses to explain the lack of extrabasinal clasts in this stratigraphic level and their presence in D14-D18 below and D19 above: (i) the ice was far from Garvellachs; (ii) the source of the sediments is different, if the dolomite was detrital; (iii) the dolomite was formed by direct precipitation from the water or by microbial action; and (iv) there were no ice bergs in the Garvellachs area to provide the extrabasinal clasts. The explanation could be one of these, or all of them together. If the sea level rose by melting of the ice-sheet and the ice oscillated (retreated) far from the Garvellachs. Thus, the dolomite could represent deposition when the ice was far from the Garvellachs or in an interglacial period (Spencer, 1966). That possibly explains the presence of rare dolomite lonestone and sandstone clasts at the base and in the lower part of the UDL respectively, and that both disappear at higher stratigraphic levels within the lithofacies. Columnar microbial structures in Fig.3.72 commonly occur in water depths less than 200 m (Le Ber et al., 2013, Fig.7 and 9).

In conclusion, the UDL was formed in a subaqueous environment <200 m of water, by microbial structures, under the influence of wave action on a tidal platform.

Chapter 4 : Members 2 and 3

4.1 Arenaceous diamictite-brown sandstone LFA (D19-D32)

Strata of this lithofacies association occur in Member 2, above the Upper Dolomite (of Member 1) and below the white sandstone and arenaceous diamictites (of Member 3). The association consists of two main lithofacies, arenaceous diamictite and brown sandstone, and two minor lithofacies, siltstone and conglomerate.

4.1.1 Arenaceous diamictite lithofacies

These strata have been studied by (Kilburn et al., 1965) who numbered the diamictite beds 19 to 32, on the E coast of GE. The present author keeps using those but groups the beds as bed-sets: 19-22, 23-26, 27-29 and 30-32. The diamictite beds are interbedded with sandstone, siltstone and conglomerate.

(a) Stratigraphic position and outcrops

The diamictite beds within this lithofacies can be grouped into four bed-sets:

D19-D22 bed-set: this comprises diamictite beds 19, 20, 21 and 22. The bed-set is well defined and can be traced through the whole of the Garvellachs outcrops except DC. The thickness of the bed-set varies between 30 m and 49 m.

D23-D26 bed-set: D23-D25 are exposed throughout the Garvellachs except DC; D26 is exposed on GE and the E coast of A'C, but thins inland towards the W and completely disappears on EaN (Fig.4.1). This bed-set varies from 16 to 40 m in thickness.

D27-D29 bed-set: This bed-set of diamictite beds is exposed on the Garvellachs in four different places: on the E and W coasts of GE; on the SC of A'C; on Sgeir Leth a Chuain and on the E, W and SC of EaN. However, on the SC of GE, A'C and Sgeir Leth a Chuain just the lower contact and several metres of the lowest part of the beds are exposed, so the thickness cannot be measured. These beds are rather variable in thickness, reaching 26m on the E coast of GE, but only 10m in the SC of EaN (Fig.4.2).

D30-32 bed-set: D30 is lies above bedded sandstone that overlies D29. D30 is exposed on the E, inland and W coasts of GE and the S coast of EaN.

On the E coast of GE, D31 is located above a thick bed-set of bedded sandstone and siltstones above D30 and beneath bedded sandstone below rhythmically laminated siltstones and sandstone. D32 is exposed only on the E coast of GE.
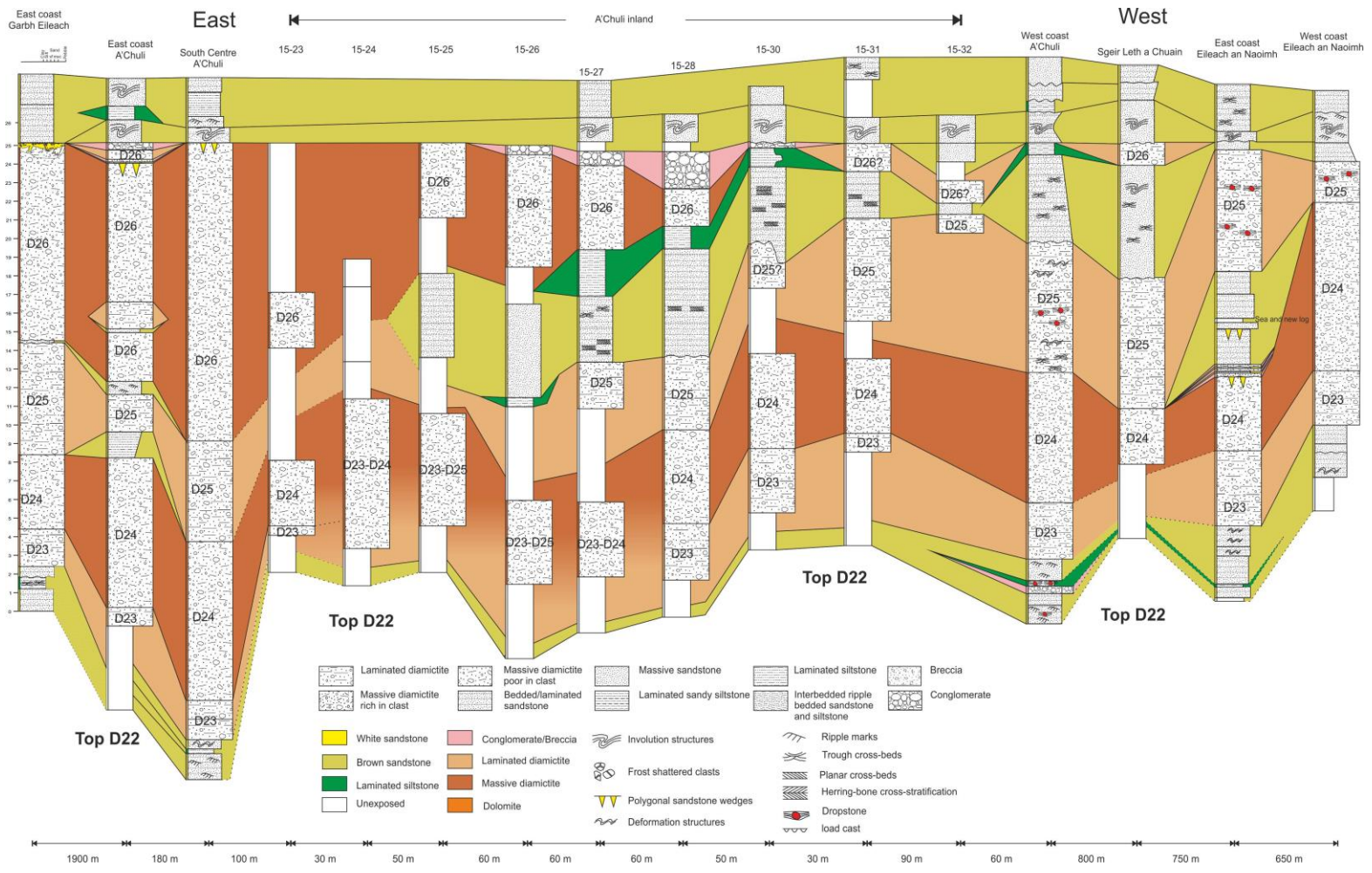
Figure 4.1: Correlation panel across the Garvellachs for D23 to D26. The base of the 'intra-bed fold sandstone' above D26 is the datum.
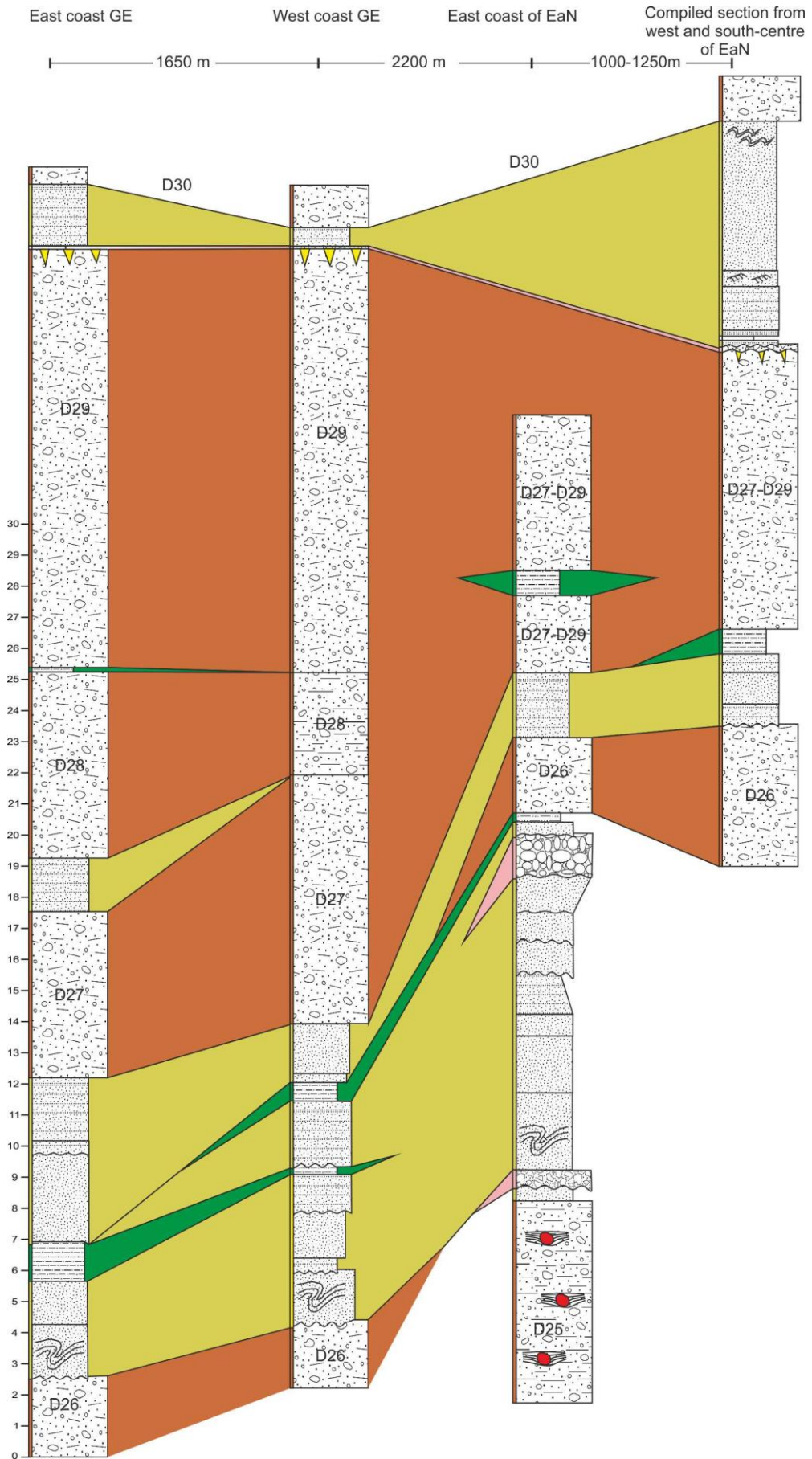
Figure 4.2: Correlation logs from the top of D26 to the top of D29. Note that the legend is the same as for Fig.4.1.

(b) Contacts

D19-D22 bed-sets: The lower contact of D19 with the underlying Upper Dolomite (UD) is everywhere sharp, and is rich in iron oxide, especially in its lower 1-2 m. One locality shows special features. This is on the W of A'C where the base of D19 is irregular and sharp with the UD (Fig.4.3), and the upper part of the UD is brecciated about 1 m just beneath D19. The amount of deformation and clast size, within this brecciated horizon, increases upward towards the base of D19. The upper contact of D22 is overlain by a complicated set of strata and structures: sandstone wedges penetrate the top of D22 and are overlain by conglomerate/breccia (Fig.4.4) and then by bedded sandstone (detail in section 6.2).

On the E coast of GE, D19 and D20 are similar, but D20 includes lenticular sandstones, while these lenses are not present in D19; also, there is a 20cm lenticular laminated siltstone between them. When this siltstone is missing, the contact looks more gradational. The contact between the two diamictite beds is, for convenience, drawn at the level of the highest bedded siltstone laminae. D20-D22 are homogeneous and unbedded and have identical lithologies and clast contents, but can be clearly separated from each other by bedded sandstone. The thickness of these beds is less than 0.5 m and they have sharp top and bottom contacts with the diamictite beds. Both sandstone beds (below D21 and D22) can be traced across the width of the raised beach outcrop (25 m), on the E coast of GE. However, because of the incomplete inland exposure, the thin sandstone beds which separate D19-D22 cannot be traced far inland. The next easily accessible and well exposed place to see this bed-set is on the E coast of A'C. There, almost the entire thickness of the bed-set is completely exposed and sandstone beds are notably absent. Thus, this diamictite intervals appear to be homogeneous and D19-D22 cannot be separated from each other.

Diamictite beds D19-D22 are completely exposed on the W coast of A'C and on the E and W coasts of EaN. Thin sandstone beds which could be correlate with those present on the E coast of GE are again absent in these localities. However, at some of these localities, thin (less than 30 cm) lenticular beds of siltstone and sandstone occur at various stratigraphic intervals within this bed-set.

D23-D26 bed-set: The lower boundary of this bed-sets shows a sharp contact with the top of sandstone beds that overlie D22. This bed-set of diamictite beds, with its interbedded sediment, varies between 22-40 m in thickness through the Garvellach outcrops. Part of this variation is probably caused by the thinning laterally to zero of D26 and the sandstone between D25 and D26 on A'C (Fig.4.1). The lateral variation of the diamictite beds within this group is obvious, but D23-D25 are more persistent than D26. Also, distinguishing between the diamictite beds of this bed-set is easier on the E coast and inland of A'C and on the E and SC of EaN, because in those places more interbeds are present than on the E and W coasts of GE.

In three places - the E and W of GE and the SC of A'C - D23-D26 form one block without any interbeds; but the three diamictites can be distinguished because of the different size and number of clasts and the presence of lamination (in D23 and D25) or massive structure (D24, D26).
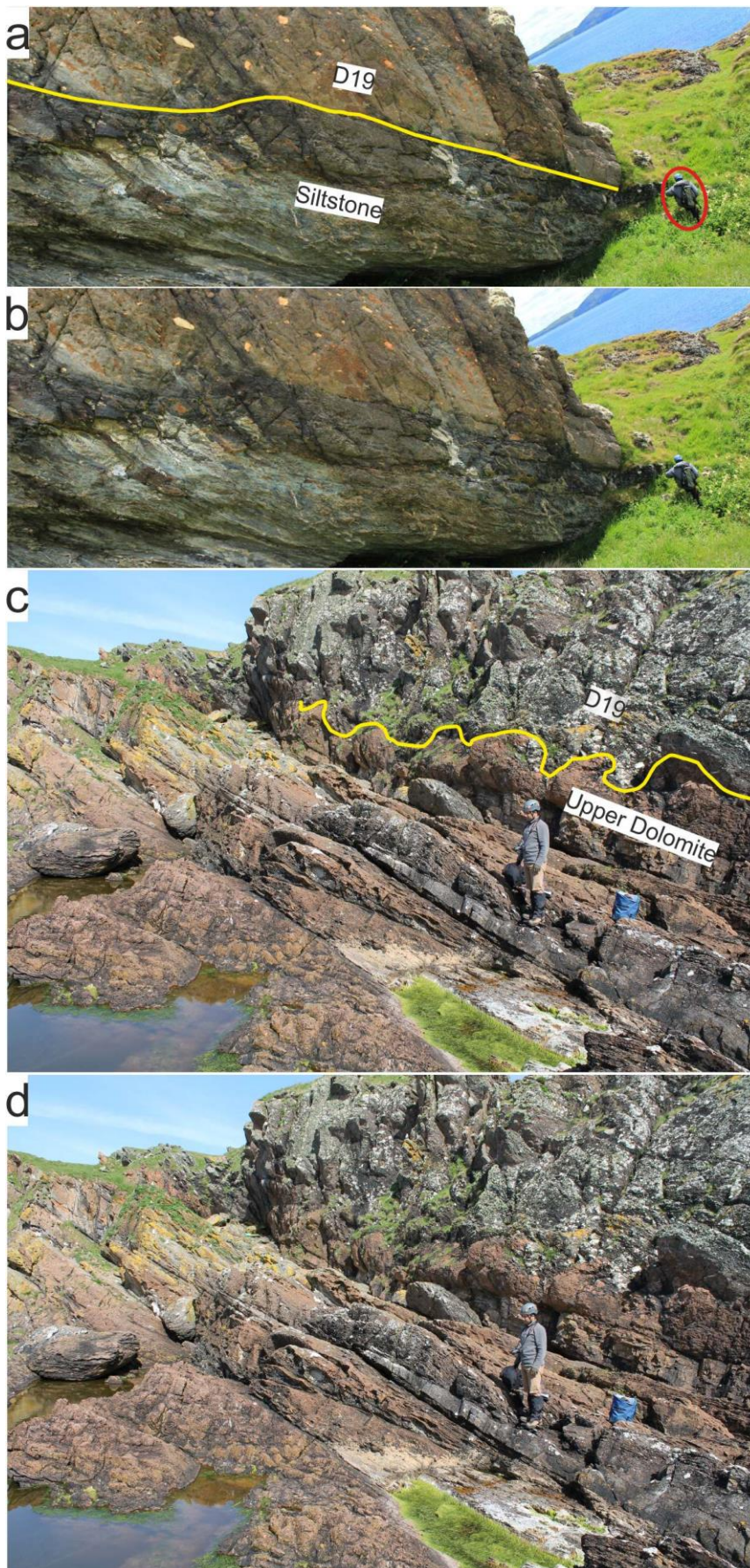
Figure 4.3: (a and b) show the base of the D19 with the underlying siltstone beneath on the W of EaN to show the difference with the irregular base of D19 (c and d) with the underlying Upper Dolomite on the W cliff of A'C.
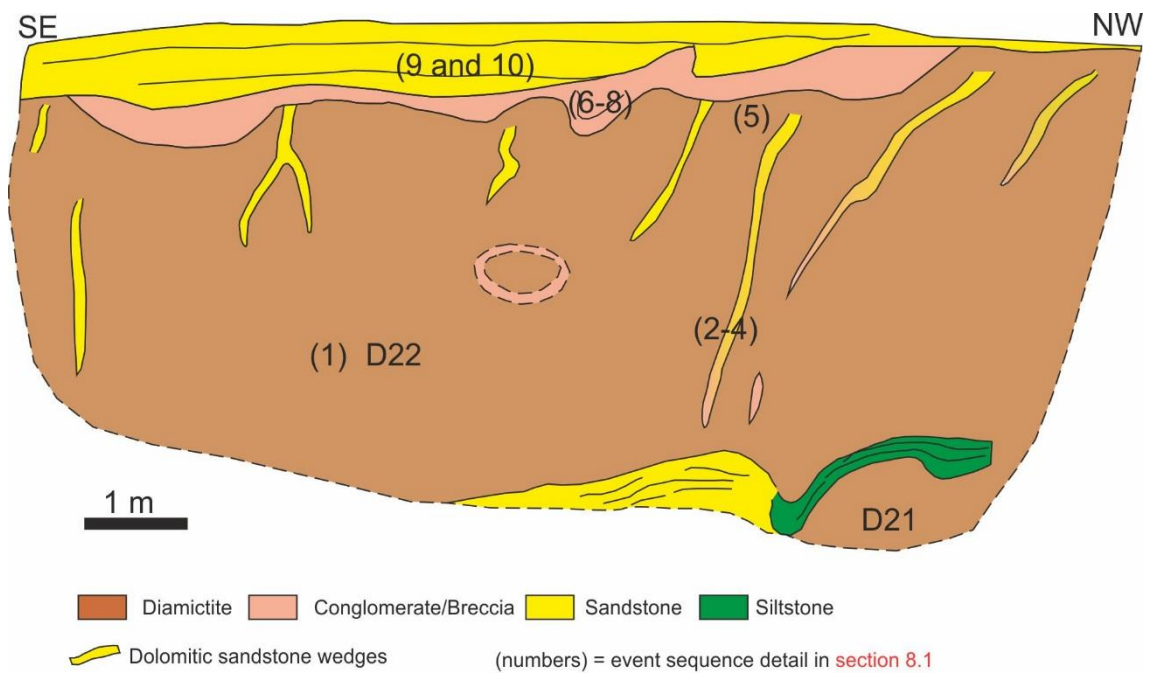
Figure 4.4: Complicated upper contact of D22 on the E coast of GE. Sandstone wedges penetrate D22, and are truncated by intra-bed folds.

The lower and upper contacts of D24 with D23 below (Fig.4.1) and D25 above are everywhere sharp. On the E coast of EaN, D24 is overlain by a 5m thick interval of conglomerate, sandstone and siltstone beds; sandstone wedges penetrate the top of D24; a second level of giant wedges occurs 2m above the top of D24 (Fig.4.1).

On GE and the E coast of A'C, D26 has a sharp and conformable base with D25; and in these places, D26 varies between 10 to 26 m in thickness (Fig.4.1). The upper contact of D26 is also sharp with the overlying sandstone beds, on GE and the SC of A'C, where they contain intra-bed folds.

A total of 16 detailed sedimentary logs have been made to investigate the lateral changes in D26 (Fig.4.1): one from the E coast of GE, 11 logs on A'C (localities 23-32 are from inland), one on SLaC and one on the E coast of EaN. On A'C, D26 thins from the SC coast section (16.5 m) towards the W and in locality 30 is almost absent, in a lateral distance of 550 m (Fig.4.1). In the same distance, D25 varies between 2 m to 6 m. In addition, a thick bedded sandstone appears between D25 and D26, between locality 15-24 and 15-25 and thins to almost zero at locality 15-32 (Fig.4.1), before thickening again towards the W and then thinning towards the E coast of EaN. These sandstone beds are medium-grained, well sorted and white. On the W of A'C, the base of the sandstone is very irregular and cuts down vertically into D25 about 1.5 m (Fig.4.5).
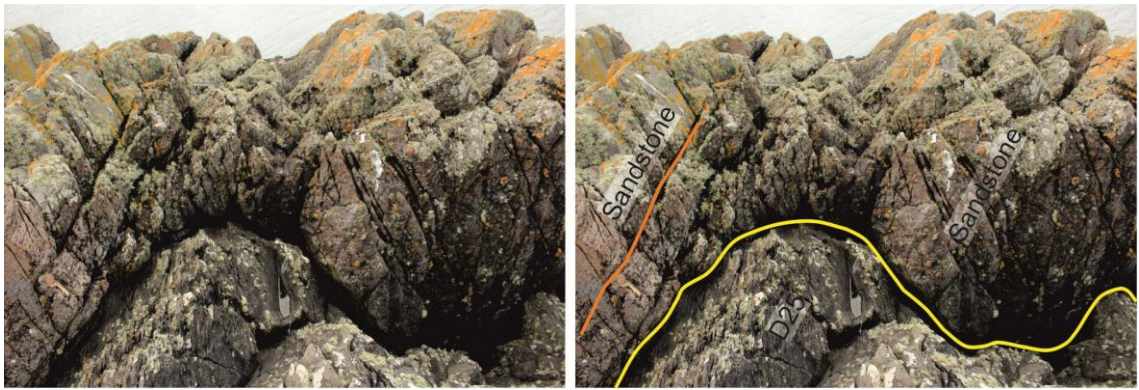
Figure 4.5: Irregular base of the sandstone bed above D25 on the W coast of A'C about 100m towards E. The orange line in the right photo is the regional bedding dip, and the yellow line represents the steep contact between D25 below and the sandstone bed above.

The upper boundary of D26 is complicated (Fig.6.14): it is overlain on GE and in the SC of A'C directly by the involuted pebbly sandstone. On the E coast of A'C, D26 is separated from a second involuted sandstone by a 3 m thick series comprising: 5 cm sandstone, 50 cm diamictite, 40 cm dolomitic pebble bed, 130-150 cm sandstone and 80 cm laminated siltstone beds. On the E coast of A'C, a beautiful series of sandstone wedges penetrate down into the top of D26 (Fig.4.6).
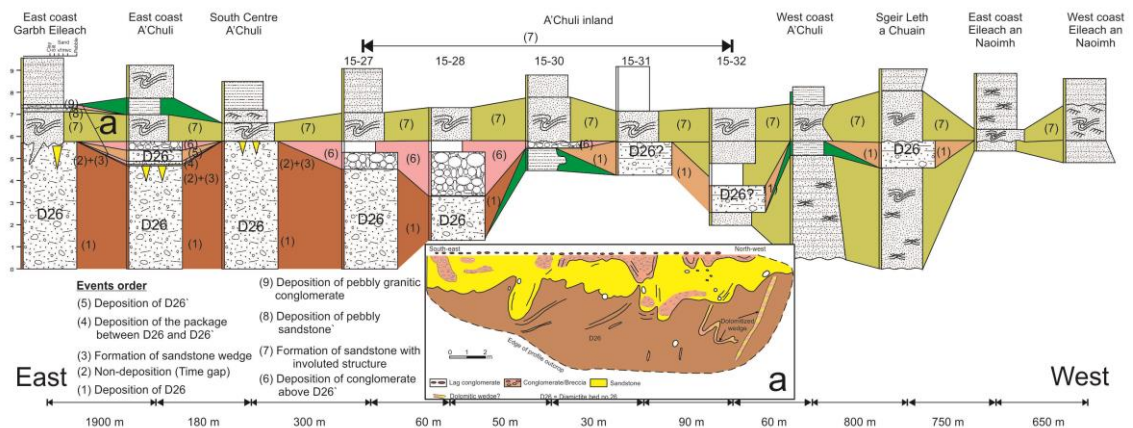
Figure 4.6: Correlation panel for the top of D26 throughout the Garvellachs. The inset diagram 'a' shows the stratigraphic relationships at the top of D26 on the E coast of GE (the left hand most column). Diagram 'a' can be seen at a bigger scale in Fig.6.14.

D27-D29 bed-set: The lower boundary of this bed-sets is sharp with the bedded sandstone above D26 (Fig.4.2). The bed-set is variable in thickness, reaching 26 m on the E coast of GE, but only 10 m in the SC of EaN. The bed-set is underlain a group of sandstone and siltstone beds everywhere, except on Sgeir Leth a Chuain where just sandstone is present. Well-developed polygonal sandstone wedges penetrate the top of D29 and are truncated by a sharp upper contact.

The lower contact of D27, on the E of GE, is partly transitional with the top of the underlying bedded sandstone; the topmost 60 cm of the sandstone bed is poorly bedded, whilst the lower 20 cm of the diamictite bed has some thin siltstone laminae which lie parallel to the bedding in the sandstone. The upper contact of D27, in the same locality, is marked by a sharp boundary with bedded sandy-siltstone sediment (170 cm thick). The lower contact of D28 is gradational with the sandy-siltstone bed.

D28 and D29 are identical in all respects and the contact is gradational between them, but on the E coast of GE they can be separated from each other by a 5cm thick and discontinuous bedded horizon. The upper contact of the D29, which coincides with the upper contact of the bed-set, is again complicated (detail in section 6.2); there are different sized sandstone wedges penetrating the top of D29 and these wedges are capped by conglomerate patches (Fig.4.7).

Figure 4.7: complicated top contact of D29 on the E coast of GE. The yellow line in the right photo is a thick sandstone wedge, the white lines represent thinner polygonal sandstone wedges chalked in pink on the outcrop (all penetrating D29), and the red circle represents a patch of conglomerate/breccia at the top of D29. Ruler is a 1 m.

In the SC of A'C, the base of D27 is again gradational with the underlying stratified sandstone and there are no interbeds there to separate diamictite beds 27 to 29 from each other. On EaN, D27 seems to be absent, and D28-D29 rests directly on the underlying bedded sandstone with a sharp contact. These diamictite beds have similar lithologies to D28 and D29 on GE and A'C, but they contain many more bedded horizons here than in those localities.

On EaN D28-D29 contains several large areas within which the matrix of the diamictite is very dolomitic and dolomite clasts outnumber granites. On the E of EaN, at the top of D28-D29 there are sandstone wedges which penetrate the diamictite bed (Fig.3.8), especially in the areas in which dolomitic patches are present. These patches have gradational contacts with the matrix of the diamictite bed.

Figure 4.8: Dolomitic patch at the highest stratigraphical level in D28-D29on the E coast of EaN. Within the patch, there are polygonal sandstone wedges which penetrate the diamictite. The yellow line is the bedding dip, the yellow arrows are sandstone wedges, and the geologist for scale.

D30-D32 bed-set: The lower contact of D30 is sharp and undulating marking the change from the underlying well-bedded sandstone to a massive diamictite bed. On the S coast of EaN, D30 is

homogeneous and unbedded and has a sharp lower contact with the underlying siltstone. On the E coast of GE, the upper boundary of D30 is sharp and undulating with the overlying bedded dolomitic sandstone (Fig. 596). On the W coast of GE and S of EaN, the upper boundary of D30 again is sharp and undulating with the fine-laminated siltstone. On the E coast of GE, D31 has sharp lower and upper contacts. Its outcrop extends towards the W, but wedges out to zero beneath the base of the overlying Member 3 (Fig.4.9) before reaching the W coast of GE.

(c) Lithology

D19-D22 bed-set: These diamictites are quite different from the dolomitic diamictites of Member 1. Their matrix is arenaceous and has a lower carbonate content than diamictite beds D1-D18. The matrix colour is blue-grey on fresh surfaces and light or dark grey coloured on weathered surfaces.

On the E coast of GE diamictite bed D19 is 8.5 m thick and its matrix is slightly more pelitic than D20-D22; in addition, it contains (1 m thick) laminated siltstone at the base of the diamictite. D20-D22 have a siltier matrix than D19 and include different types of clasts. Intra-basinal clasts still predominate but extra-basinal clasts form 30% to 40% of the assemblage.

At the E of EaN, a discontinuous series of blue laminae, rich in iron ore minerals, occur through up to 1 m of D19 and lie parallel to the top of the diamictite bed. A similar, but much less continuous horizon, occurs within this bed-set of diamictite beds at the W of EaN.
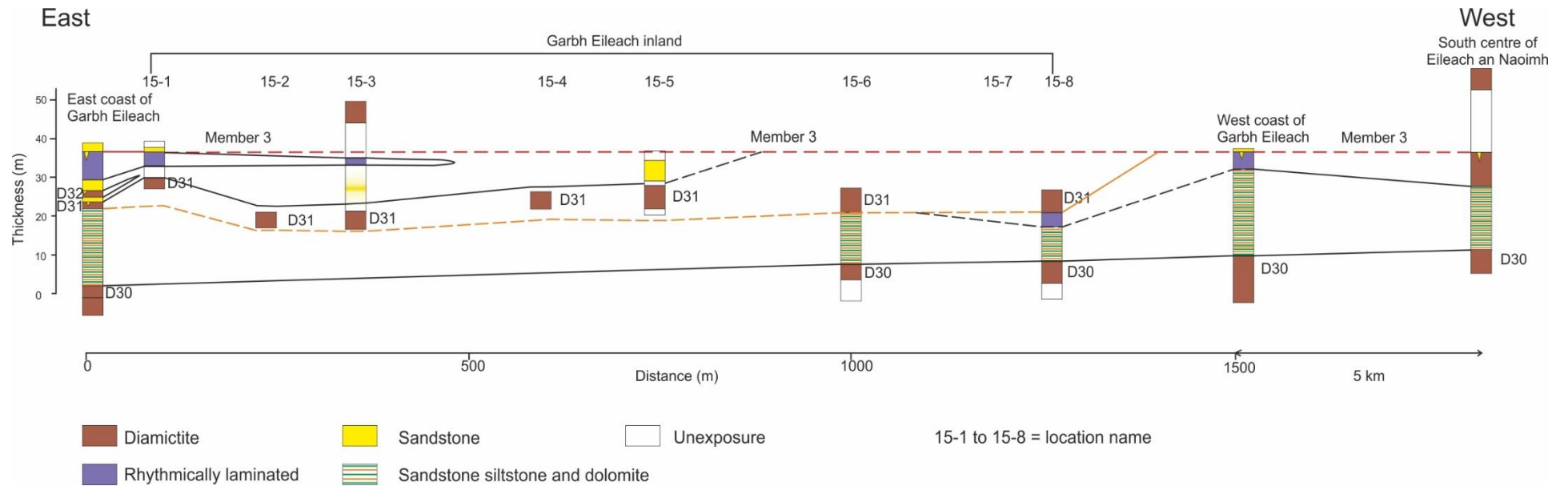
Figure 4.9: Correlation between stratigraphic logs throughout the Garvellachs from the top of D30 to the base of the Member 3.

D23-D26 bed-set: These diamictite beds resemble D19-D22 in lithology, but have a more arenaceous matrix. Also, extra-basinal clasts and intra-basinal clasts are equal in number. D23 can be separated in the field from D24 by colour (Fig.4.10); the former is a lighter grey colour than the latter. Also, D23 and D25 are laminated and consist of a fine-grained siltstone matrix (Fig.4.11) and contain sparse clasts. The thickness of individual laminae of D25 vary from 10 mm to less than 1 mm. The common size of the clast within D23 and D25 are pebble grade, but in places there are boulder size clasts such as, on the E coast of EaN. Both D23 and D25 are iron rich (10-15%, majority magnetite, some pyrite; 20% almost exclusively magnetite, respectively). The prismatic compass swings through up to 8° for hand specimens of D25. By contrast, D24 is quite normal and is a massive and homogeneous diamictite and with a fine-grained matrix containing pebble to boulder size clasts. The thicknesses of D23, D24 and D25 are variable, respectively, from 1 to 4.5 m, 4 to 10.5 m and 2 to 7 m along the outcrops of the Garvellachs. D26 is more massive and consists of a sandy-siltstone matrix (Fig.4.13A-B); it contains intra and extra-basinal clasts; it is easy to distinguish D26 from D25, because the latter is laminated while the former is massive.

Figure 4.10: Contact between D23 and D24 (yellow line) in A'C inland. The contact is sharp and clear because of the colour contrast between the two diamictite beds and D23 is laminated while D24 is massive. Ruler is 1 m scale.
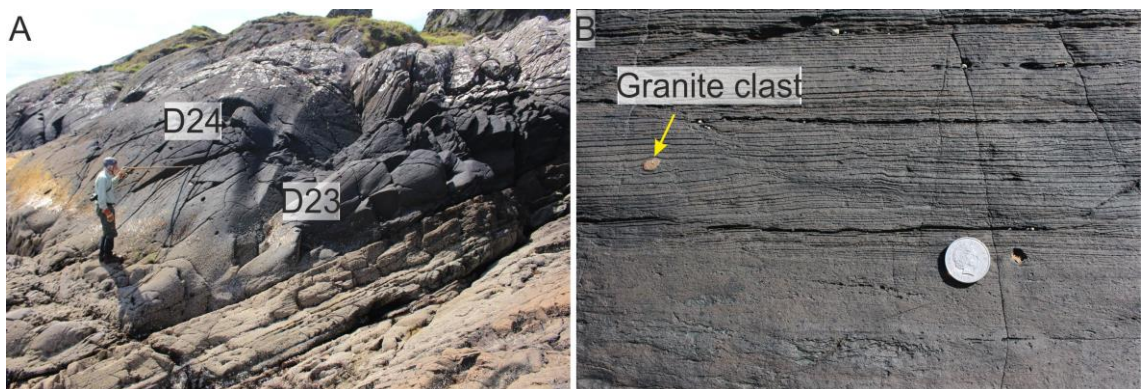
Figure 4.11: (A) Laminated D23 on the E coast of GE; the geologist (Anthony Spencer) pointing to the contact between D23 and D24. (B) Laminated D25 on the SC of the EaN. The holes represent weathered dolomite clasts; protruding and more resistant clast is granite.

D27-D29 bed-set: On the E coast of GE, D27 is homogeneous, and consists of well cleaved siltstone matrix containing relatively small numbers of clasts. Extra-basinal clasts are rare and dolomites larger

than 2 cm in diameter are uncommon. By contrast, both D28 and D29 have a coarser grained matrix, sand grade is dominant, and they contain various types and sizes of clasts; extra-basinal fragments up to 60 cm in diameter are common. D28 and D29 contain pebble, cobble and boulder sized clasts in larger numbers than any of the underlying diamictite beds in the Garvellachs succession (apart from the Great Breccia). Also, they are the first diamictite beds in the succession in which extra-basinal clasts outnumber dolomite clasts.

The tripartite division of this bed-set of diamictite beds cannot easily be recognized elsewhere in the Garvellachs. However, on the W coast of GE and on A'C, a lower diamictite bed with few clasts (corresponding to D27) can be distinguished from an upper, sandier diamictite bed with abundant clasts (corresponding to D28-D29).

D30-D32 bed-set: D30 is similar in lithology to D28-29 but contains many fewer boulder sized granite clasts than the latter and contains almost equal numbers of dolomite and extra-basinal clasts. This diamictite bed has a relatively even thickness between 6.3 - 11.3 m along its 4.1 km long outcrop. On the W coast of GE, D30 contains a boulder size (3X5m) clast composed of beds of sandstone, siltstone and dolomite which are folded in a complicated fashion and almost rests on the base of the diamictite bed (Spencer, 1971, Fig.39b).

D31 and D32 have a silty sandstone matrix and extra-basinal clasts form a greater proportion than intra-basinal clasts. At the western end of its outcrops on GE, D31 can be subdivided into a lower part with more pelitic matrix and upper part in which clasts are more abundant and the matrix is a homogeneous sandstone.

(d) Sedimentary structures

The sedimentary structures of the diamictite beds will be described in stratigraphic order, from the base to the top.

D19-D22 bed-set: At the top of D22 is a horizon of sandstone wedges. This horizon is beautifully exposed and arranged in a well-developed polygonal fashion on EaN (Fig.4.12). The wedges penetrate the top of D22 up to 2 m depth; the width of an individual wedge is from few centimetres to tens of centimetres, and the size of the polygonal shapes are about '0.5-2'm across. In addition, small numbers of sandstone wedges are present at the top of the D22 on the E coast of GE and on the W coast of A'C.

On the W coast of GE, a few discontinuous sandstone laminae in the top of D20, in the lower half of D21 and in the centre of D22. These are less than 50 cm thick and have sharp top and bottom contacts with the diamictite beds.

On the E coast of GE, at the top of D22 is an involuted pebble sandstone (Fig.4.4), which is overlain disconformably by planar bedded sandstone; and sandstone wedges penetrate as much as 3m down into D22 from beneath the involuted sandstone.

Figure 4.12: Polygonal sandstone wedges penetrating the top of D22 on the S-W of EaN.
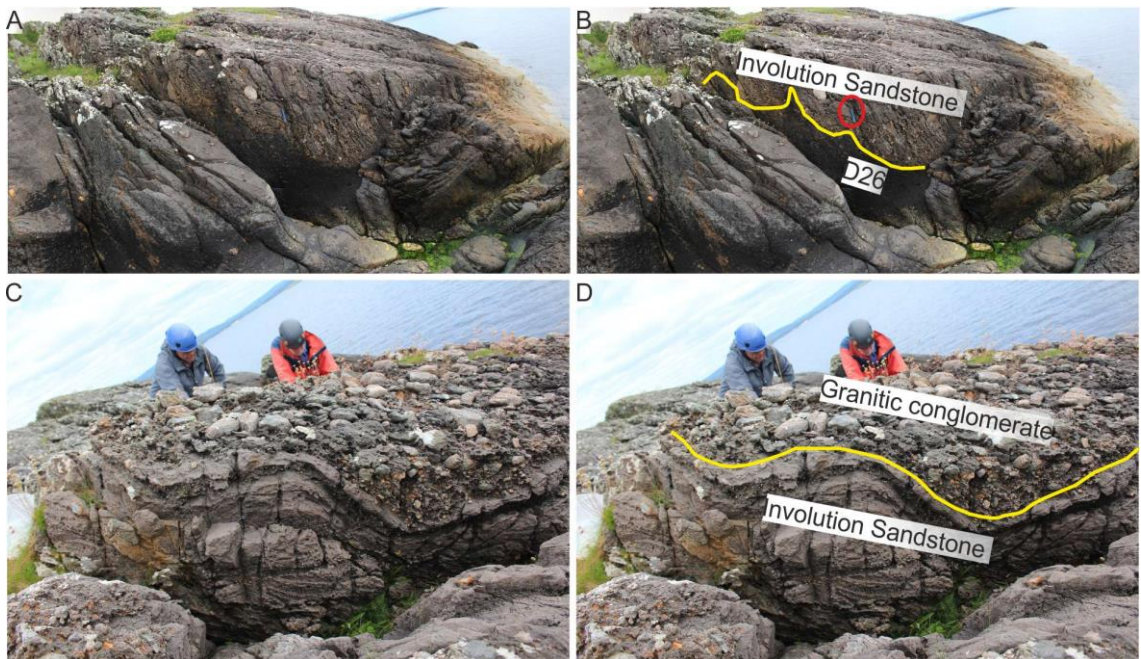
Figure 4.13: (A and B) the yellow line is the contact between D26 and the intra-bed folds sandstone downfold on the E coast of GE. Geological hammer for scale. (C and D) The contact between intra-bed folds and the overlying granitic conglomerate on the E coast of GE. Geologist for scale.

D23-D26 bed-set: D23 and D25 both have a finely laminated matrix; and in both clasts occur sparsely. On the E and W coast of EaN, out-sized clasts have been recorded within fine laminated D25 (Fig.4.14). The lithology of the clasts are granite, quartzite and dolomite. The lamination underneath the clasts are bent and deflected.
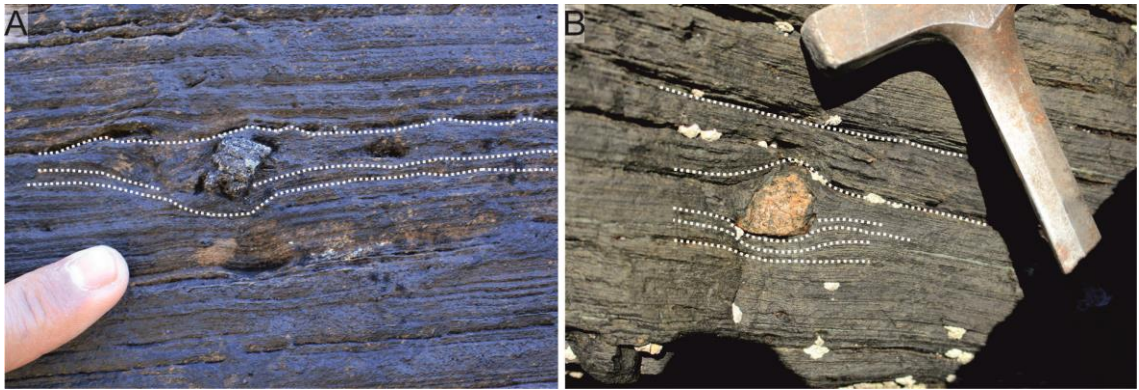
Figure 4.14: Outsized clasts within laminated D25, (A) on the E coast of EaN, quartzite extrabasinal clast within laminated siltstone matrix; (B) on the SC of EaN, dolomite intrabasinal clast within laminated siltstone matrix.

On the E coast of GE, sandstone wedges penetrate down into the top of D26 (Fig.6.14); also, a very well exposed series of these wedges penetrate down into the top of the same diamictite on the E coast of A'C (detail in section 6.2).

On the E coast of A'C, there is about 1.3 m of coarsening upward, fine to medium-grained, sandstone separating D24 from D25 (Fig.4.1); and another sandstone bed separates D25 and D26 and contains trough cross-bedding. On the W coast of A'C, the sandstone bed that overlies D25 is cross-bedded and shows palaeocurrents towards the N-NE (Fig.4.1). Also, the base of this sandstone is irregular where the bed has load casts or cuts down in places into the underlying laminated siltstone. Moreover, this sandstone is continuous in the W of A'C towards the SW and is absent only on the E coast of EaN, where the involuted sandstone rests directly on D25.

On the E coast of EaN, D24 is overlain by a conglomeratic sandstone, then a siltstone and then another sandstone before the base of D25 is reached. Both these bedded sandstones have sandstone wedges beneath them (Fig.4.1).

D27-D29 bed-set: On the E coast of GE, the top of D29 is penetrated by sandstone wedges (Fig.4.7) and overlain by well bedded sandstone (Fig.6.1e). In places, there are patches of conglomerate between the bedded sandstone and D29 (Fig.4.7), but these patches are exposed only at low tide.

D30-D32 bed-set: On the E of GE, small lenses of sandstone are present in the lowest 1.5 m of D30 (Fig.4.15); the sandstone lens has a sharp edge with the matrix of the diamictite bed. Also, discontinuous beds are present within D30; the most prominent is a discontinuous conglomerate level, which is up to 60 cm in thickness and lies parallel to the bedding about 3 m from the base of the diamictite bed.
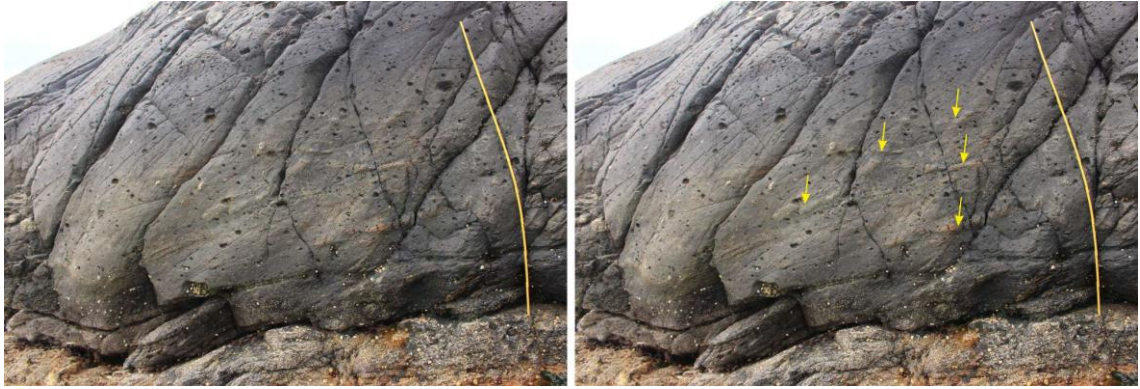
Figure 4.15: Yellow arrows in the right-hand side are sandstone lenses at the base of the D30 on the E coast of GE. Ruler is 2 m scale.

On the E coast of GE, at the top of D31, there are downfolds and basin shaped structures; these are disconformably overlain by the base of the planar bedded sandstone beneath D32 (Fig.4.16). The basin shapes are composed of thin layers of interbedded conglomerate and sandstone.

Inland, in the C of GE and about 400 m before the W coast, there are sandstone wedges penetrating the top of D31, but identifying sandstone wedges is difficult because of their similarity in lithology to the sandy matrix of the diamictite bed.

4.1.2 Brown sandstone lithofacies:

This lithofacies occurs as bed-sets between diamictite beds or within them. The sandstone is labelled 'brown' because most are dolomitic and yellowish brown or on their weathered surfaces are brown, but on fresh surfaces they are white; in addition, minor white sandstone beds occur.

(a) Stratigraphic position and outcrops:

Bed-set between D22 and D23: This bed-set is exposed in five places in the Garvellachs: E coast of GE, W coast of A'C, SC of A'C, E coast of EaN and E coast of EaN. The thickness of the bed-set ranges between 2-4 m.

Bed-set between D26 and D27: This sandstone bed-set is continuous along the whole of the outcrop in the Garvellachs and varies in thickness from 9 to 18.2 m (Fig.4.2). This bed-set is represented by bedded sandstone and some thin beds of siltstone and conglomerate.

Bed-set between D29 and D30: This bed-set is exposed on the E coast of GE, W coast of A'C and in the SC of EaN (Fig.4.2). The thickness of the bed-set varies between 8.5-2m.

Bed-set between D30and the base of M3: This bed-set is exposed throughout the Garvellachs outcrops (Fig.4.9 and 6.17). On the E coast of GE, it includes: (i) dolomitic sandstone and siltstone above D30 to the base of D31; (ii) sandstone between D31 and D32; (iii) sandstone between D32 and rhythmically laminated lithofacies; and (iv) sandstone beds above the rhythmically laminated beds to the base of the Member 3 (Fig.4.9 and 6.17).
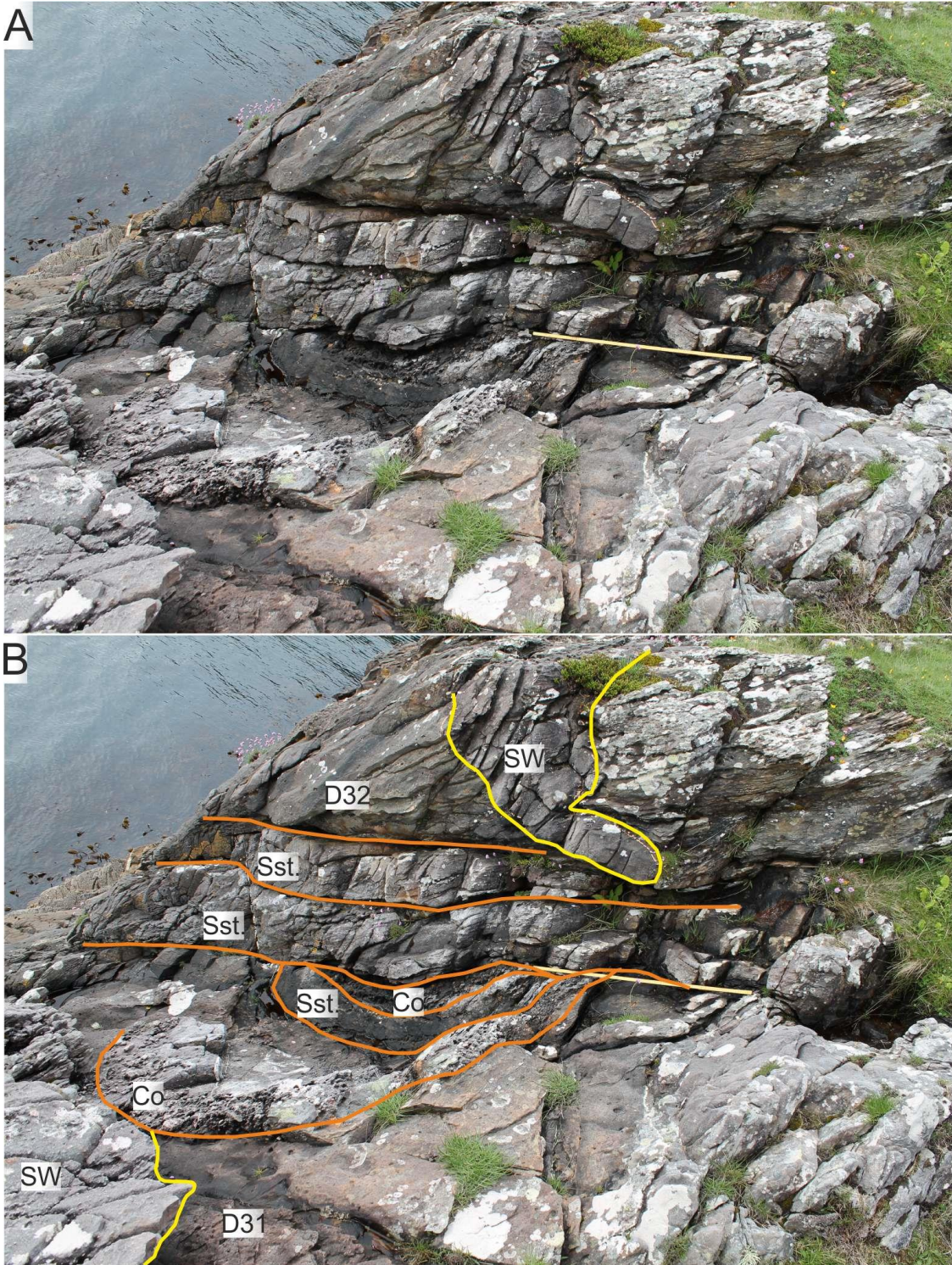
Figure 4.16: (A and B) Top D31 and D32 on the E coast of GE penetrated by sandstone wedges (SW). Between the two diamictite beds, a syncline contains alternation between sandstone (Sst.) and conglomerate (Co). The yellow lines in 'B' show the contacts between SW and diamictite beds; and the orange lines represent the contacts between sandstones, conglomerates, and diamictite beds.

(b) Contacts:

Bed-set between D22-D23: This bed-set of sandstone beds overlies the top of D22, with its well-developed system of sandstone wedge polygons; and it is overlain by D23. The lower and upper contact of this bed-set are sharp with the underlying and overlying diamictite beds.

Bed-set between D26-D27: On GE and in the SC coast of A'C, this bed-set directly rests on D26 at a sharp and undulating contact. The lower most part of the bed-set contains an involuted pebbly sandstone horizon (detail in section 6.2, and Fig.6.14). These sediments are exposed on GE, A'C and EaN.

At its base everywhere, except on the SW of EaN, is the pebbly sandstone with disturbed bedding referred to above (intra-bed folds horizon). On GE and A'C, above this bed-set of sandstone lies D27, but on SLaC and EaN the succession is more complicated, and what may be a new diamictite bed appears at or beneath the top of the bed-set.

On the E coast of GE, the sharp base of the sandstone is irregular, where the intra-bed fold sandstone rests directly on D26. The upper most part of D26, is folded, showing that the structure affecting the sandstone continues for 1 or 2 m down into the top of the diamictite bed (Fig.4.13). Elsewhere, the structure of the intra-bed fold sandstone is usually less intensely developed than on the E coast of GE.

Bed-set between D29-D30: The basal contact of the sandstone beds within this bed-set with D29 is sharp: the top of D29 is penetrated by sandstone wedges which are truncated, in places, by breccia patches.

Bed-set between D30-base of Member 3: The base of the beds within this bed-set is usually sharp with the underlying D30. The thickness of the bed-set is about 40 m, starting at the top of the D30 and finishing at the base of M3 (Fig.6.17). Another feature is that massive sandstone beds grade up into laminated sandstone, for example, on the W coast of GE (Fig.6.17).

(c) Lithology

Bed-set between D22-D23: This bed-set consists of fine to medium-grained sandstone, commonly yellowish grey in colour, and minor beds of siltstone and conglomerate. On the E coast of GE, this bed-set is about 2.8 m thick and composed of two horizons of sandstone and one horizon of siltstone (0.5 m thick) between the sandstones (Fig.4.1). The sandstone is well bedded and fine to medium-grained, while the siltstone is well laminated. The lower contact of the siltstone with sandstone is sharp and straight, while the upper contact is sharp and undulating.

On the E coast of A'C this bed-set is unexposed, but there is a lenticular conglomerate bed at the top of D22. On the SC coast of A'C, a similar succession to the E coast of GE is present, but there is a discontinuous bed of conglomerate at the top of D22 about 10-15 cm thick (Fig.4.1). A similar succession is exposed on the W coast of A'C, with two horizons of conglomerate, one at the top of D22 and the other below siltstone layers.

On the E coast of EaN, this bed-set reaches its thickest, about 4.2 m (Fig.4.1). It is composed of well bedded sandstone with thin layers, 5-10 cm, of conglomerate at the base and a 5-10 cm siltstone layer lies 1 m from the base of the bed-set. On the SC of this island, the lower part of the bed-set is unexposed, but the upper part, about 3 m, is well exposed and is a well-bedded sandstone.

Bed-set between D26-D27: Between these two diamictite beds on the E coast of GE there are bedded sandstones (Fig.5.2) about 2.1m thick, which are medium-grained and well-sorted. The upper part of the beds is more argillaceous than the lower part. On the W coast of GE, the top of D29 is separated by a 0.1 m siltstone and 0.9 m sandstone from the base of D30 (Fig.4.2).

Bed-set between D29-D30: On GE and EaN, D29 is overlain by a bedded horizon which has beneath it everywhere a well-developed system of sandstone wedges. Inland on GE, this horizon is thin (maximum 2 m) and consists of conglomerate (Fig.4.17). The predominant clasts are granite and quartzite (Fig.3.17D), while diamictite and dolomite (Fig.4.17A) occur in minor proportions. The diamictite and dolomite clasts are larger, up to 60 cm across, than granite and quartzite which are commonly 2-3 cm across. The same horizon is present in the same stratigraphic level at the SC coast of EaN. There, the horizon is represented by a thick (7-11 m) group of banded siltstones at the base of which is the thin conglomerate (15 cm) seen on GE. The top of these siltstones on the S coast of EaN is very dolomitic and contains a bed of dolomite flake breccia, in which the largest flake measures 85 mm by 4 mm in cross-section.

Figure 4.17: Conglomerate bed about 2 m thick at the top of D29 in GE inland. Geological hammer and coin are scales. (A) Diamictite clast more than 60 cm within the conglomerate bed; (B and C) the conglomerate bed from a distance and show the thickness with clast sizes; and (D) different types of clasts within the conglomerate bed.

Bed-set between D30-base Member 3: on the E coast of the GE, this bed-set is about 36m thick with D31, D32, and the rhythmically laminated lithofacies, but it thins to less than 10m on the W coast of EaN. It consists of fine-laminated dolomitic siltstone, well-bedded dolomitic sandstone, and massive sandstone.

(d) Sedimentary structures

Bed-set between D22 and D23: On the E coast of GE, the half metre of the top most sandstone bed includes trough cross-bedding, also, 1.5 m from the base of sandstone beds on the SC coast of A'C are symmetrical ripple marks.

Bed-set between D26 and D27: On the E coast of A'C, there is a diamictite bed (D26`), 3 m thick, present within the lower part of this bed-set. Within the bed-set fine-grained sandy siltstone, often with current ripple bedding structures, and sandstone with planar cross-bedding predominate, although some levels are also very dolomitic. Despite the extensive outcrops of the bed-set no extra-basinal boulders (occurring isolated in the bedded sandstone or siltstone) have been found.

Two horizons of 'involutions' are present within this sandstone bed-set (Fig.4.1), one of them is continuous along all the Garvellach Islands and the other is exposed in some localities. The former is the best developed and is well shown because of the pebbly nature of the sandstone; it occurs at the base of this sandstone bed-set. The latter is similar to the former but less developed and occurs at higher horizons in the bed-set; the most persistent of these horizons occurs at a level 1 to 2m above the base of the sandstone bed-set (Fig.4.1).

All intra-bed folds (involutions) have the following common characteristics: (1) broad rounded synclines, or basins and sharp crested anticlines; (2) the structures are sharply truncated with a sharp contact with the overlying beds, above which lie planar bedded sediments, implying that the structure must be synchronous; (3) in plan-view on the top of the bed, they show sub-circular to elliptical structure (Fig.4.18C-D). Sometimes two or more of these shapes merge and form completely irregular shapes (Fig.4.18A-B); and (4) the structures are almost always overturned towards the N-W. This overturning everywhere follows the direction of the main Caledonian cleavage.
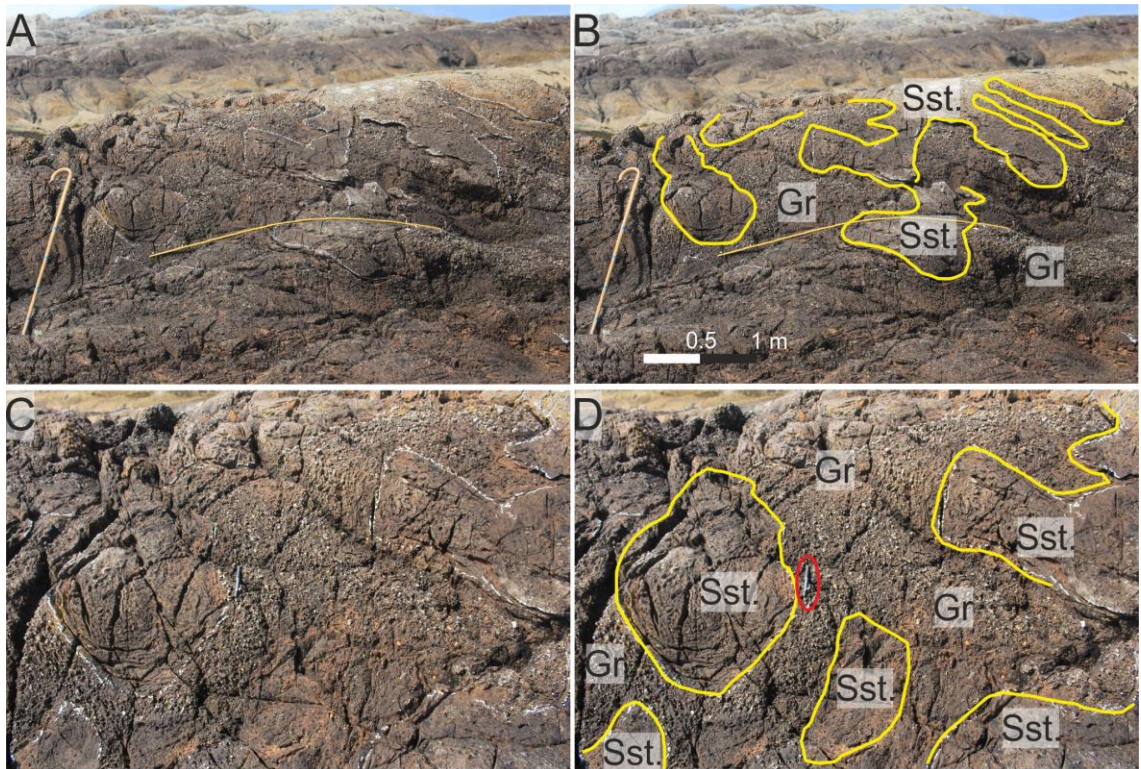
Figure 4.18: Top view of the involutions, in SLaC: (A and B) shows circular or elliptical shapes of the gritty or pebbly (Gr) and Sandy (Sst.) patches, 2m ruler and stick are scales; (C and D) a bigger scale of the top surface and shows merging shapes of the sandy and pebbly patches. Red circle (pen) is scale.

The three-dimensional shape of these structures is not known for certain; the crest of the anticlines and synclines within the intra-bed folds may have an overall orientation, although this is not obvious as the structures are similar in appearance whether seen in a N-S or E-W sections.

Bed-set between D29-D30: The sedimentary structures within this bed-set are well-bedded sandstone, well-laminated sandstone, ripple marks and some soft sediment deformation at the top part of the sandstone bed on the SC coast of EaN just beneath D30 (Fig.4.2).

Bed-set between D30- base of member 3: The sedimentary structures within this bed-set include: ripple marks (Fig.4.19A and B), two opposing side cross-stratifications (Fig.4.19C and D), deformation structures (Fig.4.19E and F), trough cross-stratification and load casts (Fig.6.12a, b and c).
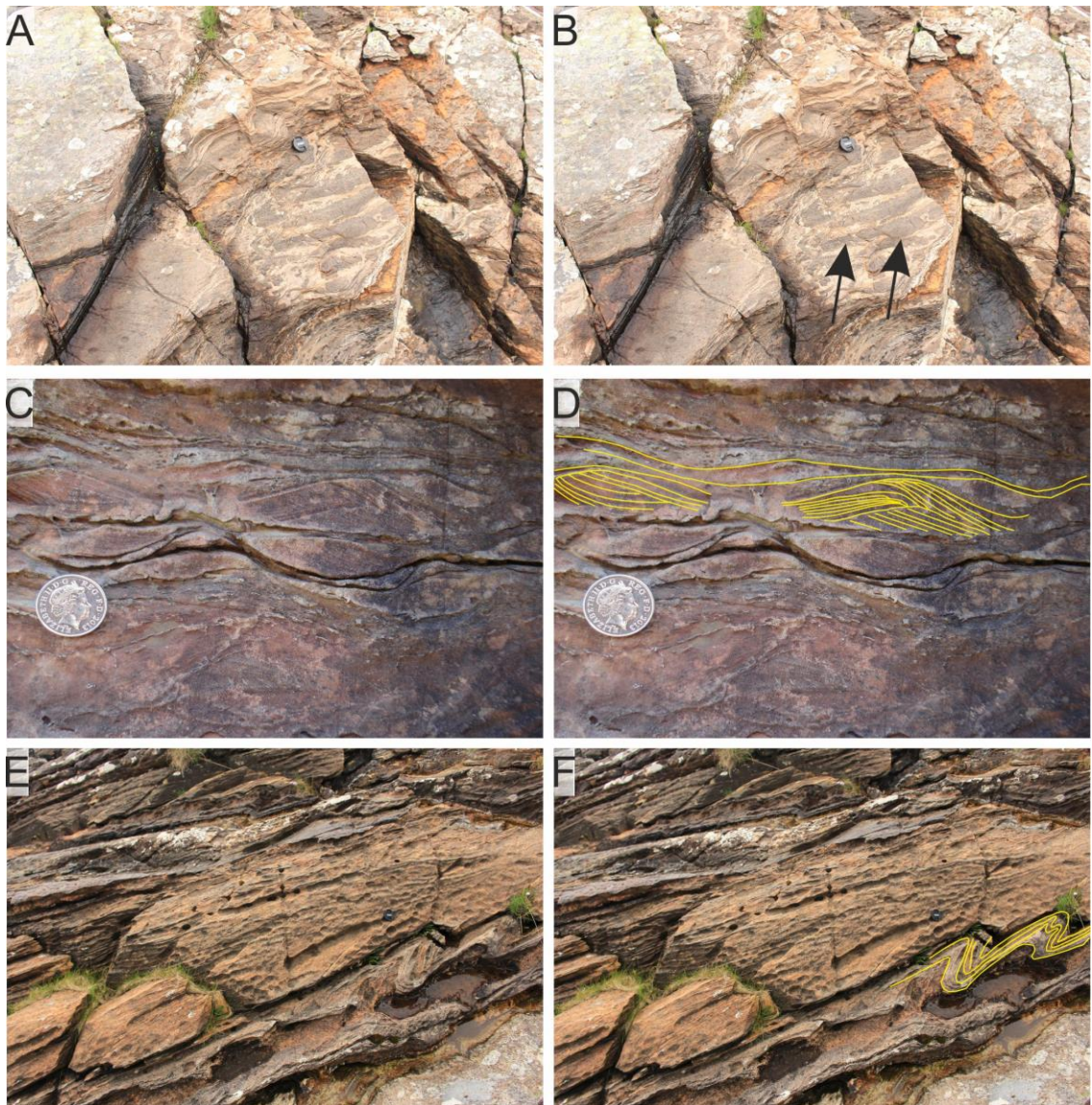
Figure 4.19: (A-B) ripple marks within sandstone strata about 2.5m below D31; (C-D) opposing side ripple marks within the sandstone just below D31. (E-F) soft sediment deformation structure within the succession between D30 and D31. All photos from the E coast of GE

4.1.3 Conglomerate lithofacies

This lithofacies occurs in two units. The first one contains mostly granitic clasts and lies 10m above the intra-bed folds on SLaC, and the second level lies in the highest stratigraphic level in the same island.

a. Lower unit

On SLaC above the intra-bed folds sandstone beds, there are two lenticular granitic conglomerate beds within the succession. The maximum thickness of the largest body is about 3m thick (Fig.4.20) and extends laterally about 100m before it dies out completely. This conglomerate is mud supported, channel shaped, and has a sharp and irregular base with the underlying rocks. Larger clasts are concentrated at the top and some of them are shattered to smaller pieces (Fig.4.21). The size of the boulders is tens of centimetres in the thickest part, while close to the edge of the channel clasts are grit size. The top boundary is sharp and the boulders protrude at the top. In the middle of the thickest part of the channel, there is a thin layer of fine material (Fig.4.20). There are lenticular shaped sandstone

clasts within the conglomerate. They have a sharp contact with the matrix, and are numerous at the edge of the channel (Fig.4.22). They are identical in grain size, lithology, colour in fresh surface, and composition with the sandstone beds underneath and next to the conglomerate unit.

Figure 4.20: Granitic conglomerate, 3m thick, above D26 on SLaC. The yellow lines show the lower and upper boundary of the bed, and the red line represents a mudstone lamina between two conglomerate beds.

Figure 4.21: Fragmented clasts at the top of the granitic conglomerate on SLaC. These probably represent the effect of frost-shattering.

Figure 4.22: Yellow arrows point to lenticular sandstone clasts within the granitic conglomerate, on SLaC.

b. Upper unit:

The second unit lies at the highest stratigraphic level exposed on SLaC. It is composed of well sorted conglomerate about 12m thick. The beds are normally-graded (Fig.4.23a and a`) and the unit is a wide channel shape. The base of the unit is sharp (Fig.4.23b and b`), also the base of the conglomerate beds is sharp (Fig.4.23c and c`). The clasts vary in lithological composition, size and shape (Fig.4.23d and d`). The amount of carbonate (dolomite) and crystalline clasts are almost the same. However, the ratio of intrabasinal (carbonate and sandstone) clasts are higher than the extrabasinal (granite and quartzite) clasts (Fig.4.23d and d`). The size of the clasts ranges between few centimetres to up to 20cm. Their shape are various from semi-spherical to blade to discoidal (Fig.4.23d and d`) in the terminology of Zingg (1935). The sandstone clasts are usually discoidal (Fig.4.23d-d` and 4.24) and become larger at the edge of the unit, in the place where the conglomerate unit dies out laterally (Fig.4.24). In addition, this unit contains some cross-stratification (Fig.4.25) and imbrication of pebbles (Fig.4.26).

The lower contact of the conglomerate unit is sharp with D30 (Fig.4.23b and b`). However, in the W coast of SLaC, it is underlain by a delicate laminated siltstone bed with a sharp contact (Fig.5.27). The siltstone shows some loading structures (Fig.4.28) and includes deformation with folding (Fig.4.29a) and brecciation (Fig.4.29b).
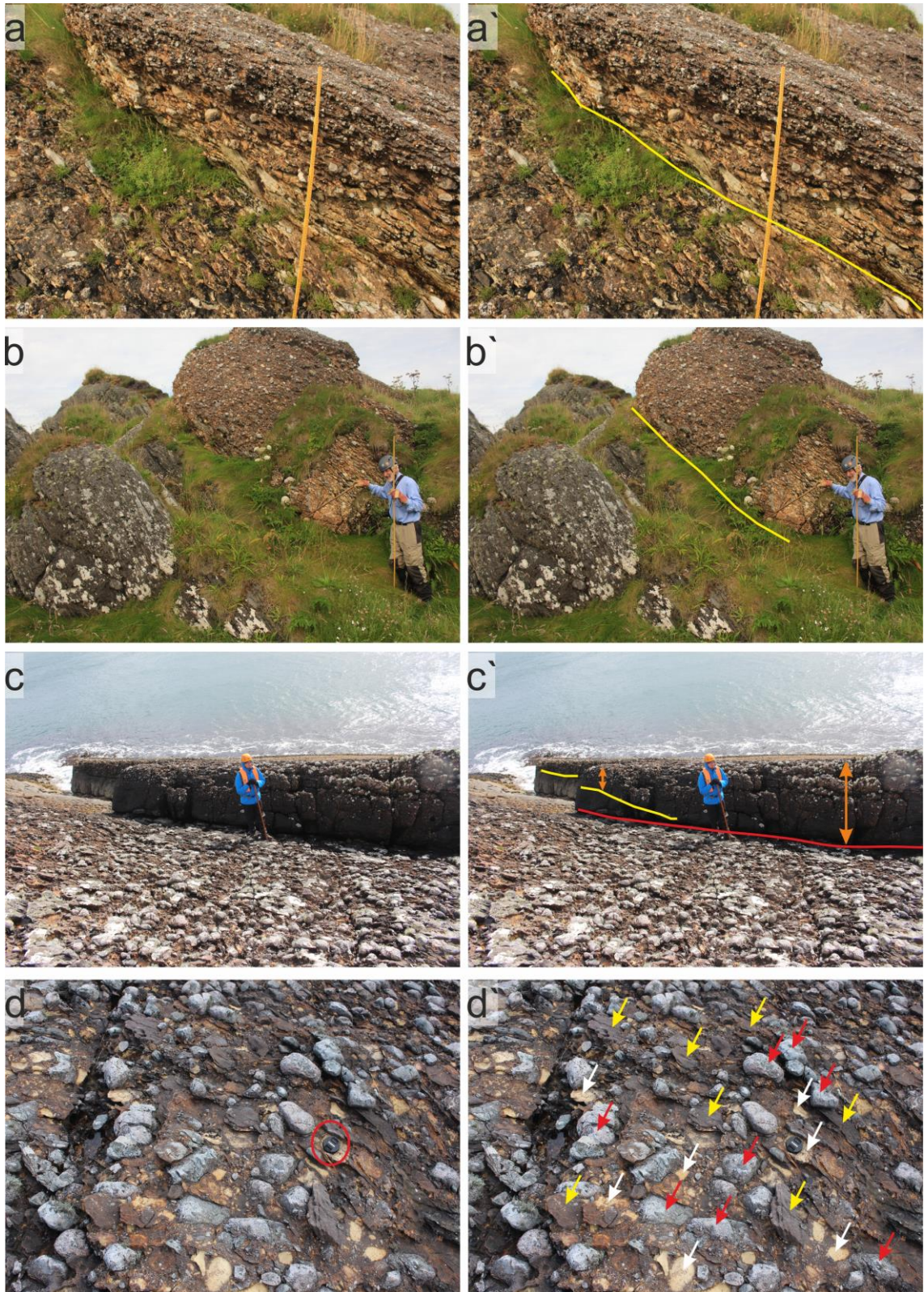
Figure 4.23: Upper unit of conglomerate lithofacies on SLaC: (a-a`) normal graded bed within the conglomerate; (b-b`) the yellow line represents the sharp base of the conglomerate with the underlying D30 on the E coast of SLaC; (c-c`) the red line shows the sharp base of a conglomerate bed; the yellow line shows the contact between sandstone and conglomerate; the double sided orange arrows show the increasing thickness of this conglomerate bed; (d-d`) various lithologies of clasts: red, white and yellow arrows respectively show crystalline, dolomite and sandstone clasts.
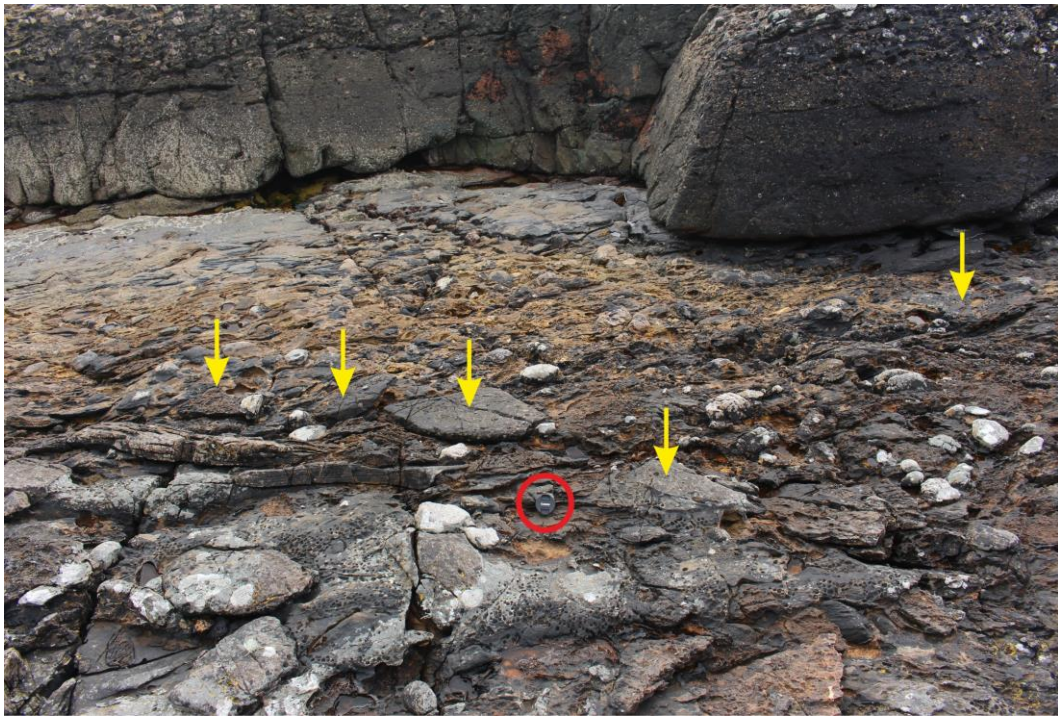
Figure 4.24: Yellow arrows show discoidal sandstone clasts at the edge of the second conglomerate unit on SLaC. For comparison see sandstone clasts close to the centre of the channel shape (Fig.4.23d and d`).

Figure 4.25: Cross-stratification within the second dolomite unit on SLaC, Lens cap 58 mm scale.

Figure 4.26: Imbrication of clasts within the second conglomerate unit on SLaC. The water current flowed to the NW.

Figure 4.27: Yellow dashed line shows the lower contact of the second conglomerate unit with the underlying siltstone bed on the W coast of SLaC. The yellow arrow points to the load structure in "Fig.4.28".
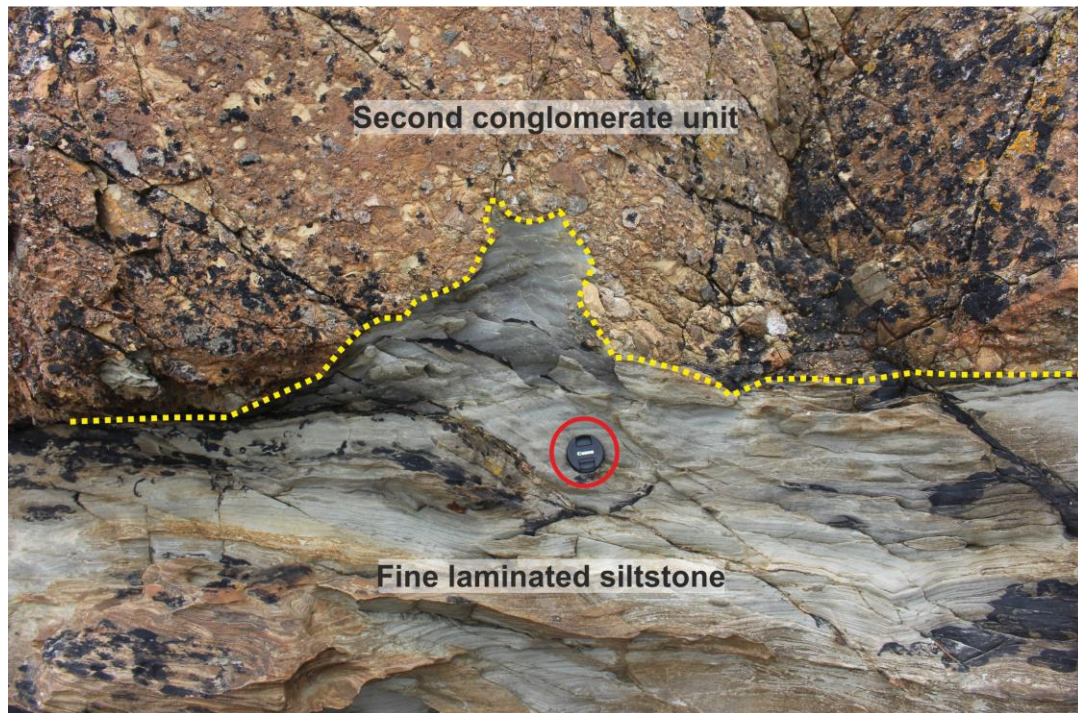
Figure 4.28: Load structure at the contact between siltstone and conglomerate.

4.1.4 Rhythmically laminated lithofacies

Between the base of Member 3 and the top of D30, there is a thick succession of sandstones, siltstones, dolomites, and two diamictites (D31 and D32), plus two beds of rhythmically laminated siltstones (Fig.6.17). They occur at two different stratigraphic levels. On the E coast of GE, a 6m succession is locate above D32; while on the W coast of GE, 4m of rhythmically laminated strata occur directly beneath D31 and are truncated by the base of the Member 3 (Fig.6.17); they show a gradational boundary with the underlying sandstones and a sharp contact with the Member 3 strata above.

On the E coast of GE, the rhythmites have a simple graded structure. Individual rhythmic laminae are thin, about 3mm, couplets of coarse and fine-grained laminated sandstone and siltstone respectively (Fig.4.30). The couplets consist of two layers, an upper of silt grade, dark brown and a lower of sand grade. The grain size change is almost always gradational fining upward. The laminae weather differently, the sandstone layers stand out, while the siltstone appear less resistive (Fig.4.30C). Some couplets are very similar in thickness along the exposure studied. In a few rhythmic couplets, up to 5 laminae are present within each. The constant lateral thickness of the couplets has allowed measurement of a section through the central part (Spencer, 1971). Also, several lenticular shaped sandstone clasts are observed inside the laminated lithofacies (Fig.4.30F); they are rounded, have a sharp contact with the host rock, and most of them have a diameter much greater than the thickness of the couplets. Most the laminae below and above the sandstone clasts are bent (Fig.4.30F). On the E coast, 50cm of the top-most part of the laminated horizon is dolomitic (Fig.4.30b and D). Also, some soft sedimentary deformation structures are recorded, especially in the dolomitic part (Fig.4.30E; 4.32). Sandstone wedges (Fig.4.33) penetrate the top of both rhythmites.
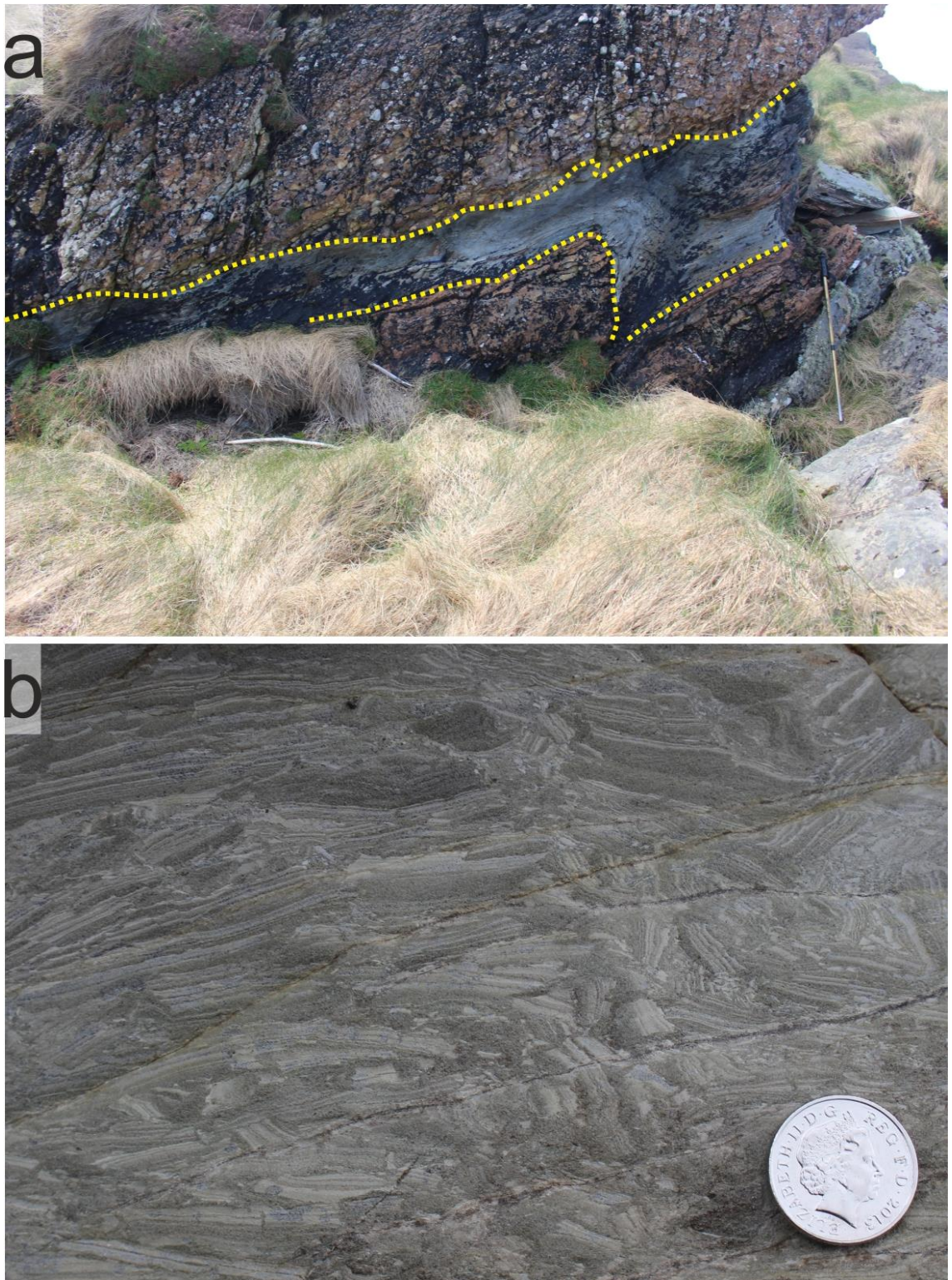
Figure 4.29: Folding and brecciation within the siltstone beneath the upper conglomerate unit on the W coast of SLaC. (a) the yellow dashed line shows the lower and upper contact of the siltstone beneath the upper conglomerate unit. Stick is 1m scale. (b) Delicate laminated siltstone has broken into angular pieces. Coin (5 pence) for scale.
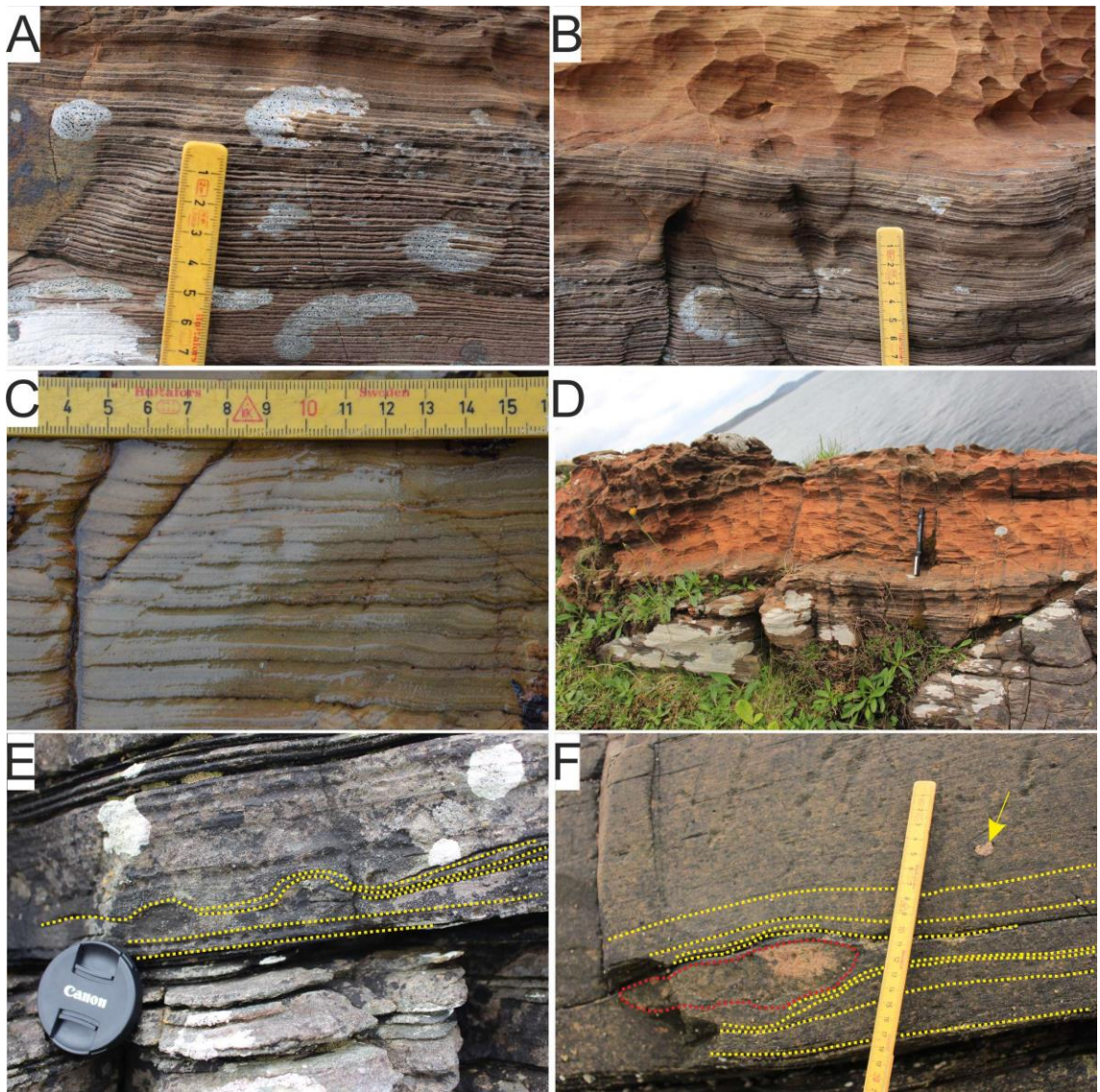
Figure 4.30: Rhythmically laminated beds above D32 on the E coast of GE. (A-C) show prominent sandstone laminae and weathered siltstone laminae. Ruler is scale. (B and D) Dolomitic part of the rhythmite. (C) Normal grading of the couplets with a reverse fault in the left-side. (E) Yellow dashed lines are deformation structure within the fine-laminated couplets. (F) red dashed line is a sandstone lens within the rhythmite and yellow dashed lines show bending underneath the lens.

On the W coast of GE, a similar horizon of rhythmically laminated rocks is exposed, but at a lower stratigraphic level (Fig.6.17). This also contains some outsize extra basinal clasts (Fig.4.31) which show some bending and puncturing of the lamination within the section.

The facies also crops out at Port Askaig on Islay at an identical stratigraphic level at the top of Member 2. The thickness of the facies on Islay is 9 m and has all the characteristics described above, except the rhythmic laminae are much thicker, couplets of up to 10 mm thickness are common (Spencer, 1971).

154
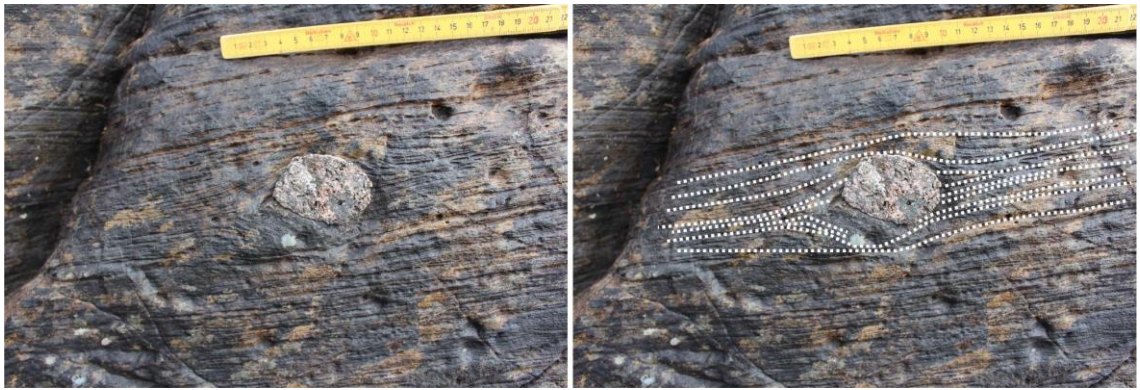
Figure 4.31: Granite dropstone within rhythmically-laminated siltstone on the W coast of GE above D30 (Fig.4.9).

Figure 4.32: Deformation structure within the dolomitic part at the top of the rhythmically laminated unit above D32 on the E coast of GE. Ruler is 20cm scale.
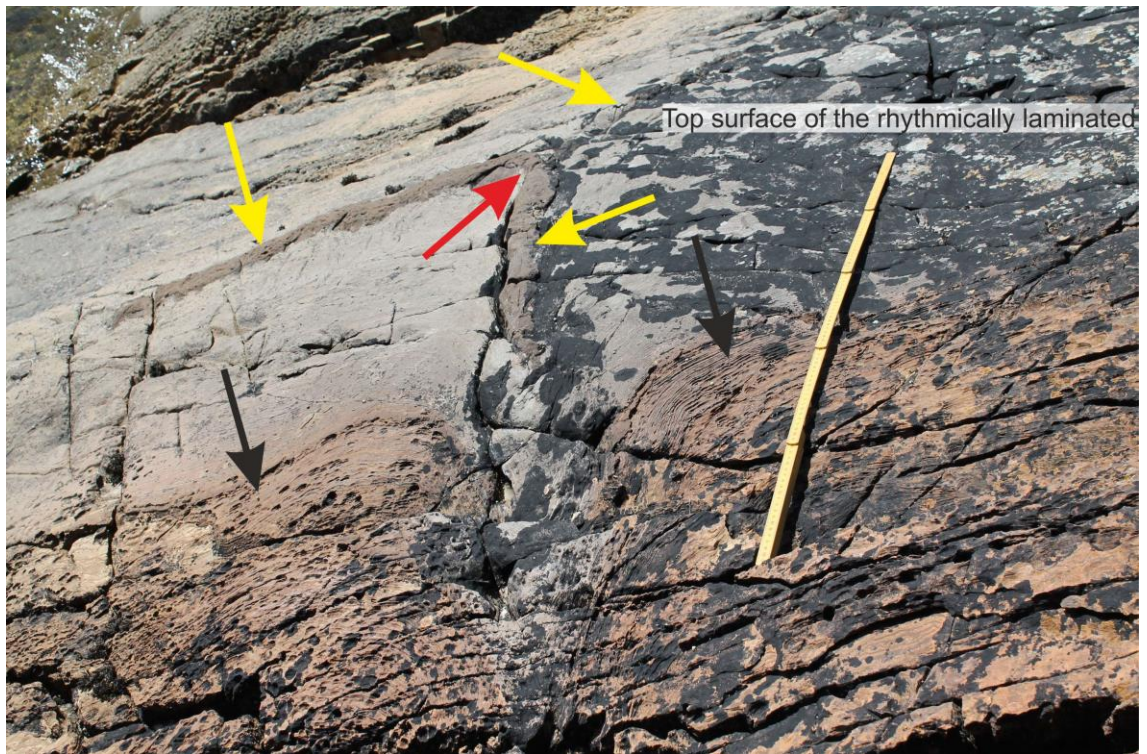
Figure 4.33: Sandstone wedges penetrating the top of the rhythmically laminated lithofacies on the E coast of GE. Red arrow is where three sandstone wedges join; yellow arrows point to the sandstone wedges; and black arrows show deformation of laminae.

4.1.5 Depositional environment of the Arenaceous diamictite-brown sandstone LFA

This lithofacies association contains the most varied lithologies and structures of all the lithofacies associations within the PAF succession. Also, it includes tens of sequence events, more than can be seen in any other lithofacies association in the succession. Because of these characters many changes in environment and depositional mechanisms must have taken place.

The main depositional hypotheses to test for these rocks are: grounded-ice, floating-ice, and mass-flow processes. The main features to be considered are (Table.4.1): (i) all diamictite beds have a sharp base; (ii) most of diamictite beds are massive and homogeneous; (iii) the topmost part of the UDL is brecciated beneath D19 on the W coast of A'C; (iv) in two localities and horizons there are laminated diamictite beds; (v) polygonal sandstone wedges occur at several horizons; (vi) frost-shattered clasts at some horizons; (vii) the presence of cryoturbation; (viii) deposition of sandstone beds in seven stratigraphic horizons; (ix) absence of dropstones in sandstone beds; (x) granitic conglomerate above D26 on SLaC; (xi) conglomerate at the highest stratigraphic level on SLaC; (xii) presence of dropstones in some stratigraphic levels; and finally (xiii) two units of rhythmically laminated couplets of siltstone and fine-grained sandstone. The author is discussing all above 13 features systematically as following:

The sharp bases of the diamictite beds are explained in detail in section 6.1. The massive and homogeneous diamictite could be formed by mass-flow or grounded–ice mechanisms. The brecciated topmost part of the UDL was recorded by Ali et al. (2018: in press) as a glaciotectonic feature; it is mentioned in detail in section 4.1.1b and Fig.4.3c-d. In addition, there is another deformation structure within the succession of the 'arenaceous diamictite-brown sandstone lithofacies association' below D31

which probably formed by glaciotectonism; this can be seen at low tide (Fig.4.34a-d). Also, about 50m towards N from the coast, there are more deformation structures in beds of sandstone and siltstone (Fig.4.34e). Glaciotectonic structures are a powerful evidence of grounded-ice.

D23 and D25 are laminated diamictites. D25 contains some lonestones (probably dropstones) on the E coast of EaN (Fig.4.1 and 4.14). Lamination of both diamictite beds and the presence of dropstones indicate deposition in water with probable presence of ice-rafting: these two diamictites could be formed by ice-rafting or/and floating ice sheet.

Polygonal sandstone wedges and frost-shattered clasts in many stratigraphic levels of the arenaceous diamictite-brown sandstone lithofacies association (discussed in detail in sections 4.5e, 5.3B and 6.2) indicate periglacial environments.

Both units of conglomerate within the conglomerate lithofacies on SLaC are probably subaerial for the following reasons: (a) angular discoidal sandstone clasts occur within these units (Fig.4.22; 4.23d and 4.24); these clasts must have been in a solid state (frozen) when deposited otherwise they would have disaggregated. (b) rolling these clasts within a mass-flow current could not have produced their angular discoidal shapes. (c) presence of frost-shattered clasts (Fig.4.21) in the same level support a subaerial environment hypothesis.

The best hypotheses for interpreting the lower and upper units, respectively, are as a local debris flow and as a glaciofluvial deposit in a periglacial environment for the following reasons. The lower unit: (i) the conglomerate is mud-supported; (ii) clasts protrude at the top of the unit and sticking up into the overlying bed: (iii) the discoidal sandstone clasts could be solid if frozen; (iv) these discoidal clasts could be from a collapsed channel edge; (v) increasing the size of the angular discoidal clasts close to the channel edge indicate that they come from the sandstone underneath and next to the channel and they have not transported for a long distance. In addition, presence of a thin fine-grained bed in the middle of the unit (Fig.4.20) separates two different debris flow events.

The upper conglomerate unit is at the highest stratigraphic level could be a fluvial (fluvioglacial??) deposit because: (i) the discoidal sandstone clasts discussed above indicate subaerial deposits (Fig.4.24); (ii) the imbrication of clasts (Fig.4.26), the cross-stratification (Fig.4.25), and sedimentary loading (Fig.4.27 and 4.28) structures indicate current activity and fluctuation of the water. All these structures together are unlikely to form by mass-flow processes or floating-ice. They could form in a periglacial environment in braided fluvial channels.

In addition to these two conglomerate units, the conglomerate at the top of D29 (Fig.4.17) is also more likely to be a fluvial deposit in a periglacial environment.

Seven sandstone beds contains cross-beds that have less than 1 m amplitude and ripples which have less than 3 cm amplitude and about 8-15 cm wavelength (Fig.4.19A-D). Based on ripple measurements on the W coast of GE, E and SE coast of A'C at the top of the intra-bed folds, Spencer (1966, Fig.71b, c,

and d) concluded that the systems must been produced over an area with one diameter of at least 700m; because the ripples measurements in these three areas are very similar to each other and plausible to come in the same system. Furthermore, the <u>absence of dropstone within sandstone interbeds</u> rules out a floating-ice hypothesis in the levels which these sandstones are occur. Also, ripple marks with presence of opposing flow directions (Fig.4.19C-D) are more likely to be formed in a tidal environment.

Sandstone intra-bed folds

Most of the features mentioned above have been described previously, except sandstone intra-bed folds. The author gives more detail of these structures here, because they are one of the important structures that helps with our understanding of the depositional environment.

Kilburn et al. (1965, p.353) first observed soft-sediment deformation structures at above D26 and suggested that they resembled glacial involutions in appearance. The name 'involution' has been retained, both for convenience and to focus attention on the structures, although it is by no means certain that they are of cryoturbation origin.

Spencer (1971) discussed the intra-bed folds (sandstone downfold structures by him) at the base of the bedded sandstone or in the top of D26 and suggest two mechanisms for producing this type of structures: (1) large-scale load-cast or the movement and rearrangement of quicksand, and (2) cryoturbation in a periglacial environment. This second structure is formed within an active layer in a subaerial exposure due to freezing and thawing during temperature changes between (0 to -5) ˚C. Spencer (1971) excluded forming such structure by slumping in the sense of lateral mass movement.

The gentle overturning inclination of the folds towards the N-W which is commonly observed is probably of tectonic origin. Moreover, the disturbed structure can be traced downwards into undisturbed sediment in several sections: SLaC and W and E coast of EaN, no marked break, which could have acted as the sole of a slump sheet, can be seen. The continuity of the involute structure horizon along the strike for 4.5 km is unlikely to form by slump, because an extensive contemporaneous slump sheet would be necessary to produce the uniform structure seen. There is no evidence of the existence of an extensive slope, of sufficient gradient to generate such a slump. The disturbed structures are not channel infilling, although some small channel structure is present. Furthermore, certainly the cross-bedding palaeocurrent direction in the overlying sandstone are random in orientation. The mechanism which produced the rearrangement is thought to have formed in situ by the shifting and rearrangement of quicksand (Selley et al., 1963; Owen and Moretti, 2011; Druzhinina et al., 2017). Any difference, even small, to minor seismic disturbances or loading can cause the rearrangement of fluid material to produce a more stable form of packing (op cit.). Both reasons: (i) mobilization of the lower part of the sandstone, and (ii) the denser nature of the upper part, may be formed by appropriate differences in lithology which would therefore sink under gravity. Differences in lithology are present within intra-bed folds here (pebbly sandstone overlying siltstone) in some localities. For example, a sandstone with well-developed intra-bed folds overlie a bedded pebbly sandstone packed with granite pebbles (Fig.4.13;

4.18). Although it is difficult to estimate the original porosity and density of lithified rock burial, it is suggested that the disturbed structures, particularly here, could not have been produced by a loading mechanism because the original density difference was the reverse of that required. The lower horizon in the sandstone bed-set is continuous and in very similar in thickness and character along 4.5 km outcrop. It must be noted, however, that the horizon with disturbed bedding occurring at higher level are not so continuous.
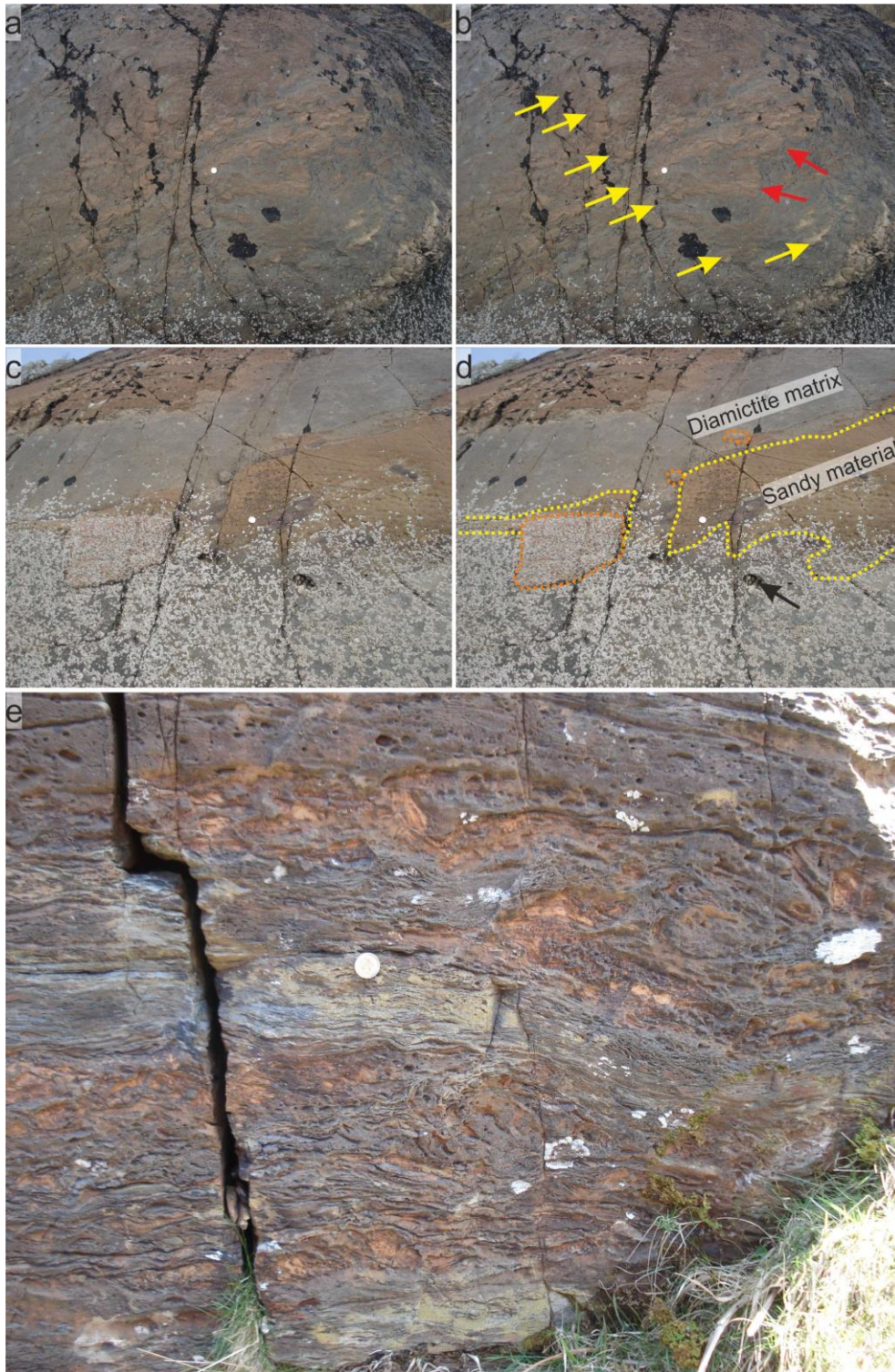
Figure 4.34: (a-d) Deformation structure within the interbeds just below D31, on the E coast of GE. (b) the red arrows show deformation structures and disrupted sandstone beds; the yellow arrows point to the sandstone beds. (d) Orange dashed-lines pointing to crystalline clasts, and yellow dashed-lines show the boundary between the matrix of D31 and sandstone beds. (e) interstratified, deformed sandstone and siltstone lamina underneath D31 showing some current activity (Fig.5.19C-D) and deformation structures, 10 m from the E coast of GE. Coin for scale.

The rhythmically laminated lithofacies with lonestone and dropstones (Fig.4.31) respectively on the E and W coasts of GE below Member 3 indicate waterlain deposition. This type of rhythmite compares to

the rhythmically laminated siltstone sublithofacies in the DB. Thus, the reader is referred to section 3.4e for a detailed interpretation.

Table 4.1: Features representing the depositional environment for the arenaceous diamictite-brown sandstone lithofacies association.

	Features	Lithofacies	Subaqueous mass-flow	Floating ice	Grounded ice	This study
A	Rhythmically laminated couplets of siltstone and fine sandstone	Rhythmically laminated (below D31, and above D32)	Not possible	Possible (Lacustrine or marine)	Not possible	Floating-ice
B	Outsize clasts within fine laminated siltstone	Rhythmically laminated (below D31)	Not possible	Possible (Lacustrine or marine)	Not possible	Floating-ice
C	Conglomerate	Brown sandstone (Above D30, Sgeir Leth A Chuain)	Not possible	Not Possible	Possible	Grounded-ice
D	Granitic conglomerate	Brown sandstone (Above D26, Sgeir Leth A Chuain)	Not possible	Not possible	Possible	Grounded-ice
E	Sandstone	Brown sandstone (Seven horizons)	Possible	Not possible	Possible	
F	Brown Sandstone deposition	Brown sandstone (in seven horizons)	Possible	Possible	Possible	
G	Cryoturbation (periglacial)	Brown sandstone (Above D26, two horizons)	Not possible	Not possible	Possible	Grounded-ice
H	Dismantled clasts (Frost-shattered in periglacial)	Arenaceous diamictite (Tops of D22, D24, D26, and D29)	Not possible	Not possible	Possible	Grounded-ice
I	Sandstone wedges (periglacial)	Arenaceous diamictite (Tops of D22, D24, D26, D29, D30, D31, rhythmically laminated bellow and above D31)	Not possible	Not Possible	Possible	Grounded-ice
J	Laminated diamictites	Arenaceous diamictite (D23, and D25)	Unlikely	Possible	Unlikely	Floating-ice
K	Brecciation of Upper Dolomite	Arenaceous diamictite (Beneath D19)	Not possible	Not possible	Possible	Grounded-ice
L	Massive nature of diamictite beds	Arenaceous diamictite (D19-D22, D24, D26, D27-D29, D30, and D31)	Possible	Unlikely	Possible	Mass-flow Grounded-ice
M	Sharp bases of diamictite beds	Arenaceous diamictite (nine levels from D19 up to D32)	Possible	Unlikely	Possible	Mass-flow Grounded-ice

Considering the above discussion about the 13 features in Table 4.1. The author concluded that the depositional environment was most likely to be grounded-ice. In addition, the table shows some levels of floating-ice in a lakelet or the sea. Additionally, many of the 13 features described above are discussed in Chapter 6 and 7.

4.2 White sandstone-arenaceous diamictite LFA (D33-D38)

This facies association is equivalent to Member 3 of Spencer (1971), which is ca.200 m thick in the Garvellachs. The association is composed of two main lithofacies (white sandstone and arenaceous diamictite) and two minor lithofacies (lonestone beds and brown dolomitic sandstone).

4.2.1 White sandstone lithofacies

(a) Stratigraphic position and outcrops

This lithofacies has four stratigraphic occurrences, from the base to the top: below diamictite beds D33 (Fig.4.35), D36 and D37 and above D38 (Fig.4.36). The four bed-sets have thicknesses of, respectively: 51-94m, 13.4m, 8.5-14m and 18.8m (Fig.4.37).

Figure 4.35: Dashed yellow line is the sharp contact between the lowest white sandstone unit and the overlying D33, E coast of GE. Anthony M. Spencer for scale.

(b) Contacts

The lower contacts of all the four sandstone units are well exposed on the S and W coasts of GE (Fig.4.37). The top contacts of the three lowest units are also well exposed there (Fig.4.37). The base of the lowest white sandstone bed-set coincides with the base of Member 3 of Spencer (1971). It lies just above the rhythmically laminated siltstone horizon on the E coast of GE; on the W coast, it rests in sharp contact upon a different laminated siltstone. The base of the second sandstone interval overlies a pebble bed (Fig.4.37) cross-cutting the sandstone wedges penetrating D35 (detail in section 4.5e) on the S of GE; it is not exposed on the W coast. The base of the third sandstone unit is a sharp contact, on the S coast of GE and on the W coast, it overlies D36; which has isolated boulders protruding at its top in both places. The fourth sandstone unit overlies D38 at a sharp contact. The tops of the lower three sandstones units are similar: the changeover from white sandstone to massive diamictite occurs either at a sharp break or within a transition no more than 50 cm thick.

Figure 4.36: The dashed yellow line shows the sharp, undulating contact between D38 and the overlying white sandstone bed-set (Fig.4.37). W coast of GE, camera lens cap is 58 mm diameter.

(c) Lithologies

The white sandstone facies comprises, thick bed-sets of white coloured, quartz rich, fine to medium grained, and well-sorted sandstone beds, which are commonly cross-bedded. The clean appearance of the white sandstones in the field helps easily to distinguish them from the grey-brown weathering dolomitic sandstones in Members I and II. Details of the four sandstone units are as follows:

i. Lowest sandstone bed-set:

This sandstone bed-set lies below D33 and consists of well-sorted, white sandstone. This is medium grained, and quartz rich. The lowest part of the bed-set includes thick planar cross-beds. These are typically about 3 m thick, up to a maximum of 8.5m on the W coast of GE. The foresets of the cross-beds vary from 5mm to 30mm in thickness. By contrast, cross-bedding is absent in the uppermost 14-24 m of this bed-set and the rocks are massive or poorly bedded.
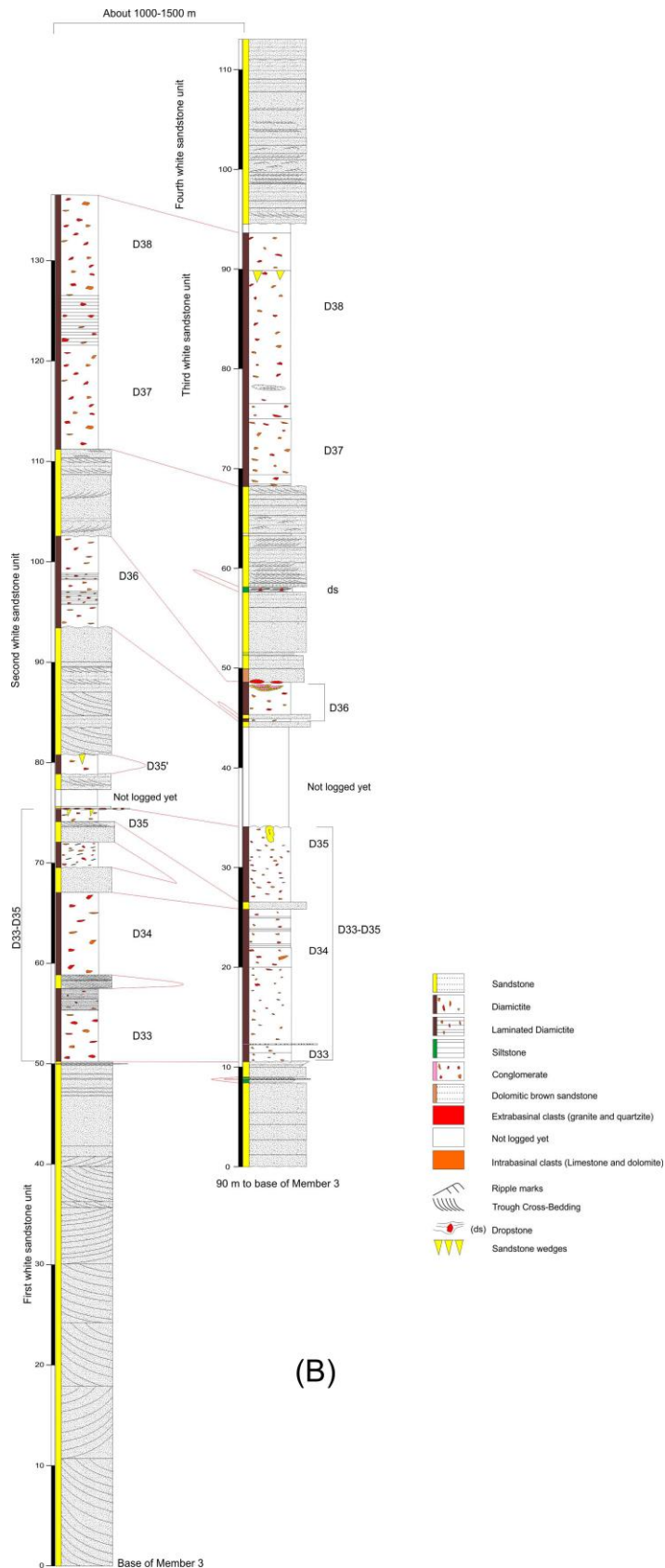
Figure 4.37: (A) Composite sedimentary log of the E and S coast of GE. (B) Sedimentary log for the west coast of GE.

ii. Second sandstone bed-set

In lithology and structure, this resembles the sandstone below D33, with a few differences listed below. The first difference is the lower contact. A stratified sandstone is underlain by a well-developed, massive, one-clast thick granitic conglomerate lens (Fig.4.38) which cross-cuts the sandstone wedges (detail in section 3.5e) in the top of D35 on the S of GE. The upper contact of the sandstone unit is sharp and planar: bedded sandstone overlain by the massive diamictite of D36. The sandstone beds show large-scale planar cross-beds, ranging from 2.5-9.5 m. Individual cross-beds cannot be correlated between the two coastal outcrops (800 m apart) of GE.

Figure 4.38: Granitic conglomerate lens above the base of the bed-sets (labelled D35 on Fig.4.37A), S of GE (Harbour). The bed is discontinuous and one clast thick. Geological hammer for scale.

The second difference between this bed-set and the lowest sandstone bed-set is the presence of a diamictite bed 1.5m above the base of the unit. It is 1.5m thick, homogeneous, structureless, poorly sorted, exposed only at low tide on the S coast of GE (Fig.4.37) and includes granitic pebbles and cobble fragments with some smaller clasts within a 15m long outcrop (Fig.4.39).

Figure 4.39: Diamictite bed in the second sandstone unit on the S coast of GE (landing jetty). The white dashed lines show the boundary of the diamictite bed and the inset photographs shows a granite clast inside the diamictite bed. Geologist and geological hammer for scale.

iii. Third sandstone bed-set

Lithologically this is identical with the other white sandstones, but has a quite different internal stratification. It is located below D37 (Fig.4.37). In the S of GE, the unit can be divided into two parts based on bedding and sedimentary structures. The lower half is composed of massive planar beds. The upper half contains small-scale planar cross-bedding; the average thickness of the foresets is 45cm, which is smaller and thinner than those in the two lower white sandstones.

iv. Fourth sandstone bed-set

This bed-set is exposed only on GE and consists of fine grained, well-sorted, white sandstone. The sedimentary structures recorded in this unit are lamination, ripple-marks, and cross-beds. The thickness of the laminated layers reaches up to 10mm; some of them include spectacular ripples in cross section (Fig.4.40). The ripples are particularly common in beds 5.2m-8.0m above the base of the unit. At this level, some ripples are loaded and form downfold structures (Fig.4.41). The cross-beds exhibit 5 cm thick gentle and planar foresets (Fig.4.42). Spencer (1971) constructed a rose diagram for eight sets to determine a palaeocurrent direction, six trend approximately NNE-SSW (Fig.4.37).

Figure 4.40: Cross-section through asymmetrical ripple marks in the fourth white sandstone bed-set above diamictite no.38. W coast of GE (Fig.4.37), camera lens cap is 58mm
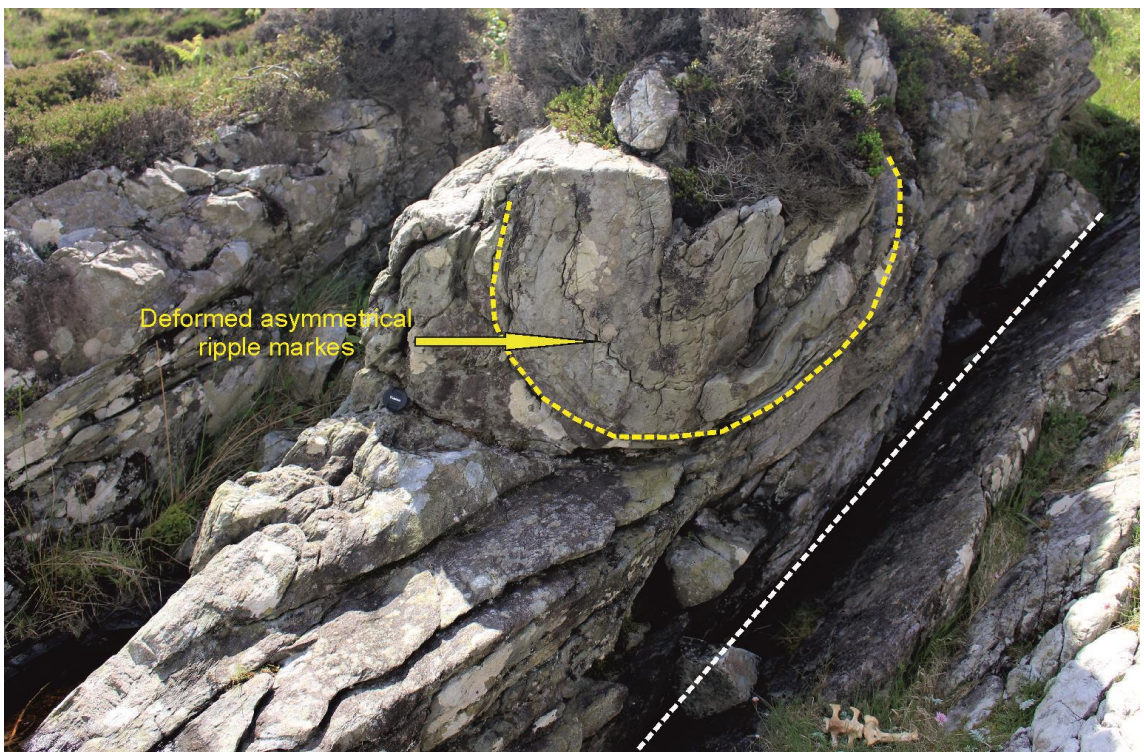
Figure 4.41: Yellow dashed lines shows a loaded ripple mark level in a synformal structure in the fourth white sandstone bed-set (Fig.4.37) above diamictite no.38. The white dashed line is the normal structural dip. W coast of GE. Camera lens cap is 58mm

Figure 4.42: Cross-lamination in the fourth white sandstone bed (weathered colour is brown here), above diamictite bed 38, W coast of GE. Ruler is 20X20 cm.

(d) Sedimentary structures

Several sedimentary structures have been recorded in the white sandstone facies: giant cross-beds (up to 14.5 m thick (Fig.4.43)) of both parallel and trough set types, massive beds, and parallel lamination. The facies includes asymmetrical ripples (Fig.4.41) of several cm height and wavelength, some of which show climbing geometries. Some of the climbing ripples are down folded (Fig.4.42). A few soft-sediment deformation structures are present: convolute bedding, load casted basal contacts and deformed lenticular sandstone beds.

Current rose diagrams constructed by Spencer (1971 pp.26-29) from the measurements of these beds exhibit varied palaeocurrent directions. The main current direction of the cross-beds in two lowest sandstones is N to S. A similar pattern occurs in 'figure 10 c' Arnaud (2004). The current direction in the third sandstone is towards the N in 'figure 13h Spencer (1971)' and 'figure 5D Arnaud (2004). The cross-bed sets typically reduce in thickness up section in the set (Fig.4.37). Furthermore, the grain size becomes finer in the uppermost sandstone bed.
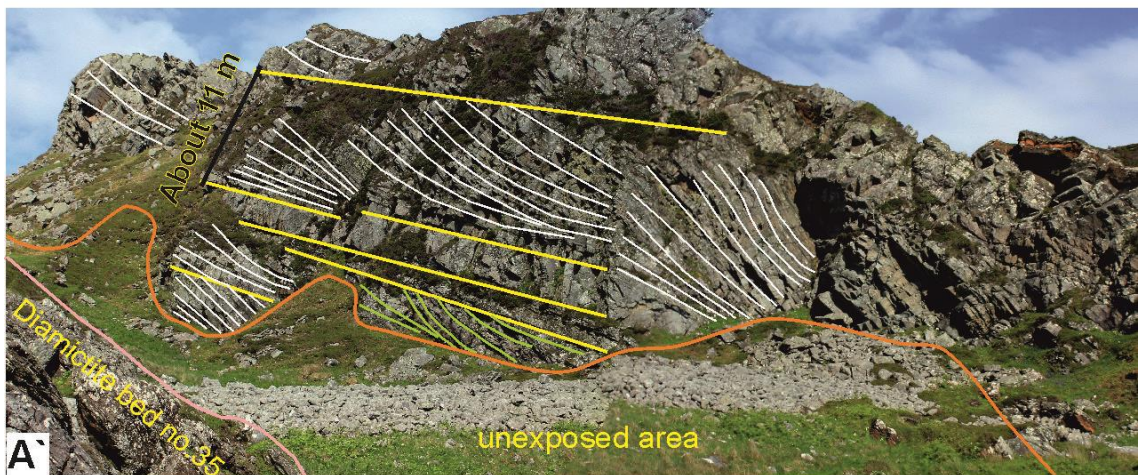
Figure 4.43: (A) and (A`) Panoramic view of the giant cross-stratification in the second sandstone unit, W coast GE. Yellow lines show the set boundary of the cross-bed, the white lines show forset, green lines show low angle cross-bed, pink line is the upper contact of D35 and the orange line is the edge of an unexposed area.

4.2.2 Diamictite lithofacies

The diamictites in Member 3 of Spencer (1971) correspond to diamictite nos.33-38 of Kilburn et al. (1965). We here term them diamictites and retain those numbers but label them: D33-D35, D36, and D37-D38. These lithofacies are interbedded with the white sandstone bed-sets of the previous lithofacies. Eyles (1988) and Arnaud (2012) have also investigated these rocks.

(a) Stratigraphic position and outcrops

D33-D38 occur in Member 3 and are well exposed on the Garvellachs, principally on the SE, S and SW coasts of GE, but they also crop out on some islets S of the main islands. The five diamictites numbered by Kilburn et al. (1965) fall into three units - D33-35, D36 and D37-38 – separated by thick, continuous, white sandstones. The stratified beds separating D33 from D34, D34 from D35 and D37 from D38 are quite different: they are discontinuous and where they are absent those diamictites cannot be separated from each other.

The thicknesses of the diamictites varies from bed to bed and location to location. On the SE coast of the GE, D33 and D34 are 17.2m and 12m thick; whilst on the SW coast they are 8.6m and 5.9m thick. D35 in

the S of GE is 2.3m thick but 7.6m in the SW of the island. D36 varies laterally from 4.5 to 6m thick. D37 and D38, with the white sandstone layers which lie in between, form a bed-set about 23-30m thick.

(b) Contacts

The contacts of the diamictites on the white sandstones (i.e. the bases of D33, D36 and D37), are all generally sharp. On the W coast of the GE, the base of D33 is sharp. There it rests on a brown-weathering sandstone bed; this bed is absent on the E coast of GE where D33 instead rests on white sandstone with a knife sharp contact (Fig.4.44). At the landing jetty on the S coast of the GE, the white sandstone bed is cross-bedded and fine to medium grained except in the topmost 1 m, which shows a lesser degree of stratification, and contain 12 granitic pebbles in the uppermost 50 cm in a 20 m long outcrop. The contact of this 1m bed with the overlying massive diamictite is sharp and when traced laterally shows an irregular surface. At the same place, the base of D36 is gradational in 50 cm, because in this location there are similarities in colour and grain size between underlying sandstone beds and the matrix of D36.

On the SW coast of GE, the lower contact of D37 with the underlying sandstone bed is sharp; the lowest 1m of the diamictite show some lamination. On the S coast of GE, the lower contact of this diamictite is again sharp. In its lowest 2 m the diamictite contains lenticular shaped, granular sandstone laminae which lie sub-parallel to the base of the diamictite bed.
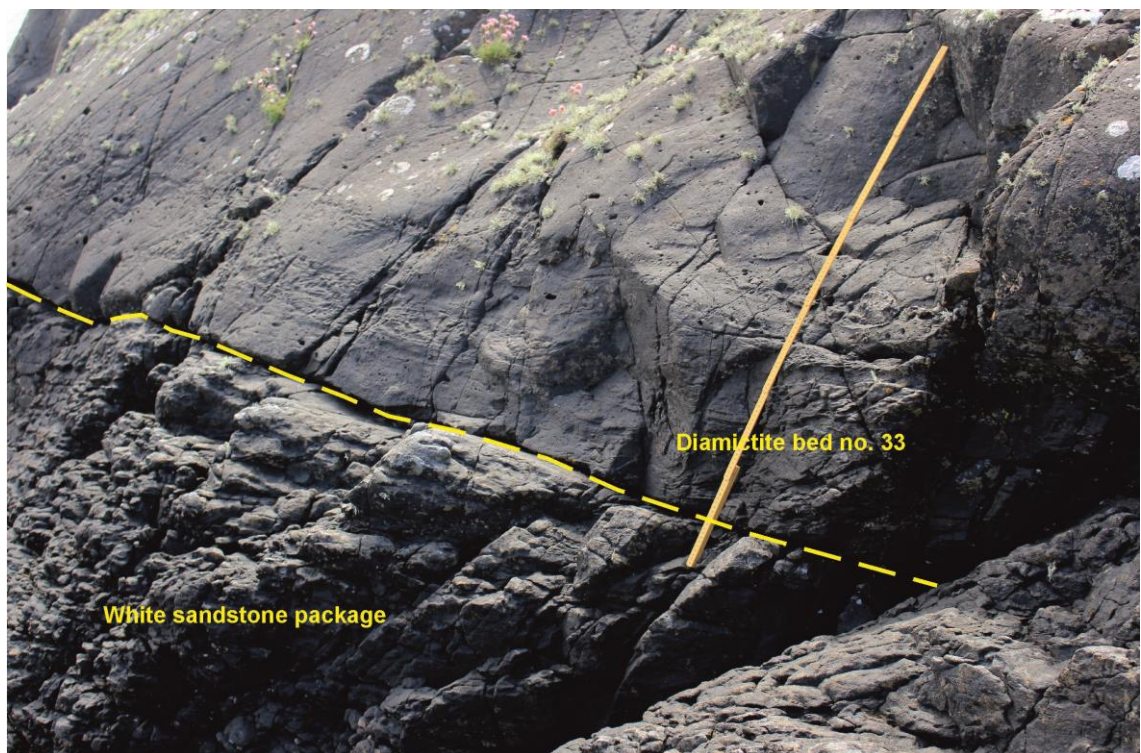
Figure 4.44: Yellow dashed line is the lower contact of diamictite no.33 with the underlying white sandstone beds on the E coast of GE. The ruler is 1m scale.

The upper contacts of diamictites D35, D36 and D38 are, where they are overlain by the white sandstone units above, planar and sharp.

The best exposure of the upper boundary of D35 is on the S of GE near the landing jetty. Analysis of this horizon over a few metres at this locality exemplifies its complexity (Fig.4.45). The top of the diamictite bed is penetrated by a polygonal network of sandstone wedges: each polygon varies from 1.5-2m across. The wedges contain well sorted, fine to medium grained sandstone. They penetrate down into the diamictite bed for depths from tens of centimetres up to 1 metre. The wedges are truncated by a discontinuous granitic conglomerate bed. This bed overlies D35 and separates the massive diamictite bed from the overlying white sandstone. The conglomerate has sharp lower and upper contacts, respectively, with the underlying D35 and overlying sandstone bed. The thickness of the conglomerate bed is about 15-20cm; it has a granular to sandy matrix, including various sizes of clasts ranging from a few centimetres to 70 cm. The largest granite clast measures about 70X25X15cm and is embedded within the conglomerate. The majority of clasts are granite with a minor portion of quartzite. The clasts in the conglomerate are very similar to those in D35 in type, size and shape; and it is poorly sorted, and clast-supported; the granite clasts have sharp contact with the groundmass (Fig.4.38).

Near the W coast of GE, about 100 m inland from the sea, there are 5 sandstone wedges penetrating D35 and overlain by small patches of granitic conglomerate. Boulders and cobbles of coarsely crystalline granite within the top of D35 here show a special structure (Fig.4.46). These clasts consist of angular pieces of crystalline granite, 0.5-25cm in size, separated from each other by diamictite matrix.
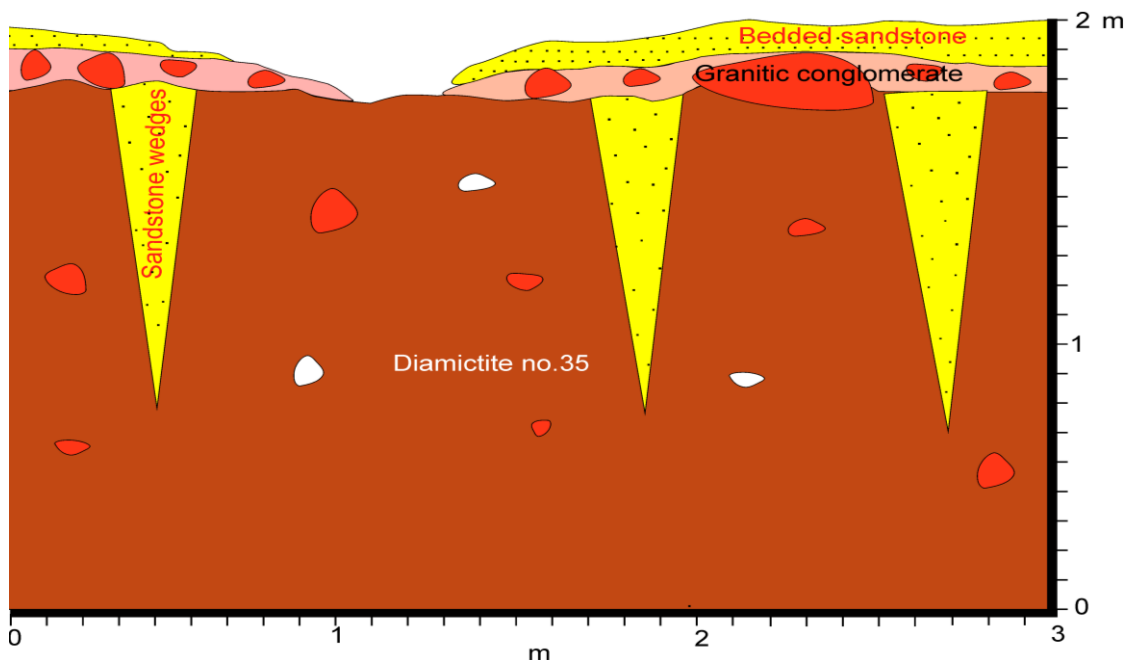
Figure 4.45: A cartoon explaining the stratigraphic relationship (horizon analysis) of the top of diamictite no.35, in the S coast of GE. Sandstone wedges penetrate diamictite bed no35 and are overlain by a granitic conglomerate bed.
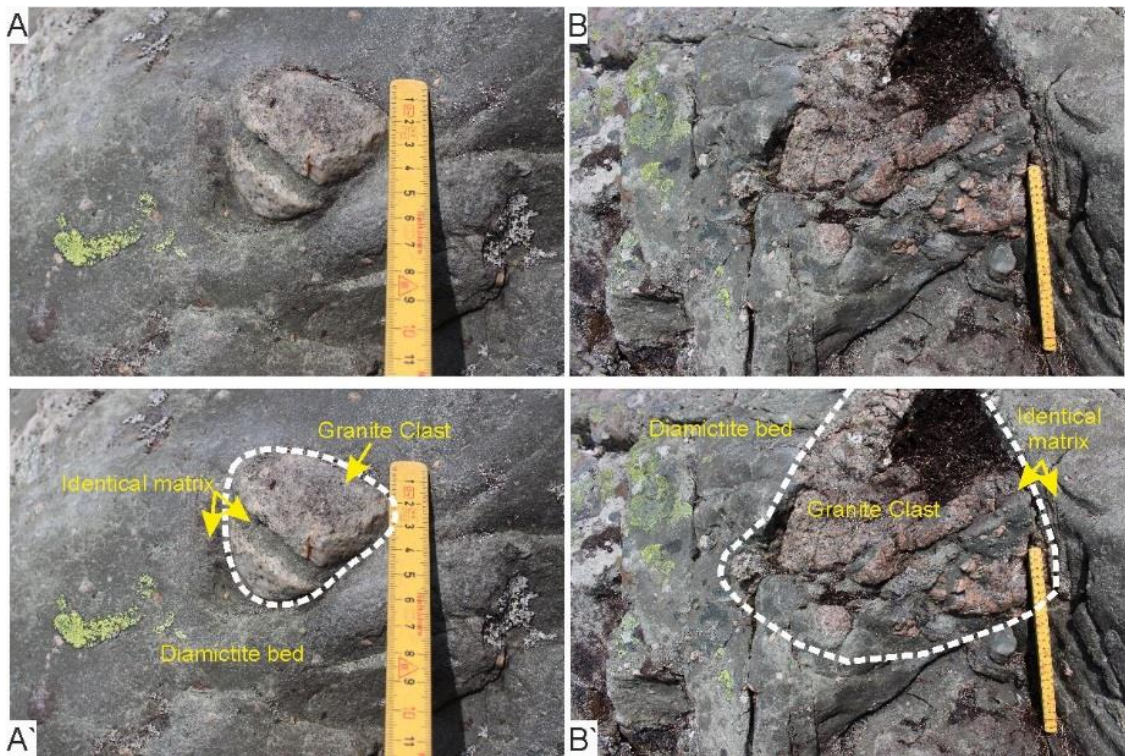
Figure 4.46: Fractured and dismembered clasts, with diamictite matrix protruding into and separating the clast fragments. About 100 m inland from the W coast of GE, at the top of diamictite no.35. (A) and (A`) Granite clast broken into two pieces and separated by matrix identical to the matrix of the host sediment. (B) and (B`) example of a granite boulder fragmented into tens of angular pieces. In both photos, the ruler is the scale and white dashed lines are the outer boundary between the original granite clast and the matrix.

The granite pieces resemble the pieces of a jigsaw: the components of a former single, but now fragmented clast. Similar fragmented clasts were recorded at the same stratigraphic level about 100 m further W (Fig.4.47).

On the SW coast of GE, the upper contact of D36 shows the change between the massive diamictite bed and the overlying well-bedded white sandstone strata. The contact is sharp and irregular; some cobble and boulder-sized granitic clasts occur at the contact and protrude upwards into overlying sandstone (Fig.4.48 and 4.49). Furthermore, on the S coast of the same Island, the same feature has been recorded. Diamictite 38 is overlain at a sharp contact by white sandstones. These white sandstones correspond to the topmost exposed stratigraphic level on the GE.
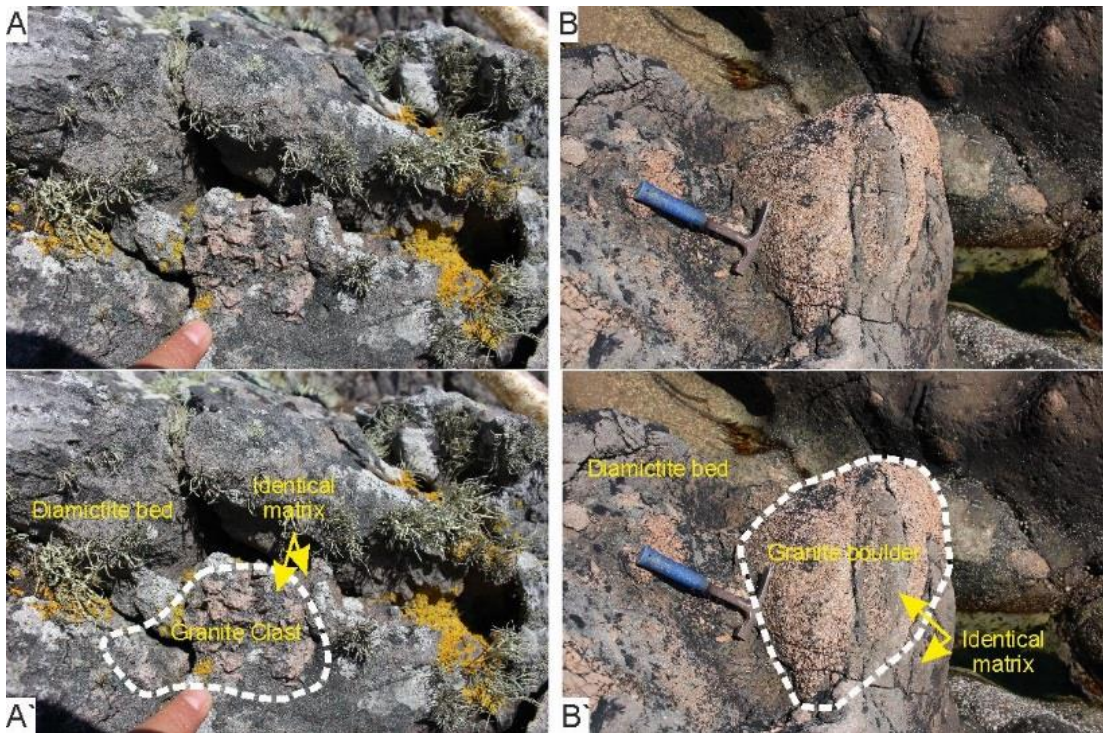
Figure 4.47: Diamictite matrix protruding into dismantled clasts and separating the clast fragments. W coast of GE at the top D35. (A-A`) Granite clast broken apart into tens of angular pieces and separated by matrix identical to the matrix of the host sediment. (B-B`) examples of granite boulders fragmented into tens of angular pieces. In both photos, the geological hammer and finger are the scale, and white dashed lines are the outer boundary between the original granite clast and the matrix.
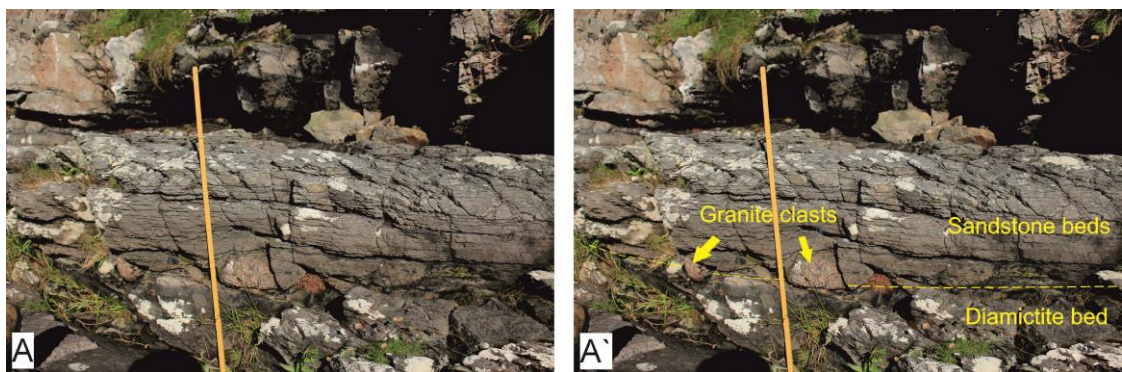
Figure 4.48: (A-A`) W coast of GE. Granite clasts lying at the contact between D36 and the overlying sandstone bed. The dashed yellow line represents the contact between them. The clasts protrude into the overlying sandstone bed. Ruler 1 m scale.
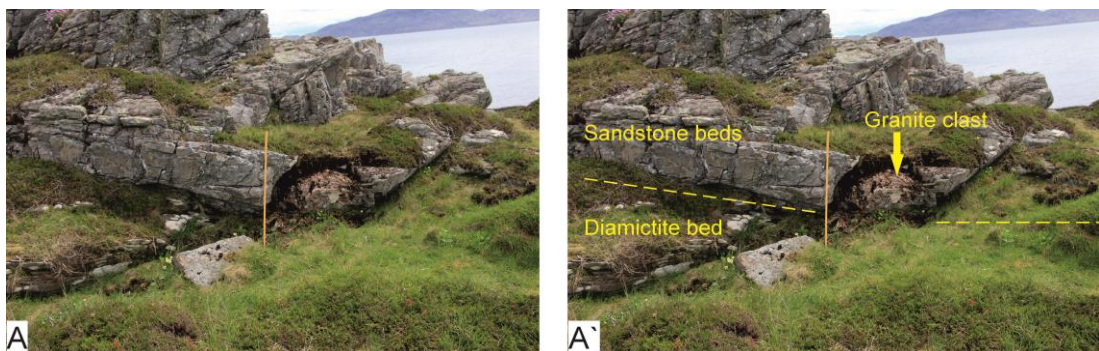
Figure 4.49: (A-A`) Granite boulder at the contact between D36 and the overlying sandstone beds. W coast of GE. The dashed yellow line represents the contact between them. Ruler is 2 m scale.

(c) Lithologies

The beds of diamictite have a muddy or fine sandy matrix and contain boulder and cobble size clasts. Diamictites 33, 34 and 35 are separated by discontinuous sandstone beds. The matrices of D33 and D34 are more argillaceous and well-cleaved, while D35 has a massive arenaceous matrix. The clasts exhibit different lithology, size, and ratio. The proportion of different clast types is shown on 'Fig.4.50'. Extra-basinal clasts (granite, quartzite and unidentified crystalline clasts) are the main clast types; intra-basinal clasts (dolomite and limestone) are much less abundant. For instance, extra-basinal clast percentages, respectively, are 74.4%, 82.1%, and 51.7% for D33, D34, and D35; also, intrabasinal clast percentages are 25%, 12.8%, and 48.4% for D33, D34, and D35 respectively (Fig.4.50). Clasts in D35 are generally larger than the clasts in D33 and D34; the latter is poor in clasts compared with the other two diamictites. The lithology of D36 is similar to D35, but D36 contains less boulder sized clasts than D35.
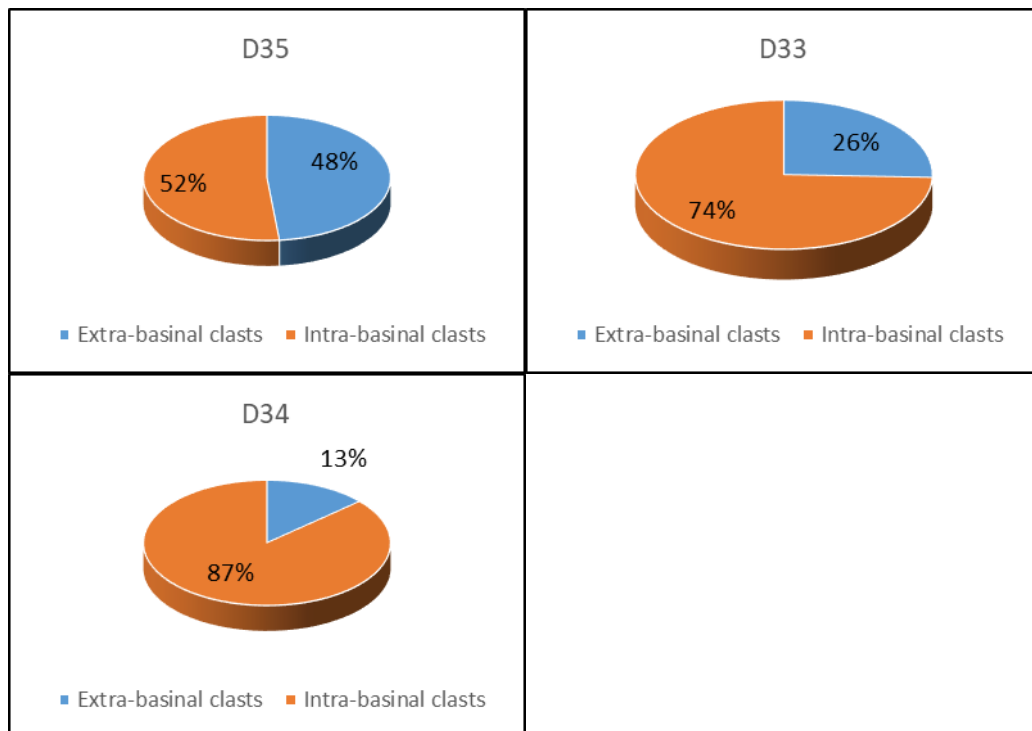
Figure 4.50: Pie chart show the proportions of the extra- and intra basinal clasts within D33, D34 and D35.

Diamictites D37 and D38 are similar to D33-D35 described above. Lithologically, they have silty sandstone matrices, are well cleaved and have a light blue-grey colour in fresh surface. These diamictites contain clasts of various lithology. The granite clasts are abundant and form the largest clasts, while quartzite and carbonate lithologies occur in minor proportions; the amount of carbonate clasts in both diamictite beds is less than 10%. The clasts have sharp contacts with the diamictite matrix and the diameters vary from some centimetres up to 80 cm. D38 is more homogeneous than D37 and the latter contains a few lenses of stratified sandstone or siltstone, on the S coast of GE.

(d) Sedimentary structures

The beds of diamictite are mainly massive with some faint lamination at a few stratigraphic levels. The lower boundary to all three diamictite beds is planar and shows a sharp change from bedded white sandstone to massive diamictite beds.

D33 and D34 are easily separated, by a discontinuous sandstone bed which varies in thickness; for example, on the E coast of GE a 1m sandstone beds occurs between D33 and D34 (Fig.4.37). On the W coast of the same Island, the contact is sharp, and 4 m of sandy laminae occur in the lowest part of D34 and are parallel with the contact. Also, 9 m above the base of D34 a 1.2 m thick bedded sandstone layer occurs and can be traced about 300 m before disappearing. Both beds of diamictite are massive, except for a few faint laminations 2 m above the base of the D34 in the SW of GE.

The contact between D34 and D35 is marked by a complicated bedded horizon 0-7.5 m in thickness which can be traced through much of the outcrop on GE. The horizon is composed of siltstone, weathered brown sandstone, pebbly sandstone and breccia rich in cobble and boulder sized clasts. On the E coast of GE, this breccia overlies the lowest sandstone and shows large basin shaped structures.

In the SW of GE, there is a group of lenticular beds of sandstone and conglomerate, about 30 m long and 2.5-3m thick occurs, within D36 (Fig.4.51 and 4.52) and tens of centimetres below the third white sandstone unit. These lenticular bodies are separated from the overlying third sandstone by a diamictite bed about 20 cm thick, which pinches out to the NW (Fig.4.51) and which has isolated boulders sticking up at its top (Fig.4.48 and 4.49). Within the sandstone-conglomerate lens, each individual group is a few metres long and about one metre thick.
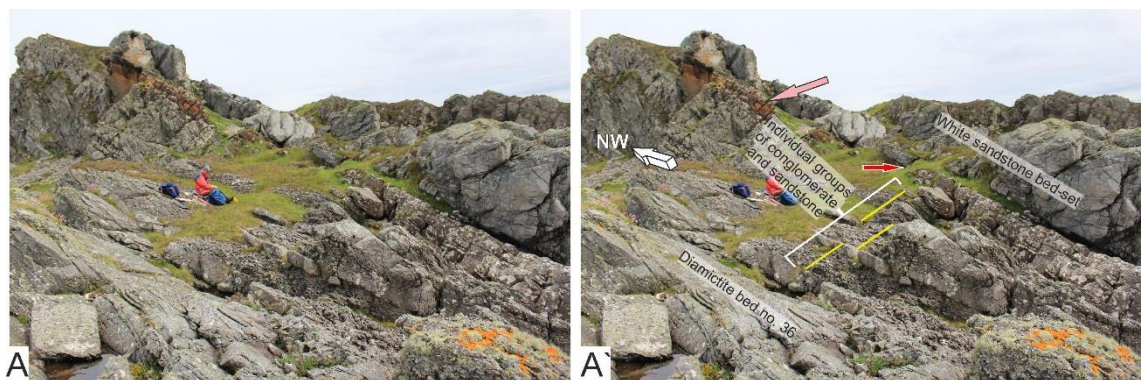
Figure 4.51: White lines represent a thickness of the individual lenticular group of conglomerate and sandstone (side view) within uppermost part of diamictite no.36. The red arrow represents the location of the granite boulder in Fig.4.49 and the pink arrow shows the brown-weathered sandstone bed.

Each group contains conglomerate and sandstone beds. The conglomerate beds contain various clast types (mostly granite), are poorly sorted and the clasts are <1cm to few centimetres in diameter; they are interbedded with white sandstone beds. The thickness of the conglomerate and the sandstone beds, respectively, are approximately 70cm to 30cm. The sandstone beds include low angle cross-beds with foresets about 15cm high (Fig.4.53).
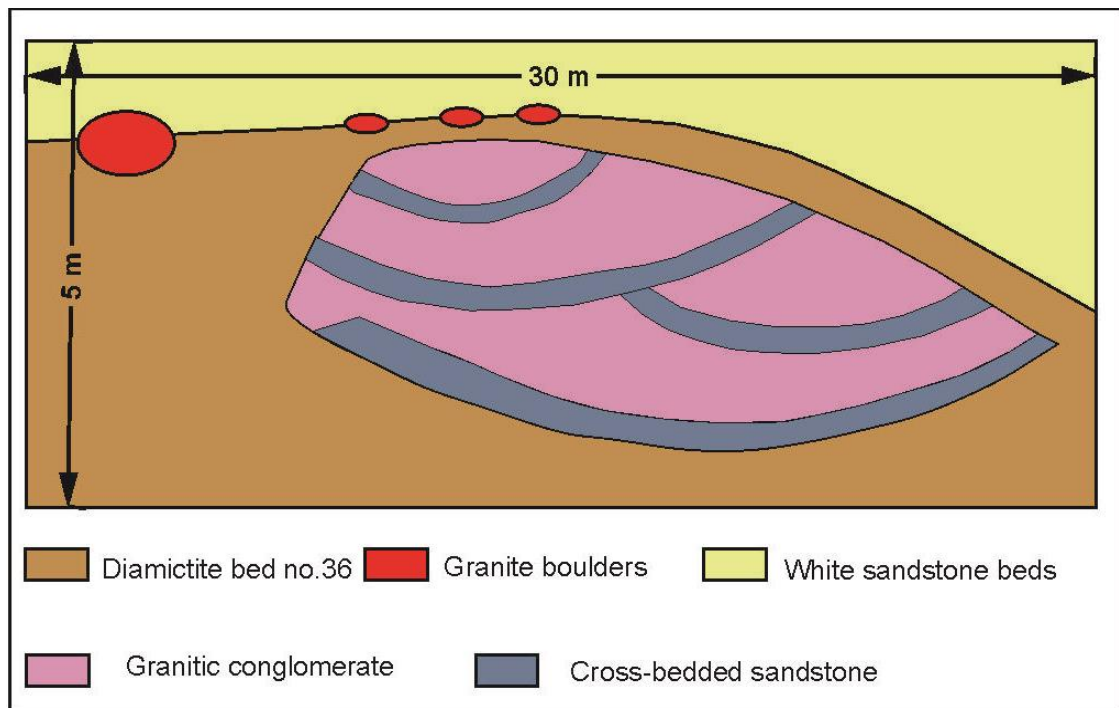
Figure 4.52: A cartoon showing the lens of lenticular groups of interbedded granitic conglomerate and sandstone within D36. W coast GE.

Figure 4.53: Interbedded groups of conglomerate and sandstone within D36. On the W coast GE; geological hammer for scale.

Stratification at the D37/D38 contact: The upper contact of D37 is sharp beneath a trough cross-bedded sandstone on the W coast of GE. D37 and D38 are sometimes separated by a series of pebble-free sandstone beds. Separation between these two diamictites is impossible when the sandstone beds are absent between them. The thickness of sandstone is about 3.6 m and shows current flow toward the E and SE. The lower contact of D38 with the sandstone is erosional and sharp, and the diamictite bed

176

includes some fine lamination in its lowest 50cm, which is parallel to the base of the diamictite. On the SW coast of GE, the lowest 1m of the D37 shows some lamination. Here, D37 can be subdivided: the basal 2.5m is clast rich, and the centre part (6 m thick) of the diamictite bed contains a smaller number of clasts, however, these internal details cannot be traced through the island toward the E coast and are absent in the S coast section.

4.2.3 Lonestone-bearing lithofacies:

On the SW coast of GE, thin laminated, yellowish-green siltstones occur 13.3m above the base of the third white sandstone unit. This bed contains well-rounded and spherical outsized clasts (Fig.4.54) of up to 30cm across. This bed is the only bed that occurs in member 3 that contains outsize clasts. It needs to be treated as a separate lithofacies from the white sandstone lithofacies in which it is enclosed.
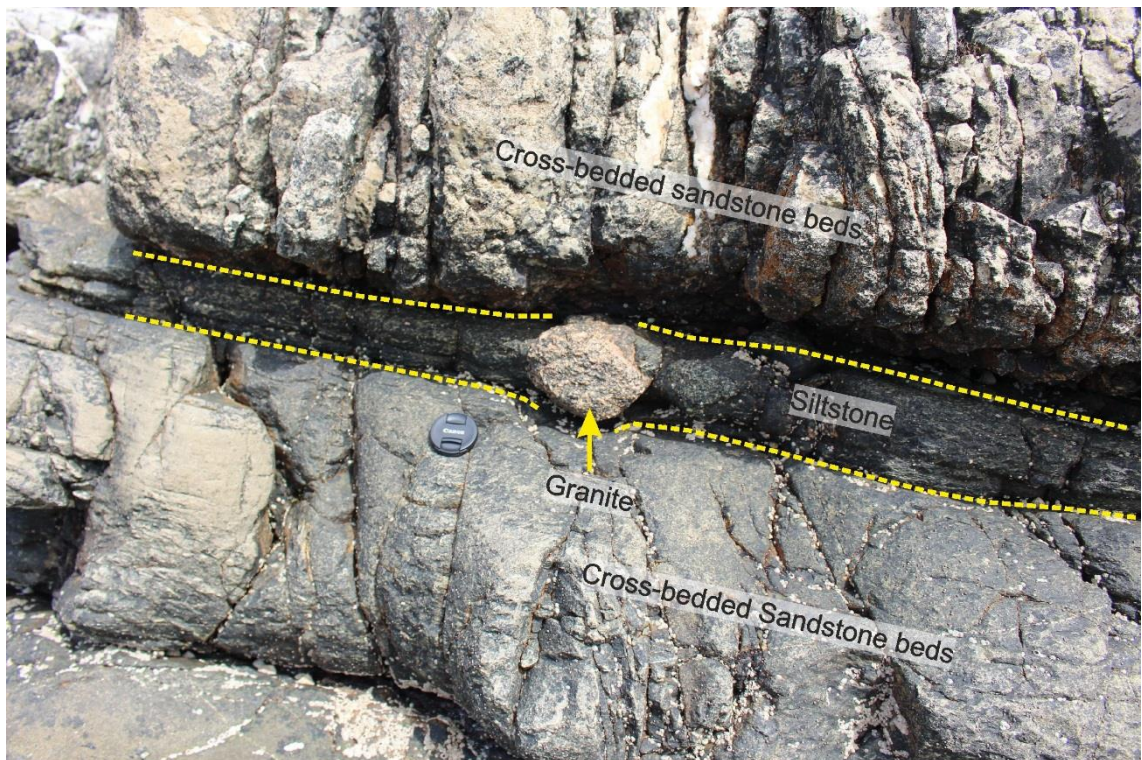
Figure 4.54: Laminated siltstone including lonestones (dropstone) lying between two cross-stratified sandstone beds. W coast GE. Camera lens cap is 5 mm.

4.2.4 Discontinuous brown-weathering horizons:

These occur at two levels within the lowest sandstone unit. They are dolomitic sandstone and sandy dolomites. On Sgeir nam Marag, a discontinuous brown-weathering sandstone bed, 3-13m thick, occurs just beneath D33 and includes intra-bed folds (Fig.4.55). The involutions occur in a medium to coarse grained sandstone which is finely laminated. The involutions have an amplitude up to 1m and, in cross-section, show broad basin shapes separated by sharp and narrow anticlines which are truncated by an erosional surface above. The synclines are faintly trough cross-laminated. This horizon is similar to the intra-bed folds at the top of D26 but they are more organized. The same level of dolomitic sandstone is seen on the W coast of GE (Fig.4.51 and 4.55).
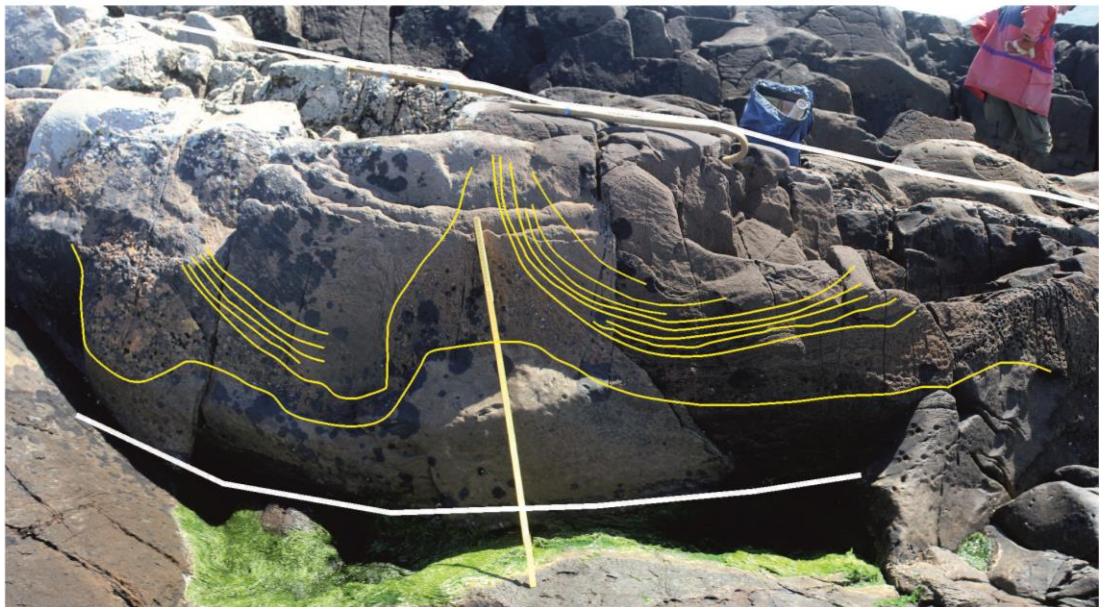
Figure 4.55: White lines show the boundary of the brown-weathered sandstone bed. Yellow lines represent convolute structures. Sgeir Nam Marag, ruler is 1m for scale.

4.2.5 Depositional environments of the white sandstone-arenaceous diamictite LFA

Micromorphological study is not suitable for the PAF, because the rocks are highly strained due to the Caledonian orogeny. Therefore, interpretation of the depositional origin depends on outcrop scale and comparable data. The main features of the white sandstone-diamictite facies association which require interpretation are: (i) white sandstone, lithology and sedimentary structures. (ii) Diamictite, lithology and sedimentary structures; (iii) Contact surfaces between the white sandstone and the diamictites, together with their associated sandstone wedges and shattered clasts.

a) Depositional environments of the white sandstone lithofacies

One of the main features of the white sandstone facies is the presence of large cross-beds (dunes). Large dunes are found in a wide range of sedimentary environments: aeolian, rivers experiencing flood discharge, tidally influenced shallow seas, and outer shelves with tidal and/or geostrophic currents

(Coleman, 1969; Brookfield, 1977; Ashley, 1990; Berne et al., 1998). Tidal and/or geostrophic currents are most likely as the depositional environment of the white sandstones.

i. Subaerial settings
Aeolian settings:

Arnaud (2004) stated that the large cross beds of the lowest and second unit white sandstone bed-sets show similarities with the compound internal structure in ancient aeolian deposits that described by Brookfield (1977). However, typical aeolian feature such as grain-fall lamination, adhesion surfaces, sub-critical climbing to translate strata, and steeply inclined cross sets have not been found (Brookfield, 1977; Hunter, 1977).

Fluvial settings:

The migration of a large river channel can create large scale-cross strata, notably as point bars in a meandering system. Eriksson et al. (1998) and Ielpi and Rainbird (2016) suggested that Precambrian rivers were commonly braided due to the lack of channel-bank stabilizing land plants. The white sandstone beds are unlikely to be of fluvial origin because they do not exhibit several typical characteristics of Precambrian braided deposit: (i) they lack various thickness of cross-bedded sandstone; the bed thickness do not decrease up-ward; also, they lack shallow scours or channels (metre-scale depth and tens of metres wide) filled in with cross-bedded sandstone (Rainbird, 1992; McCormick and Grotzinger, 1993); (ii) they lack mud-chip breccias and lenticular siltstones with desiccation cracks and evaporites, or sheet-like conglomerates that line scoured surfaces (Rainbird, 1992; McCormick and Grotzinger, 1993); (iii) no transitional facies has been founded between the glaciomarine sediment of Member 2 and the cross-bedded sandstone of Member 3, (e.g., shoreface or intertidal deposits).

ii. Subaqueous settings
Based on the above, the cross-beds in Member 3 are unlikely to have been deposited in a subaerial environment. It has been suggested that they formed as a result of the migration of submerged dunes in subaqueous settings (Spencer, 1971; Eyles, 1988; Arnaud, 2004).

The giant cross-beds in the white sandstone facies could have formed by migration of subaqueous bedforms under unidirectional currents, as ripples and cross-beds (small and medium dune). Deposition under upper flow regime conditions produced parallel-laminated sandstone and rapid deposition created massive beds (Spencer, 1971; Eyles, 1988; Arnaud, 2004). Processes that can cause unidirectional currents are tidal, longshore, and geostrophic currents and/or shoaling waves in marine (Arnaud, 2004) or lacustrine (Ainsworth et al., 2012) settings. These strata were more likely to have formed under the influence of substantial tidal and/or geostrophic surface current based on the scale of the inferred bedforms (Arnaud, 2004).

Tidal settings

The giant cross-beds were interpreted as having formed under strong tidal current in a relatively shallow marine setting (Spencer, 1971; Eyles, 1988). There is a similarity between the internal organization of the giant cross-beds documented here and the internal structure of modern tidal subaqueous dunes on the Northern French Coast (Berne et al., 1998) and the internal organization of predominant unidirectional tidal current Class IV sand waves described by Allen (1980). However, some common features of tidal deposits are absent: herring-bone cross-bedding or antidunes relative to the larger-scale slip face on which it developed (Levell, 1980; Kamp et al., 1988; Smith and Tavener-Smith, 1988; Ashley, 1990; Smith, 1992). Moreover, the typical characteristics of inner shelf and near shelf tidal settings are conspicuously absent; such as mud clasts, mud drapes and tidal bundles indicative of tidal current reversals and fluctuation from high- to low-energy depositional regimes (Allen, 1982; Johnson and Baldwin, 1996). Therefore, based on the scarcity of this evidence Arnaud (2004) suggested a relatively deeper setting than initially proposed by Spencer (1971) and Eyles (1988).

Geostrophic settings

There is similarity between the scales of the dunes and internal structures formed in tidal and in geostrophic settings. Therefore, large-scale geostrophic currents might have produced the giant cross-bedded sandstone of the PAF. Arnaud (2004 in table.1) made a comparison between ancient and modern analogues of the sedimentary characteristics, facies association and deposition setting of tidal and geostrophic settings in different places in the world. As modern examples the Agulhas current on the Kwazulu-Natal shelf off SE Africa produces compound bedforms with heights up to 17 m and lee slopes dipping at 8° (Ramsay et al., 1996; Arnaud, 2004: Table 1; Terry and Goff, 2014). At the shelf edge of the Bungo channel in Japan corresponding bedforms were documented under the influence of the Kuroshio currents (Ikehara, 1998). The inferred 'geostrophite' model of Ramsay et al. (1996) is applicable to the internal structure of the white sandstone facies (Arnaud, 2004). The typical features of sand deposits modified by shallow-water bottom currents in 50-300m depth (Macdonald et al., 2013), and those of the white sandstones appear similar.

Combined tidal and geostrophic settings

The cross-bedded white sandstones in Member 3 may also have formed as a result of a combination between tidal and geostrophic processes. The large-scale cross-beds in the Bungo channel off SW Japan, are not only found in a restricted area, but also formed under the influence of the Kuroshio geostrophic current at the mouth of the channel and shelf edge (Ikehara, 1998). The giant cross-beds in the Palaeozoic Vryheid Formation of S Africa are 12 to 40m thick and <28° dip angle; and the Cenozoic Tekuiti Group of New Zealand contains cross beds <4.5 m thick and <20° dip angle formed by both tidal and geostrophic currents (Selley et al., 1963; Smith, 1992; Arnaud, 2004: Table. 1). Based on the palaeogeography of the New Zealand shelf and modern New Zealand margin Gilbert (1983) preferred a combined current interpretation there.

It is difficult to fully deduce the origin of the white sandstone facies (i.e. whether tidal, geostrophic or combined tidal-geostrophic) owing to the similar internal structure of compound cross-bedded sets or facies associations predicted for each of these settings.

b) Depositional environment of the arenaceous diamictite facies

The diamictite beds of the PAF were first suggested by Thomson (1871) as a glacial origin, then Kilburn et al. (1965) proposed them as a glacial deposit and Spencer (1971) concluded they were glacial tills. The mechanisms of diamictite formation are controversial, ranging between direct deposition from ice (subaerial) and/or ice rafted processes (Spencer, 1971) and subaqueous debris flows (Eyles, 1988). Thus, the diamictite lithofacies association may have formed by any of four mechanisms: (i) as terrestrial moraines, (ii) as sub-glacial deposits below lake-or –the sea; (iii) by ice-rafting or (iv) by downslope mass movement of sediments from any of the first three mechanisms.

Mass-flow settings

A glaciomarine depositional model has been suggested for PAF diamictite beds based on (Eyles and Eyles, 1983; Eyles, 1988; Arnaud and Eyles, 2006): (i) stratigraphic context; (ii) palaeogeographic settings of other upper Precambrian diamictite beds of similar age; (iii) their assertion that there is a lack of evidence of traditional processes associated with ice movement, such as lodgement, striated and faceted clasts, bullet-shape boulders and boulder pavements, the lack of organized conglomerate and sandstone deposits typical of outwash fans found at ice margins, and glaciotectonic deformation structures; and (iv) the shear deformation typical of subglacial till (Pratt, 2002) has not found in diamictite beds of the PAF. Eyles (1988) studied the diamictite beds of the PAF on the Garvellachs and based on their tabular outcrop geometries, and lack of a glaciotectonic structures, suggested that the diamictite beds are similar to the glaciomarine Late Cenozoic Yakataga Formation of the Gulf of Alaska. The deposition of the Yakataga Formation took place in a glacially-influenced shallow marine shelf setting (Helwig, 1970; Eyles, 1988; Vandenberghe, 2011). The massive and stratified diamictite beds there formed as a result of sediment rainout from ice-rafting (Eyles, 1988); the fine-grained sediment was supplied by sediment-laden plumes in a glacially-influenced marine environment (Gilbert, 1983; Plaziat et al., 1990; McCarroll and Rijsdijk, 2003).

The lower contacts of the diamictite beds of the PAF are commonly knife sharp and planar or slightly irregular. Deposition of the diamictite beds must be as a result of the flow of mass mudflow or ice-sheets across these surfaces or, alternatively, rafting from ice-bergs must have commenced on these surface (Spencer, 1971: pp. 11). Eyles et al. (1985) interpreted the abrupt change between the underlying beds and the diamictite as a change in energy regime and sediment supply consequent on punctuated glacio-isostatic or tectonic subsidence and eustatic sea level changes. Furthermore, the upper boundaries of some diamictite beds in the PAF succession, such as D35 and D36 are overlain by a granitic lag conglomerate that formed by re-working the upper part of the diamictite bed (Eyles et al., 1985). Moreover, the granitic pebbles within the siltstones in the cross-bedded sandstone above D36 are apparently ice-rafted and indicate the onset of floating ice in the basin prior to mud accumulation

(Eyles, 1988). In addition, synsedimentary, polygonal sandstone wedges, which penetrate the top of diamictite beds, were interpreted as expressions of loading in response to reverse density gradients (Eyles and Clark, 1985). D36 and D38 may have formed as a result of 'rainout' or sediment gravity depositional processes or a combination of both, because do not show characteristics to distinguish between them; also, it was suggested that the diamict originally formed by rainout processes may have been subsequently remobilized on subaqueous slopes (Arnaud and Eyles, 2006).

Grounded-ice settings

A grounded-ice process as an ice-contact deposit, is the second suggestion for the formation of the diamictite beds in Member 3. Spencer (1971: pp.12) argued that to explain these sharp contacts by ice-rafting was difficult for two reasons: (i) during uninterrupted sedimentation in a subaqueous environment ice-bergs should produce a gradational sequence from normal bedded sediment to unbedded diamictite, due to the gradual increase in the number of icebergs to glacial maximum; that is not the case here. (ii) The change in lithology from bedded white sandstones to massive diamictite beds is not gradational and continuous; it is abrupt and sharp. 'Discontinuous sedimentation could result in sharp lower contacts to ice-rafted diamictite, if the mechanism of sedimentation of the interbeds came to a halt and was replaced–after some interval– by iceberg sedimentation alone' (Spencer, 1971). Such a process cannot be ruled out, but it is implausible to explain all the ubiquitous sharp contacts of the diamictite beds in this way.

Thus, according to Spencer (1971) the diamictites formed from grounded ice sheets, due to in situ basal melt-out, giving rise to the sharp lower contacts of the diamictite beds and the nature of the internal bedding in the diamictites. The lenticular shapes of bedded sandstones and conglomerates within diamictite beds (e.g. D36) were formed in sub or englacial tunnels, and could not have been created by the winnowing action of marine currents action on open sea floor (Spencer, 1985). The sandstone wedges that penetrate the top of several diamictite beds at different stratigraphic horizons (e.g. D35) were considered as subaerial (permafrost) features (Spencer, 1985; Le Heron et al., 2013).

Benn and Prave (2006) disputed with Arnaud and Eyles (2002) about the definition of till; it should not be used in a simple, narrow, genetic sense and cannot be recognized just by special characteristic, such as, bullet shaped boulder, striated, facetted, oriented clasts or shear planes (Menzies, 2000; Nogueira et al., 2003). Till has a more complex definition and sometimes is a complicated stratigraphic unit, part of which may contain large thrust bounded, fold chalk rafts , for instance, the Cromer Till that occurs in the Pleistocene of N Norfolk (Benn and Prave, 2006).

The diamictite beds in Member 3 are most likely to have been formed from grounded ice-sheet as a result of in situ basal melt-out rather than as glaciomarine mass mudflows because: First, the sharp basal diamictite contacts are unlikely to result from onset of ice-rafted sedimentation (Spencer, 1971; Spencer, 1985). Second, polygonal sand wedges are permafrost contraction cracks formed in subaerial setting (Boggs, 2014). Finally, the most important features are the fragmented granitic clast (Fig.4.46

and 4.47). These clasts are likely to be frost-shattered cryogenic in situ weathered deposits, supporting the periglacial interpretation (Spencer, 1971; Spencer, 1985). These periglacial features confirm that the environment was subaerial at the end of diamictites deposit, implying that the diamictites were deposited from grounded-ice.

The lenticular shapes of interbedded conglomerates and sandstone groups within diamictite bed-sets (e.g. D36) may have formed as a result of tunnels underneath ice by sub- or en-glacial processes (Spencer, 1971). An alternative mechanisms could be debris flows in a periglacial environment (Fairchild, 1991). Also, a complex scheme proposed showing how conglomerate structures could form in a deformed subglacial bed (Van der Wateren et al., 2000; Knight, 2016; Menzies et al., 2016).

The clasts near the upper contact of D36 and protruding into overlying white sandstone beds are too big (up to 75 cm across) to have been moved by the traction current that transported sand or silt. Thus, there are three ways to interpret how these clasts were formed. Firstly, compaction or loading of sand into the sandy siltstone matrix of the diamictite can be ruled out because no evidence for loading occurs beneath the boulders. A second hypothesis is that they formed by ice-rafting processes. This can be ruled out because there is no evidence for dropstones and the boulders coincide with the contact between diamictite and sandstone beds. Also, frost-shattered clasts, sandstone wedges and cryoturbation structures occur at this stratigraphic level. The third hypothesis is that they were left isolated as a result of re-working of the surrounding fine sediment by the traction currents in conjunction with melting ice and transition into an ice-free environment. This third interpretation is preferred and explains multiple occurrences because: (i) there is no evidence of deflation of strata beneath the boulder; (ii) there is no puncturing and/or abrupt termination of laminae against the margins of the clasts, and no-deformation above the boulders; (iii) the boulders are identical in size, shape, and lithology to the boulders of the D36; and (iv) the boulders occur in two different lithologies: lower half inside D36, and upper half inside white sandstone bed.

c) Lonestone-bearing facies

This facies comprises fine-grained (i.e. siltstone-grade) strata that host lonestones. The clasts are extra-basinal and occur in laminae that are thinner than the diameter of the clasts. Beneath the clasts, disruption of underlying laminae is common. This includes thinning and attenuation of laminae, and local truncation of laminae at the margins of the clasts (Le Heron, 2015). These clasts must have been transported by ice-rafting (Spencer, 1971; Eyles, 1988).

d) Brown-weathered sandstone facies

Dewatering structures similar to the intra-bed folds of the brown-weathering sandstone have been recorded in a outwash subaqueous environment near Ottawa in Canada (Eyles and Eyles, 1983). Anderton (1988) mentioned structures like that in Slettjökull, the northern part of the ice cap Myrdalsjökill, S Iceland formed as a result of dewatering processes in outwash environment. They might also be subaerial cryoturbation structures (Arnaud and Etienne, 2011). As a result, the intra-bed folds in

the brown-weathered sandstone facies might be formed as a result of dewatering after the ice melt-out or by cryoturbation.

Table 4.2: Features related to the depositional environment for the white sandstone-arenaceous diamictite lithofacies association

Features	Lithofacies	Subaqueous mass-flow	Floating ice	Grounded ice	This study
Ice rafting	Lonestone-bearing (in D36-D37 sandstone)	Not possible	Support	Not possible	Floating-ice
Sandstone deposition	White sandstone (four bed-sets mostly tidal)	Indirectly oppose	Possible	Possible	Tidal deposits Geostrophic
Sandstones lacking dropstones	White sandstone (four bed-sets, mostly tidal)	Indirectly oppose	Not Possible	Possible	Tidal deposits Geostrophic
Cryoturbation (periglacial)	Brown sandstone (Beneath D35)	Not possible	Not possible	Possible	Periglacial
Frost-Shattered stones	Diamictite (Top D35, and Top D36)	Not possible	Not possible	Possible	Periglacial
Sandstone wedges (periglacial)	Diamictite (Top D35, Top D36, Top D38)	Not possible	Not Possible	Possible	Periglacial
Boulders protruding at top of diamictite bed	Diamictite (D36)	Unlikely	Possible	Possible	Grounded-ice
Stratified lenticular beds within diamictites	Diamictite (D34-D35, in D36, and D37-D38)	Unlikely	Unlikely	Possible	Grounded-ice
Massive nature of diamictite beds	Diamictite	Possible	Unlikely	Possible	Grounded-ice Mass-flow
Sharp bases of diamictite beds	Diamictite	Possible	Unlikely	Possible	Grounded-ice Mass-flow

Chapter 5 : Islay area

In this thesis, the information from Islay is presented differently from that on the Garvellachs. For members 2 and 3 on Islay the outcrops are much poorer than those on the Garvellachs, so only brief information is given. Member 1 is much thinner on Islay but a few important differences compared to the Garvellachs are represented here. More information is presented on Members 4 and 5, which do not crop out on the Garvellachs.

The type locality of the PAF is on Islay and all five members are exposed in this area. However, the quality of the outcrops compared with the Garvellachs is poor. On the Garvellachs, the whole continuous succession of the lower three members is exposed along the coastline and raised beach. On Islay, most of the rocks are poorly exposed except along a few parts of the coastline or some exposures inland near the lakes or farms. The main differences compared with the Garvellachs are: (i) Members 4 and 5 are present; (ii) the Great Breccia and Disrupted Beds are quite different in geometry and thickness; and (iii) D1-D12 are not present on Islay.

Visited and logged outcrops (Fig.5.1):

1) Around Loch Lossit: Beannan Buidhe, Dun Boraraic, and Lossit farm (Member 1).

2) Along and close to the coastline: Am Meal and Creagan Loisgte (Members 2 and 3).

3) Around Loch Nam Ban: W Loch Nam Ban (Member 3), and Torrabus (Member 1).

4) Around Loch Allen: Port na Seilich next to hydroelectric power station (Member 4).

5) Around Port Askaig: Port Askaig road-cut, and Port Askaig pier to Caol Ila distillery (Members 3 and 4).

In the above sections, the base of the PAF and Member 1 or part of it are only exposed in Beannan Buidhe (Fig.5.1), Dun Boraraic, Am Meal, and Torrabus (Table.5.1). However, Member 2 is exposed at Am Meal and Creagan Loisgte; while Member 3 is exposed in Creagan Loisgte, Port Askaig pier and road-cut and W of Loch nam Ban (Table.5.1). Member 4 is best exposed around Port Askaig and in the cliff N to Caol Ila. Member 5 is exposed best in the Con Tom section (Table.5.1).

Table 5.1: Localities of the visited exposures for each Member within the PAT on Islay.

Exposures	Base	Member 1	Member 2	Member 3	Member 4	Member 5
Con Tom						√
Caol Ila coastline				√	√	
Port na Seilich (Loch Allen)					√	
PA road-cut				√	√	
PA Pier				√	√	
Creagan Loisgte			√	√		
West Loch Nam Ban		√	√			
Am Meal	????	√	√			
Torrabus Farm		√				
Lossit Farm	√	√				
Dun Boraraic	√	√				
Beannan Buidhe	√	√				
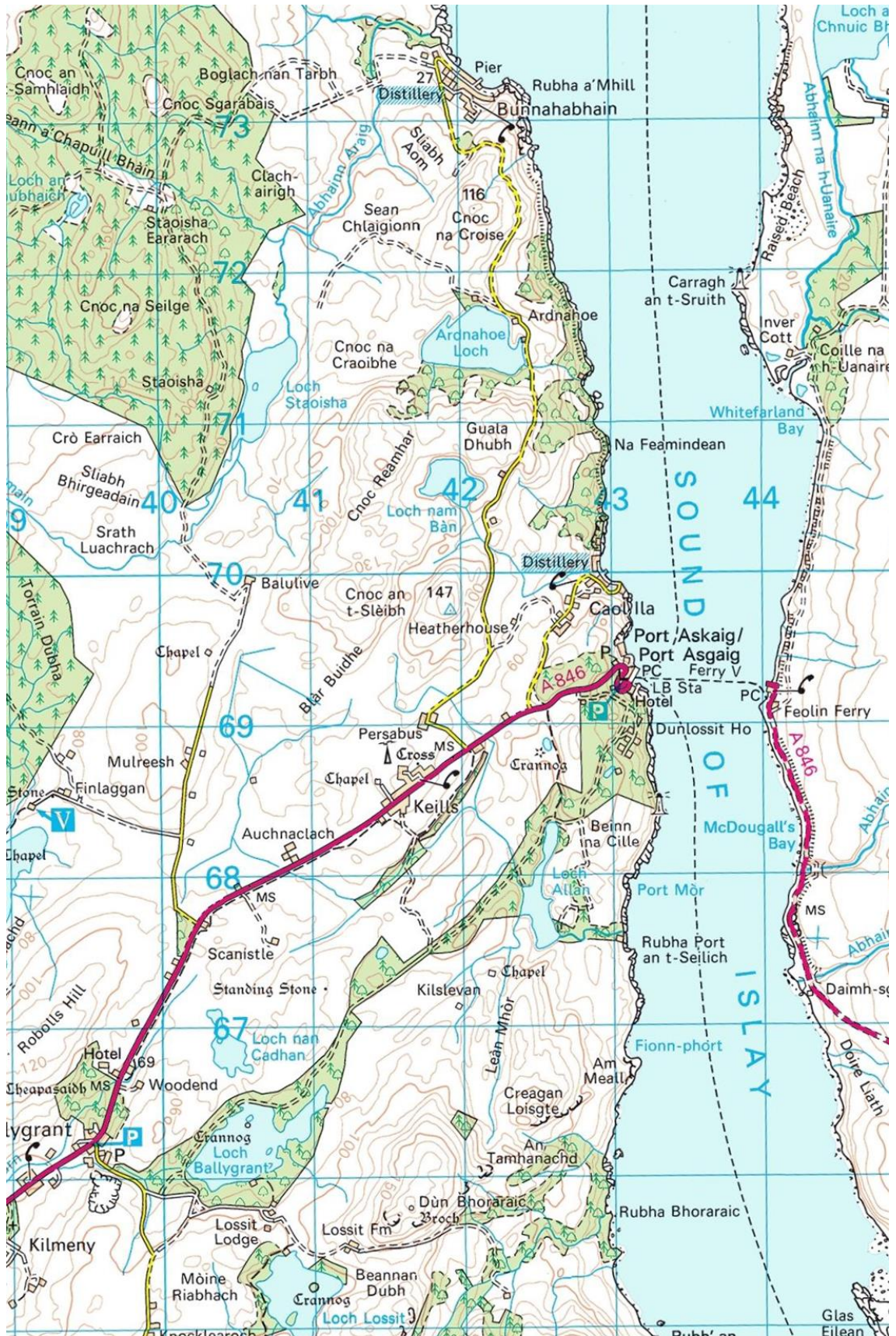
Figure 5.1: Location map for the Islay outcrops. The map is from the United Kingdom ordnance survey, and the scale is the national grid (each square is 1 km).

5.1 Lossit Formation:

The carbonate beds just beneath the PAF exposed at Beannan Buidhe belong to the top 50 m of the Lossit Formation (Arnaud and Fairchild, 2011). They consist of light or dark-grey bedded carbonates. The thickness of the beds ranges between 0.2-0.75 m organised in bed-sets more than 5 m thick. About 5 m below the contact of the overlying PAF, there are alternations between dark grey, massive, fine-grained dolomite and mottled, fine-grained limestones with flake breccia (Fig.5.2).

Figure 5.2: Flake breccia limestone bed alternating with massive dolostone; about 5 m below the contact between PAT and Lossit Formations.

The unit that includes the mottled structure overlies at least one of the stromatolite horizons. Spencer (1971) recorded a 4 m thick white dolomite immediately beneath the lowest diamictite bed on Beannan Dubh (Fig.5.2); the bed exhibits finely laminated concentric structures. Ovoid shapes and rounded pebbles of limestone are present with the mottled (flakes breccia) horizons.

5.2 Depositional environments of the Lossit Formation

Carbonates are usually formed and produced in a carbonate factory area within the sea (Bonnand et al., 2013; Boggs, 2014, pp.319; Fairchild et al., 2016) but some carbonate beds are detrital or lacustrine (Fairchild, 1991; Fairchild and Kennedy, 2007; Boggs, 2014, pp.226; Fairchild et al., 2016). The mechanism and conditions that affect carbonate production are different from terrigenous sediments. This is because most carbonates need: (i) close to tropical conditions; (ii) warm water; (iii) clear water; (iv) low sediment input, and (v) oxygenation (Banner and Lord, 1982; Armstrong and Brasier, 2013). In the Lossit Formation, the presence of stromatolites (Section 3.2.1d, Fig.3.11) indicates a shallow marine environment. Spencer (1966, pp.350) suggested extreme shallow water comparing the oolites within the Lossit Formation to those of the modern Bahamas. For the mottled carbonates (flake breccia), there are several mechanisms to form such a structure:

a. **Dolomitization:** Differing chemical composition of the various carbonate components influence selective dolomitization processes (Gingras et al., 2004). However, the mottled structure is limestone, which means this possibility can be ruled out.

b. **Desiccation cracks**: it is possible these flakes were formed by desiccation. However, the desiccation flakes should be concentrated at the top of the bed and show an organized trend (Le Heron, 2012). The flakes in the Lossit Formation, by contrast, are present through the bed, from base to the top. So, desiccation seems unlikely.

187

c. **Fracture controls:** Mottled structures can be formed due to fractures being used as channels for fluid movement and sometimes hydrocarbons. This possibility can be ruled out, because no hydrocarbons are recorded and both light grey and dark grey patches are limestone.

d. **Limestone pseudo-conglomerates**: conglomerate can form due to mechanical rupture by deformation (by storms or earth quake) and pore overpressure as a result of overburden stress from overlying sediments and sea water (Chough et al., 2001; Chen et al., 2009). This seems unlikely because the mottled structures are flakes commonly 2-3 mm; while the size of the clasts within limestone pseudo-conglomerate are more than 2 cm.

e. **As microbial structures:** the shape of the structure is not like regular stromatolite bodies, but the undulating lower and upper contacts of the bed, and the shape of the flakes, even the ovoid shapes, are similar to the thrombolite microbalite structures (Kennard and James, 1986; Feldmann and McKenzie, 1998; Johnson and Grotzinger, 2006; Shapiro and Awramik, 2006, Fig.6 and 7).

This latter hypothesis is preferred, owing to their size, shape, lithology and geometry.

5.3 Member 1 of the PAF

Diamictite beds on Islay have not been numbered as in the Garvellachs by Kilburn et al. (1965). However, Spencer (1971) used a member system for comparison and correlation between the Garvellachs and Islay.

5.3.1 The basal contact and Member 1 of the PAF:

The basal contact of the PAF with the Lossit Formation is exposed in: Beannan Buidhe, Dun Boraraic, near Lossit Farm, and Torrabus (Fig.5.3). Spencer (1966, Fig.133) illustrated the base of the formation in Beannan Buidhe by a field sketch. In that sketch, the base is irregular and sharp between a breccia and the dolomite beds of the upper part of Lossit Formation. The contact between the two formations on Garvellachs is normally sharp but occasionally gradational, for instance, on DC and on the E coast of GE (Ali et al., 2018: in press; Fairchild et al., 2018: in press); by contrast on Islay, it is sharp everywhere.

On Islay, Member 1 is different from the Garvellachs. It consists of a diamictite breccia bed (same lithostratigraphic level as the Great Breccia), Disrupted Beds, and D14 to D18 (Fig.5.4, 5.10); while D1-D12 are not present here. The thickness of the breccia is about 3.5-4 m and it is formed from one lithofacies not three as in the Garvellachs. Also, D14-D18 are thinner and only three diamictite beds are present on Islay instead of five on the Garvellachs.

The diamictite breccia bed is the first diamictite bed at the base of PAT on Islay (Fig.5.3-5.5). The matrix of this diamictite bed consists of dolomitic sandy siltstones and contains various sizes, and shapes of clasts. The lithology of clasts is dolomite, which is identical to the underlying formation. Despite excellent outcrops but no extrabasinal clasts have been found in this breccia. The size of the clasts ranges between a few cm up to 2 m across; and the shapes are sub-angular to sub-rounded. The identification of the clasts with the underlying dolomite lithology is easy due to the distinctive fine

laminated lithology of both and the presence of microbial structures. The latter also helps to identify the way up and orientation of the clasts. Beneath some boulder sized (*sensu* Terry and Goff, 2014) clasts there is bending or deformation (Fig.5.5). Those clasts seem to be allochthonous, although sometimes it is difficult to see the contact between the boulders sized clast and the underlying Lossit Formation, while a few metres laterally the contact is obvious and clear.

On Dun Boraraic in the same stratigraphic position within the succession, there is an identical breccia (Fig.5.3). Here the diamictite breccia bed is in patches of lenticular shape within the sandstone with dispersed pebble-sized clasts (Fig.5.3). The contact between the diamictite breccia bed and the sandstone is gradational and the matrix of the diamictite breccia bed is identical with the sandstone host rock (Fig.5.3C-D). Also, the contact between the Lossit Formation and the diamictite breccia bed is sharp (Fig.5.3A-B; E-F).
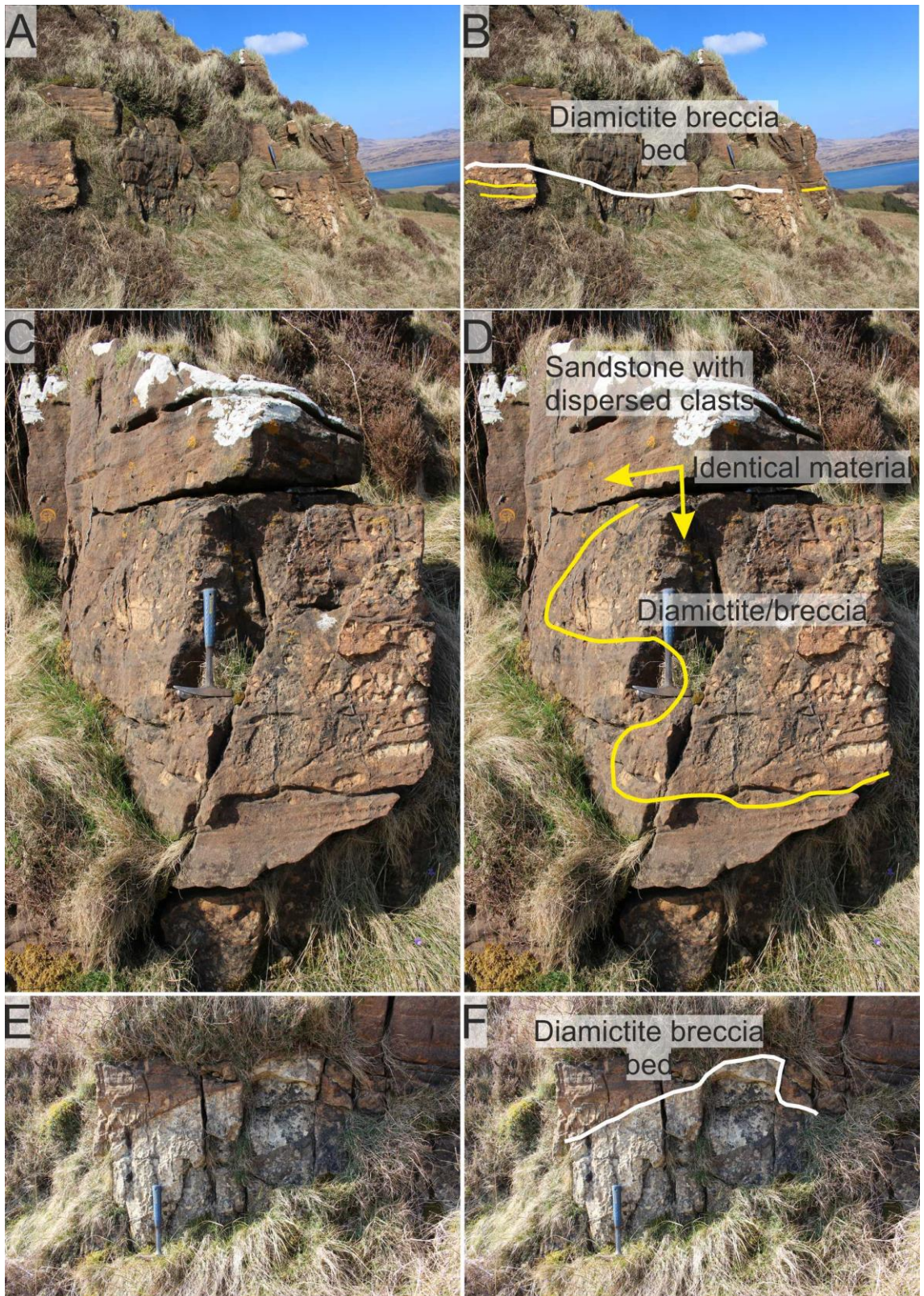
Figure 5.3: Diamictite breccia at the base of the PAF at Dun Boraraic. (A, B, E, and F). (E and F) the white line shows the irregular contact between the diamictite breccia bed, at the base of PAF, and the Lossit Formation (probably a clast). (C-D) the yellow line shows the gradational contact between patches of the diamictite breccia bed with the sandstone with dispersed pebble-sized clasts.
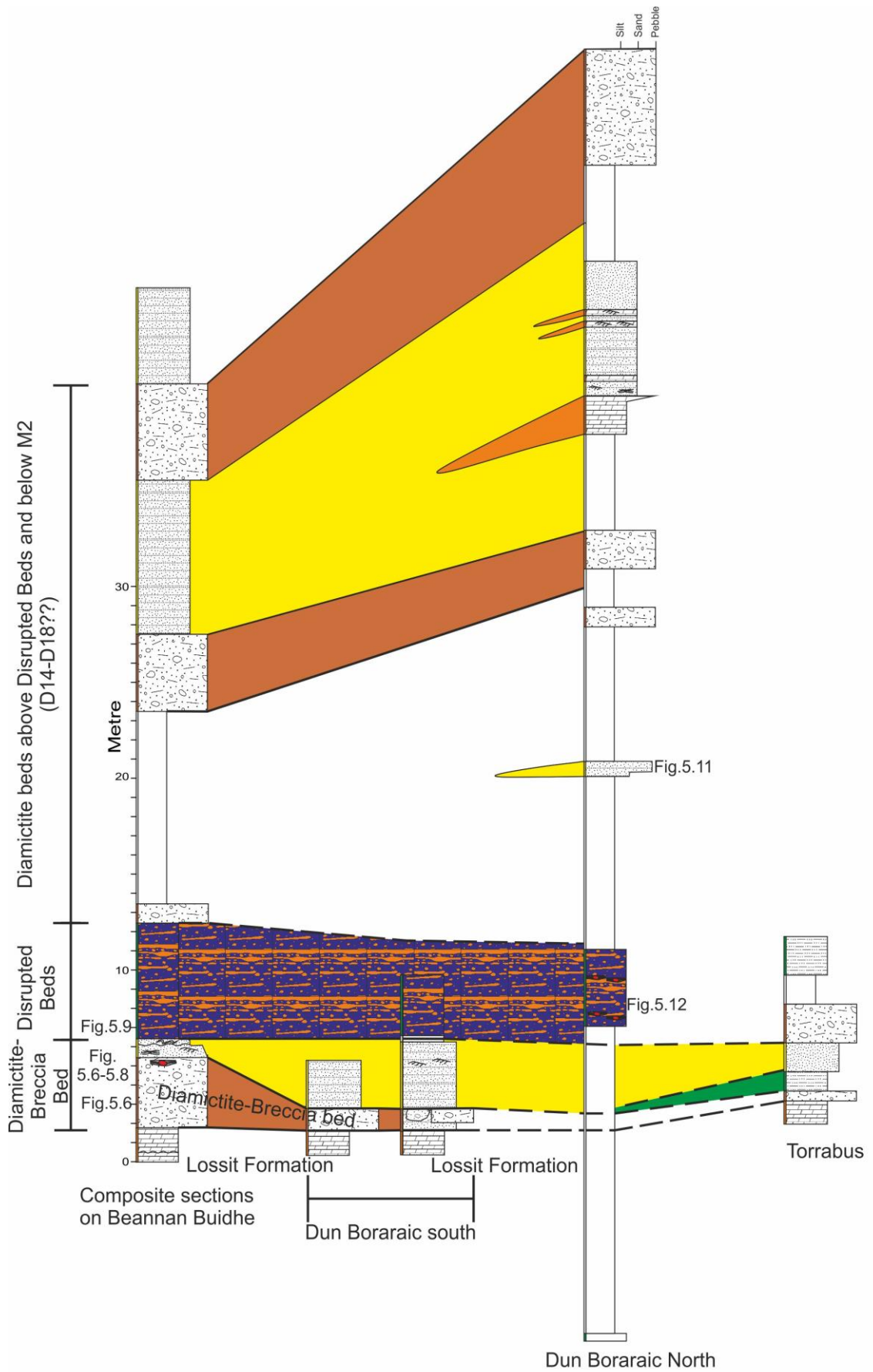
Figure 5.4: Correlation logs of Member 1 in different localities of the PAF on Islay.

Figure 5.5: Diamictite breccia bed at the base of the PAF at Beannan Buidhe. The clast can be easily recognised by its colour.

In places in the Beannan Buidhe section (N 55°48'446''; W 06°07'779'') and at the base of the diamictite breccia bed, lenticular sandstone beds occur. They show evidence of palaeocurrents and some sedimentary structures (Fig.5.6). The 50 cm thick sandstone is medium to coarse grained, and brown in colour on weathered surfaces (Fig.5.8a-b), pinching out over 30 m laterally (Fig.5.7). In the same outcrop and underneath the lenticular sandstone bed there are fine-laminated sandy siltstones (Fig.5.8a-d). The thickness of the bed is about 100 cm, and thins to 30 cm after 8 m laterally in both directions, then dies out completely along strike. This siltstone contains lenses of conglomerate, and dolomite and quartzite outsized clasts (Fig.5.8c-f). There is some bending and deformation underneath the outsized clasts.

Figure 5.6: Sandstone bed, within the diamictite breccia at the base of the PAF on Beannan Buidhe, shows planar and trough cross-stratification trending towards NE.
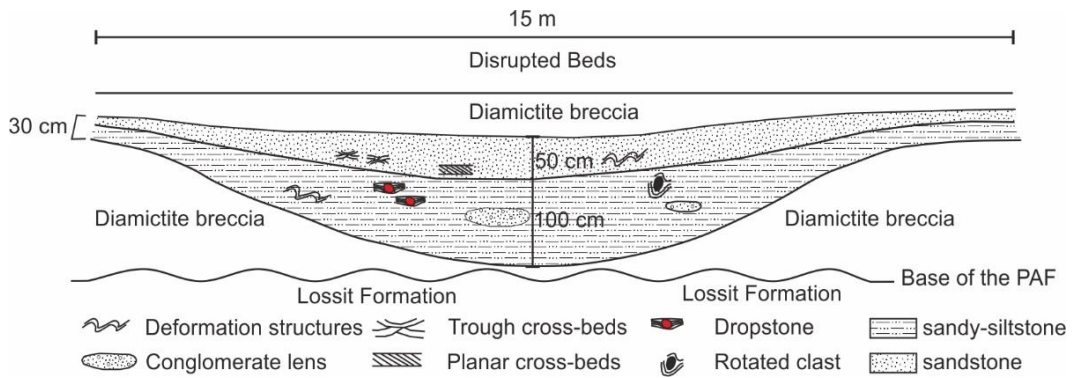
Figure 5.7: Field sketch of lenticular sandstone and siltstone bed above the diamictite breccia bed at the base of the PAF on Beannan Buidhe. The sandstone bed contains trough and planar cross-stratification with some signs of deformation structure; the siltstone bed contains deformation structures, lenses of conglomerate, and some lonestones.

Figure 5.8: (a and b) Sandstone and siltstone beds within the diamictite breccia at the base of the PAF on Beannan Buidhe. The dashed yellow line is the boundary between sandstone and siltstone beds; the red line looks like a fault but is an illusion. The orange rectangle is the place of 'figures c-f'. The black dashed line is the possible contact between PAF and Lossit Formations. (c-f) Lonestone within the sandy siltstone bed.

In this study, the term 'diamictite breccia bed' is preferred instead of breccia bed (Great Breccia on Islay) because:

a. The stratigraphic position of this breccia is similar to the D1-D12 and Great Breccia lithofacies association on Garvellachs.

b. The term 'Great Breccia' is restricted to a lithofacies association in this study, rather than one sole facies, and thus the term is inappropriate.

c. The thickness of the lithofacies is just 3.5-4 m which is very thin compared to the 48 m thick Great Breccia on Garvellachs.

d. It lacks extrabasinal clasts, whereas the Great Breccia contains some quartzite clasts.

e. No lenticular beds of siltstone and sandstone are recorded underneath the Great Breccia on Garvellachs; while on Beannan Buidhe there are siltstone and sandstone lenticular beds at the base of the diamictite lithofacies.

5.3.2 Disrupted Beds (DB)

On Beannan Buidhe and Dun Boraraic a 4-6 m thick interval of deformed strata overlies the diamictite breccia bed and is very similar to the DB on the Garvellachs (Fig.5.4 and 5.9). Spencer (1966, pp.352) suggested five reasons to correlate this lithofacies with DB on the Garvellachs: (i) a 2m thick ore band at the base of the lithofacies in Crags S of Beannan Dubh; this is very similar to that found at the base of the DB on the Garvellachs; (ii) the discontinuous nature of the dolomite beds and irregular bedding of the lithofacies (Fig.5.9) are features shared with the DB of the Garvellachs; (iii) colour contrast between the blue siltstones and dolomite beds and clasts (Fig.5.9); however, the lithology of the Disrupted Beds on Islay is not identical to those in Garvellachs: on Islay, this lithofacies is more arenaceous, composed principally of sandy, pebbly dolomites and dolomitic siltstones; (iv) like the Garvellachs, intrabasinal clasts are common; however, extrabasinal clasts are rarely recorded on Islay, in contrast to the relatively large numbers of extrabasinal clasts present within the DB in the Garvellachs; and (v) in the crags to the S of Beannan Dubh (Fig.5.12a-b and g-h), finely laminated siltstones occur at the base of the DB containing outsize dolomite pebbles of up to 5cm across; similar laminated siltstones with outsize clasts occur in the DB of the Garvellachs (Fig.3.41-3.43).

Figure 5.9: Disrupted Beds on Beannan Buidhe: discontinuous, orange coloured dolomite beds and blue siltstone beds.
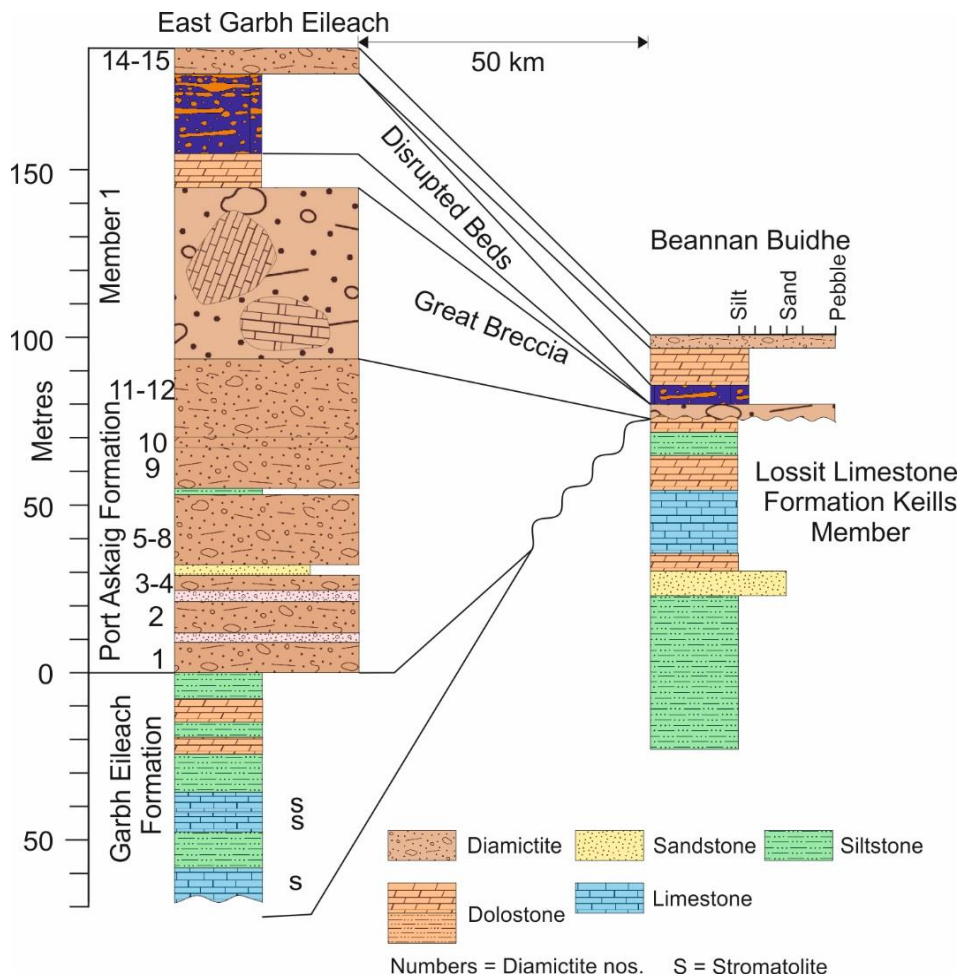
Figure 5.10: Correlation of logs between Garvellachs (E Garbh Eileach) and Islay (Beannan Buidhe and Dun Boraraic). D1-D12 are absent on Islay, and the Great Breccia thins to 4 m. The Disrupted Beds unit is also thinner on Islay than on the Garvellachs.

Within laminated siltstone at the base of the Disrupted Beds on the N of Dun Boraraic, there is a dolomite clast about 40cm across (Fig.5.12a-b) and surrounded by smaller clasts within a sandy siltstone matrix. The matrix at the top of the clasts shows lamination bending around the top of the clast (Fig.5.12a-d). Also, within the sandy siltstones, just 20 cm above the previous boulder, there are smaller dolomite clasts which appear to show rotation (Fig.5.12c-d), imbrication and deformation (Fig.5.12e-f) and outsize clasts (Fig.5.12g-h). At the top of the Disrupted Beds on Dun Boraraic, there is a bed, 80 cm thick, of breccia (Fig.5.11). It consists of brown, gritty sandstone matrix that contains orange dolomite breccia clasts. The clasts are angular and commonly about 5 cm across.

Figure 5.11: Brecciated dolomite clasts at the top of the Disrupted Beds. (a) angular dolomite clast within the bed at the top of Disrupted Beds. (b) outcrop of the Bed in figure 'a'. Coin and geological hammer are scales.

The DB on Islay cannot be studied in comparable detail to the Garvellachs, owing to the lack of exposures. Thus, the four lithofacies of the Garvellachs cannot be recognised. However, the 'bluish siltstone diamictite-disrupted dolomite lithofacies' is obvious and recognisable due to its colour contrast between dark blue sandy siltstone matrix and reddish orange clasts and bands of dolomite (Fig.5.9, and 5.12). The base of the Disrupted Beds is not seen, while the upper contact is irregular and sharp with, 20 cm, discontinuous sandstone beds. The latter is truncated by a thick (7m) diamictite bed.
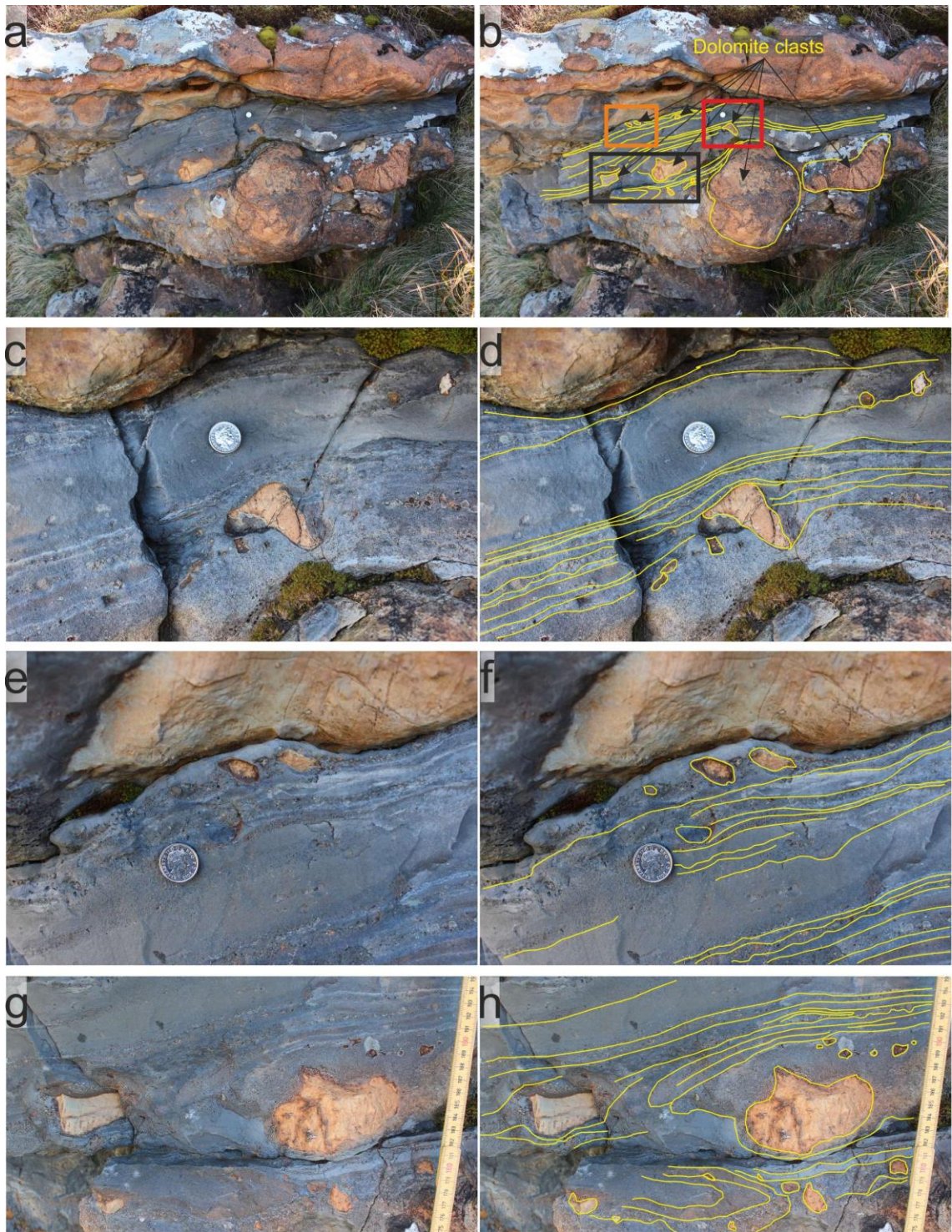
Figure 5.12: Disrupted Beds on the N of Dun Boraraic. (a-b) show outsize dolomite clasts wrapped by fine laminated sandy siltstone lamina. The largest dolomite clast is about 40 cm across in cross-section. The red, orange, and black rectangles show the places of figures 'c-d, e-f, and g-h' respectively; coin is a scale. **(c-d)** rotated dolomite clast within fine laminated sandy siltstone matrix. **(e-f)** exhibit imbricated dolomite clasts within fine laminated sandy siltstones. **(g-h)** outsize dolomite clasts within the fine laminated sandy siltstone matrix.

5.3.3 Dolomitic diamictites (equivalent to D14-D18)

On the north side of Beannan Dubh and Dun Boraraic, there are three diamictite beds between DB and Member 2 (Fig.5.4). The two lower diamictites have an arenaceous matrix and sparse clasts. Most of the clasts are intrabasinal; extrabasinal clasts are rare. However, the upper diamictite bed has a dolomitic

sandy siltstone matrix that contains about 25% extrabasinal clasts. In all three diamictite beds the clasts are mostly of pebble grade.

The middle diamictite bed is massive, while the lower and upper beds show crude bedded structure, especially in the upper diamictite bed due to more dolomitic or sandy horizons. Also, the lower two diamictite beds can only be seen in the crags S of Beannan Dubh; the upper diamictite bed thins laterally to zero in the exposure at Beannan Buidhe, where it overlies bedded dolomite and dolomite conglomerates with an irregular contact.

Spencer (1966, 1971) suggested that these three diamictite beds may be equivalent to D14-D18 on the Garvellachs. However, based on this study in 'Fig.6.16' and 'section 3.5a' D16-D18 die out within the Garvellachs outcrops towards the W. Thus, these three diamictite may be equivalent to D14-D15.

On the Garvellachs, D14-D15 have a dolomitic matrix (details in section 3.5b) and contain more than 30% extrabasinal clasts (Fig.3.57-3.60); while the two lower diamictites here have an arenaceous matrix and are poor in extrabasinal clasts. The upper diamictite here has a dolomitic matrix and contains 25% of extrabasinal clasts, which is similar to D14-D15 on the Garvellachs. As a result, it is not plausible to correlate the two lower beds with D14-D15 on the Garvellachs; they may be two new beds at a stratigraphic level below D14-D15 but above the DB compared with the Garvellachs.

Disconformity surfaces
There are two disconformity surfaces: one at the base of the formation; and the other at the base of the three diamictite beds (Spencer, 1971; pp.89). The new field data partly agree with Spencer (1971) that there are at least two unconformity surfaces: one at the base at the PAF; but the other at the base of Member 2, not beneath the lowest of the three diamictite beds here. However, there are couple of other candidates. For instance, the Main Dolomite in the Garvellachs is missing on Islay, and the thickness of the DB is about 40 m in the Garvellachs but is thin on Islay. Thus, the question is whether the MD can be represented by an unconformity surface on Islay. Also, the Upper Dolomite on the Garvellachs, is absent on Islay: is it an unconformity surface on Islay, or was there just no deposition?

5.3.4 Depositional environments of Member 1
On the Garvellachs, Member 1 was interpreted in various ways because it consists of four lithofacies associations. But on Islay M1 cannot sub-divided in the same way, because the lithofacies associations on the Garvellachs do not exist on Islay. Nevertheless, the depositional mechanisms are probably similar because of the similarity in lithologies, bed geometry and sedimentary structures and features in both areas.

The microbial material that occurs within limestone and dolomite beds in the underlying Lossit Formation indicates a shallow marine environment (Le Ber et al., 2013). It is difficult to envisage the large clasts at the contact between the Lossit and PAF Formations (Fig.5.3C-D, 5.4 Dun Boraraic South) could be moved by water currents. Most of the clasts are angular and cannot have been transported for a long distance, and some of them are still attached to the underlying bed. These clasts must need a

powerful force to pluck them, and move them even for a short distance. Thus, a glacial transport mechanism via grounded-ice is tentatively suggested.

Channel geometry, lenticular sandy-siltstone and sandstone beds in Fig.5.7 could be formed in fluvioglacial channels or lakelets in a periglacial environment, or ponds or tunnels in a subglacial environment under the ice-sheet. Fine-laminated siltstone with lonestone (Fig.5.7, 5.8a-d) underlying the sandstone indicate deposition in water and quiet conditions with ice-rafting. However, the complicated geometry of the bed and of the contacts with the underlying and overlying beds, when followed 50-100 m laterally, are most likely to have form in a grounded-ice setting.

With respect to the three mechanisms-grounded-ice, mass-flow and floating-ice-evaluated in this study for the Garvellachs, it is difficult to explain the ice-rafted, laminated siltstone and sandstone lenticular beds in the same stratigraphic level as the breccia bed.

The DB on Islay (Fig.5.9) is almost identical to the Garvellachs, but is different in thickness and has fewer facies on Islay compared with the Garvellachs. This is attributable to the poorer outcrop quality. Many similarities between the localities suggest that the depositional mechanisms for both the Garvellachs and Islay were similar.

The DB in 'Fig.5.9' was interpreted by Spence et al. (2016; Fig.7c) as containing concretion lenses of dolomite separating siltstones with detrital and secondary magnetite. The brecciated dolomite clasts at the top of the DB (Fig.5.11) are more likely to be frost-shattered clasts than detrital breccia: they are angular, have identical matrix with the host rock, are similar to frost shattered clasts in the Garvellachs, and have a sharp and irregular upper contact with the overlying sandstone bed.

Interpretation of the DB features shown in 'Fig.5.12' is not easy, because the delicate laminated siltstone punctured by dolomite clasts indicate a subaqueous environment; by contrast, the rotated clasts and imbrications can have formed in subglacial or periglacial environments. However, all these features can be formed in the block diagram shown in 'Fig.5.52' for the Garvellachs.

Similarly, the base of the diamictite beds that lie above the DB are sharp; they are at a stratigraphic level that Spencer (1971) correlated with D14-18 on the Garvellachs. Although, this study suggests that this correlation does not work, the author agrees with Spencer (1971) that they may have formed from grounded-ice, similar to the Garvellachs.

5.4 Member 2 (D19-D32)
These rocks are exposed at Creagan Loisgte, Am Meal, Beannan Dubh, and An Tamhanachd. The complete section is exposed on An Tamhanachd to Creagan Loisgte; and the best exposed section is at Am Meal, but unfortunately there is a fault at the top of the section there, at the contact between M2 and M3 (Fig.5.13).

Spencer (1971) chose the contact between M1 and M2 at a 2m thick siltstone bed, which contains green fragments. The siltstone has fine-stratification and shows some deformation structures (Fig.5.14). At Am

Meal, about 50 m above the base of M2, there are seven examples of sandstone wedges (Fig.5.13); also, they occur at An Tamhanachd and at Eileanan Gainmhich. At Am Meal, above these sandstone wedges, most of the rest of the section is unexposed until the fault between M2 and M3; only a 4 m diamictite bed is seen about 9 m above the sandstone wedges (Fig.5.13).

To the SW of Loch nam Ban, the sandstone wedge horizon just described is probably overlain by a sandstone bed, succeeded by thicker diamictites than at Am Meal or An Tamhanachd. At Loch nam Ban and An Tamhanachd, the top of M2 contains a similar arenaceous diamictite which is poor in clasts and in which dolomite clasts are rarely recorded (Spencer, 1971). This arenaceous diamictite beds lies in the "sandstone with dispersed clasts" category of the Hambrey and Glasser (2012) classification.
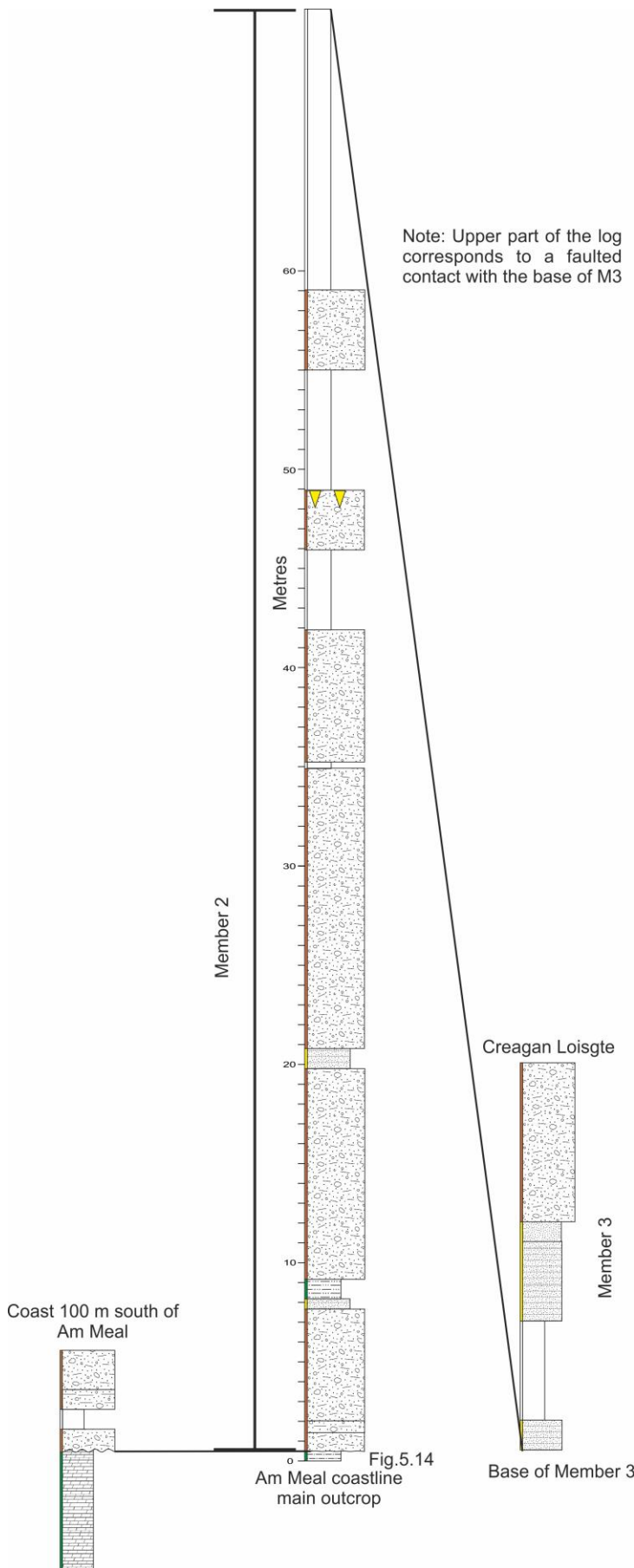
Figure 5.13: Correlation logs of Member 2 of the PAF in different localities on Islay.

201

Figure 5.14: Siltstone bed at the contact between M1 and M2 at Am Meal. The yellow lines show the deformation structure within the siltstone beds; white line represent bedding plane; and the red line shows the cleavage. Coin is a scale.

5.5 Depositional environment of Member 2

The explanation and interpretation of the M2 sediments on Islay cannot be given in the same detail as for the Garvellachs, owing to poorer outcrop quality. The rocks, clast percentages, lithologies, sedimentary structures and one level of the sandstone wedges are similar to Garvellachs. Thus, a similar environmental interpretation is appropriate.

5.6 Member 3

This member is similar to M3 on the Garvellachs in containing diamictite beds and thick sandstone interbeds. The member consists of diamictite and interbed lithofacies; the latter lithofacies comprises one main sublithofacies (sandstone) and three minor sub-lithofacies (granitic conglomerate, siltstone, and dolomite).

5.6.1 Diamictite lithofacies:

The number of the diamictite beds in this member are six in the Garvellachs, while here, there are only three diamictite beds as follows:

a) Basal diamictite bed

This study does not agree with Spencer's (1971) correlation on his plate 10E for the base of M3: the base of the M3 seems lower than he suggested. Some sandstone beds previously counted with M2 belong to M3 because they are white sandstone (not brown) and have characteristics more similar to M3 than M2. The basal diamictite bed is exposed on the S-side of the wall at Creagan Loisgte, about 12.5 m from the base of M3. It has a sandy matrix and contains sparse pebble-sized clasts. Based on Spencer (1966, pp.359, 1971, pp.90), this bed is correlated with the D33 in the Garvellachs. However, the number of clasts is very small, so this is a sandstone with dispersed clasts according to the Hambrey and Glasser (2012) classification. Thus, this study follows more updated classification than Spencer's work. The thickness of this bed is about 8 m (Fig.5.15) on Creagan Loisgte. The basal contact is sharp with the underlying disturbed sandstone beds, and the upper contact is poorly exposed.

b) Middle diamictite bed

This is exposed at the north-side of the wall in Creagan Loisgte and is about 14 m thick. It is faintly laminated (Fig.5.16A-B) and has a sandy-siltstone matrix that contains up to boulder-size extrabasinal clasts (Fig.5.16C-D). The lower contact of the bed is unexposed, while the upper contact is gradational with the overlying granitic conglomerate lithofacies (Fig.5.15). Also, this bed is exposed in the Port Askaig road-cut.
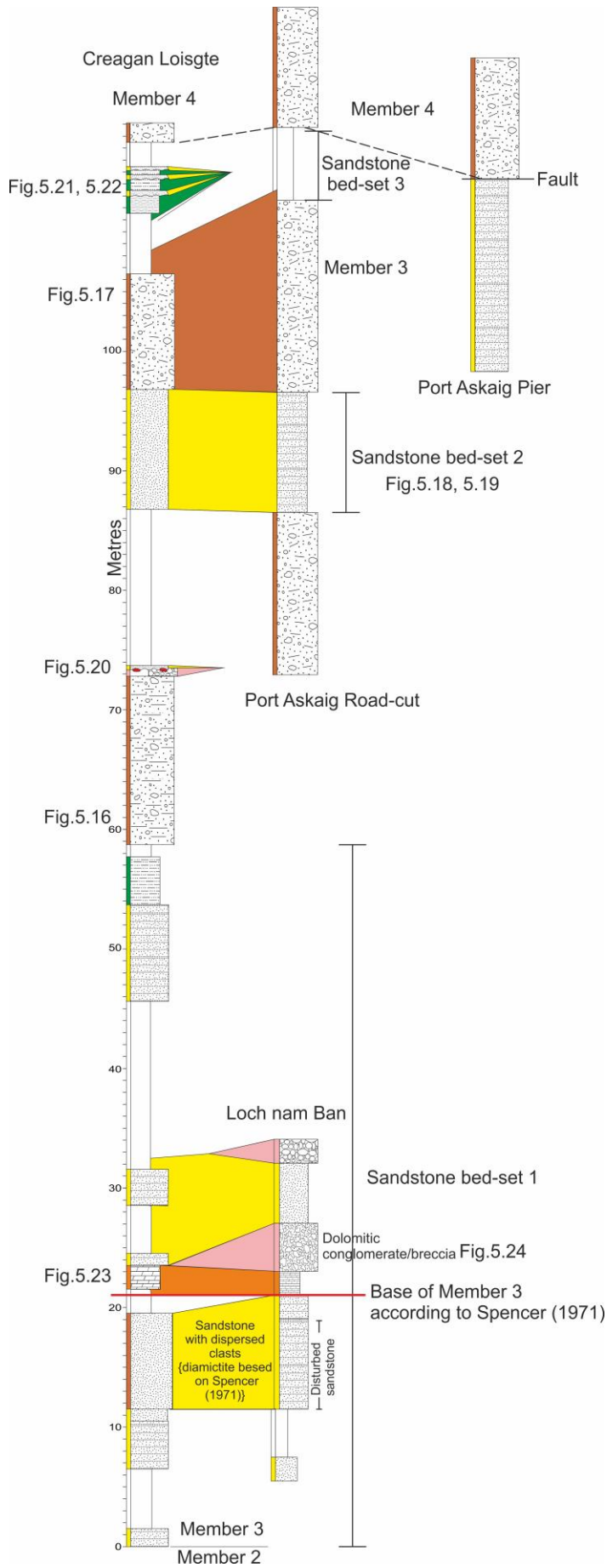
Figure 5.15: Correlation sedimentary logs of Member 3 of the PAF in different localities on Islay.
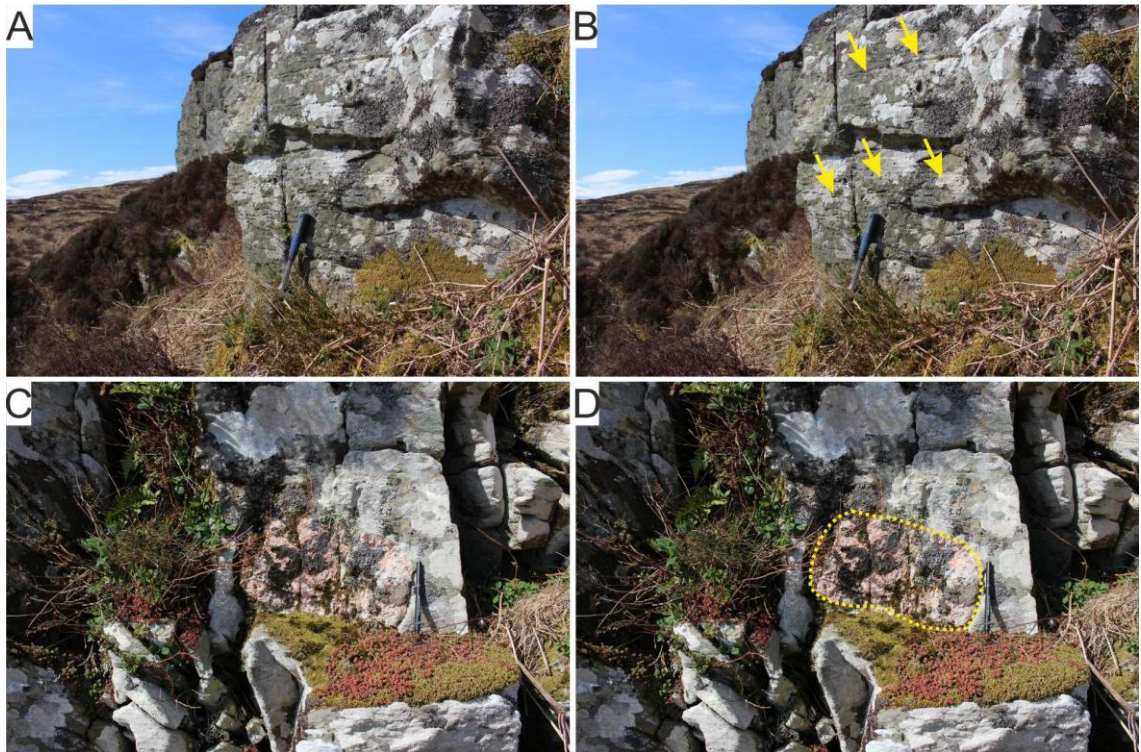
Figure 5.16: (A-B) yellow arrows shows faint lamination within the middle diamictite bed on Creagan Loisgte. (C-D) the dashed line shows a granite extrabasinal clast within the same diamictite bed. Geological hammer and pen for scale.

A similar bed occurs at the same stratigraphic level and has similar thickness at Loch nam Ban (Fig.5.15). However, the latter outcrop is better quality and shows alteration between cross-stratification and planar bedding. The thickness of each cross-bed foreset is about 1.5 m, and individual planar bed thickness is about 1 m. The lower contact is unexposed here, while the upper contact is gradational with the overlying brown sandstone beds.

c) Upper diamictite bed

This is exposed N of the wall at Creagan Loisgte and is about 10 m thick. It has a silty-sandstone matrix which contains some gritty patches with pebble-size granites, but fewer clasts than the middle diamictite bed. Granite clasts are more frequent than quartzite, and a few dolomite clasts are present. In the upper part of the bed there are discontinuous conglomerate lenses (Fig.5.17). They consist of granite and quartzite clasts floating in the matrix of the diamictite. These conglomerate lenses have a gradational contact with the diamictite bed.

Figure 5.17: Yellow dashed lines show the lenticular conglomerate lenses within the upper diamictite bed on Creagan Loisgte. Coin for scale.

1) Interbeds lithofacies

This lithofacies is similar to the white sandstone lithofacies in the Garvellachs (Section 4.2.1), but is thinner here and fewer events are preserved. It consists of well-sorted, fine to medium grained sandstone, white on fresh surfaces and grey or light brown on weathered surfaces. It comprises one main sub-lithofacies (sandstone) and three minor sub-lithofacies (conglomerate/breccia, siltstone, and dolomite).

5.6.2 Interbed lithofacies

(a) Sandstone sub-lithofacies

This sub-lithofacies is exposed completely at Creagan Loisgte and partly in the Loch nam Ban section (Fig.5.14). There, above M2, the first sandstone bed-set exposed is about 50 m thick (Fig.5.15). It is similar in lithology, grain-size, sorting, colour, and bed geometry to the white sandstone lithofacies in the Garvellachs.

There are three bed-sets within M3 from the base to the top as follows: (i) bed-set no.1 at the base; (ii) bed-set no.2 about 15 m from the base; and (iii) bed-set no.3 above a granitic conglomerate sub-lithofacies in the north-side of the wall at Creagan Loisgte (Fig.5.15).

They are all characterised by planar or cross-stratified sandstone beds about 0.3-1.5 m thick, mostly with sharp lower contacts, but gradational in a few places. The planar beds are mostly structureless, but some show planar lamination or ripple laminations. The foresets of the cross-stratified beds are up to 1 m thick, and some of the sandstone beds contains scattered pebbles of extra and intrabasinal clasts.

On the Port Askaig road-cut the succession is affected by some faults (Fig.5.18). Most are minor and show small displacements; one large fault forms the contact between M3 (this lithofacies association) and M4 (the next lithofacies association).

Figure 5.18: Yellow lines are faults in the M3 on the Port Askaig road-cut section. The white-dashed line shows the contact between two, diamictite and sandstone, lithofacies. The red lines are bedding planes of the strata. Van is a scale.

On the Port Askaig road-cut, the sandstone beds are well-bedded and well-sorted, brown to greenish grey on the weathered surface, and white to light grey on the fresh surfaces (Fig.5.18, 5.19). The lower and upper contacts of the beds are sharp with the underlying and overlying diamictite beds.

Figure 5.19: Well-bedded sandstone of the sandstone lithofacies and diamictites on the Port Askaig road-cut. The white-dashed lines are sharp contacts between sandstone and diamictite beds

(b) Granitic conglomerate sub-lithofacies

This sub-lithofacies is exposed at Creagan Loisgte and at Loch nam Ban. It consists of poorly sorted, mud-supported, coarsening upward conglomerate. The clast size is up to boulder size, and most are granite with some quartzite and minor proportions of dolomite (Fig.5.20). The lower contact of the lithofacies is gradational with the underlying diamictite bed, and the upper contact is sharp and irregular with the overlying sandstone bed (Fig.5.20).
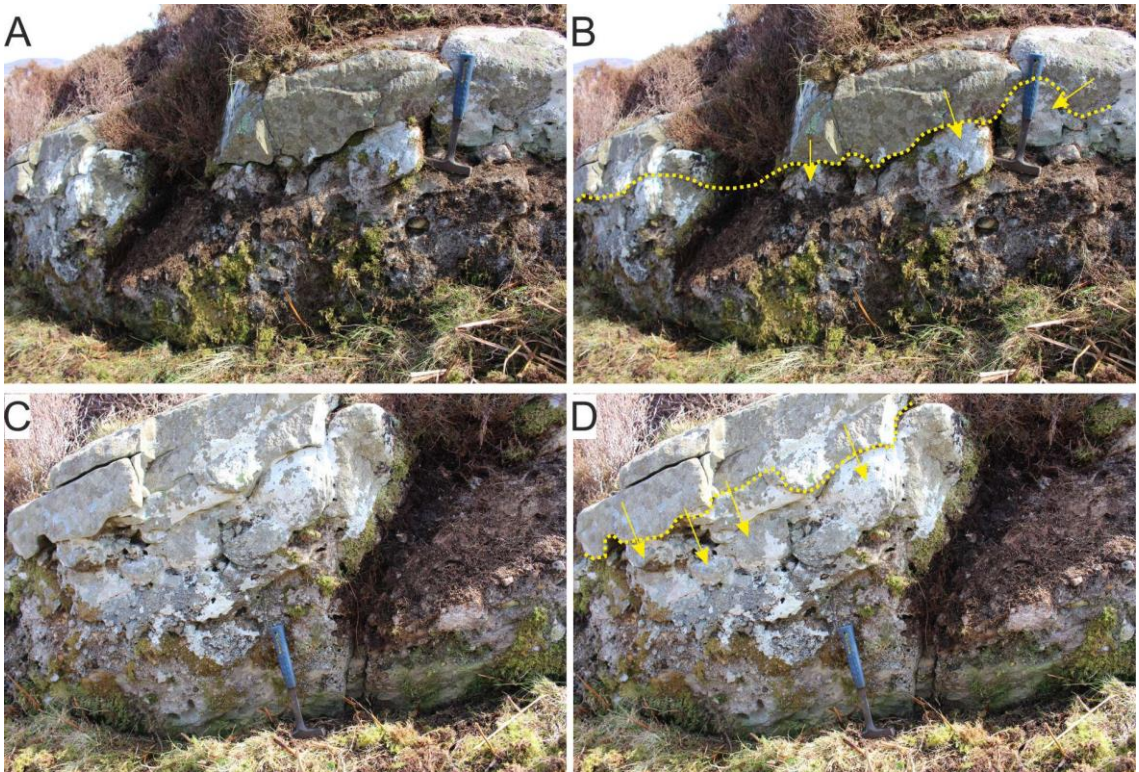
Figure 5.20: Mud-supported and coarsening upward granitic conglomerate on Creagan Loisgte. The yellow dashed-lines in B and D shows the contact between the conglomerate and the sandstone bed above, and the yellow arrows show clasts protruding into the overlying sandstone bed.

(c) Siltstone sub-lithofacies

This sub-lithofacies is exposed only at Creagan Loisgte at two different stratigraphic levels: (i) below the middle diamictite bed, and (ii) at the top most part of M3, just below M4 (Fig.5.15). It is characterised by fine-grained, and highly cleaved sandy-siltstone and siltstone, dark greenish-grey colour on weathered surfaces (Fig.5.21-5.22) and grey on fresh surfaces. The lower and upper contacts of the sub-lithofacies are not clear because of the quality of the outcrop.
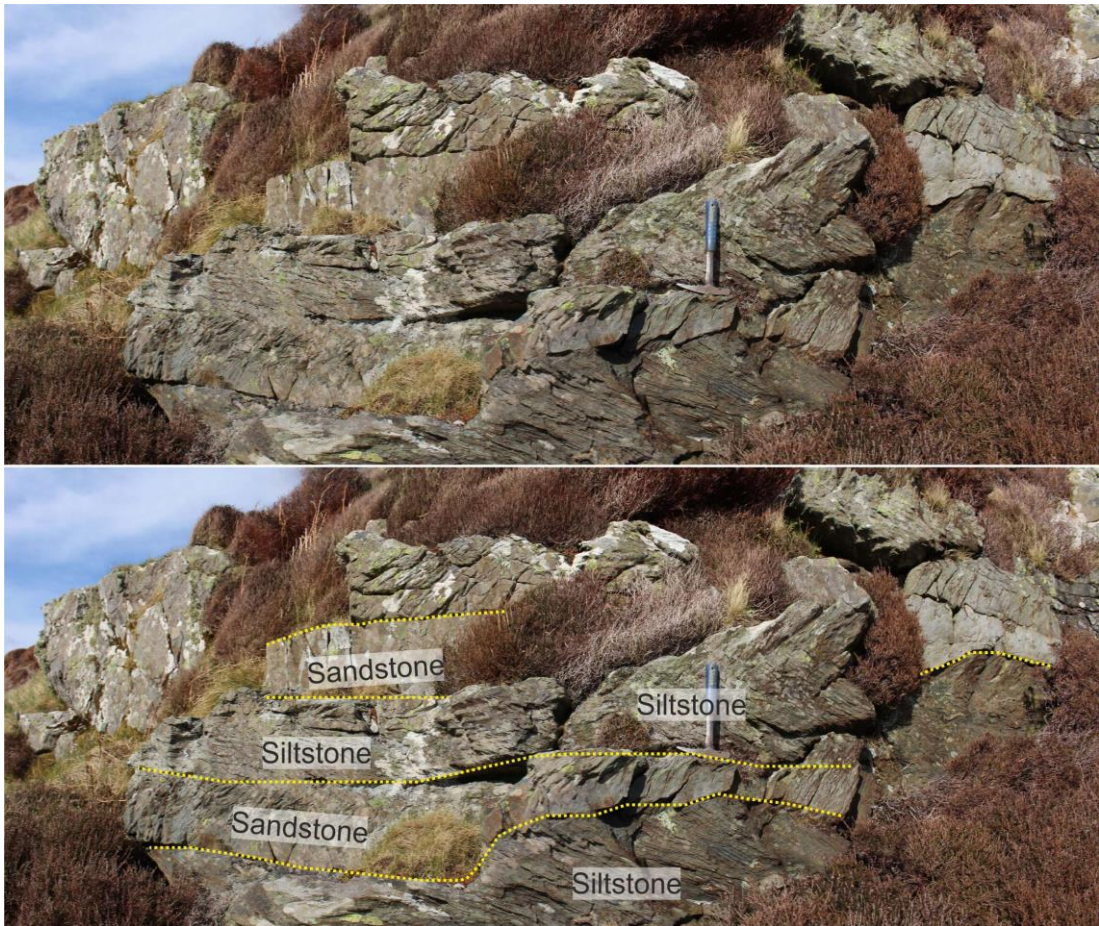
Figure 5.21: Dark greenish-grey siltstone on Creagan Loisgte. The yellow dashed-lines show the contact between highly cleaved siltstone and less cleaved, channelised sandstone.

The bed-set that lies just below M4 contains some channel geometries (Fig.5.21). They are about 10 m wide and 0.1 to 0.6 m thick and consist of medium-grained sandstone, well-sorted and well rounded. They can easily be distinguished from the siltstone; the latter is highly cleaved and greenish-grey colour, while the former is less affected by tectonism and white on weathered surfaces (Fig.5.21-5.22).
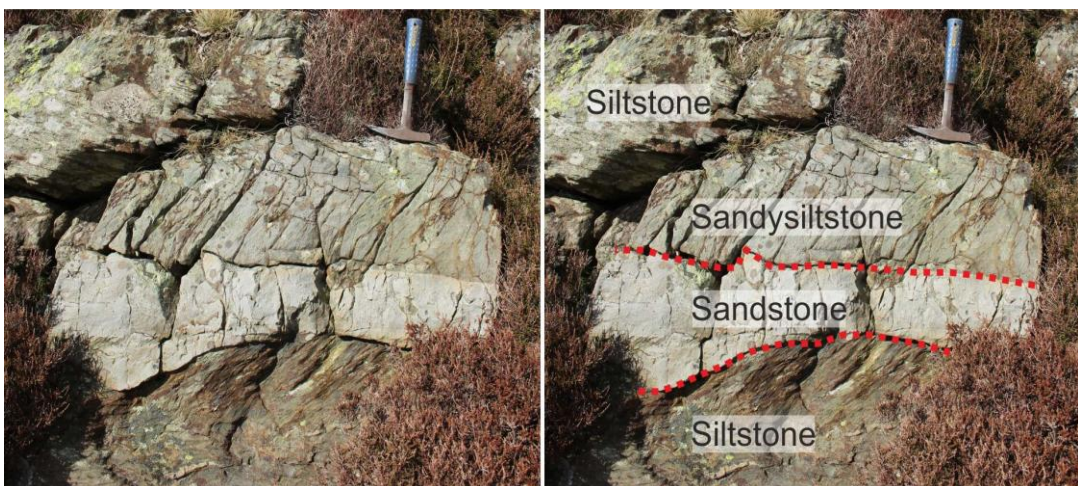
Figure 5.22: Channel geometry sandstone within the fine-laminated siltstone on Creagan Loisgte

(d) Dolomite sub-lithofacies

This lithofacies is exposed on the S-side of the wall at Creagan Loisgte and in the Loch nam Ban section (Fig.5.15). It is located about 2 m above the disturbed sandstone bed in both localities (Fig.5.15). It consists of well-bedded, brown dolomite beds, with sand-sized grains, in places with a fine-lamination structure (Fig.5.23).
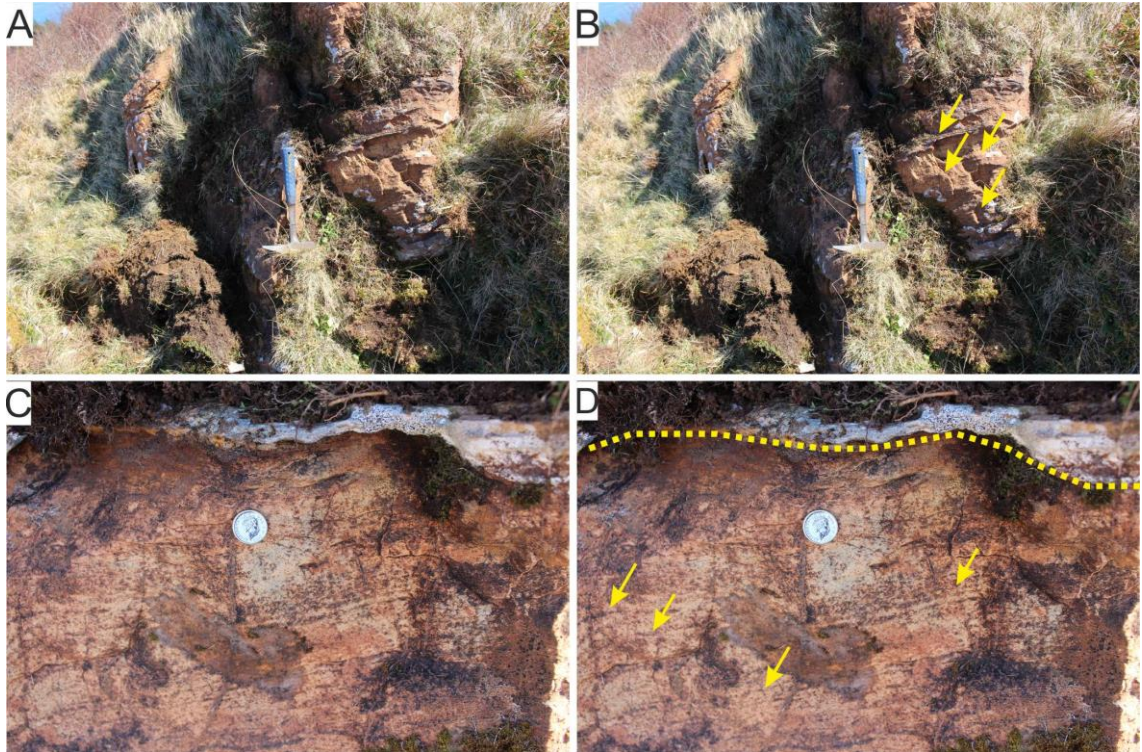
Figure 5.23: Dolomite sub-lithofacies north-side of the wall on Creagan Loisgte. Yellow arrows in B and D show the lamination within the dolomite, and the yellow dashed-line in D shows the sharp upper contact of the dolomite with the overlying sandstone.

There is another dolomitic level at Loch nam Ban, but this is conglomeratic/brecciated rather than bedded or laminated (Fig.5.24). This conglomerate is lenticular and at its thickest reaches 6 m (Fig.5.15). It has a gradational lower contact with the overlying sandstone, and a sharp upper contact with overlying conglomerate. The lower part contains clasts up to boulder size within grey coloured sandy matrix, while in the upper part more pebble to cobble sized clasts occur within a dark brown sandy matrix (Fig.5.24).
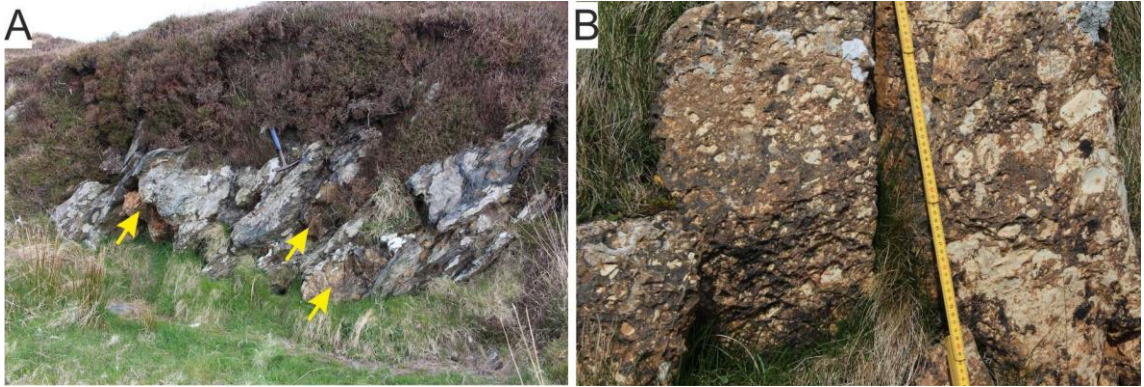
Figure 5.24: Dolomite conglomerate/breccia bed W of Loch nam Ban (Fig.5.15). (A) Lower part of the dolomitic conglomerate/breccia shows clasts up to boulder size. The yellow arrows show the dolomite clasts within the sandy matrix. (B) Upper part of the conglomerate/breccia shows finer sized clasts and there is some angularity.

5.7 Depositional environment of Member 3

The general characteristics, lithologies, succession, and sedimentary structures of the rocks on Islay are identical to those on the Garvellachs. The diamictite beds represent glacial deposits, but the question is whether they were deposited by grounded-ice or IRD. It is difficult to decide between these, because on Islay there are no records of subaerial exposure or ice-mass movement activity, nor any record of IRD.

5.8 Thick diamictite lithofacies association (D39-D44)

This association is only exposed on Islay in Member 4: (i) Port Askaig pier; (ii) Port na Seilich (Loch Allen); and (iii) Caol Ila coastline (Fig.5.25). The lithofacies association consist of two lithofacies: diamictite and sandstone.

5.8.1 Diamictite lithofacies

This lithofacies consist of six thick and homogeneous diamictite beds, D39-44 sensu Spencer (1971). These diamictite beds are thick and interbedded with the much thinner sandstone lithofacies. The diamictite beds are homogeneous, their thickness ranges between 25-68 m (Fig.5.25), and they consist of sandy-siltstone matrix which contains various sizes and lithologies of clasts. Extrabasinal clasts (Fig.5.26) are dominant and intrabasinal clasts are present in minor amount. In some horizons, there are greater concentrations of clasts (Fig.5.27).
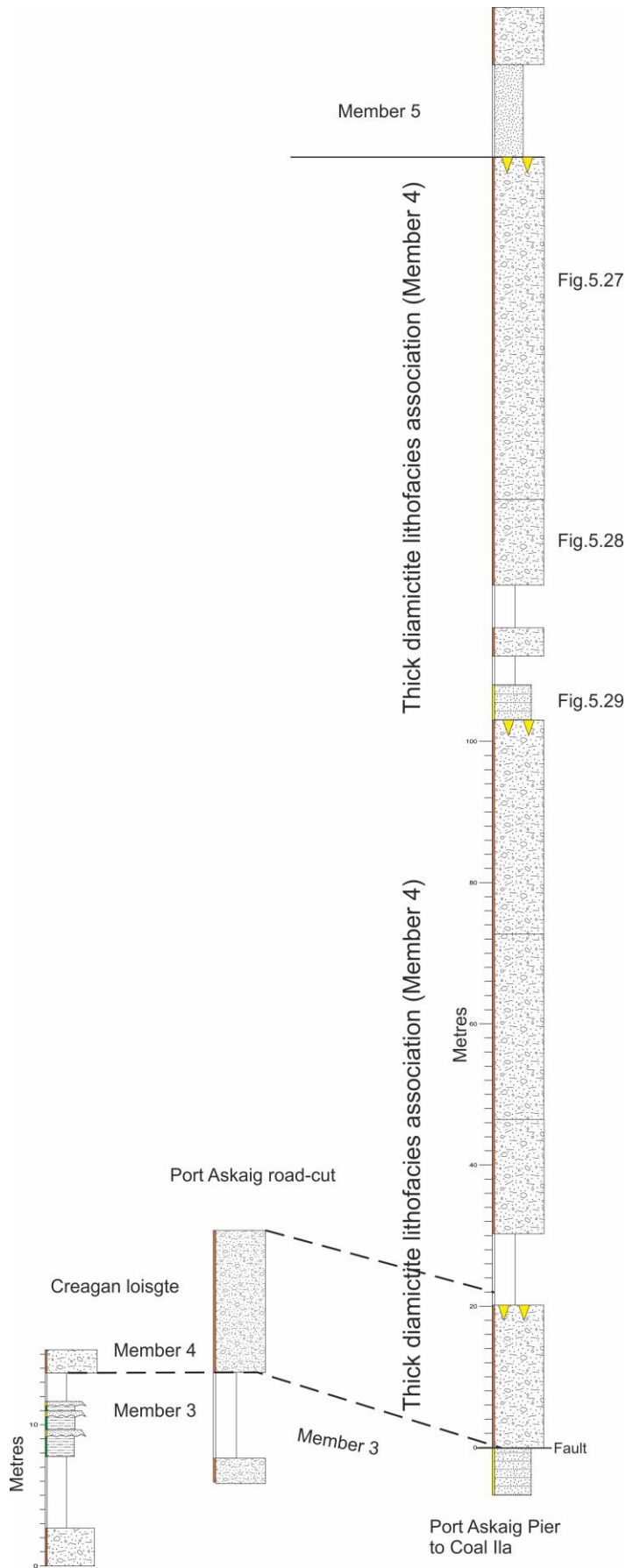
Figure 5.25: Correlation panel of Member 4 of the PAF in different localities on Islay.
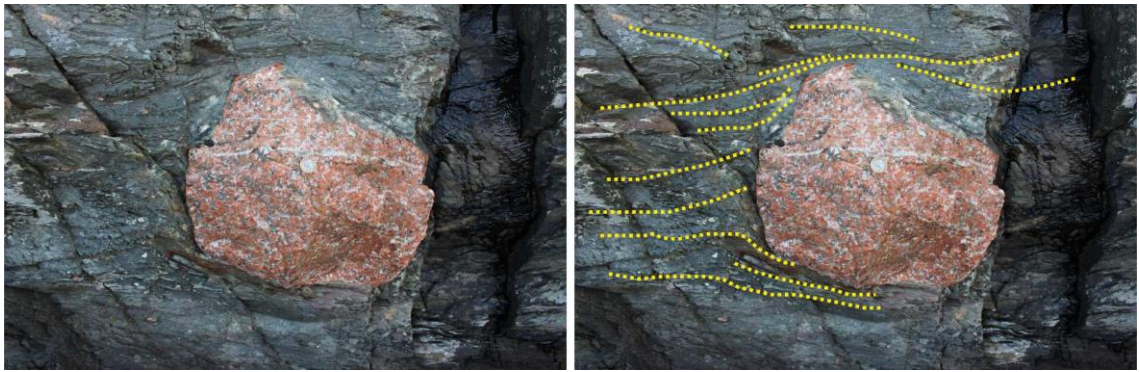
Figure 5.26: Granite clast within homogeneous diamictite bed of the diamictite lithofacies on the Port Askaig pier to Caol Ila coastline. The 'lamination' (yellow-dashed lines) is due to cleavage. Coin for scale.
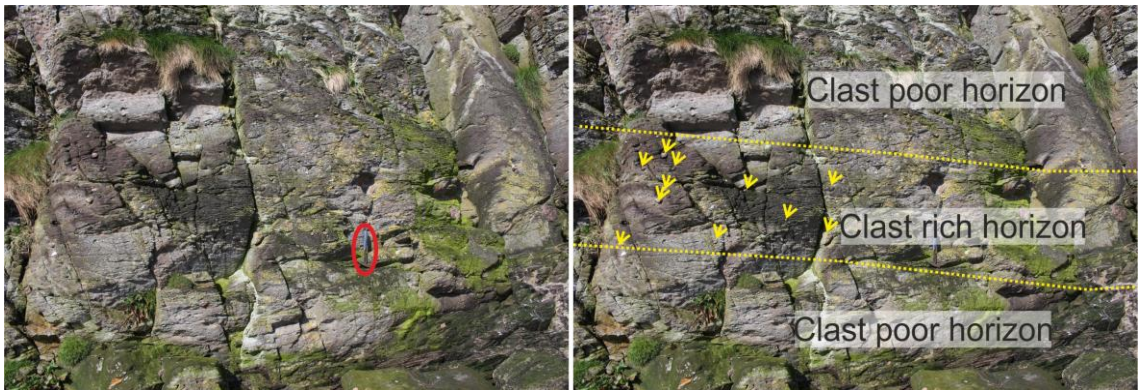
Figure 5.27: Clast rich and clast poor horizons within the diamictite beds of diamictite lithofacies close to Port Askaig pier. The yellow arrows show granite clasts within a clast rich horizon in the diamictite. Geological hammer is a scale.

The diamictite beds of this association are distinctive by their thickness (Fig.6.3), because they are the thickest part of the diamictite bed-set in the PAF succession, even thicker than the Great Breccia lithofacies association. Also, the interbeds between these six diamictite beds are not continuous and two of them do not extend for a long distance laterally. Thus, this lithofacies association (Member 4) can be subdivided into four groups: (i) D39-D40; (ii) D41; (iii) D42-D43; and (iv) D44 (Fig.6.3).

5.8.2 Sandstone lithofacies

This lithofacies consists of three sandstone bed-sets that separate the four diamictite beds (groups). They are located between: (i) D39-40 and D41; (ii) D41 and D42-43; and (iii) D42-43 and D44. Also, the interbeds of this lithofacies are much thinner compared with those at other stratigraphic levels of the PAF, except some interbeds near the base of the succession within the dolomitic diamictite lithofacies association (Fig.6.3).

The sandstone beds are grey on weathered surfaces and white or light grey on fresh surfaces (Fig.5.28). They consist of well-bedded, and well-sorted sandstone; the lower and upper contacts of the beds with the underlying and overlying diamictites are sharp (Fig.5.28)

Figure 5.28: The yellow-dashed line shows the contact between diamictite and sandstone lithofacies; and the white-dashed lines show the lamination within the sandstone bed. On the coast of the Port Askaig Pier toward Caol Ila.

On the Port Askaig Pier coast line towards Caol Ila, there are three horizons of sandstone wedges penetrating the top of D39-40, top of D42-43, and top of D44. They are light brown on weathered surfaces and white to light grey on fresh surfaces. They can be distinguished from diamictite by their weathered colour: diamictite matrix is bluish grey while the wedges are light brown (Fig.5.29).
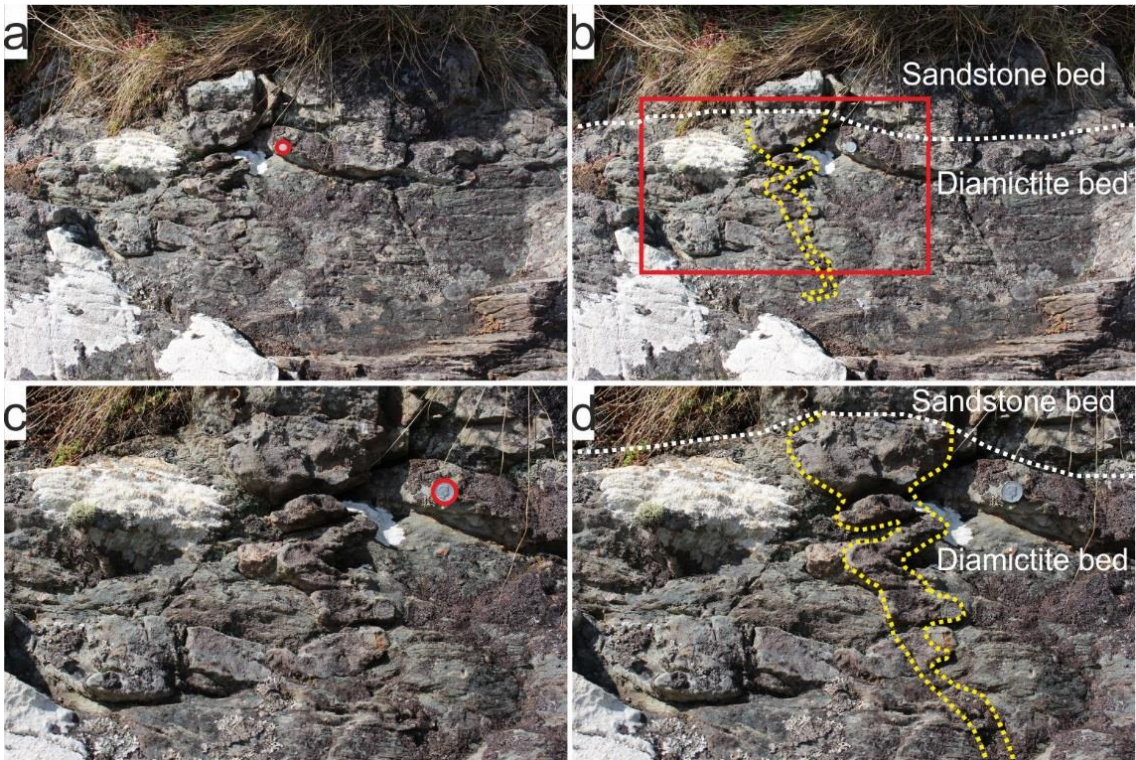
Figure 5.29: Sandstone wedge penetrating the top of D39-40 on the coastline between Port Askaig pier and Caol Ila. The yellow-dashed lines are the contact between sandstone wedges and diamictite bed; and the white-dashed line is the contact between diamictite and sandstone beds. The red-rectangle is the magnification of (c-d). Coin is a scale.

At Caol Ila, there is a horizon of sandstone wedges at the top of D44 (Fig.5.30). Some of the wedges are isolated, whereas others form networks of polygons.

Figure 5.30: View downwards onto top surface of D44 showing sandstone wedges (yellow lines) penetrating top of D44 at Caol Ila.

At Port an Seilich, there is another level of sandstone wedges penetrating the top of D42-43; in addition, there is a 2 m granitic conglomerate (Fig.5.31) in this stratigraphic level. The latter has a sandstone to sandy siltstone matrix, contains different shapes, sizes, and lithologies of clasts. Extrabasinal clasts are dominant (Fig.5.31). Some sandstone lenses exist within the conglomerate; in places, they are sheared and deformed. The contact of the conglomerate with the underlying diamictite bed is gradational (Fig.5.31c-d).
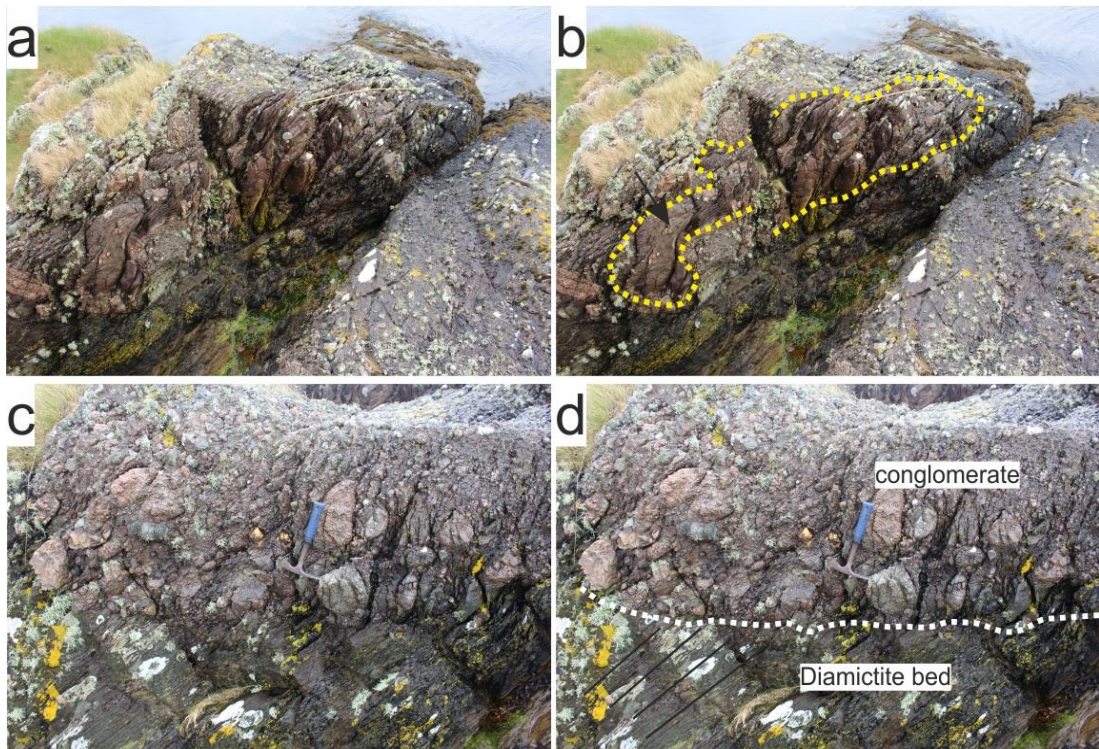
Figure 5.31: Granitic conglomerate at the top of D42-43 at Port an Seilich. The yellow-dashed line is the contact of a sandstone lens inside the conglomerate bed. The white-dashed line is a gradational contact between the conglomerate bed and the underlying diamictite bed. The black arrow is the deformation and shearing within the sandstone lens. The black lines are cleavage. Geological hammer and 2 m ruler for scale.

5.9 Thick sandstone lithofacies association (Member 5)

This association lies at the top of the PAF succession. Like M4, it is only exposed on Islay and does not crop out on the Garvellachs. It consist of two lithofacies: diamictite and thick sandstone.

5.9.1 Thick sandstone lithofacies

This lithofacies consist of four bed-sets of sandstone. These are the thickest interbeds in the PAF succession (Fig.5.32, 6.3), even thicker than the sandstone bed-sets in M3. The thickness of each individual bed-set ranges 18.5-229 m; and the total thickness of the association is about 375 m. The sandstone beds consist of medium-grained and well-sorted sandstone; light-grey on weathered surfaces and white or light-grey on fresh surfaces. The outcrops of this lithofacies association are poorly exposed inland N of Ardnahoe Lock and those on the coastline are only partly accessible.

5.9.2 Diamictite lithofacies

It consists of three beds of diamictite (D45-D47) mainly represented by boulders on the beach on the E coast of Islay. They are homogeneous and consist of sandy-siltstone matrix containing different sizes and lithologies of clasts. Extrabasinal clasts are common, while intrabasinal are minor proportion. The diamictite beds of this lithofacies are distinctive; because they are thin, 3.5-7 m, compared with lower stratigraphic levels. All basal and lower contacts are sharp, and there is a horizon of sandstone wedges penetrating D46 from the top (Fig.5.32).
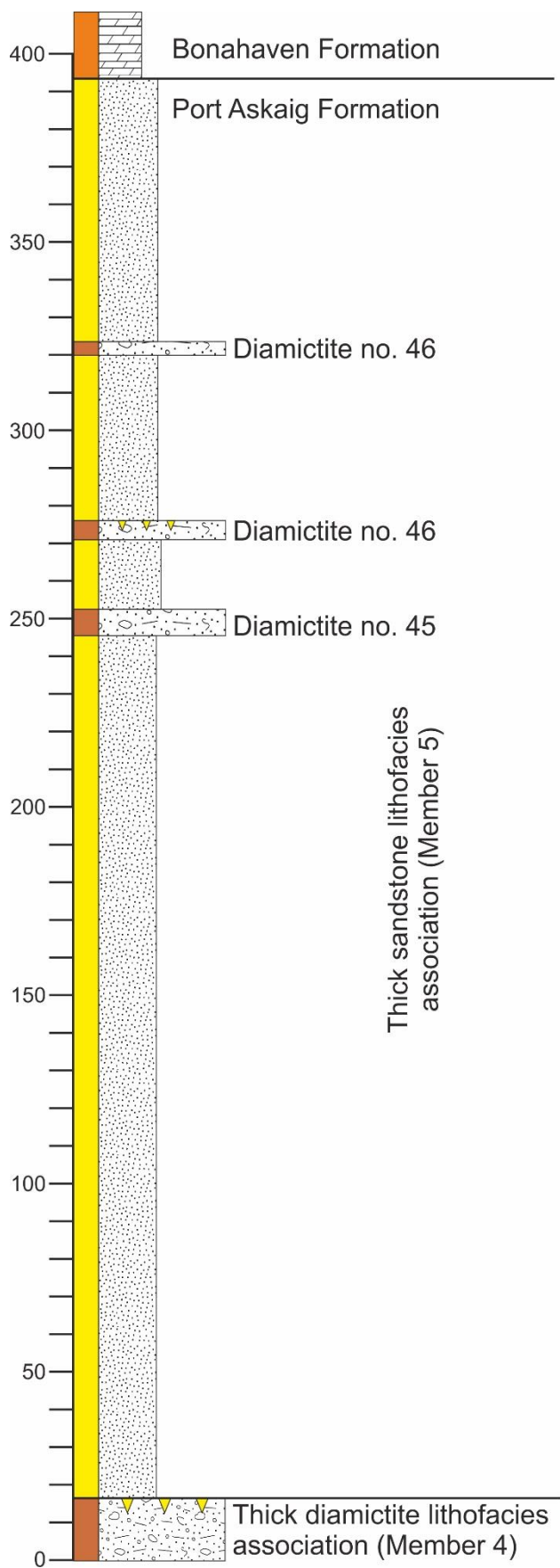
Figure 5.32: Sedimentary log of Member 5 of the PAF at Con Tom on Islay (Re-drawn after, Spencer 1971).

5.9.3 Fallen blocks on the coastline S of Con Tom

The best examples of the lithology of D46 are in fallen blocks on the coastline S of Con Tom (Fig.5.33, 5.34). They have probably come from the adjacent inaccessible cliff; because they are angular and up to 2.5 m across. The lithologies of these blocks are diamictite, unsorted granitic conglomerate, dolomitic conglomerate, layered dolomite, and sorted granitic conglomerate. These blocks were counted in a 60X15 m area: (i) 23 diamictite; (ii) 14 layered dolomite (Fig.5.34c-d); (iii) 8 unsorted conglomerate/breccia (Fig.5.34e-f); (iv) 4 dolomitic conglomerate; (v) one sorted conglomerate. The surprise observation none of them was sandstone that can be similar to the thick sandstone within this facies association. Also, some blocks consist of more than one lithology, and show the contact between them: (i) 11 blocks show contact between diamictite and unsorted granitic conglomerate; (ii) 11 blocks show contact between dolomite and diamictite (Fig.5.34a-b).

Figure 5.33: Panoramic view of the blocks on the coastline on Con Tom.

Is it possible to suggest the stratigraphy of D46 from the observations of these fallen blocks? D46 is underlain and overlain by the thick sandstone lithofacies of this facies association. Granitic conglomerates occur at the top of diamictite beds within the PAF succession: for instance, the granitic conglomerate at the top of D26 on A'C (Fig.4.1) and SLaC (Fig.4.20), the conglomerate above D29 on GE (Fig.4.17), and the granitic conglomerate at the top of the middle diamictite bed on Creagan Loisgte (Fig.4.19). Thus, the conglomerate is more likely to be at the top of the D46. Dolomite beds can be at the top or base of diamictite beds; however, if the conglomerate is at the top, then the dolomite might be at the base. This suggestions for the stratigraphy of D46 are shown on 'Fig.5.35'.
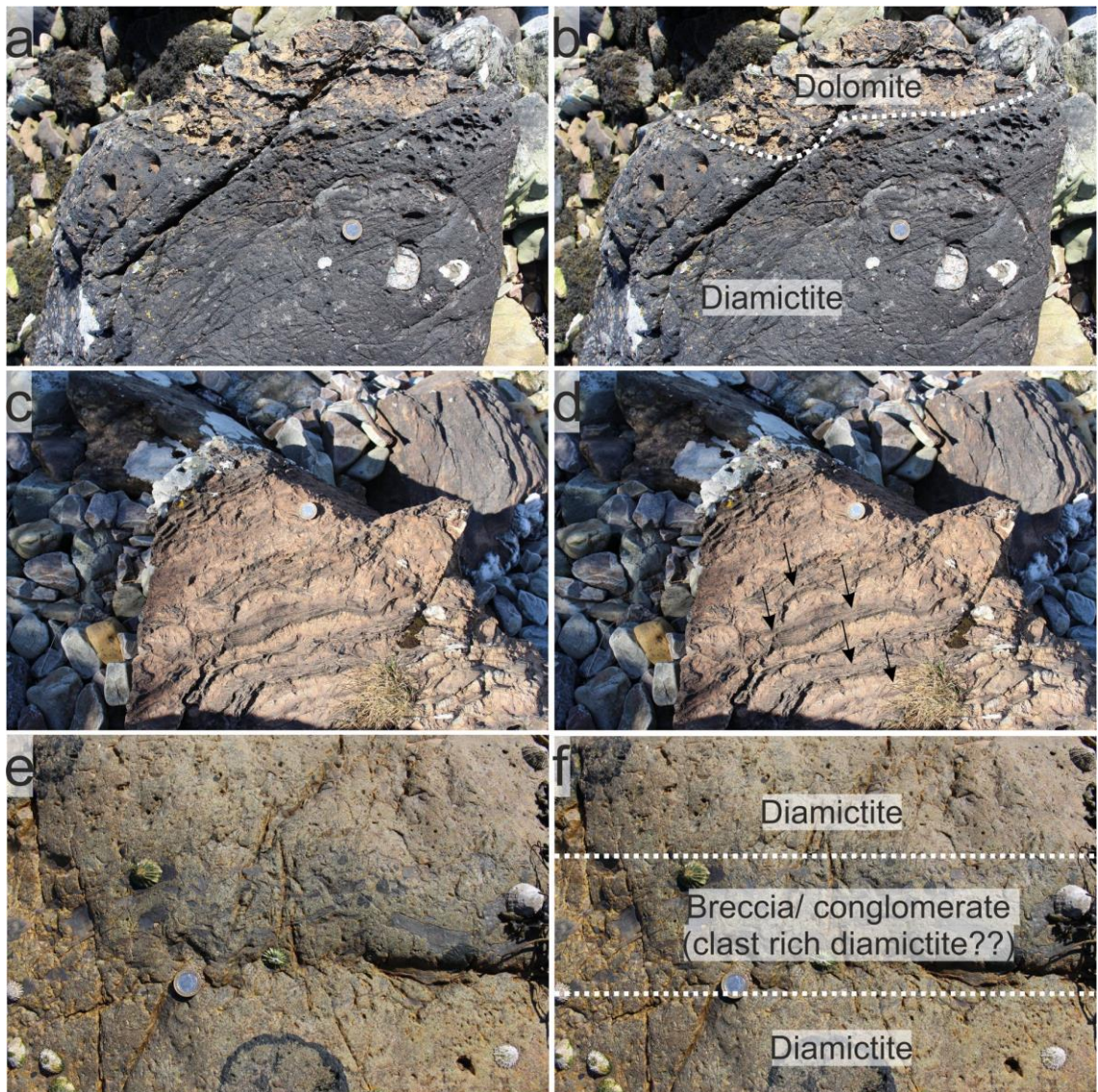
Figure 5.34: Fallen blocks on the coast S of Con Tom from D46, (a-b) the contact between dolomite and diamictite lithologies; (c-d) laminated dolomite; (e-f) unsorted conglomerate/ breccia within diamictite with a gradational contact.
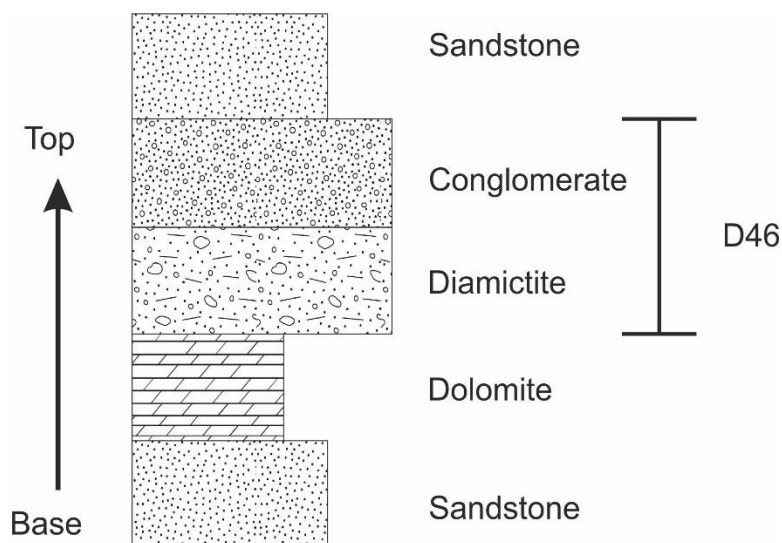
Figure 5.35: Possible stratigraphic order of the lithologies of the fallen blocks on the Con Tom coastline representing D46. Scale is not provided, because they are blocks (not beds).

Below is the stratigraphic log correlation between all five members on Islay:
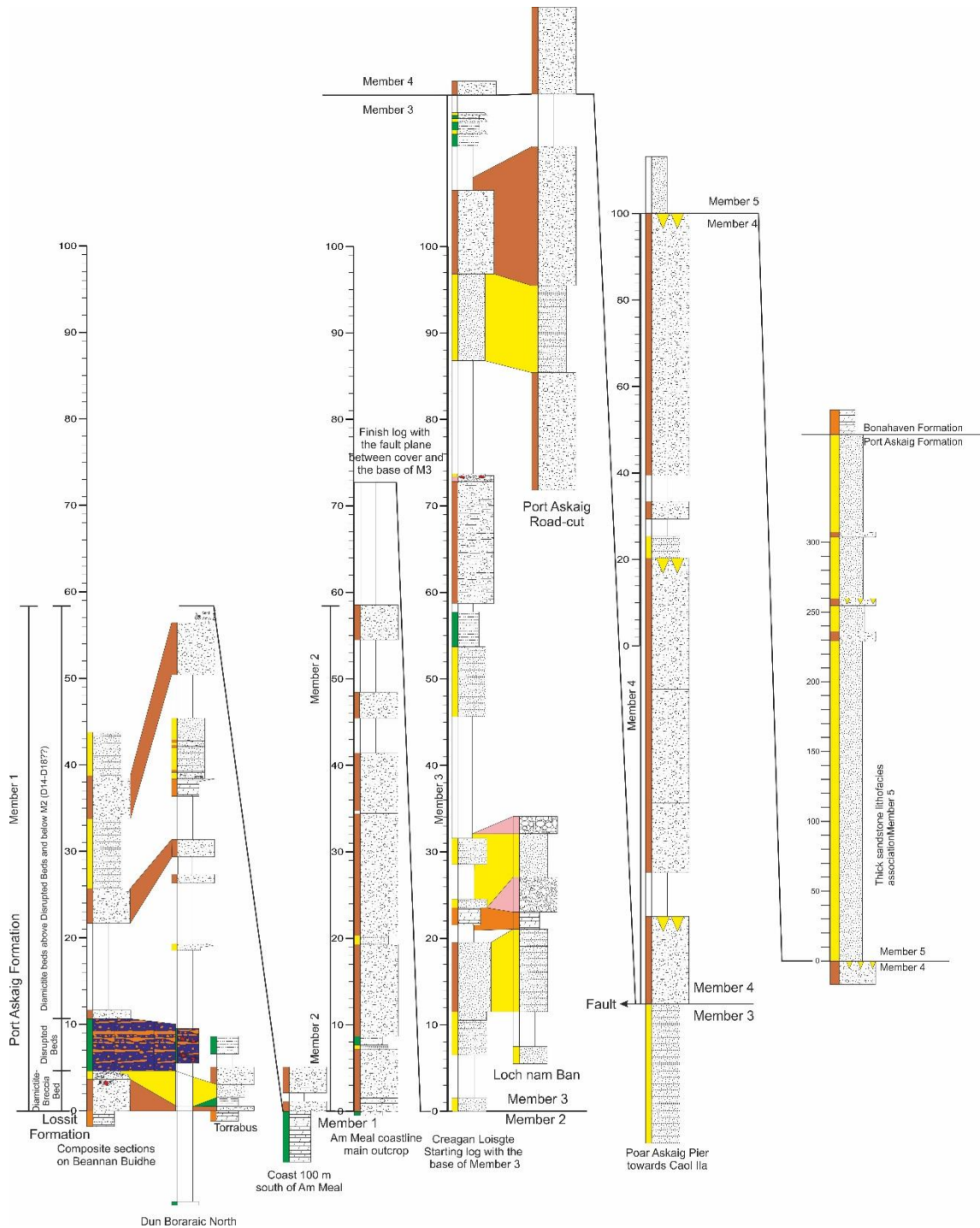
Figure 5.36: Correlation panel for members 1-5 on Islay in different locations. Note that the scaling purposes logs are drawn at different scales. Members 1, 2, and 3 have the same scale; while members 4 and 5, have an identical scale which is different from scales of the three previous members.

5.10 Depositional environments of M4 and M5

The obvious features in the thick diamictite lithofacies association (D4) are: (i) thick diamictite beds; (ii) thin sandstone bed-sets; (iii) three horizons of sandstone wedges similar to sandstone wedges horizons on Garvellachs in Ma and M3; (iv) presence of granitic conglomerate in 'Fig.5.31'; and sharp bases of the diamictite beds. Previously, the sandstone wedges were interpreted in this study as contraction cracks

in a periglacial environment. Also, the granitic conglomerate bed in 'Fig.5.31' is looks similar to the granitic conglomerate lithofacies on SLaC (Fig.4.20). The latter was interpreted as a possible subaerial debris flow in a periglacial environment. The sandstone beds are similar to sandstone beds in Member 3, and the diamictite beds are homogeneous with the sharp contact. The diamictite beds more likely to be grounded-ice than mass-flow deposits.

In addition, the thick sandstone lithofacies association (M5) is similar to the thick diamictite lithofacies in the presence of: (i) interbeds of diamictite and sandstone lithofacies; (ii) the presence of sandstone wedge; (iii) the sharp bases of the diamictite and sandstone beds. So, their depositional mechanism could be similar. However, they are exactly opposite in thickness of the beds. The diamictite beds in M4 are thick, while sandstone interbeds are thick in M5. This may indicate some differences in depositional mechanisms; for instance: (i) during the deposition of M4 the basin was tectonically still active and subsiding (Ali et al., 2018: in press), so there was enough accommodation space for the diamictites to form thick beds, while during M5 the subsidence was not similar to M4; (ii) there was a longer glacial period in M4 and a shorter one in M5 (explaining why the glacial diamictite beds are thick in M4 and the non-glacial sandstone is thick in M5); (iii) diamictite beds in M5 may have been removed by erosion.

Chapter 6 : Stratigraphic Boundaries

This chapter introduces the reader to information about the stratigraphic boundaries in the PAF. It starts with the nature of the basal contacts of the diamictites-sharp or gradational. The top surfaces of the diamictite beds show three important features, sandstone wedges, frost-shattered clasts, and sandstone cryoturbations. At a few levels unconformity surfaces and major boundaries can be inferred by correlation between sedimentary logs in different localities.

6.1 Basal contact of the diamictite beds

The basal surface of a diamictite is especially important because across this surface the mudflow or ice-sheet which deposited the diamictite must have flowed or, alternatively, on this surface the deposition of material from floating icebergs must have commenced (Spencer, 1971). First, Kilburn et al. (1965; P.351) noted the sharp basal contact of the diamictite beds and lack of gradational transitions; these were highlighted by Spencer (1971; P.11) but have not been given weight by subsequent observers (e.g. Eyles and Eyles, 1983; Eyles, 1988; Arnaud and Eyles, 2006).

The basal contacts of all of the 47 diamictite beds in the PAF are knife sharp with the underlying strata. There is usually an abrupt change from dolomite, siltstone, sandstone, and breccia/conglomerate to diamictite (Fig.6.1) (Ali et al, 2018). The only exceptions are the base of D1 on DC (Fig.3.2a), the bases of D36 and D37 in the harbour of GE (Fig.6.2a), and the base of D24 on the E of GE (Fig.7.1d). D1 has a gradational contact with the underlying GEF on DC, but the reason for the gradation is explained in detail in section '3.1.c'. Also, the base of D36 is discussed in section 4.2.b; while the base of D37 (Fig.6.2a) in the harbour on GE, is represented in Spencer (1971; Fig.3). Furthermore, the base of D24 is slightly gradational (Fig.6.1d) on the E coast of GE because of weathering in the intertidal zone; otherwise it is sharp on A'C.

In general, these slightly gradational surfaces, at the base of some diamictites, can be seen in 20-50 cm thicknesses. None of the diamictites have gradual, transitional bases. Ali et al. (2018, in press) emphasize that no examples have been observed where stratified sediments lacking clasts pass gradually upwards, through stratified sediments with clasts, into stratified diamictite and finally into unstratified diamictite.
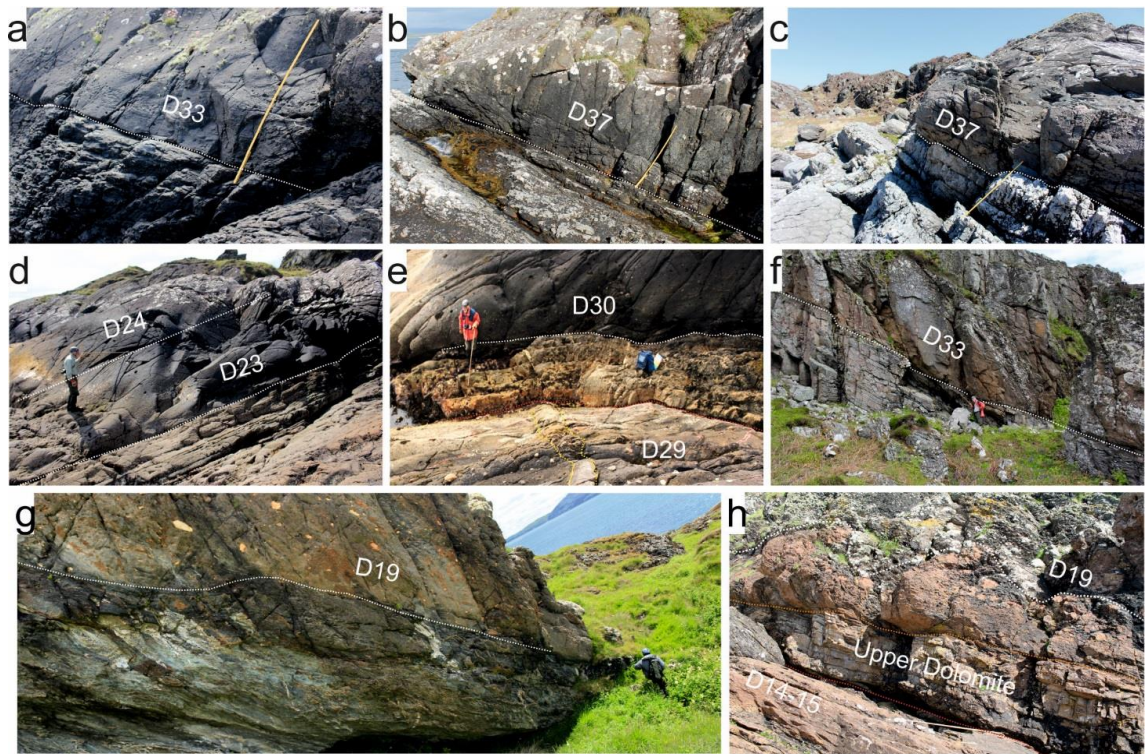
Figure 6.1: Examples of the sharp basal contacts of diamictite beds in Member 3 (a-c, f) and Member 2 (d, e, g, h) in the Garvellachs. (a-c, f) Show diamictites in Member 3 which overlie tidal sandstones. (d) The massive, clast-rich Diamictite 24 overlies sharply the laminated, clast-poor Diamictite 23 (ice-rafted?) which rests on tidal/fluvial sandstones. (e) Diamictite 30 overlies a 2m tidal/fluvial sandstone whose base cuts across the sandstone wedges penetrating the top of Diamictite 29. (g) Diamictite 19 has a sharp, undulating base above a siltstone with deformed stratification. (h) Diamictite 19 overlies with an irregular contact a 2 m dolomite breccia (glaciotectonism?); this overlies sharply the Upper Dolomite, the base of which cuts across sandstone wedges (w) penetrating the top of Diamictites 14-15; the contact of Members 1 and 2 of the PAF is here at the top of the Upper Dolomite beneath the dolomite breccia. Localities: a, b, d, e, f – E coast of GE; g – SW coast of EaN; h – W cliff of A'C. Scales: a-c, h – 2 m ruler; others – person (reproduced from Ali et al., 2018: in press).

Figure 6.1 shows several examples of diamictite basal surfaces which are well-exposed and sharp in Members 1 to 3 in the Garvellachs. In Fig.6.1 the photos are arranged in stratigraphic order. In Member 3 the diamictites overlie tidal sandstones (Fig.6.1a-c, and f): the sandstones lack any clasts and the diamictites are massive. The topmost metre of the sandstone sometimes has poor stratification (but normally no clasts); occasionally the lowest metre of the diamictite has homogeneous sandstone lenses with few clasts (Fig. 6.2a); but mostly the basal contact of these diamictites are knife sharp. In Member 2, D30 and D23 again have sharp bases (Fig.6.1d); while D24 seems gradational in 'Fig.6.1d' but this is due to weathering in the intertidal zone. D23 is laminated and contains spare outsize clasts; it may have been ice-rafted. Nevertheless, it both has a sharp base and has a sharp top beneath the unstratified D24.
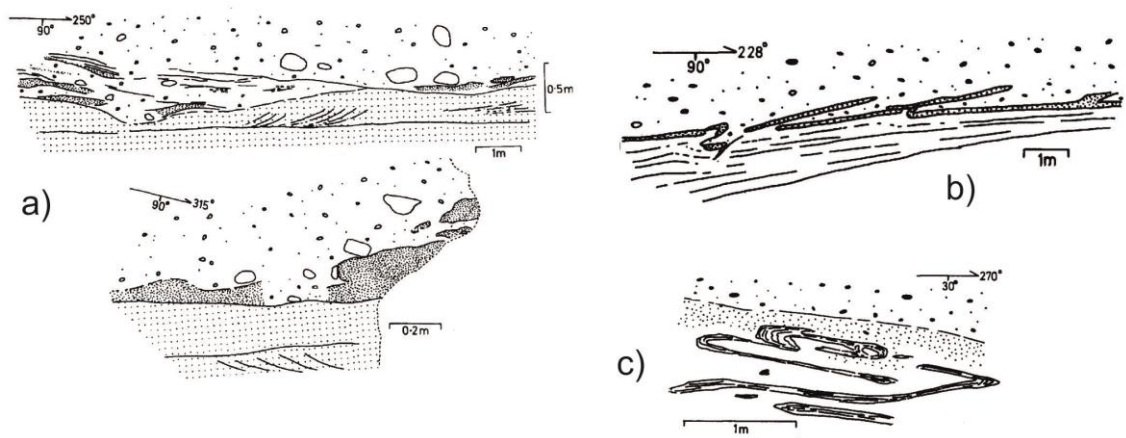
Figure 6.2: (a) Field sketch of the base of D37 at S Garbh Eileach. The strike and dip of the surface of the exposure are indicated (Spencer, 1971; Fig. 3); (b) base of D15, E coast of A'C; (c) base of D1, NE coast of GE.

Previous observations have concluded that the basal contacts of the diamictites in the PAF normally show no evidence of glaciotectonism except for subtle, small-scale disturbance structures noted by Spencer (1971) and Spencer (1966), which may have been overlooked (Fig.6.2b, c; and Fig.3.7). Ali et al. (2018: in press) provided another example, illustrating the dolomite breccia present at the base of D19- which appears to be composed of fragments of the Upper Dolomite that are being ripped-up (Fig.6.1h).

The sharp basal contacts must indicate change over from two different environments, from non-glacial to glacial. Also, such contacts are repeated at least 25 times in the PAF implying that such environmental changes occurred, and were preserved, at least 25 times (Ali et al., 2018: in press).

6.2 Top surfaces of the diamictite beds

The top surfaces of the diamictite beds in the PAF are sharp, but exhibit more complicated stratigraphic features compare with the basal surfaces. Kilburn et al. (1965; Fig.4) were the first to recognize cryoturbation and polygonal wedges at the tops of the diamictite beds. They were described by Spencer (1971), who illustrated and documented many levels of 'sandstone downfolds' and recorded sandstone wedges at 27 horizons.

The recent fieldwork provides important data on the repeated preservation of detailed environmental changes throughout the stratigraphy. Below are sections to assess the stratigraphic occurrence of the three features: frost-shattered clasts, sandstone wedges, and intra-bed folds. These followed by a summary of the stratigraphic occurrences where these three features occur together.

6.2.1 Horizons with frost-shattered clasts

Perhaps the most important piece of new data is that frost-shattered clasts have been found at least in 10 different stratigraphic levels in Member 1, 2 and 3 in the Garvellachs (Table.6.1). Seven levels show high quality examples; the others are of poorer quality due to lack of exposure, weathering, or intertidal location (Fig.6.3).

Table 6.1: Stratigraphic levels of frost-shattered clasts within PAF succession in the Garvellachs.

Sr.	Members	Top of the beds	Description	Quality of the outcrop
10	3	D36	Thin bed	Good
9	3	D35	Thin bed	Good
8	3	D34	Bed of frozen siltstone plate like clasts	Acceptable
7	2	D32	Patches discontinuous + thin bed	Good
6	2	D29	Thin bed	Good
5	2	Sst. above D26	Thin bed	Good
4	2	D26	Patches + thin bed	Good
3	2	D22	Thin bed	Good
2	1	D14-15	Patches of angular fragments poor quality	Acceptable
1	1	Below D1	Top of the dolomite bed	Acceptable

The frost-shattered clasts of five of the stratigraphic levels are located at the tops of diamictite beds. Coarse-grained granite clasts, up to boulder size, appear to be dismantled in-situ, with the interstices between the fragments filled with diamictite matrix (Fig.6.4 a, b, d, e, g-i, k). At another level the top of a dolomite bed or dolomite clasts appears to be shattered into angular fragments, with sandstone matrix between the separated parts of the clasts (Fig. 6.4 g, h, j, l). At another level, quartzite clasts appear to be disaggregated into angular fragments, with diamictite matrix between the separated parts of the clast (Fig.6.4 c); this photograph also shows angular quartzite debris to the right of the clasts (Ali et al, 2018: in press).
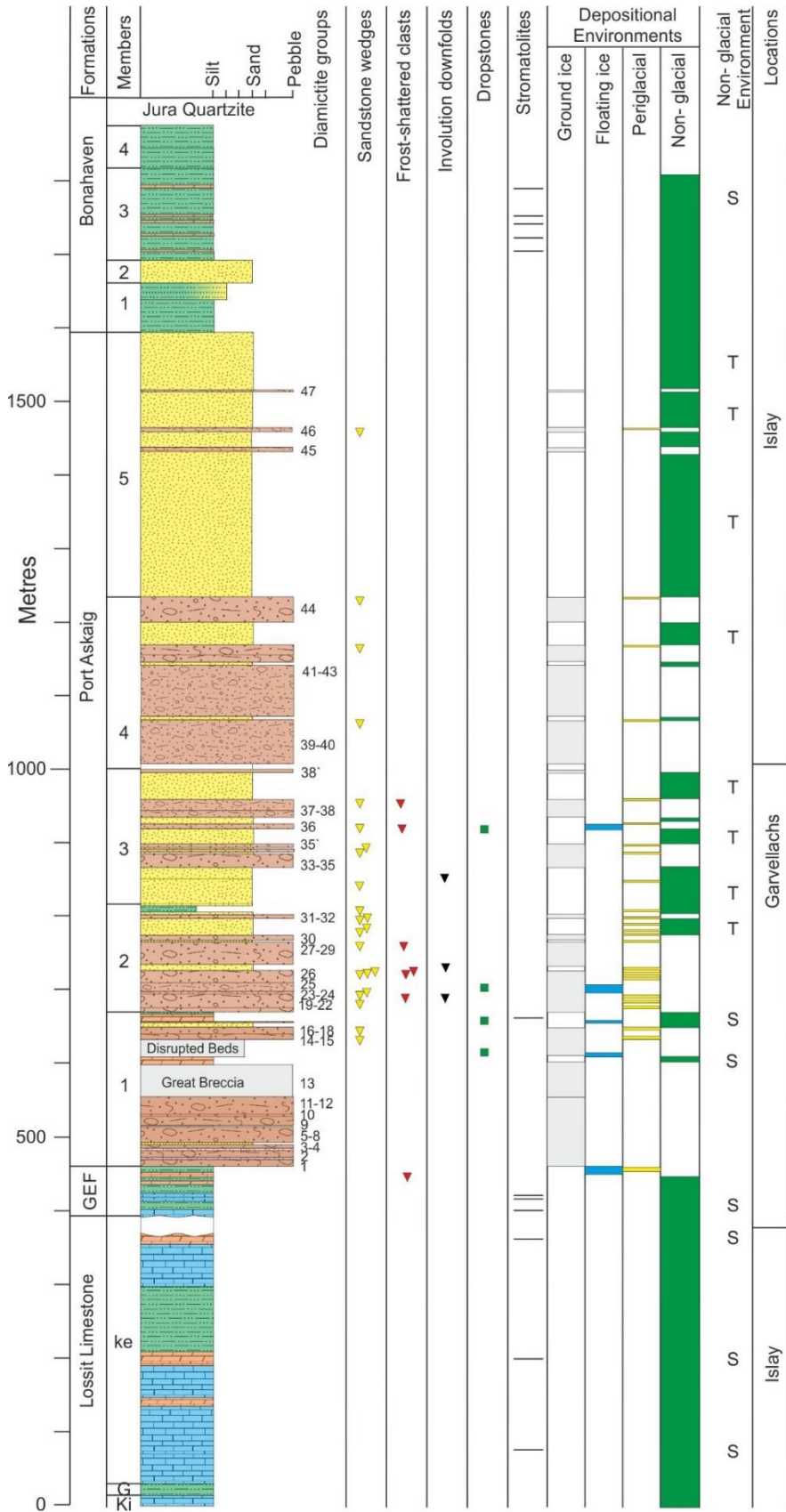
Figure 6.3: Types of the depositional environment based on structures recorded at different stratigraphic levels
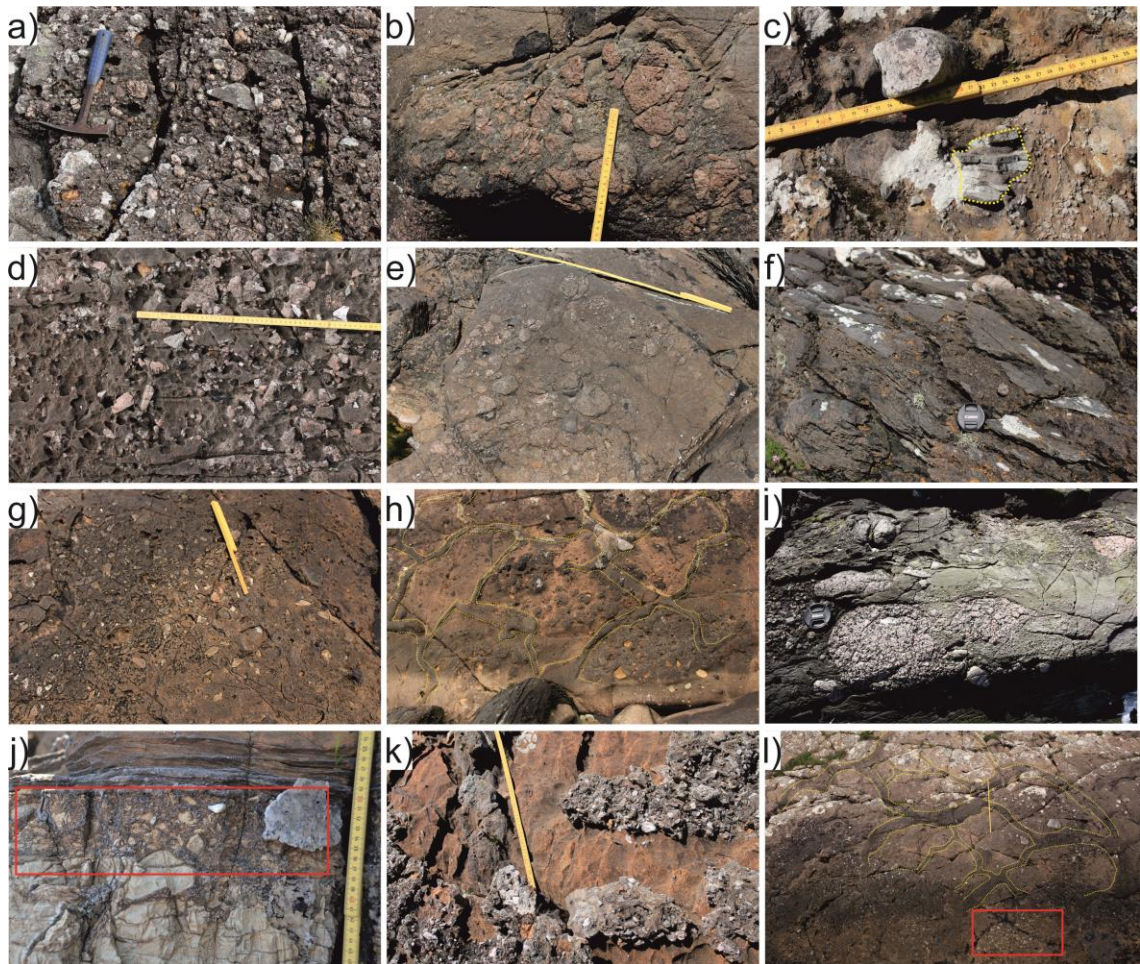
Figure 6.4: Frost-shattered clasts at different stratigraphic levels on Garvellach Islands:
(a-c, and f) from Member 3.
(a and b) granitic angular clasts from S and W coasts of GE at the top of D35.
(c) fragmented quartzite clast at the top of D36 on the W coast of GE.
(d, e, g-i, and l) disaggregated clasts in Member 2.
(d and e) fragmented granite clasts at the top of sandstone downfold horizon above D26 on the S coast of A'C and Sgeir Nam Marag (SNM).
f) thin, plate-shaped siltstone clasts imbricated were frozen during deposition.
(g, h, and l) dismembered clasts at the top of D22, from NE (h) and SW (g, l) coasts of the EaN. The red rectangle in 'l' represents the location of (g).
(i) disassembled granite clasts at the top of D26 on Sgeir Leth a Chuain (SLaC).
(j and k) fractured clasts in Member 1. (k) at the top of D14-15 on the E coast of A'C; (j) red rectangle outlines the brecciated top of a dolomite bed below D1.

A comparable analogue for frost-shattered clasts is shown 'Fig.6.5' from the surface of an Icelandic sandur. In a 1991 surge, various lithologies of pebble-sized clasts were mixed up; despite many clasts remaining intact, one tuffaceous lithology has been shattered into thousands of pieces (Fig.6.5). In general, all lithologies can be affected by weathering and shattering, as a result of disruption by freezing of water that has entered initially slightly fractured lithologies. Thus, the product of frost-shattering is highly dependent on their initial physical state; over a longer period of time, all lithologies are susceptible to this kind of mechanical weathering. In the PAF case, most clasts have remained intact but a minority are fractured or have disintegrated.

Figure 6.5: Frost-shattered tuffaceous clast, Icelandic sandur. Part of geological notebook for scale (Photo by: Professor Ian Fairchild).

Polygonal sandstone wedges are another feature that are common on the top surfaces of diamictites (Fig. 6.6). The name is derived from the shape of the structure (Spencer, 1971; p.40). In cross section, they are V-shaped (Fig.6.7a) with widths up to 1 m (Fig.6.6) decreasing to zero downwards; and the length is between tens of centimetres to few hundreds of centimetres; and the amount of penetration ranges between few centimetres up to 200 cm. They are mostly infilled with a medium grained sandstone (Fig. 6.6), except six wedges which infilled with dolomitic siltstone. In plan view, they form a branching or polygonal (Fig.6.6c, d) network (Spencer, 1971; Ali et al., 2018: in press).

6.2.2 Horizons with sandstone wedges

Ali et al. (2018: in press) tabulated sandstone wedges as occurring at 23 stratigraphic levels, 19 of them exposed in the Garvellachs (Table.6.2); at 17 of these 23 levels the wedges penetrate the top of diamictite beds (Table 6.2). The best example of a polygonal system of wedges is in the top of D22 on the W of EaN (Fig.6.6d). This horizon extends to the E of the island, one kilometre away, and polygonal wedges are again exposed (Fig.6.4h, l) associated with frost-shattered clasts. The similar characters between sandstone wedges in various stratigraphic levels encouraged Spencer (1971) to suggest they were produced by the same geological process or processes. Based on Spencer (1971) and Ali et al. (2018: in press) these structures are recorded at least at 23 horizons (Table.6.2; 6.3). Therefore, the process that produced sandstone wedges must have been repeated at least 23 times during deposition of the PAF. Sandstone wedges also occur penetrating stratified sediments (Fig.6.7a-b, g-h). Generally, the top of the wedges are always truncated at an erosion surface, often underneath a lag conglomerate (Fig.6.7a-b and Fig.6.8a-c) and sometimes underneath sandstone downfolds (Fig.6.8d).
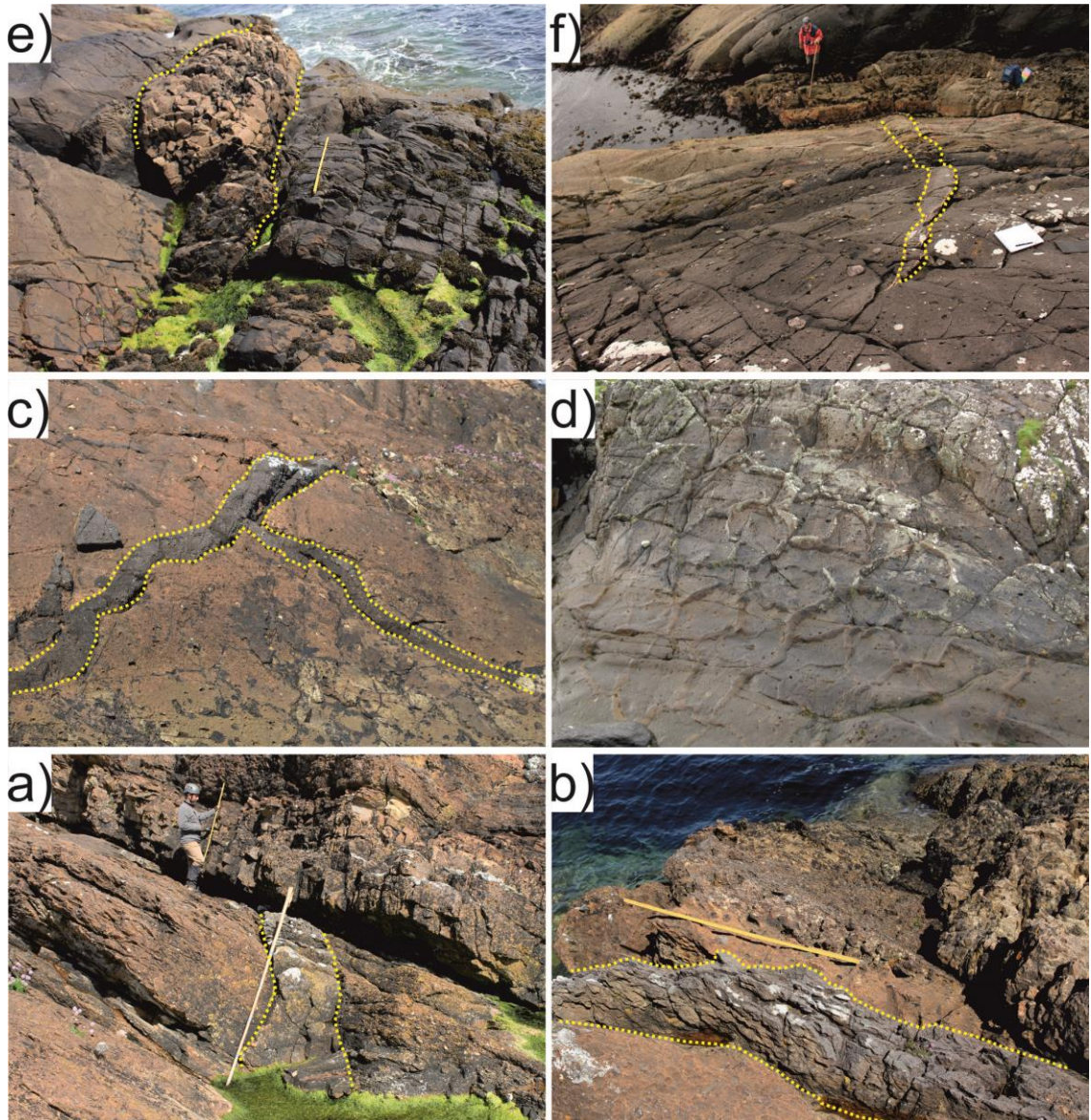
Figure 6.6: Sandstone wedges at various stratigraphic levels (yellow dashed lines). (a-c) Sandstone wedges penetrating D14-D15, respectively, on W of A'C, E coast of EaN, and E coast of GE. (d) Polygonal sandstone wedges at the top of D22 on the SW coast of EaN. (e) Thick sandstone wedge penetrating a sandstone bed 2.5 m above D24 on the E coast of EaN. (f) Sandstone wedge penetrating top of D29 on the E coast of GE. One metre ruler and geologist are for scale.
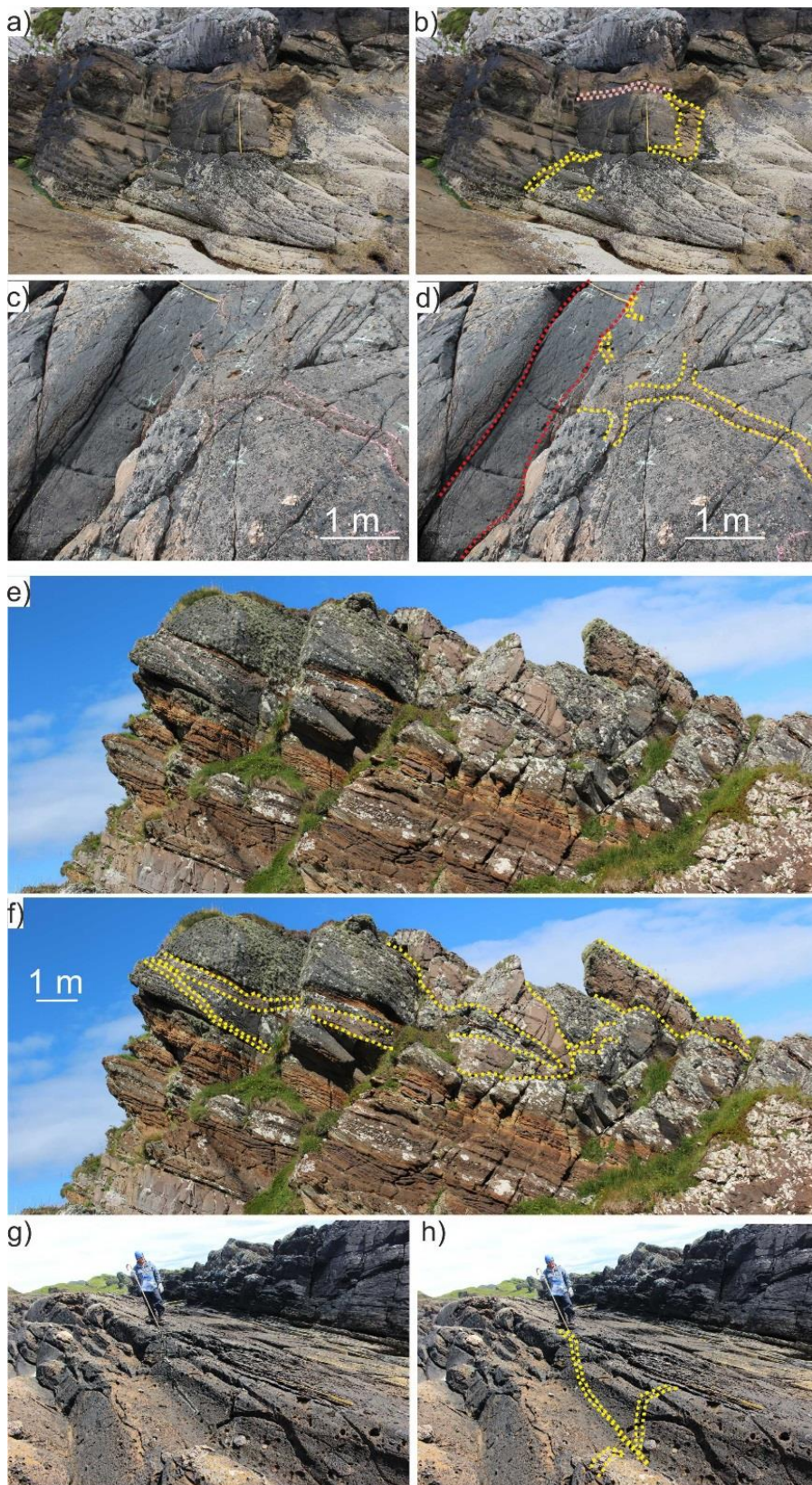
Figure 6.7: Sandstone wedges, yellow dashed lines, in cross-section.
(a-b) Wedges are penetrating laminated siltstone with dropstones, above D30, W coast of GE. The pink dashed line represents the lag conglomerate at the top of the wedge. The Ruler is 1 m scale.
(c-d) wedges penetrating D26 on the S coast of A'C. The wedges are truncated by diamictite bed (D26`) and the red dashed line represents the upper and lower contacts of D26`.
(e-f) sandstone wedge penetrating laminated siltstone. Above D30 on S coast of EaN.
(g-h) wedges piercing top of D22 on the W coast of A'C. Geologist (Hamid Daleq) for scale.

Table 6.2: Sandstone wedges at various stratigraphic levels within the PAF succession in the Garvellachs and Islay. D=diamictite bed no., E=east, W=west, S=south, DC=Dun Chonnuil, GE=Garbh Eileach, A'C=A'Chuli, SLaC=Sgeir Leth a Chuain, EaN=Eileach an Naoimh, SD=Sgeir Dubha.

Nr.	Member	Penetrating	Locations	Islands
23	4	D44	Caol Ila	Islay
22	4	D43	Caol Ila	Islay
21	4	D42	Caol Ila?	Islay
20	4	D40	Loch Allan, Caol Ila	Islay
19	4	D39	Caol Ila	Islay
18	3	Within D38	W GE	Garvellachs
17	3	D36	E SD	Garvellachs
16	3	D35`	SD	Garvellachs
15	3	D35	S GE, W GE	Garvellachs
14	2	Rhythmically laminated	W GE	Garvellachs
13	2	Rhythmically laminated	E GE	Garvellachs
12	2	D32	E GE	Garvellachs
11	2	Sst. and congl. bed-sets above D31	E GE	Garvellachs
10	2	Brown sandstone above D30	W GE, W EaN	Garvellachs
9	2	Siltstone at the top D30	W GE	Garvellachs
8	2	D29	E GE, W GE, S A'C, W A'C, E EaN, W EaN	Garvellachs
7	2	D26`	E EaN	Garvellachs
6	2	Conglomerate (Congl.) at the top D26	SLaC	Garvellachs
5	2	D26	E GE, W GE, E A'C, S A'C	Garvellachs
4	2	Sandstone (Sst.) above D24	E EaN	Garvellachs
3	2	D22	E GE, E A'C, W A'C, E EaN, W EaN	Garvellachs
2	1	D18	E GE	Garvellachs
1	1	D14-15	E GE, W GE, E A'C, W A'C, E EaN	Garvellachs

Table 6.3: Statistics of periglacial features in the PAF. The 47 numbered diamictites in the Formation belong to at least 26 groups of diamictites. These groups often show periglacial features at their top: 18 tops have sandstone wedges; 5 tops have frost-shattered clasts; one top has cryoturbation. Most of these tops show only wedges (13), but at 4 tops there are wedges and frost-shattered clasts and at one top all three features are present. More horizons of periglacial features occur within bedded sediments in the Formation: wedges (5), frost-shattered clasts (1), Cryoturbation (2) and frozen sedimentary fragments (2). The data from Members 1-3 are from the Garvellachs; those from Members 4-5 are from Islay (Ali et al., 2018: in press).

Members		1	2	3	4	5	Grand total
Thickness (m)		200	140	180	220	350	ca. 1100
Number of diamictite (D) groups		> 5	9	6	3	3	>26
Number of wedge (W) horizons	W penetrating D	2	7	5	3	1	18
	W penetrating bedded sediments	0	5	0	0	0	5
	Total	2	12	5	3	1	23
Horizons with Frost-shattered clasts (FSC)	FSC on the top of D	0	3	2	0	0	5
	FSC on the top of bedded sediment	0	1	0	0	0	1
	Total	0	4	2	0	0	6
Horizons with involution downfolds (ID)	ID at the top of D	0	1	0	0	0	1
	ID at the top of bedded sediment	0	1	1	0	0	2
	Total	0	2	1	0	0	3
Horizons of frozen sedimentary fragments		0	1	1	0	0	2
Tops of diamictite groups	Horizons with only W	2	4	3	3	1	13
	Horizons with W + FSC	0	2	2	0	0	4
	Horizons with W + FSC + ID	0	1	0	0	0	1
Total numbers of horizons with periglacial features							25
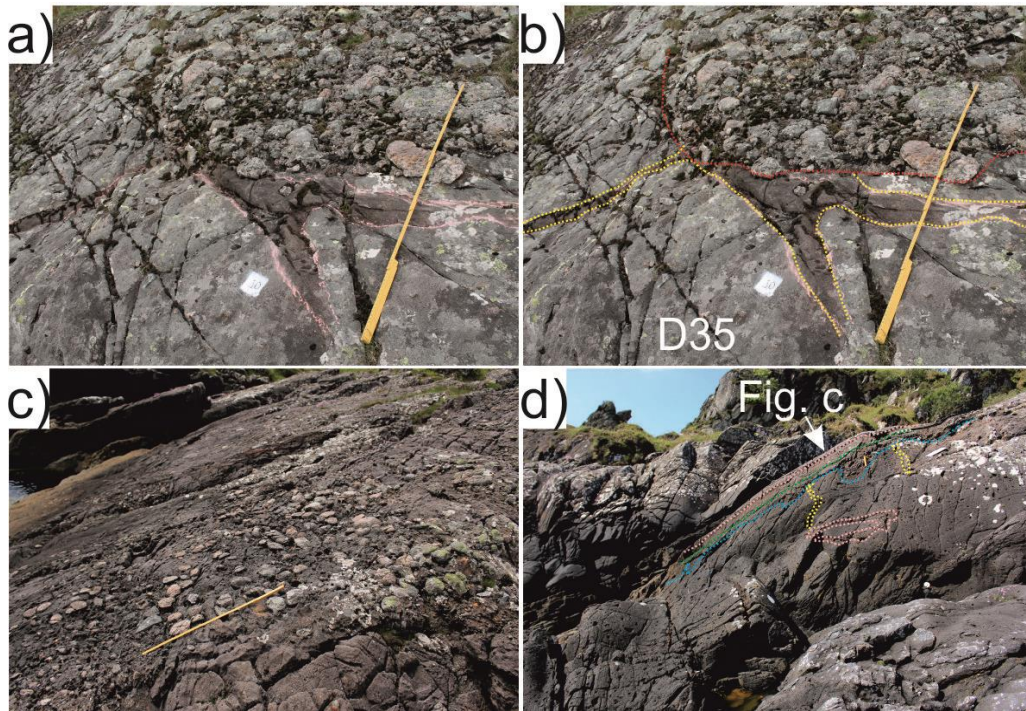
Figure 6.8: Upper contact of diamictite beds on the S (a and b) and E (cand d) coasts of GE; (a and b) view looking down on branching sandstone wedges (yellow dashed lines) penetrating the top of D35, both are overlain uncomfortably by a granitic lag conglomerate (red dashed line). (c) lag conglomerate at the top of D26; (d) shows D22 penetrated by sandstone wedges (dashed yellow lines), both are truncated by sandstone downfolds layer (dashed blue lines) which is overlain by another sandstone bed in turn truncated (green line) by a lag conglomerate at the top (dashed pink line). See also Fig.4.4 for a sketch of relationships at (d).

Spencer (1966; 1971) suggested that the production of each of these horizons of sandstone wedges needs a period of time and the sequence of events: (i) wedge shape must be formed after deposition of a particular bed, extending downward from the top of the bed; (ii) then the wedge-shape was infilled by sand-grade material from the top; (iii) when the cracks had filled with sand, either the source bed of sand was removed or the transport of the sand to the area ceased; (iv) time gap before a new bed deposited; (v) deposition of bedded sediment disconformably on the wedge structure.

The present author agrees with Spencer (1966; 1971) that this sequence of events occurred at each sandstone wedge horizon within the PAF succession. However, Spencer (1966; 1971) was focussing on a particular location at one individual horizon for counting the events. By correlating a particular horizon of sandstone wedges laterally, many more events are recorded. For example, in 'Fig.6.9' the number of events recorded, at A'C inland and SC of A'C, is much more than three: (i) deposition of D24; (ii) possible time gap (non-deposition); (iii) deposition of D25. By contrast, on the E coast of EaN, the number of events recerded are about ten (Fig.6.9): (i) deposition of D24; (ii) non-deposition of sedimentary beds (time-gap); (iii) formation of the first horizon of the sandstone wedges; (iv) deposition of the sandstone and conglomerate bed-set; (v) deposition of the sandstone above the bed-set; (vi) non-deposition of the sedimentary beds; (vii) formation of the second horizon of the sandstone wedges; (viii) deposition of the sandstone beds; (ix) sharp contact between sandstone and D25; and finally (x) deposition of D25.
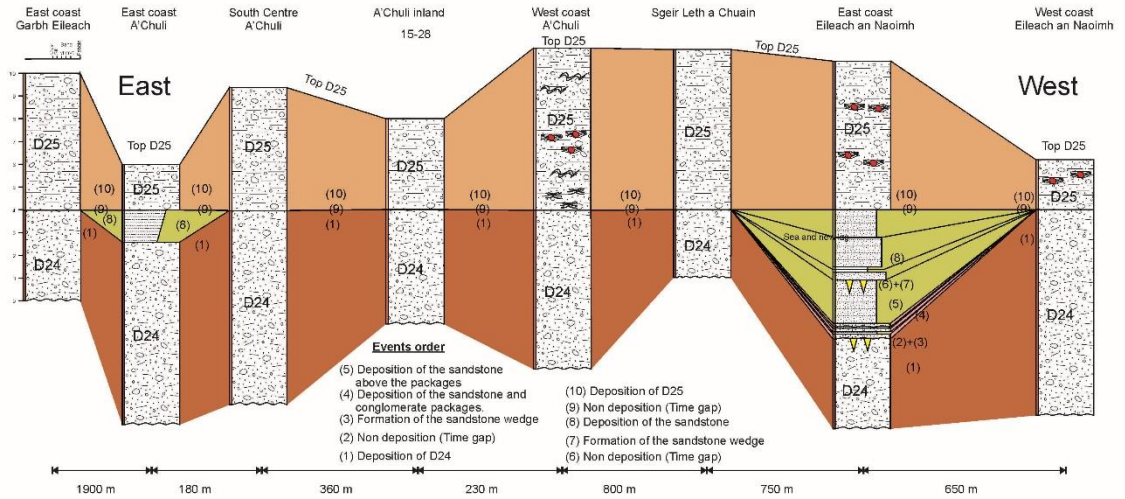
Figure 6.9: Correlation log through Garvellach Islands, showing events at the contact between D24 and D25.

6.2.3 Horizons with intra-bed folds

Intra-bed folds are another distinctive feature within the PAF succession. Spencer (1971) recognised 15 horizons of this structure at different stratigraphic levels; some of them lie above homogeneous diamictite beds (Figs.6.10 a, c, e, f, g; 6.11 c, d) and others occur within sandstone beds (Figs.6.10 b, d, i; 6.11 c, d). Laterally, they cover few hundreds of metres to several thousands of metres, and vertically they disturb bedding up to 3.5 m; lying either in the tops of diamictite beds or within bedded sandstone. They are mostly basin-shaped in three dimension (Figs.6.10, 6.13); and their internal architecture exhibits bedding parallel to the wall of the structure (Fig.6.10), except in few cases (Fig.6.12).
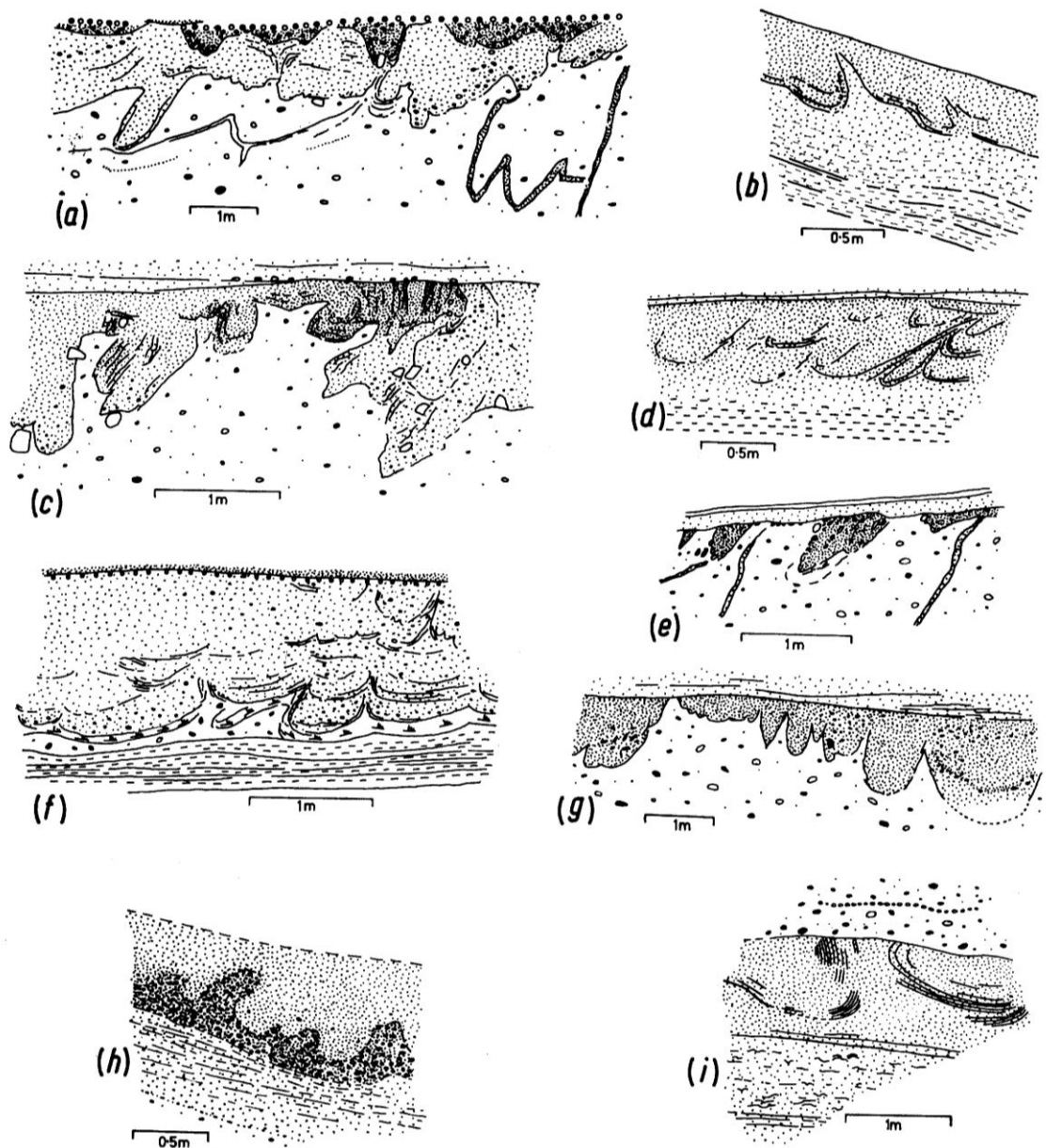
Figure 6.10: Field sketches of cross-sections of sandstone downfold structures from the Garvellachs (Spencer, 1971; Fig.10). (a, c, f, and h) the pebbly sandstone which overlies D26, respectively, on the E coast of GE, E coast and W coast of A'C; (b and d) within the sandstone between D26 and D27 on the E and W of A'C respectively; (e and g) the top of D22 and D16, respectively, on the E coast of GE; (i) the sandstone just beneath D33 (Fig. 5.11a) on Sgeir Nam Marag.

At least three of these horizons originated as periglacial cryoturbations (Fig.6.3). Usually the downfold structures are overlain disconformably by planar bedded sediments showing that the intra-bed fold was penecontemporaneous (Figs.6.10, 6.11, 6.13). However, sometimes the overlying sandstone is continuous with the sandstone basin (Fig.6.12), probably this example is a loading structure, because it shows horizontal parallel lamination within the basin shape. The best example to show intra-bed folds is located on the E coast of GE on top of D26 (Fig.6.11 c, d).The detailed events sequence of this outcrop is recorded by a field sketch in 'Fig.6.11c and d; Fig.6.14a' and the detailed stratigraphic column 2 km to the W is represented by 'Fig.6.14b' (Ali et al., 2018: in press).

234
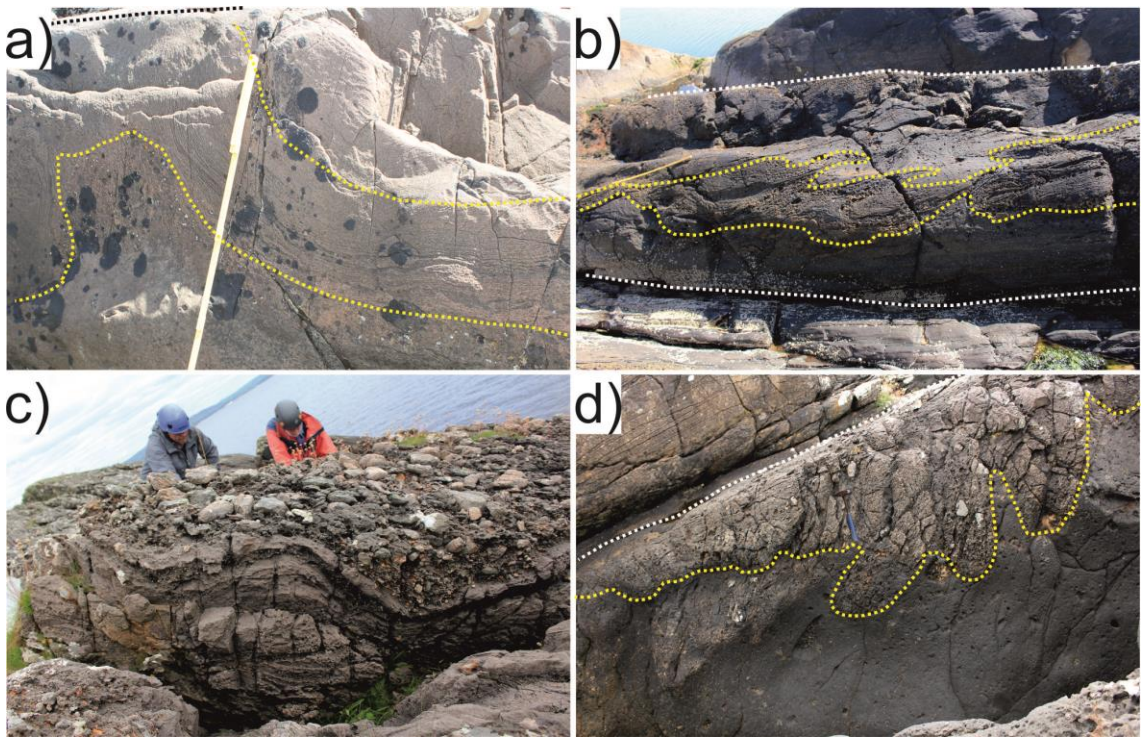
Figure 6.11: Sandstone downfolds in cross-section (yellow dashed lines). (a) Downfolds within pebbly sandstone just beneath D33 on Sgeir Nam Marag, the black dashed line represent bedding, ruler is 65 cm scale; (b) Downfolds on the top of D26 on the E coast of A'C, ruler is one metre scale; (c and d) downfolds on the top of D26 on the E coast of GE, geologists and the geological hammer are scales.
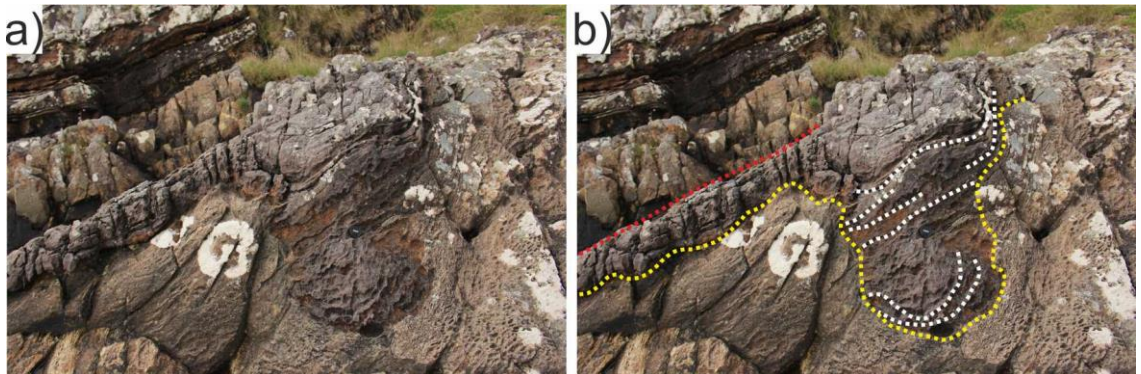
Figure 6.12: Loading structure on the top of dolomitic siltstone bed just above D30, on the E coast of GE. Within (b), the red dashed line represents bedding of the strata, the yellow dashed line shows loading structure, and the white dashed line exhibit the stratification inside the loading. Lens cap is 58 mm scale.
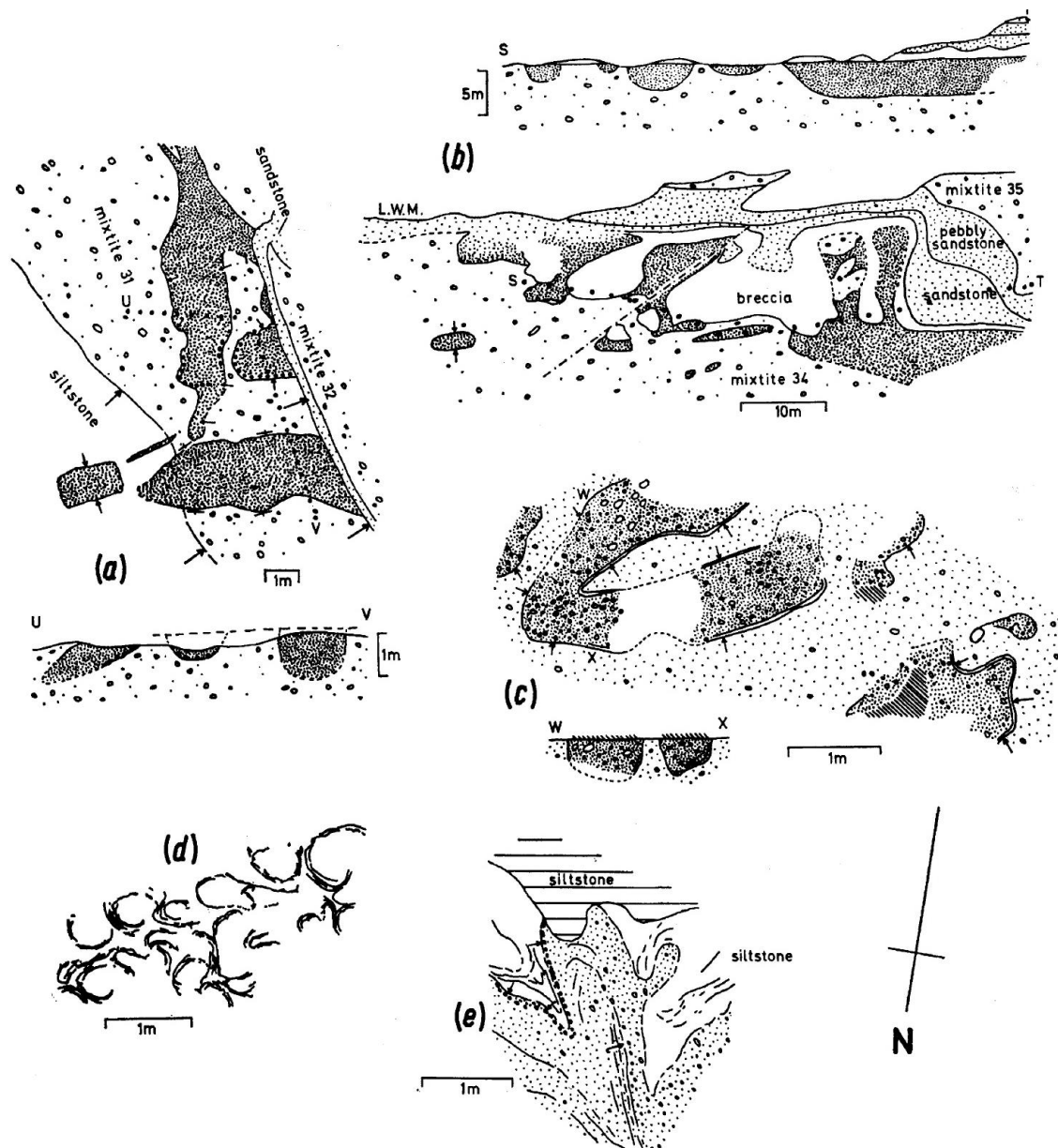
Figure 6.13: Plan view and cross section of sandstone downfold structures in the Garvellachs (Spencer, 1971; Fig.9). (a) The top of D31 at E coast of GE. (b) the top of D34 at S GE (GE); (c) The pebbly sandstone above D26 (not shown) on the E coast of GE; (d) plan view of downfolds in the pebbly sandstone above D26 on the W coast of A'C (A'C); (e) Plan view of folds affecting pebbly sandstone, overlain by undisturbed siltstones, all contained within D24 on the SW coast of EaN.

6.2.4 Horizons with combinations of frost-shattered clasts, sandstone wedges and intra-bed folds

Three types of episode represented in the PAF have been tallied: glacial, periglacial and non-glacial (Table 2). Diamictites 1–12 are there treated as one group, but require further study. The 26 diamictite groups, plus two beds of laminated siltstones with ice-rafted debris (IRD) in Member 2 (one shown in Fig. 7g), add up to a total of 28 glacial episodes. The horizons with periglacial features total 25. These glacial plus periglacial episodes are separated by 23 non-glacial episodes. Thus in the ~1100m of strata of the PAF there are a total of 76 climatically-related depositional episodes preserved.

236

Based on 'Table 6.3 and 6.4' at least 6 different horizons show sandstone wedges combined with frost-shattered clasts; however, sandstone wedges, frost-shattered clasts, and sandstone downfolds all in combination occur only at 1 horizon. The coexistence of these features in the same levels must be due to related depositional conditions and mode of formation. The author has not seen any mass-flow processes that can explain all these feature in the same stratigraphic level, but they can all form in periglacial settings. The sandstone wedges can be formed as a result of contraction cracks as Spencer (1966; 1971) suggested, and frost-shattered clasts and sandstone downfolds can be produced within an active layer by cryoturbation mechanisms. As a result three points can be concluded from these stratigraphic features at the top of diamictite beds: (i) Many glacial environmental details have been preserved within the PAF succession; (ii) the presence together of sandstone wedges, frost-shattered clasts, and sandstone intra-bed fold features in the same stratigraphic level records periglacial environments, transitional between the diamictite (glacial) and the later stratified sediments (non-glacial); and (iii) 'taking the record of these periglacial horizons, in the PAF as a whole, such conditions are preserved at 25 levels in the ca. 1100 m stratigraphic column' (Ali et al., 2018: in press)

Table 6.4: Summary of the main climatically-related episodes represented in the PAF (taken from Ali et al., 2018, table 2). Fig.6.3 shows the members, diamictite groups, and periglacial horizons in the PAF.

Member	Thickness (m)	Diamictite bed number	Diamictite groups	Glacial episodes	Periglacial	Non-glacial episodes	Totals, all episodes
5	350	45-47	3	3	1	3	7
4	220	39-44	3	3	3	3	9
3	180	33-38	6	6	6	6	18
2	140	19-32	9	11	13	8	32
1	200	1-18	5	5	2	3	10
Grand total	~1100	47	26	28	25	23	76
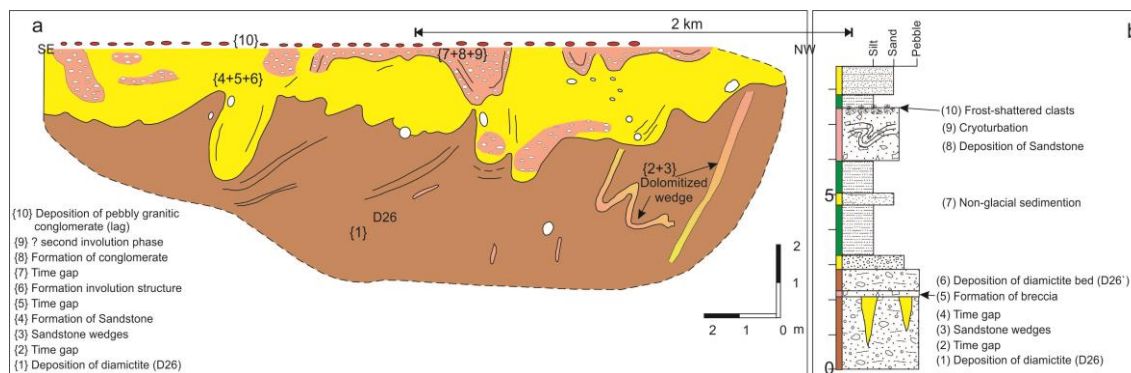
Figure 6.14: Examples of the many events recorded by the periglacial features at the top of Diamictite 26: (a) measured profile, E coast of GE; (b) stratal column, E coast of A'C. In locality (b) four extra events – (4) to (7) – are present in the time gap [5] in locality (a). The cryoturbated sandstone bed – [6] and (9) – is present along all of the outcrops for 5km throughout the Garvellachs. See Figure 4.1 (i) for a photograph showing the events (1) to (7) of (b) in outcrop (Ali et al., 2018, in press).

6.3 Unconformities

There are three unconformity candidates within the PAF succession: (i) base of the formation with the underlying Lossit Formation on Islay; (ii) base of the Upper Dolomite; and (iii) base of Member 3. In addition to these three unconformities, there are another two major boundaries but not obvious like these three. The detailed explanations for these two are mentioned in section 6.4.

The base of the formation is an unconformity on Islay: (i) The two distinctive lithofacies associations 'diamictite breccia bed' and 'Disrupted Beds' can be both recognized on Islay and Garvellachs Islands (Fig.6.15), but are much thinner at the first locality (Spencer, 1966, 1971; Ali et al., 2018: in press); (ii) on Islay the 'diamictite breccia bed' (Previously Great Breccia) rests with a clear unconformity on the Lossit Formation; and (iii) D1-12 are only present on the Garvellachs (Fig.4.15) and more than 100 m thickness is missing in the lowest part of Member 1 on Islay (Spencer, 1971).

An unconformity occurs near the top of Member 1. Spencer (1971, plate 11a) deduced an unconformable relationship between D18 and the overlying Upper Dolomite on GE. D14-D18 have been followed in detail through the Garvellachs (Fig.6.16) and this work confirms that the base of the Upper Dolomite is unconformable. Starting on the E coast of GE, underneath this bed D18 thins and dies out towards the W after 350 m; then D16-17 merge together, thinning and thickening, towards the W again until they also disappear completely on the W coast of GE (Fig.6.16).
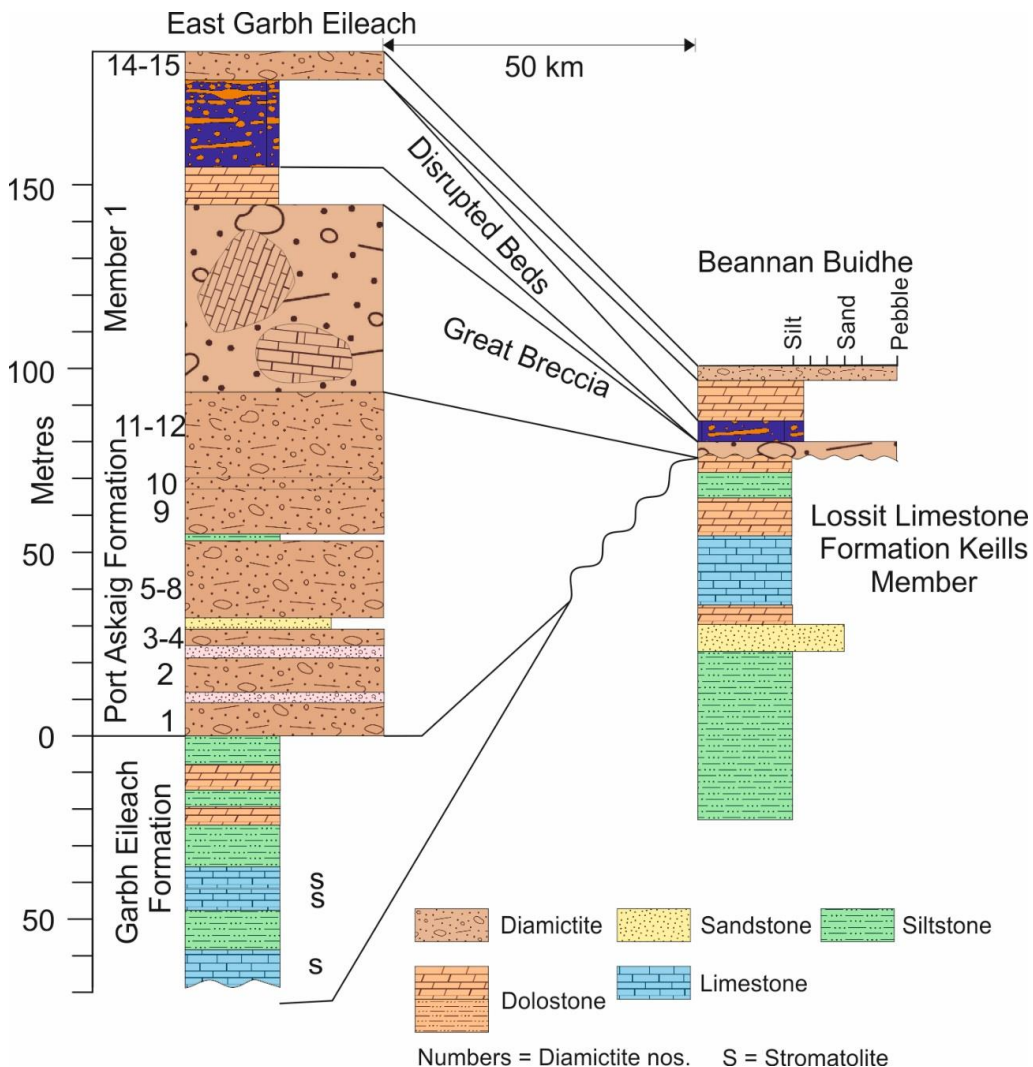
Figure 6.15: Comparison of the Lossit Limestone to Disrupted beds sections of the Garvellachs and Islay. Two distinctive beds – the Great Breccia and the Disrupted Beds – can be recognized in both localities, but are thicker in the Garvellachs. Diamictites 1 – 12 are missing on Islay: there the Great Breccia rests unconformably on the dolomite bed at the top of the Lossit Limestone (Ali et al., 2018: in press, Fig.9).

The third unconformity occurs at the top of the Member 2 and the base of the Member 3. This relationship was inferred by Spencer (1966), who suggested an unconformable relationship at the base of the large cross bedded (up to 14 m foreset), white sandstone in Member 3. New detailed fieldwork, following the boundary between Member 2 and Member 3, from the E coast of GE to the W coast of the same island is shown in 'Fig.6.17'. On the E coast of GE, the brown sandstone on the top of rhythmically laminated siltstone thin and dies out towards W; then the rhythmically laminated siltstone thins to zero towards the W. Also, the brown sandstone underneath the siltstone thins towards the W and D31 thins and has disappeared on the W coast of GE. Another level of rhythmically laminated siltstone comes in below D31 but is not seen on EaN. Both of the rhythmically laminated siltstones, from the E and W coasts of GE, are penetrated by sandstone wedges. Subsequently all the beds were truncated by an unconformable surface that separates Member 2 from Member 3.
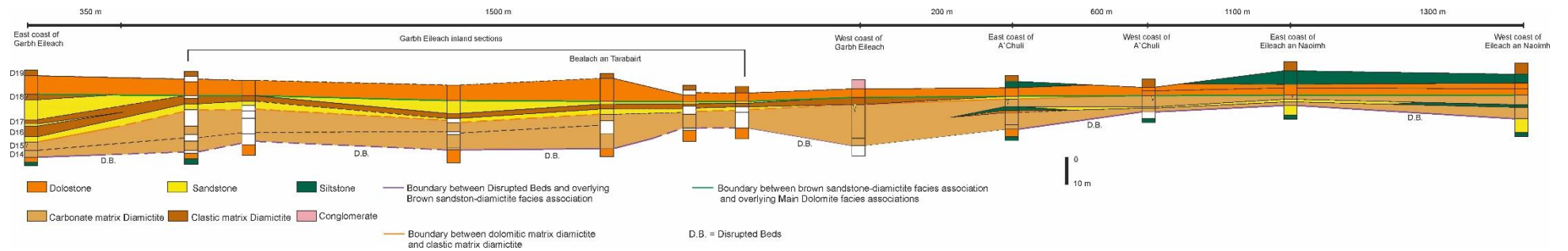
Figure 6.16: Correlation of the uppermost beds of Member 1 in the Garvellachs, showing their subcrop below the Upper Dolomite. The section on the E coast of GE contains 18m of strata that are progressively cut out when traced 5km to the W. Thus on the E coast the section records more events: three diamictites (16-18), the intervening sandstones and siltstones and a sandstone wedge horizon (top of Diamictite 18).
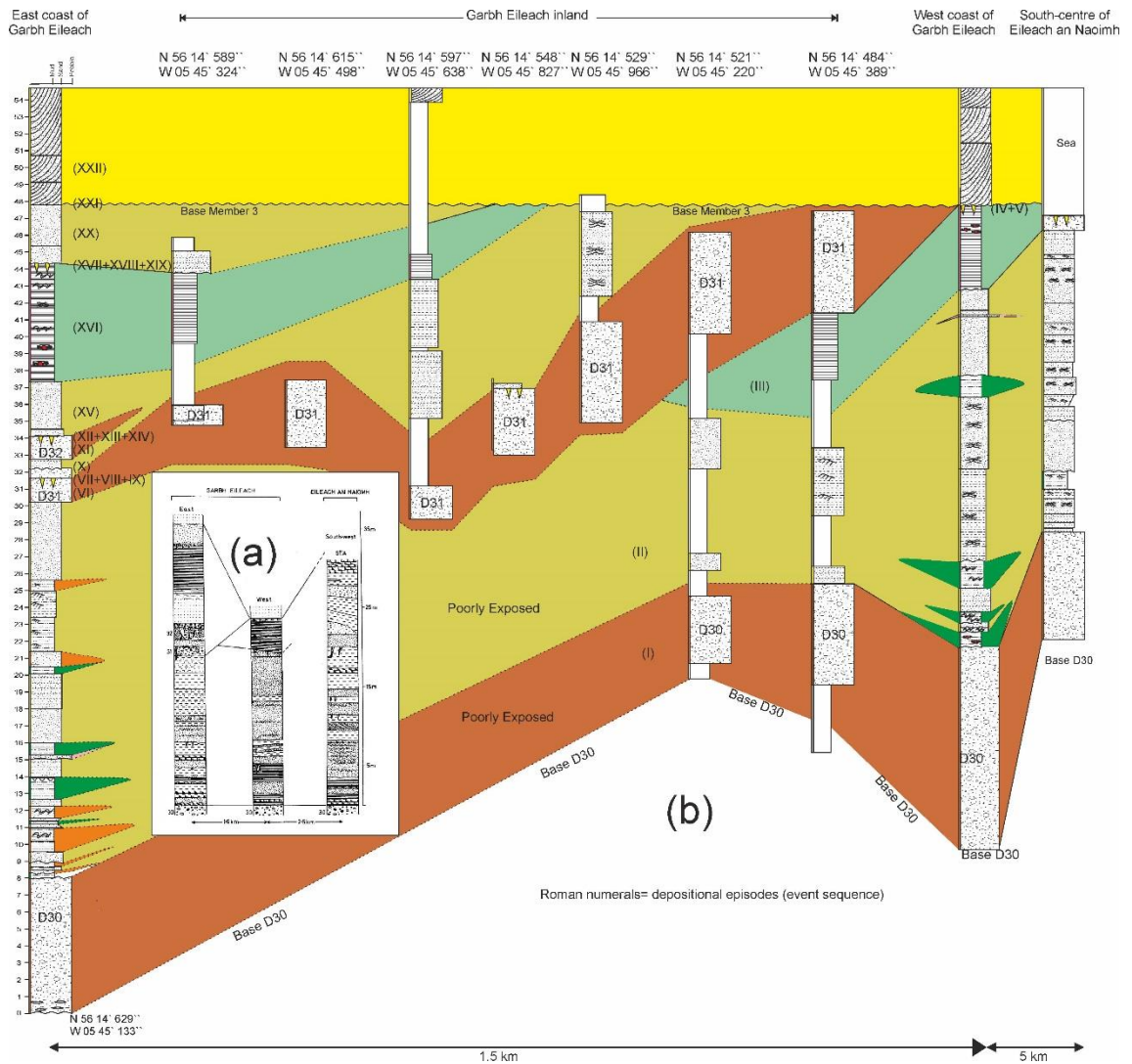
Figure 6.17: (a) Correlation of the uppermost beds of Member 2 on GE from Spencer (1971). **(b)** Result from the new fieldwork showing the correlation of the uppermost beds of Member 2 on GE, and their subcrop below Member 3. The section on the E coast of the island contains 20m of strata which are progressively cut out when traced 1.5km to the W. Thus on the E coast the section records several more events: two diamictites (31, 32), three horizons of sandstone wedges and the unit of 'rhythmically laminated' siltstones (Ali et al., 2018: in press).

These three stratigraphic levels also show that more stratigraphic units are preserved in the section on the E coast of GE than further to the W (Ali et al., 2018: in press). For instance, the E coast of GE contains more diamictite beds (D16-18, D31, and D32) and more periglacial episodes, such as sandstone wedge above D18, D31, D32 and above rhythmically laminated siltstones (Ali et al., 2018: in press). These facts are an indicator of more complete section on the E coast of GE compared with the other localities to the W.

6.4 Major boundaries

The succession of the PAF has been divided into Members 1-5 (Spencer, 1971). These divisions are based on clast content, matrix composition, lithology, and the thickness of the beds. Three important boundaries have been mentioned previously (base D1; base Upper Dolomite; and base Member 3).

Three others are the boundary between Members 1 and 2; above the sandstone that overlies D38 and the boundary at the top of D44.

In the formation we recognise five major stratigraphic boundaries:

First, the base of the PAF with the underneath Lossit Formation. The lithology changes from bedded carbonate and sandstone to diamictite and interbeds.

Second, the boundary between Members 1 (Chapter Three) and 2 (section 4.1 in Chapter Four) which is taken at the top of the Upper Dolomite, i.e. just above the unconformity at the base of the Upper Dolomite. This is also mentioned previously in 'section 3.5' and discussed in detail there. The differences between the two Members are: (i) matrix lithology is dolomitic siltstones for diamictite beds in Member 1; but in M2 they are sand-rich dolomitic siltstones to dolomitic, silty arenites; (ii) gradual upward change in clast types from intrabasinal carbonate (dolomite and limestone) to extrabasinal (granite and quartzite) clasts; in M2 the two types occur in almost equal amounts; (iii) in both the interbeds are dolomitic siltstone and sandstone; (iv) in Member 1 most interbeds are lenticular and die out in very short distance laterally and maximum thickness of the interbeds is about 5m; while in Member 2 they are more continuous and thicker.

Third, the boundary between Members 2 and 3. The detailed characterization of this boundary is mentioned in 'Chapter Four'. As well as being an unconformity in the Garvellachs this boundary makes a major change from M2 to M3. M3 is different from M2: (i) the matrix of the diamictite beds are silty-arenites; (ii) extrabasinal clasts are predominant and intrabasinal clasts are minor in proportion; (iii) the interbeds are mostly white sandstone with large cross stratification, up to 14 m foresets, and extend for a long distance laterally; (iv) the thickness of the diamictite and interbeds are similar.

Fourth, the boundary between Members 3 and 4 (Fig.6.3). The two members are quite different in lithostratigraphy, M4 is characterized by: (i) the matrix of the diamictite beds is silty-arenites; (ii) the extrabasinal clasts are dominant and intrabasinal clasts few; (iii) the interbeds are thin white sandstone; (iv) diamictite beds are very thick compared with the interbeds.

Finally, the boundary between M4 and M5 (Fig.6.3). The two members are different in lithostratigraphy; the diamictite beds in M5 are very thin compare with the thick white sandstones.

Chapter 7 : Event Stratigraphy

This chapter describes examples of repetitive events which occur through the whole PAF. The repetitive events preserve fine stratigraphic details, at very high resolution which can be tabulated and analysed.

7.1 Repetitive, fine-detail events

There are several horizons within the PAF succession which exhibit repetitive event packages. The horizons are similar in their appearance and the types of occurring features. One of the repetitive event packages involves periglacial features on the top of a diamictite beds. In this study, five stratigraphic horizons are selected to illustrate these repetitive horizons: (i) top of D22; (ii) top of D24; (iii) top of D26; (iv) top of the rhythmically laminated beds above D30; and (v) top of D35 (Fig.6.3). Some of these horizons were described in 'section 6.2', and the rest will be described in ascending stratigraphic order:

a) Top of D22: This contact is complicated and the most complete outcrop is located on the E coast of GE. There D22 is penetrated by sandy/dolomitic sandstone wedges. Some of the wedges are truncated by a lenticular bed of conglomerate/breccia (Fig.6.4g,h,l; 6.6d; 6.7h; and 6.8d). This breccia bed is overlain by a sandstone bed. If we list the sequence of events, then it is not simple like counting lithologies. 'Fig.4.4' shows the sequence of events present in this horizon: (i) deposition of D22; (ii) non deposition (time-gap); (iii) initiation of the wedge shapes; (iv) filling the wedge shapes by dolomitic or sandy materials; (v) continuous deposition of D22 in places and, possible, erosion of the sandstone wedges; (vi) non-deposition (time-gap); (vii) deposition of conglomerate/breccia; and (viii) deformation of the conglomerate/breccia; (ix) deposition of the sandstone bed; (x) formation of the sandstone downfolds.

The top surface of D22 is not the same in all the different localities along strike. On the E coast of GE, it is as described above; while on the W coast of the same island, there are only sandstone wedges.

The outcrop of the top D22 is poor on the E coast of A'C: there are some small sandstone wedges (Fig.7.1), and about 10 cm thick patches of the conglomerate/breccia. On the W coast of A'C, sandstone wedges are present (Fig.6.7l, h), but no sandstone downfolds or conglomerate/breccia were recorded.

Figure 7.1: Outcrop of the D22 on the E coast of A'C; (a) the yellow line outlines a conglomerate/breccia patch on the top of D22; (b) the yellow line shows a poor weathered sandstone wedge penetrating top of D22. Ruler is 1 m.

On the E coast of EaN, polygonal sandstone wedges are recorded with patches of conglomerate/breccia within them; also, on the SW coast there is a well-developed system of polygonal sandstone wedges with few patches of conglomerate/breccia within them; frost-shattered clasts have also found in the top of D22 (Fig.4.4 g, h, l).

b) Top of D24: This horizon and the top of D26 are described in detail in section 6.2 and Fig.6.9. To avoid repetition the author does not repeat them here. However, comparing them with the other stratigraphic horizons is important. The top of D24 is different from the other stratigraphic levels as sandstone wedges occur in some places and not in others (Fig.6.9). Also, D24 exhibits two separate stratigraphic horizons of sandstone wedges (Fig.6.9), on the E coast of EaN. One penetrates the top of D24 and the other penetrates a sandstone bed about 2.5 m above the top of D24 (Fig.6.6e). At other stratigraphic levels just one horizon of sandstone wedges occurs at the top of a diamictite bed.

On the E coast of EaN, the sequence of events at this stratigraphic level above the top D24 is (Fig.4.1, 6.9): (i) deposition of D24; (ii) time gap (non-deposition); (iii) initiation of the wedges; (iv) filling the wedge with sandy material; (v) time gap (non-deposition); (vi) deposition of the bed-set between the lower and upper horizons of the sandstone wedges; (vii) deposition of the sandstone above the bed-set; (viii) time gap (non-deposition); (ix) initiation of the wedges in the upper horizon; (x) filling the wedge with sandy material; (xi) formation of the sandstone beds above the upper horizon of the sandstone wedges; (xii) time gap (non-deposition); and finally (xiii) deposition of D25.

However, on the E coast of A'C only four events are recorded (Fig.6.9): (i) deposition of D24; (ii) deposition of a sandstone bed; and (iii) non deposition; and (iv) deposition of D25. Whereas, on the SC coast of A'C, A'C inland, W coast A'C and SLaC none of the events were recorded and D25 directly rests on the top of D24.

c) Top of D26: At the top of D26 in addition to sandstone wedges there is a horizon of sandstone downfold structures and angular fragments. The most complete sequence of this stratigraphic horizon is exposed on the E coast of GE and the E coast of A'Chuli (Fig.4.1).

On the E coast of GE, the event sequence at this stratigraphic level is: (i) deposition of D26; (ii) non-deposition (time gap); (iii) initiation of the wedge shape; (iv) filling the wedge shape by sandstone material; (v) deposition of pebbly sandstone bed; (vi) formation of the cryoturbation structures; and (vii) deposition of a pebbly granitic conglomerate bed.

On the E coast of A'C the sequence of events is slightly different: (i) deposition of D26; (ii) non-deposition (time gap); (iii) formation of the wedge shape; (iv) filling the wedge shape by sandstone material; (v) deposition of the bed-set between D26 and D26`; (vi) deposition of D26`; (vii) deposition of conglomerate above D26`; (viii) formation of cryoturbation structures and frost-shattered clasts.

A correlation and composite section from the E coast of GE and A'C gives the following sequence of events (Fig.7.2): (i) deposition of D26; (ii) non-deposition (time gap); (iii) formation of the wedge shape;

(iv) filling the wedge shape by sandstone material; (v) deposition of the package between D26 and D26`; (vi) deposition of D26`; (vii) deposition of conglomerate above D26`; (viii) deposition of the pebbly sandstone and formation of the cryoturbation structure; (ix) deposition of pebbly granitic conglomerate; (x) deposition of the siltstones (xi) deposition of the pebbly sandstone and formation of the cryoturbation structure (Fig.7.2).
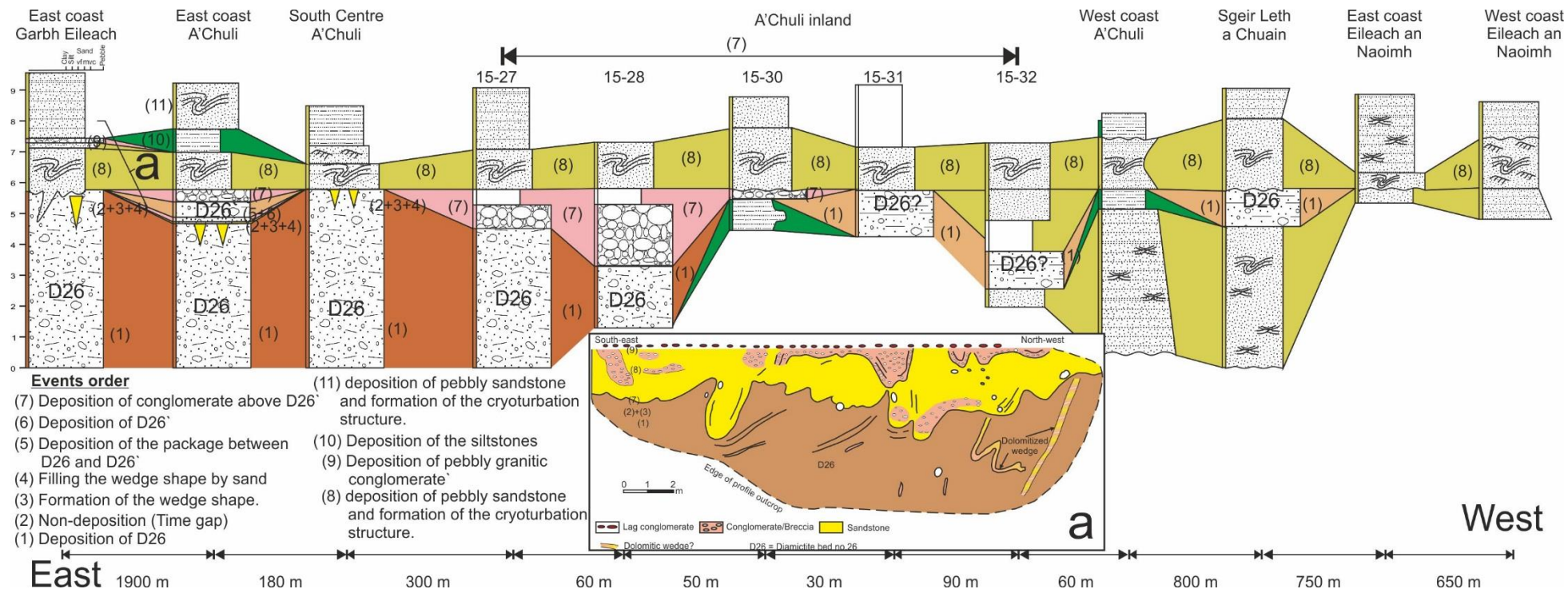
Figure 7.2: Correlation logs of the upper part of D26 through the Garvellachs. (a) is a field sketch for the top of D26 on the E coast of GE. The preserved sequences of events are different from place to place which can be seen using this detailed log correlation.

d) Top of D35: This horizon is another where periglacial features can be seen. One of the differences of this horizon compared with the others is that in one place, in the S of GE, patches of the diamictite within the sandstone wedge polygons are dolomitic; this is the only place where one can see this observation (Fig.7.3). However, about 100 m towards the W, these dolomitic patches are absent and a one clast layer of conglomerate/breccia overlies D35 and the sandstone wedges that penetrate its top (Fig.6.4a-b and 6.8a-b). The orders of the events recorded here are the same as for the top of D22.
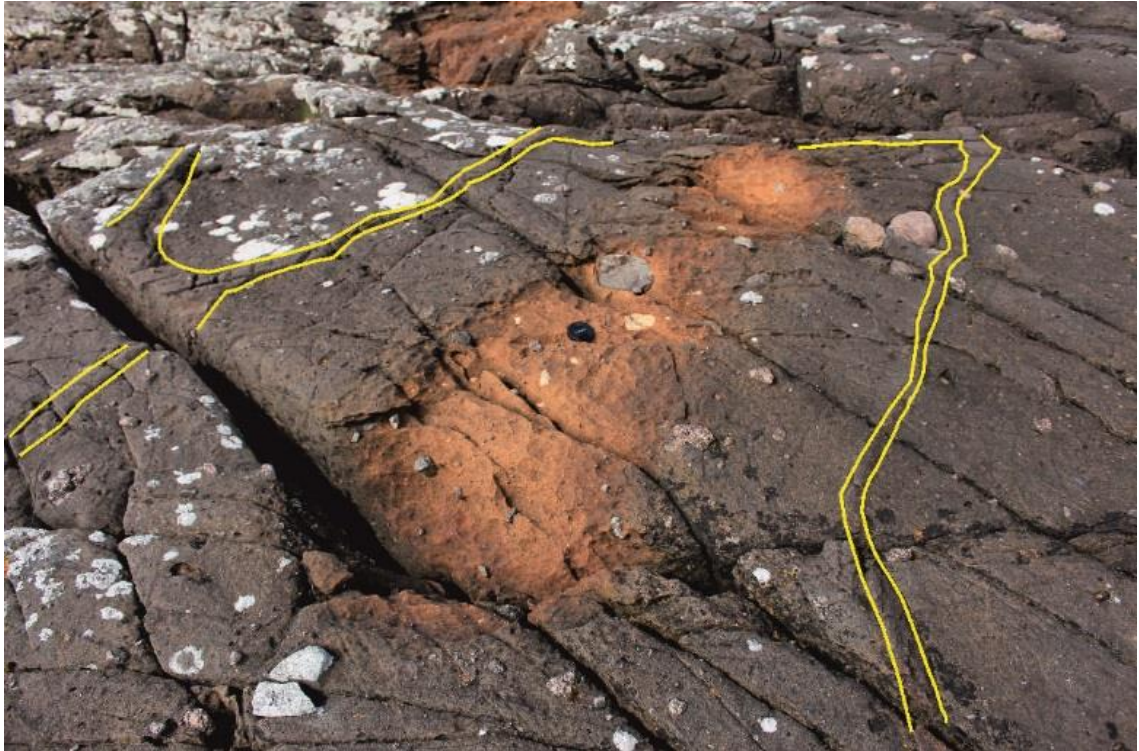
Figure 7.3: Sandstone wedge (yellow lines) at the top of D35 on the S coast of the GE E side of the harbour. The orange colour shows dolomitic patches within the polygons of the sandstone wedge. Camera lens cap is 58 mm.

On GE, the S and E coast outcrops of this horizon were described in detail in section 4.2.2.b. At the W coast, about 100 m inland from the sea, there are frost-shattered clasts on the top of the D35 associated with sandstone wedges (Fig.4.46).

The sequence of events of this stratigraphic horizon are: (i) deposition of the D35; (ii) non-deposition (time gap); (iii) initiation of the wedge shape; (iv) filling a wedge shape by sandy material; (v) frost-shattering of clasts; (vi) deposition of the conglomerate; and (vii) deposition of the sandstone bed above.

e) Top of the rhythmically laminated beds above D30: The reason behind choosing these horizons is because sandstone wedges here penetrate fine laminated siltstone instead of diamictite beds (Fig.6.7a-b). The best outcrops of these horizon are on the E and W coasts of GE. On the W coast of GE, the sandstone wedges penetrate fine laminated siltstones; but this horizon is at a lower stratigraphic level than the E coast (Fig.6.17). On the W coast the rhythmically laminated siltstones include dropstones (Fig.4.31) and the sandstone wedges are overlain by patches of conglomerate/breccia (Fig.6.7a-b).

The full sequence of events, taking account of both outcrops, is shown in Fig.6.17. This is redrawn in the form of a Wheeler diagram below (Fig.7.4). The numbered sequence is as follows : (I) deposition of D30; (II) deposition of the bed-set above D30 and below the rhythmically laminated sediments on the W coast of GE; (III) deposition of the rhythmically laminated siltstones on the W coast of GE; (IV) non-deposition (time gap); (V) formation of the sandstone wedges; (VI) deposition of D31 on the E coast of GE (with glaciotectonic disturbance of the siltstone below) and GE inland; (VII) non-deposition (time gap); (VIII) formation of the new level of the sandstone wedges (Fig.6.17); (IX) non-deposition (time gap); (X) formation of the package between D31 and D32 (sandstone and conglomerate); (XI) deposition of D32; (XII) non-deposition (time gap); (XIII) formation of sandstone wedges at the top of D32; (XIV) non-deposition (time gap); (XV) deposition of the sandstone beds above D32 and below rhythmically laminated on the E coast of GE; (XVI) deposition of the rhythmically laminated siltstone on the E coast of GE; (XVII) non-deposition (time gap); (XVIII) formation of the sandstone wedges on the top of the rhythmically laminated; (XIX) non-deposition (time gap); (XX) deposition of the brown sandstone above laminated siltstone; (XXII) Erosional surface (Unconformity?); and (XXIII) deposition of the sandstone of Member 3. The wheeler diagram below (Fig.7.4) show all the events that mentioned above. Figure 7.4 shows that the number of preserved events is much more than can be seen in one outcrop. Both the number and succession of the events are much more than recorded in one sedimentary log at any section.
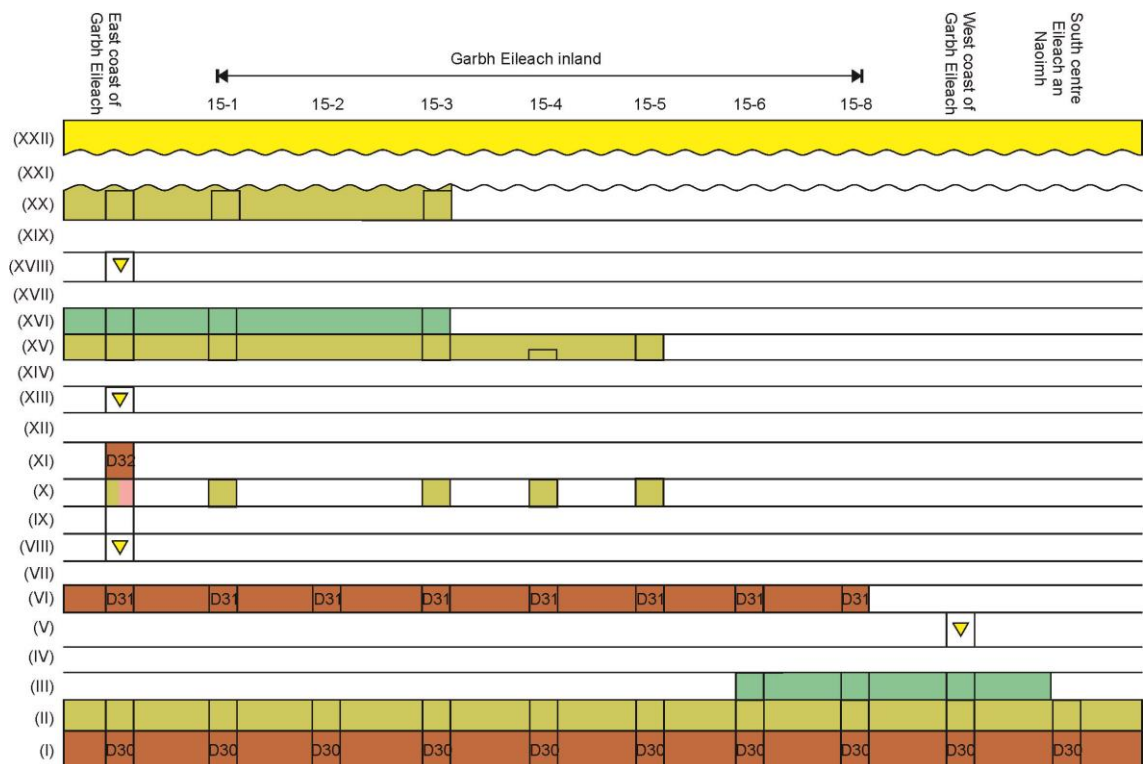
Figure 7.4: Wheeler diagram shows all chronological events from D30 up to the base of the M3.

Chapter 8 : Glacial sequence stratigraphy

8.1 Introduction

This chapter integrates fundamental aspects of the previous chapters, focussing on integrating all the sedimentological data and interpretations into a sequence stratigraphic context, with a critique of the available methodologies. Building on this, an analysis of ice-sheet cycles is attempted, drawing also on comparison to Neoproterozoic successions elsewhere. The PAF is discussed in terms of its relation to the Snowball Earth hypothesis, including a reflection of the extent to which the evidence in this thesis upholds this idea.

8.2 Glacial record of the PAF

This thesis has revealed evidence of multiple changes from glacial to periglacial to non-glacial conditions throughout the PAF (Chapters 3-7). The PAF (Fig.6.3) commences with diamictite beds (glacial condition) at the base, with a trend to thicker diamictite beds in the middle of the formation, and thinning trends toward the top. The complete succession, from the top part of the underlying GEF/Lossit Formation which shows a shallow marine setting, thus appears to record a sudden change to a glacial environment, then the ice-sheet maintained a stationary line in the middle of the succession, and retreated at the upper part of the sequence; and finally the Bonahaven Formation records another shallow marine environment. These changes (shallow marine-glacial-tidal-shallow marine) look like one cycle of glaciation. Another interesting observation within the succession is the abrupt change from the non-glacial to glacial which is represented by the sharp bases of the diamictite beds; while the changes from glacial to non-glacial are gradually in most stratigraphic levels, from diamictite beds (glacial), to sandstone wedges (periglacial), frost-shattered clasts (periglacial), and cryoturbation structures (periglacial), finally to interbeds (non-glacial).

Relationship between the PAF and the Snowball Earth hypothesis

The snowball Earth hypothesis predicts low latitude ice masses at sea level, and a prolonged period of glaciation in which the hydrological cycle was shut down (Allen and Etienne, 2008). If it is considered that the PAF is a Sturtian-age deposit, then the diamictites discussed in this thesis may record up to ca. 55 Myr of sedimentation based on geochronology of the Rapitan in Canada (Rooney et al., 2014). Originally, the Snowball Earth hypothesis posited that the diamictites represented outwash during the final retreat of ice sheets (Hoffman and Schrag, 2002). With careful study, however, the author has revealed that multiple sedimentation cycles exist, and which are discussed more fully below: these may potentially relate to a much more nuanced waxing and waning of the ice masses. The occurrence of multiple interbeds, multiple levels of periglacial phenomena, and the development of thick dolostones may support this idea. It should be noted that the carbonate beds shows microbial structures indicative of primary carbonate sedimentation (Fig.3.30, 3.72). Two hypotheses may explain their occurrence. The

first is that they are cap carbonates, recording discrete and major deglaciation episodes. If this is the case, more than one glacial episode may be represented in the PAF. In the second hypothesis, carbonate accumulated in response to ice oscillation during Sturtian, rather than major deglaciation events, when ice retreated far from the Garvellachs. The second hypothesis is more realistic; because there are two panglacial ice-age period (as mentioned before) within the Cryogenian and there are at least four carbonate levels related to the PAF: (i) GEF/Lossit Formation underlying the PAF; (ii) Main Dolomite lithofacies between GB and DB lithofacies associations; (iii) Upper Dolomite lithofacies association at the top of M1; and (iv) Bonahaven dolomite Formation overlying PAF. Moreover, there are three glacial periods during Neoproterozoic: Sturtian, Marinoan, and Gaskiers (Sawaki et al., 2010).

8.3 A sequence stratigraphic approach to the PAF

8.3.1 Overview

This topic is new in glaciology and in its initial stage of progress. There are controversies between scientists about terminology, drawing sedimentary logs, sequence boundaries, and principles that can be built for interpreting glacial sequence stratigraphy:

1) Terminology

As with other scientific approaches that are at an early stage, the terminology of glacial sequence stratigraphy has not yet distilled into a universal framework, meaning that alternative schemes and frameworks exist. In glacial sequence stratigraphy, a "sequence" records a single ice sheet oscillation cycle, but there are a handful of ways in which this can be defined. For instance, Pedersen (2012) used *glaciodynamic events* to define a sequence that hinged on the significance of soft-sediment deformation structures (predeformation-syndeposition-sedimentation-post deformation). By contrast, other authors followed the traditional terminology developed by classic sequence stratigraphic approaches, by using system tracts (ST) modified by the noun 'glacial' (Brookfield and Martini, 1999; Powell and Cooper, 2002; Lang et al., 2012; Busfield and Le Heron, 2014); for example, glacial erosion surface (GES). However, In the present study, a systems tract approach (Brookfield and Martini, 1999; Powell and Cooper, 2002; Lang et al., 2012; Busfield and Le Heron, 2014; Busfield and Le Heron, 2016), is favoured over the glaciodynamic framework of Pedersen (2012). This is because whilst spectacular soft-sediment deformation structures do occur in the PAF they do not recur with sufficient stratigraphic frequency for the author to develop a meaningful interpretation. Here, the systems tract terminology of Powell and Cooper (2002) is adopted. In this framework, a glacial sequence consists of a glacial advance system tract (GAST), a glacial retreat system tract (GRST), an ice-maximum system tract (GMaST), and an ice-minimum system tract (GMiST). Sequences and systems tracts are separated by key stratigraphic boundaries as follows. These include a glacial boundary surface (GBS), a glacial advance surface (GAS), and an iceberg-rafting termination surface (ITS). This approach has met with some success in its application to Sturtian successions in South Australia (Busfield and Le Heron, 2014), and thus there is a precedent which can be used and critiqued. It should be noted, however, that the approach is not without its drawbacks: Powell and Cooper (2002) specifically developed their glacial sequence

stratigraphic models to apply to temperate, mid latitude ice sheets. It is a moot point whether the ice sheet that deposited the PAF reflects these characteristics, but the approach can at least serve as the basis for a first-order analysis. A further rationale is that development of new terminology may serve to confuse the community, rather than to aid communication of interpretations.

2) Data collation and sedimentary logs styles

Surprisingly, whilst a group of geologists may make the same observations of a diamictite in the field, multiple possibilities exist with how these rocks are recorded and ultimately presented in log format. This is a far from trivial issue because the style of presentation of grain size data can have profound implications regarding inferences about ice dynamics. Owing to the fine-grained nature of some diamictite matrices, some authors prefer drawing beds with a low relief style, closely resembling siltstones or mudstone beds (Arnaud and Eyles, 2002; Busfield and Le Heron, 2014; Busfield and Le Heron, 2016). In stark contrast, other authors have represented essentially the same lithologies as muddy conglomerates, emphasising the large clasts within the matrix of diamictite beds (Lang et al., 2012; Pedersen, 2012). This variation in drawing styles shows exactly opposite changes in grain-size through the succession, and arguably highlights a major problem in the empirical study on ancient diamictites that needs to be overcome. For example, Pedersen (2012) drew the diamictite beds, in Fig.14 of his paper (Fig.8.1B), in high relief ("conglomerate style") that he used to argue for a coarsening-upward profile typical of his glaciodynamic sequence. Nevertheless, Busfield and Le Heron (2014) and Busfield and Le Heron (2016) drew the diamictite beds as a low relief ("mudstone style") in their sedimentary logs (Fig.8.1A and C); these observations then underpinned recognition of fining-upward successions. This inconsistency of approach may be one reason why sequence stratigraphy has not been more widely embraced by glacial sedimentologists, and highlights the need for a quantitative or semi-quantitative approach that is more rooted in empirical observation than subjectivity. These problems occur in spite of suitable classifications for poorly sorted rocks (e.g. Hambrey and Glasser (2012)).
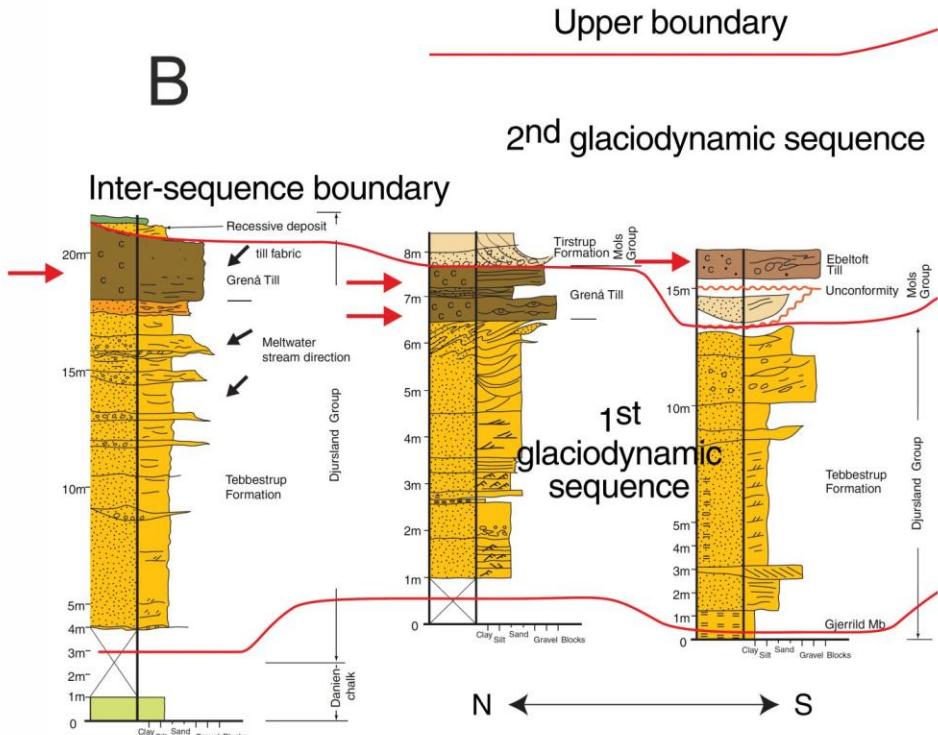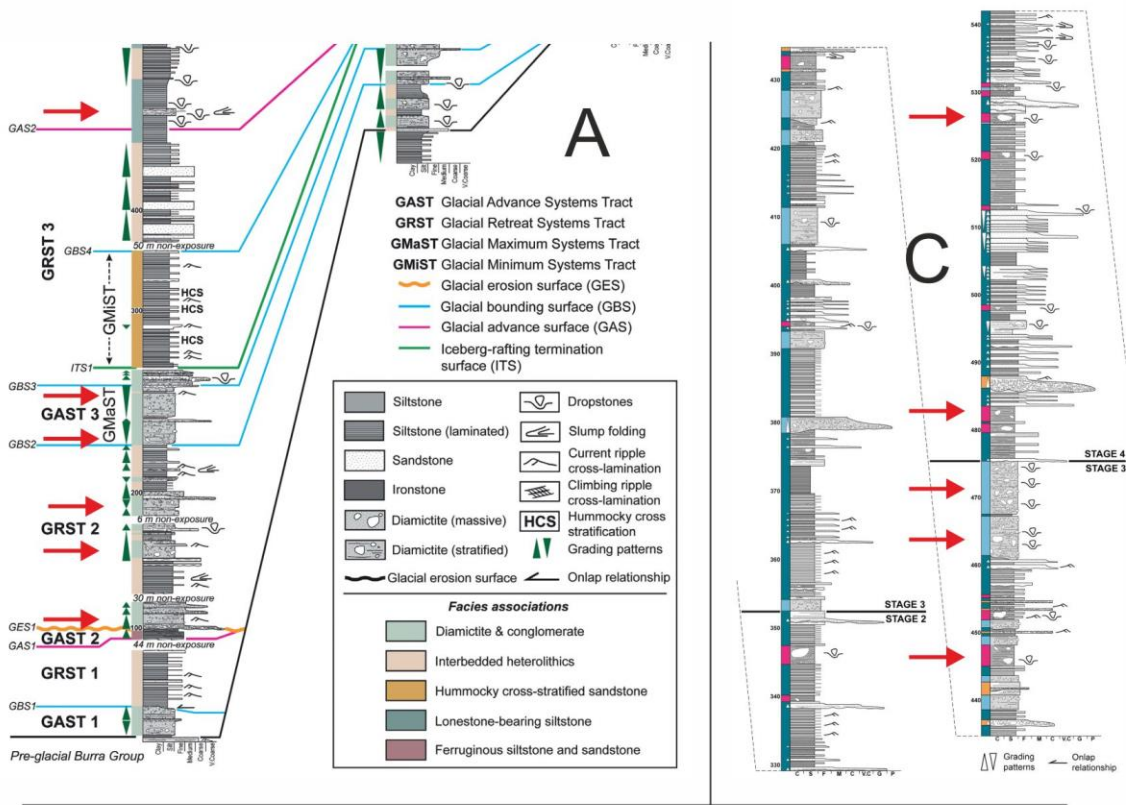
Figure 8.1: Different logs by various authors show inconsistency in drawing in diamictites (red arrows): (A) and (C) low relief; (B) high relief. (A and C) Part of Fig.2 and Fig.7 in Busfield and Le Heron (2016) and Busfield and Le Heron (2014), respectively. (B) Fig.14 in Pedersen (2012).

3) *Sequence boundaries*

In traditional sequence stratigraphy, sequence boundaries are recognised by significant erosional unconformities (on land) and their correlative conformities (in subaqueous settings); the development

of these boundaries is controlled by sea level changes (Catuneanu et al., 2011). By contrast, the sequence boundary in glacial successions can be recognised either by a glacial erosion surface (GES) or glacial bounding surface (Lang et al., 2012; Busfield and Le Heron, 2014). Note that these surfaces may not necessarily relate to sea level changes, and that ice sheet waxing will control the location of the GES in the succession, rather than sea level draw-down. This does not, however, preclude the two processes operating in tandem. Whilst relative sea level changes may determine the architecture of a sequence deposited in a non-glacial context, other factors contribute in a glacial setting. They include, but may not be restricted to, tectonic processes (glacio-isostatic depression and rebound) and changing sediment input points that reflect the subglacial plumbing (Fig.8.2b). The relative influence of these factors may be difficult to discern, but the advantage of the PAF for a sequence stratigraphic analysis is the stratigraphic repetition of similar facies which may imply a somewhat more simple set of controls, which the author explores below.

4) *Principles*

As might be inferred from above, and as noted by Brookfield and Martini (1999), the application of sequence stratigraphy in non-glacial (carbonate, clastic, and mixed marine and non-marine) sequences differs appreciably to that in glacial successions. These workers argued that the traditional (non-glacial) sequence stratigraphy is controlled by two key factors: (i) water depth, the water level relative to the depositional surface (which controls accommodation space) and (ii) input points, controlling the location of sediment delivery to the basin. In glacial successions, water depth and input points can vary independently of glacial isostacy, glacial eustacy and ice margin oscillation. According to the glaciodynamic model of Pedersen (2012), multiple, sequential phases of development of soft-sediment deformation structures exist. These include pre-deformation, syn-deformation, sedimentation, and post-deformation phases, in turn building up the "glaciodynamic sequence". A significant drawback to this approach is that understanding palaeo-ice sheet dynamics based on deformation alone requires full preservation of each deformation phase. Thus, the author considers this approach to be useful for particular basins that record full preservation, but it cannot claim to work as a general hypothesis.

In spite of all of the complexities above, sequence stratigraphy in glacial successions has much in common with "traditional" sequence stratigraphy in the sense that sea-level is the most important factor that affects facies changes at the largest scale. The author prefers to interpret the PAF on the basis of ice-sheet oscillation rather than following the sea-level change because it affects: (i) facies distribution (rock units); (ii) sediment input points by Brookfield and Martini (1999); (iii) glacial sequence events by Pedersen (2012); (iv) sea-level changes; and (v) glacial depression and rebound. Also, tectonism cannot be neglected, especially in tectonically active basin.

8.3.2 Alternative scenarios in glacial sequence stratigraphy

Fig. 8.2 contrasts sequence stratigraphic scenarios for non-glacial and glacial sequences. Considering the overall relative sea-level control on stratigraphic architecture (notwithstanding the issues of sediment input points shifting as noted above), the "traditional" sequence stratigraphic model (i.e. that developed

for non-glacial sequences) may apply well to glacial successions provided that the ice margin does not reach the sea (Fig.8.2b scenario A). If the ice maximum coincides with the development of a tidewater ice margin, however (i.e. it reaches the sea) (Fig.8.2b scenario B), or if an ice shelf develops (Fig.8.2b scenario C), the "traditional" model faces challenges. Ice-rafted debris becomes important in such settings, producing textures ranging from weakly stratified diamictite to mudstones with dispersed dropstones, depending on sediment concentrations within the ice shelf / at the ice margin. Thus, whereas the "traditional" sequence stratigraphic model predicts progressive basinal fining of sediment, interrupted by occasional mass flows, ice-rafting will produce comparatively coarser sediment in a comparable bathymetric setting. In Fig.8.2b scenario A, sea level and tectonism are key factors that affect lithofacies changes, whereas in 'Fig.8.2b, scenarios B and C' there are more factors affecting lithofacies changes: (i) sea level changes; (ii) tectonism; (iii) glacial depression and rebound; (iv) sediment input points. The most important factor of all is (v) ice-sheet position and its oscillation. Thus, ice-sheet position and mass-movements derived from rapid sedimentation rates are more important than sea level and tectonism in glacial sequence stratigraphy. This is the rationale for adopting the schemes of Powell and Cooper (2002) in this study rather than alternative frameworks.
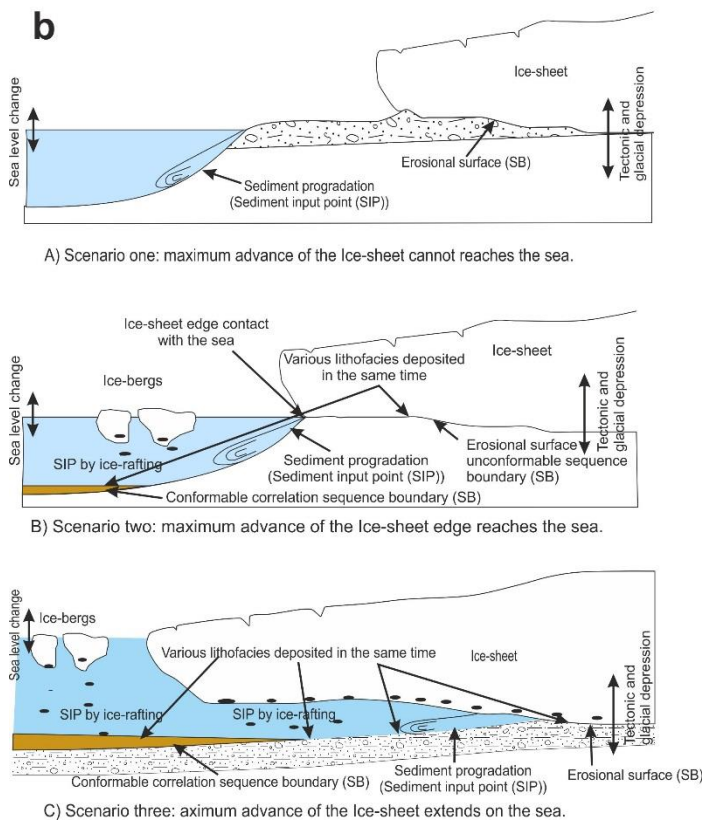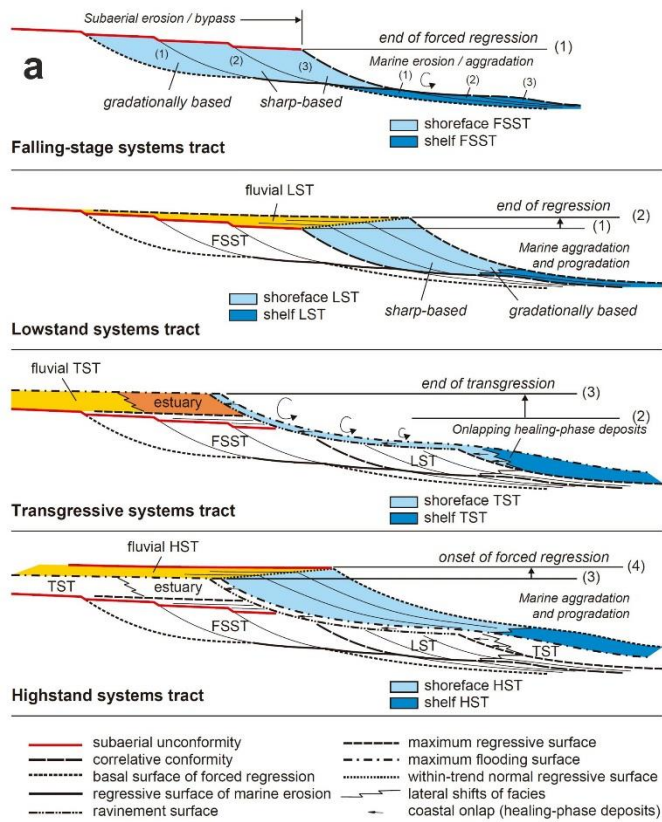
Figure 8.2: Comparison between traditional (carbonate and terrigenous) and glacial sequence stratigraphy. (A) Traditional sequence stratigraphy, an example of the detailed architecture of system tracts and stratigraphic surfaces in the transition zone between fluvial and shallow-marine environments (Catuneanu, 2006, Fig.5.6). (B) Schematic glacial sequence, explaining factors that affect facies changes compare with the traditional sequence stratigraphy.

8.4 Synthesis: interpretation of changing sedimentary environments

Our planet may have been frozen from pole to pole at least twice in Neoproterozoic time (Sturtian and Marinoan) according to the Snowball Earth hypothesis. Such 'snowball' conditions could suggest that the water cycle was completely inactive and shut down. Evidence for the advance and retreat of ice sheets, indicating a dynamic water cycle, might therefore conflict with the 'snowball' hypothesis (Eyles and Eyles, 1983). The Marinoan glacial succession on Svalbard has recently been studied from this point of view. Benn et al. (2015) analysed sedimentary rocks in the Wilsonbreen Formation, northern Svalbard. The formation was deposited within a broad, long-lived intracratonic basin when Svalbard was formed part of the eastern, tropical, part of Rodinia (Donnelly, 1963; Spencer, 1975) during the Marinoan ice age, about 650-630 Ma ago (Fairchild, 1985b; Cofaigh and Dowdeswell, 2001). Benn et al. (2015) concluded that the weathered zone at the base of the Wilsonbreen Formation represents frost-shattered clasts which formed in a subaerial environment when the sediment was exposed to the atmosphere during glaciation. This weathered zone was purported to represent a direct record of global glaciation. Analysis of oxygen and sulphur isotopes led Benn et al. (2015) to suggest three cycles of glacial advance and retreat over a short (perhaps 100,000 year) period.

The Port Askaig Formation is probably Sturtian (>700 Ma) (Brasier and Shields, 2000; Benn and Prave, 2006; McCay et al., 2006; Prave et al., 2009). The M3 succession described in this study is, however, analogous to the Svalbard succession in showing evidence of repeated glacial and interglacial cycles. The white sandstone-arenaceous diamictite lithofacies association, about 160 m thick, represents three cycles of glacial ice advance and retreat. The white sandstone lithofacies (Fig.8.3) records four episodes of deposition in a tidal sea. The diamictite facies shows three episodes of direct deposition from the ice. The lonestone-bearing facies records one episode of deposition from ice-bergs. The brown-weathered sandstone facies records one episode of dewatering or cryoturbation probably in a fluvioglacial setting in front of the ice body. In addition, sandstone wedges and frost shattered clasts record three episodes of periglacial conditions. Taken together, this evidence of changing environments in Member 3 records three cycles: glacial advance–melting–periglacial condition–marine transgression.

Now, if the 160m of the rock succession in M3 record three oscillations of ice-sheet advance and retreat; then how many cycles and oscillation can be expected in a formation that has a thickness about 1100m? Based on Ali et al. (2018: in press) there are evidence at least for 25 periglacial horizons in various stratigraphic level.
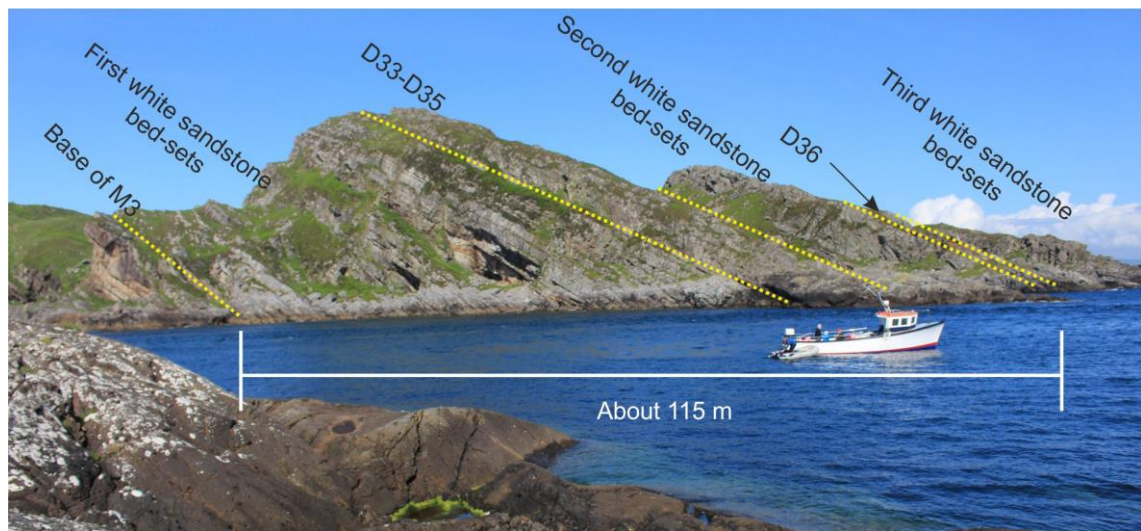
Figure 8.3: Panoramic view for the white sandstone and arenaceous diamictite facies on the W coast of GE Island.

8.5 Glacial cycles in the PAF

In previous chapters, particularly chapter six, the author discussed the data for at least five stratigraphic boundaries within the PAF succession, and at least three of them have been interpreted as unconformities. These boundaries represent major changes in lithology, geometry of the beds, clast patterns, and structures. These boundaries are interpreted as the products of glacial cycles (Fig.8.4).

An attempt to integrate the key sedimentological data in this thesis by geographic locality and to interpret them in terms of glacial cycles is shown on Fig. 8.4. Given the stratigraphic and spatial distribution of key phenomena such as emergent surfaces / periglacial structures, diamictite interbeds, and glaciotectonic structures, an "ice sheet oscillation curve" is presented (Fig.8.4). This shows that there were at least ten ice advance and retreat cycles in the area studied (Argyll). Further, minor ice-oscillation cycles are proposed between Garvellachs and Islay. These cycles are discussed below.

The lowermost cycle commences with the base of the formation and extends up to the top of the MD (Fig.8.4). D1-D12 are interpreted as an initial glacial advance systems tract (GAST 1), culminating in deposition of the GB. The lower contact of the MD is sharp in the BaT, and represents the first glacial erosional surface (GES 1) (Fig.3.17). The non-glacial MD with microbialites (Fig.3.30) represent the first glacial retreat system tract1 (GRST 1) (Fig.8.4).

Above these rocks, the second cycle starts with GAST 2 at the base of the DB. The sedimentology of this GAST includes the deposits of lakelets bearing dumpstones and dropstones, modified glaciotectonically to produce galaxy structures, sheared clasts, and intense folding (section 4.4e). This systems tract extends to the base of the Upper Dolomite on the E coast of GE. Upsection, GES 2 truncates D16-D18 (section 4.5g and Fig.6.16) from E coast of GE to W coast of EaN. The UD represents GRST 2.

GAST 3 represents the onset of the third cycle, and is represented by D19-D26 (Fig.8.4). At the top of D26, there is a continuous bed recording sandstone cryoturbation. This glacial boundary surface (GBS)

forms the basal surface of GRST 3, with its sandstone wedges with frost-shattered clasts representing a periglacial environment (Fig.4.1, 8.4).

Regarding the fourth cycle, the base of D27 up to the top of the D32 (Fig.8.4) represents GAST 4. Several sharp based diamictite beds characterise this interval, together with evidence for glaciotectonism, culminating in GES 3 (Fig.6.17). The dropstone-bearing, rhythmically laminated deposits above, together with the tidal sandstones, represent GRST 4 (Fig.8.4, 6.17).

The fifth cycle starts with the base of D33 and extends up to the top of the sandstone bed above D38 (Fig.8.4). GAST 5 is represented by diamictite beds, and the GBS is represented by frost-shattered clasts, sandstone wedges penetrating diamictite beds from the top. GRST 5 corresponds to a tidal sandstone between each diamictite bed-set (Fig.8.3). Finally, the uppermost cycle is defined by the base of D39 to the top of D44 (Fig.8.4). Similarly to cycle five, the diamictite bed-sets record GAST 6; the sandstone wedge-bearing horizons define a GBS. The sandstone bed-sets represent GRST 6.

There is evidence for more than the six cycles mentioned above. However, the data from D44 to the base of the Bonahaven Dolomite Formation do not reveal systems tracts to an adequate degree of resolution. For this reason, no further sequence stratigraphic interpretation is attempted for the uppermost rocks. Nonetheless, the six major cycles discussed above are also divisible into finer-scale sub-cycles. For instance, cycle five includes at least three horizons of sandstone wedges, three horizons of frost-shattered clasts, three diamictite bed-sets, and four sandstone bed-sets. Thus, it is plausible that at least three higher frequency ice margin oscillation events occur within this larger-scale cycle. It is interesting to note that the thickness of the bed-sets, features, and succession are similar to the Wilsonbreen Formation of Svalbard where an orbital control on sedimentation has been posited (Benn et al., 2015).

If glacial cycles controlled the tempo of sedimentation in the PAF, what was the direction of sediment delivery to the basin? Spencer (1971) proposed that the PAF was deposited on a regionally flat area, with no discernible palaeoslope, owing to the absence of any trend within his palaeocurrent dataset. Reappraising this data, the present author considers that this interpretation is invalid because the data were not adequately discriminated or separated with regard to types of sedimentary structure (i.e. ripples vs cross-beds) on stratigraphic position. Here, the data are replotted (Fig.8.5). Indeed, re-plotting all 364 palaeocurrent data from Spencer (1971) reveals several interesting trends. In Fig.8.5 all rose diagrams from ripple marks represent unidirectional ripples, except the two diagrams from D1-D13 and D13-D19 which represent wave ripples.

In summary, a range of palaeocurrent flow directions is recognised in the lower portion of the PAF, with flows toward the NE-SW, NE-SW and NW-SE, and SW and SE directions respectively from the base of the formation. Flows toward the NE are recognised in each of these. The upper portion of the formation (upper three rose diagrams in Fig.8.5) show a dominant NE-ward palaeocurrent dispersal. Thus, a NE-

directed palaeoslope (Fig. 8.5) is inferred. It is thus proposed that this slope influenced the behaviour of ice sheets, with those areas to the SW lying close to the sediment source (i.e. glacier-ward).
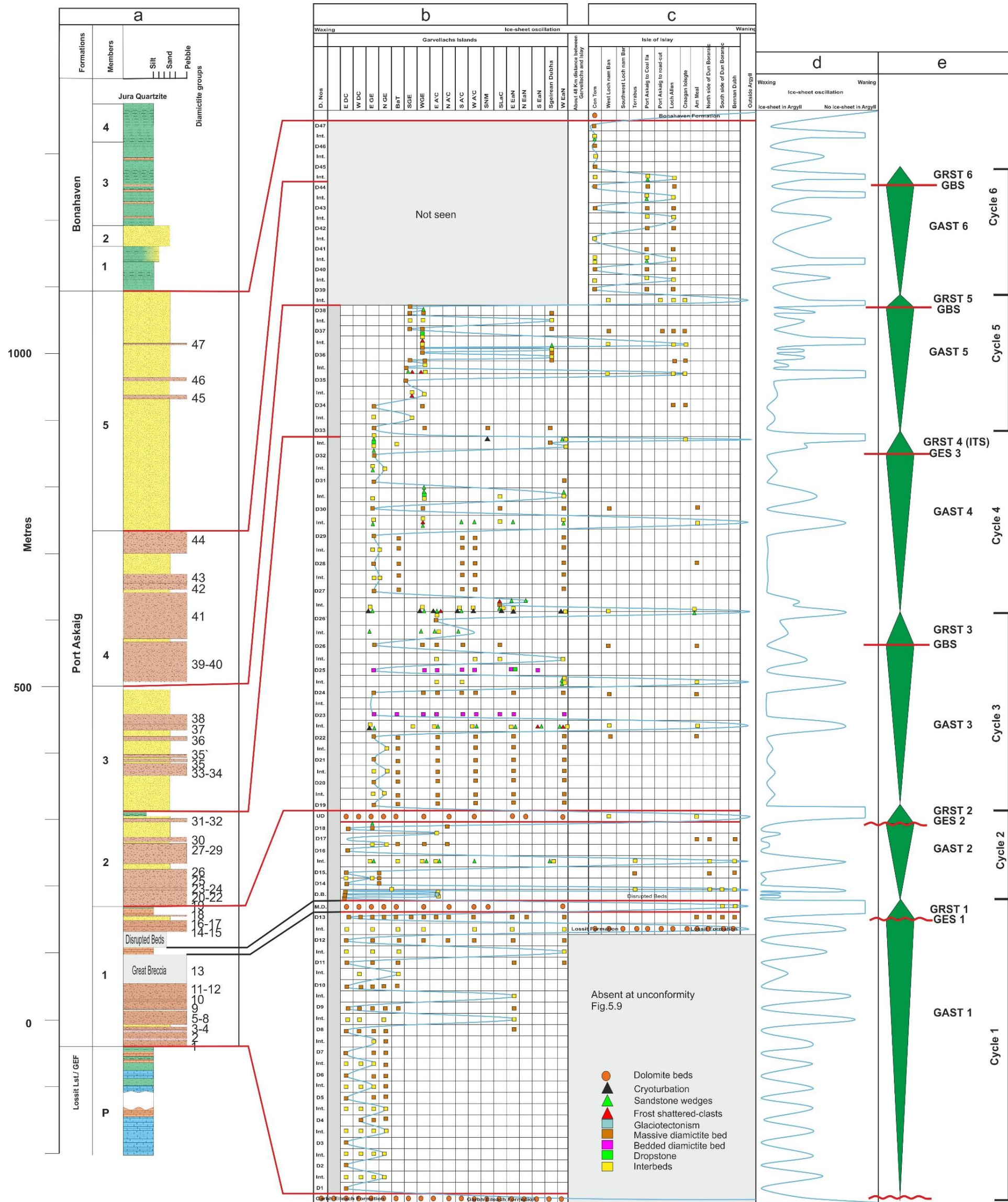
Figure 8.4: Ice-sheet cycles/oscillations based on various parameters and different localities on the Garvellachs and Islay: (a) composite stratigraphic column for Garvellachs and Islay. (b) Environmental interpretation of outcrops on Garvellachs. (c) Environmental interpretation of outcrops on Islay. (d) Ice-sheet oscillation curve. Numbers of the ice-sheet oscillation curve are when the ice-sheet was out of the Argyll area. (e) Cycles of glacial advance (GAST) and retreat (GRST).
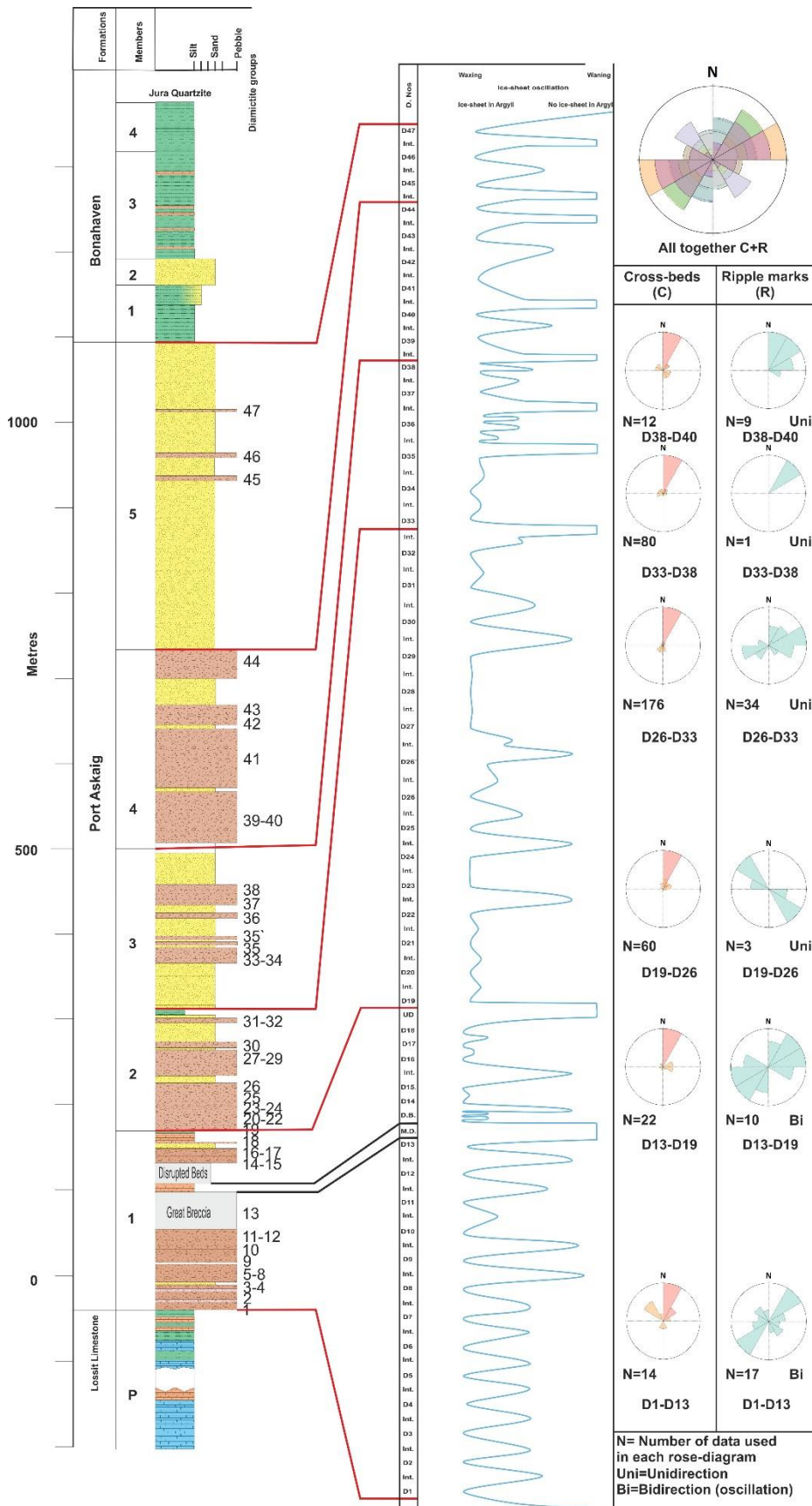
Figure 8.5: Palaeocurrent direction throughout the PAF succession up to the sandstone above D38. The green rose-diagrams represent ripple marks, and the orange and pink colours show cross-stratification. The colourful rose-diagram at the top represent the total measurements (cross-beds and ripple marks) which used for plotting these data.

262

Chapter 9 : Conclusion and recommendation

9.1 Summary and Perspectives

- The Port Askaig Formation was deposited under the direct influence of highly dynamic, oscillating ice sheets. There were three climatically controlled sedimentation types. Intervals of diamictite sedimentation (<u>glacial</u>) were punctuated by time periods where ice sheet influence was far less obvious, or even entirely absent (<u>non-glacial</u>); many intervening episodes record <u>periglacial</u> conditions.

- Detailed facies analysis of the <u>glacial</u> episodes reveals that the majority of the diamictite beds were deposited by grounded ice, although deposition from floating ice and from mass flow processes was locally important. Diamictites deposited by these processes show similarities, but a robust assemblage of features allows them to be assigned to each of the processes. The thesis builds on earlier recognition of glaciotectonic structures in the PAF (Benn and Prave, 2006) by proposing the widespread occurrence of glaciotectonic structures in at least three horizons of the PAF. The co-occurrence of galaxy structures, sheared clasts, folds, dumpstone, and dropstone has been used to differentiate diamictites deposited beneath floating ice. Collectively, the entire assemblage of structures, and each type of diamictite, is broadly indicative of ice-marginal processes throughout most of the PAF.

- The <u>non-glacial</u> interbeds (conglomerates, sandstones, siltstones, and dolomite) shed considerable new light on the depositional environments of their encasing diamictites, and enable the depositional model for them to be greatly refined. This author observes that fluvial channels, tidal deposits, lakelets and marine sediments are recognised. Some of these intervals were associated with the deposition of carbonates including the Main Dolomite and the Upper Dolomite. Intervals of carbonate sedimentation are tentatively allied to glacial minima, with climatic conditions permissive of microbalite sedimentation. Microbalites are recorded for the first time within the PAF succession.

- Many horizons show evidence of <u>periglacial</u> conditions, for example, frost-shattered clasts, sandstone wedges, and cryoturbations, often at the same horizons. These features point to subaerial conditions.

- Climate cycles (glacial to periglacial to non-glacial) of unspecified duration occur in abundance within the PAF when the diamictites and the interbeds are considered together. Both in the chapters of this thesis, and in the paper (Ali et al., 2018: in press) deriving directly from it, we recognise abundant switches from glacial to non-glacial environments throughout the

263

stratigraphic column. Evidence of periglacial environments occurs at 25 horizons. The evidence includes sandstone wedges (at 23 levels), cryoturbation (at 3 levels) and frost-shattered clasts (at 6 levels). The succession in the PAF records 28 glacial, 25 periglacial and 23 non-glacial episodes, thus representing a total of 76 climatically related depositional episodes.

- Developing the concept of climatically-driven depositional episodes, this thesis has also delivered the first attempt to analyse the PAF using sequence stratigraphy. Built using the foundations of a detailed facies analysis, multiple glacial advance systems tracts and glacial retreat systems tracts are proposed. Moreover, integration of the key depositional indicators allows an "ice oscillation curve" to be produced for the first time. The ice sheet that supplied sediment to the basin clearly expressed cyclicity / oscillation. The driving force behind this oscillation is not yet known.

- The recognition of the climatically-related depositional episodes (76) within the succession of the PAF does not fit well with the Snowball Earth hypothesis, because that hypothesis predicts that the hydrological cycle has been shut down.

9.2 Gaps in knowledge and future research

- Spencer (1966, 1971) utilized clast counting for correlation between diamictite beds in different localities on Garvellachs and Islay. Also, this study follows Spencer's methodology used for clast counting in addition to matrix lithology. However, using heavy mineral groups for correlation would add more accuracy in the future.

- The author call for a conference to discuss: terminology, drawing sedimentary logs, sequence boundaries, and the principles of glacial sequence stratigraphy. Because inconsistency in these topics has caused confusion for me.

- The geological age and duration of the PAF are not well known. Chemostratigraphic data suggest it is Sturtian, but there are no radiometric data to confirm this. This also means that the duration of the 1100 m of PAF strata is not known. Progress to increase the knowledge about the age and duration is really worthwhile.

- The underlying Islay and overlying Bonahaven Formations were deposited in environments close to sea level. The exceptional total thickness (~1100 m) of the PAF must be close to the amount of the tectonic subsidence during its deposition. Also, the Dalradian succession itself is enormously thick. It is difficult to understand these great thicknesses. What was the tectonic

setting of the basin? This makes comparing the PAF with the other Cryogenian glacial formations problematical.

- Considering that the top and bottom contacts of the PAF represent the same climatic changes that were responsible for other Sturtian glacial units, then is the unique character of the PAF due to what, for Neoproterozoic glacial deposits, was a fortuitous tectonic context?

- The last three topics need further study; to determine the rate of subsidence, and the duration of the PAF, so as to compare it with other Cryogenian glacial formations.

References

Aber, J. S., Croot, D., and Fenton, M. M., 1989, Glaciotectonic Landforms and Structures Kluwer Academic Publishers, Dordrecht.

Ainsworth, R. B., Hasiotis, S. T., Amos, K. J., Krapf, C. B., Payenberg, T. H., Sandstrom, M. L., Vakarelov, B. K., and Lang, S. C., 2012, Tidal signatures in an intracratonic playa lake: Geology, v. 40, no. 7, p. 607-610.

Alfaro, P., Moretti, M., and Soria, J., 1997, Soft-sediment deformation structures induced by earthquakes (seismites) in pliocene lacustrine deposits (Guadix-Baza Basin. Central Betic Cordillera): Eclogae Geologicae Helvetiae, v. 90, no. 3, p. 531-540.

Ali, D. O., Spencer, A. M., Fairchild, I. J., Chew, K. J., Anderton, R., Levell, B. K., Hambrey, M. J., Dove, D., and Le Heron, D. P., 2018, Indicators of relative completeness of the glacial record of the Port Askaig Formation, Garvellach Islands, Scotland: Precambrian Research.

Allen, J., 1980, Sand waves: a model of origin and internal structure: Sedimentary geology, v. 26, no. 4, p. 281-328.

-, 1982, Sedimentary structures, their character and physical basis, Elsevier.

Allen, P. A., and Etienne, J. L., 2008, Sedimentary challenge to snowball Earth: Nature Geoscience, v. 1, no. 12, p. 817-825.

Anderton, R., 1979, Slopes, submarine fans, and syn-depositional faults: sedimentology of parts of the Middle and Upper Dalradian in the SW Highlands of Scotland: Geological Society, London, Special Publications, v. 8, no. 1, p. 483-488.

Anderton, R., 1985, Sedimentation and tectonics in the Scottish Dalradian: Scottish Journal of Geology, v. 21, no. 4, p. 407-436.

Anderton, R., 1988, Dalradian slides and basin development: a radical interpretation of stratigraphy and structure in the SW and Central Highlands of Scotland: Journal of the Geological Society, v. 145, no. 4, p. 669-678.

Armstrong, H., and Brasier, M., 2013, Microfossils, John Wiley & Sons.

Arnaud, E., 2004, Giant cross-beds in the Neoproterozoic Port Askaig Formation, Scotland: implications for snowball Earth: Sedimentary Geology, v. 165, no. 1, p. 155-174.

-, 2012, The paleoclimatic significance of deformation structures in Neoproterozoic successions: Sedimentary Geology, v. 243, p. 33-56.

Arnaud, E., and Etienne, J. L., 2011, Recognition of glacial influence in Neoproterozoic sedimentary successions: Geological Society, London, Memoirs, v. 36, no. 1, p. 39-50.

Arnaud, E., and Eyles, C. H., 2002, Catastrophic mass failure of a Neoproterozoic glacially influenced continental margin, the Great Breccia, Port Askaig Formation, Scotland: Sedimentary Geology, v. 151, no. 3, p. 313-333.

-, 2006, Neoproterozoic environmental change recorded in the Port Askaig Formation, Scotland: Climatic vs tectonic controls: Sedimentary Geology, v. 183, no. 1, p. 99-124.

Arnaud, E., and Fairchild, I. J., 2011, The Port Askaig Formation, Dalradian Supergroup, Scotland: Geological Society, London, Memoirs, v. 36, no. 1, p. 635-642.

Arnaud, E., Halverson, G. P., and Shields-Zhou, G., The geological record of Neoproterozoic glaciations2011, Geological Society of London.

Ashley, G. M., 1990, Classification of large-scale subaqueous bedforms: a new look at an old problem-SEPM bedforms and bedding structures: Journal of Sedimentary Research, v. 60, no. 1.

Banner, F. T., and Lord, A. R., 1982, Aspects of micropalaeontology: papers presented to Professor Tom Barnard, Unwin Hyman.

Benn, D., and Evans, D., 2010, Glaciers and Glaciation. 802 pp: Hodder Education, London.

Benn, D. I., and Evans, D. J., 1996, The interpretation and classification of subglacially-deformed materials: Quaternary Science Reviews, v. 15, no. 1, p. 23-52.

Benn, D. I., Le Hir, G., Bao, H., Donnadieu, Y., Dumas, C., Fleming, E. J., Hambrey, M. J., McMillan, E. A., Petronis, M. S., and Ramstein, G., 2015, Orbitally forced ice sheet fluctuations during the Marinoan Snowball Earth glaciation: Nature Geoscience.

Benn, D. I., and Prave, A. R., 2006, Subglacial and proglacial glacitectonic deformation in the Neoproterozoic Port Askaig Formation, Scotland: Geomorphology, v. 75, no. 1, p. 266-280.

Ber, A., 2007, Glaciotectonism. Developments in Quaternary Science, Elsevier Science & Technology.

Berne, S., Lericolais, G., Marsset, T., Bourillet, J. F., and De Batist, M., 1998, Erosional offshore sand ridges and lowstand shorefaces: examples from tide-and wave-dominated environments of France: Journal of Sedimentary Research, v. 68, no. 4.

Boggs, S. J., 2014, Principles of sedimentology and stratigraphy, Pearson.

Bonnand, P., James, R., Parkinson, I., Connelly, D., and Fairchild, I., 2013, The chromium isotopic composition of seawater and marine carbonates: Earth and Planetary Science Letters, v. 382, p. 10-20.

Boulton, G., and Hindmarsh, R., 1987, Sediment deformation beneath glaciers: rheology and geological consequences: Journal of Geophysical Research: Solid Earth, v. 92, no. B9, p. 9059-9082.

Brasier, M., and Shields, G., 2000, Neoproterozoic chemostratigraphy and correlation of the Port Askaig glaciation, Dalradian Supergroup of Scotland: Journal of the Geological Society, v. 157, no. 5, p. 909-914.

Brookfield, M., 1977, The origin of bounding surfaces in ancient aeolian sandstones: Sedimentology, v. 24, no. 3, p. 303-332.

Brookfield, M., and Martini, I., 1999, Facies architecture and sequence stratigraphy in glacially influenced basins: basic problems and water-level/glacier input-point controls (with an example from the Quaternary of Ontario, Canada): Sedimentary geology, v. 123, no. 3, p. 183-197.

Busfield, M., and Le Heron, D., 2014, Sequencing the Sturtian icehouse: dynamic ice behaviour in South Australia: Journal of the Geological Society, v. 171, no. 3, p. 443-456.

Busfield, M. E., and Le Heron, D. P., 2013, Glacitectonic deformation in the Chuos Formation of northern Namibia: implications for Neoproterozoic ice dynamics: Proceedings of the Geologists' Association, v. 124, p. 778-789.

Busfield, M. E., and Le Heron, D. P., 2016, A Neoproterozoic ice advance sequence, Sperry Wash, California: Sedimentology, v. 63, no. 2, p. 307-330.

Calver, C., Crowley, J., Wingate, M., Evans, D., Raub, T., and Schmitz, M., 2013, Globally synchronous Marinoan deglaciation indicated by U-Pb geochronology of the Cottons Breccia, Tasmania, Australia: Geology, v. 41, no. 10, p. 1127-1130.

Catuneanu, O., 2006, Principles of sequence stratigraphy, Elsevier.

Catuneanu, O., Galloway, W. E., Kendall, C. G. S. C., Miall, A. D., Posamentier, H. W., Strasser, A., and Tucker, M. E., 2011, Sequence stratigraphy: methodology and nomenclature: Newsletters on stratigraphy, v. 44, no. 3, p. 173-245.

Chen, J., Chough, S. K., Chun, S. S., and Han, Z., 2009, Limestone pseudoconglomerates in the Late Cambrian Gushan and Chaomidian Formations (Shandong Province, China): soft-sediment deformation induced by storm-wave loading: Sedimentology, v. 56, no. 4, p. 1174-1195.

Chough, S., Kwon, Y., Choi, D., and Lee, D., 2001, Autoconglomeration of limestone: Geosciences Journal, v. 5, no. 2, p. 159-164.

Cofaigh, C. Ó., and Dowdeswell, J. A., 2001, Laminated sediments in glacimarine environments: diagnostic criteria for their interpretation: Quaternary Science Reviews, v. 20, no. 13, p. 1411-1436.

Coleman, J. M., 1969, Brahmaputra River: channel processes and sedimentation: Sedimentary Geology, v. 3, no. 2, p. 129-239.

Cowan, E., Cai, J., Powell, R., Seramur, K., and Spurgeon, V., 1998, Modern tidal rhythmites deposited in a deep-water estuary: Geo-Marine Letters, v. 18, no. 1, p. 40-48.

Cox, G. M., Halverson, G. P., Poirier, A., Le Heron, D., Strauss, J. V., and Stevenson, R., 2016, A model for Cryogenian iron formation: Earth and Planetary Science Letters, v. 433, p. 280-292.

D'hondt, S., Jørgensen, B. B., Miller, D. J., Batzke, A., Blake, R., Cragg, B. A., Cypionka, H., Dickens, G. R., Ferdelman, T., and Hinrichs, K.-U., 2004, Distributions of microbial activities in deep subseafloor sediments: Science, v. 306, no. 5705, p. 2216-2221.

Domack, E. W., and Hoffman, P. F., 2011, An ice grounding-line wedge from the Ghaub glaciation (635 Ma) on the distal foreslope of the Otavi carbonate platform, Namibia, and its bearing on the snowball Earth hypothesis: Geological Society of America Bulletin, v. 123, no. 7-8, p. 1448-1477.

Donnelly, T. W., 1963, Genesis of albite in early orogenic volcanic rocks: American Journal of Science, v. 261, no. 10, p. 957-972.

Downie, C., 1971, A palynological investigation of the Dalradian rocks of Scotland, HM Stationery Office.

Druzhinina, O., Bitinas, A., Molodkov, A., and Kolesnik, T., 2017, Palaeoseismic deformations in the Eastern Baltic region (Kaliningrad District of Russia): Estonian Journal of Earth Sciences, v. 66, no. 3.

Dunn, P., Thomson, B., and Rankama, K., 1971, Late Pre-Cambrian glaciation in Australia as a stratigraphic boundary: Nature, v. 231, no. 5304, p. 498-502.

Eriksson, P. G., Condie, K., Tirsgaard, H., Mueller, W., Altermann, W., Miall, A., Aspler, L., Catuneanu, O., and Chiarenzelli, J., 1998, Precambrian clastic sedimentation systems: Sedimentary Geology, v. 120, no. 1, p. 5-53.

Eyles, C., Eyles, N., and Miall, A., 1985, Models of glaciomarine sedimentation and their application to the interpretation of ancient glacial sequences: Palaeogeography, Palaeoclimatology, Palaeoecology, v. 51, no. 1, p. 15-84.

Eyles, C. H., 1988, Glacially-and tidally-influenced shallow marine sedimentation of the Late Precambrian Port Askaig Formation, Scotland: Palaeogeography, palaeoclimatology, palaeoecology, v. 68, no. 1, p. 1-25.

Eyles, C. H., and Eyles, N., 1983, Glaciomarine model for upper Precambrian diamictites of the Port Askaig Formation, Scotland: Geology, v. 11, no. 12, p. 692-696.

Eyles, N., and Clark, B. M., 1985, Gravity-induced soft-sediment deformation in glaciomarine sequences of the Upper Proterozoic Port Askaig Formation, Scotland: Sedimentology, v. 32, no. 6, p. 789-814.

Eyles, N., and Januszczak, N., 2004, 'Zipper-rift': a tectonic model for Neoproterozoic glaciations during the breakup of Rodinia after 750 Ma: Earth-Science Reviews, v. 65, no. 1, p. 1-73.

Fairchild, I. J., 1991, Origins of carbonate in Neoproterozoic stromatolites and the identification of modern analogues: Precambrian Research, v. 53, no. 3-4, p. 281-299.

Fairchild, I. J., Fleming, E. J., Bao, H., Benn, D. I., Boomer, I., Dublyansky, Y. V., Halverson, G. P., Hambrey, M. J., Hendy, C., and McMillan, E. A., 2016, Continental carbonate facies of a Neoproterozoic panglaciation, north-east Svalbard: Sedimentology.

Fairchild, I. J., and Kennedy, M. J., 2007, Neoproterozoic glaciation in the Earth System: Journal of the Geological Society, v. 164, no. 5, p. 895-921.

Fairchild, I. J., Spencer, A. M., Ali, D. O., Anderson, R. P., Anderton, R., Boomer, I., Dove, D., Evans, J. D., Hambrey, M. J., and Howe, J., 2018, Tonian-Cryogenian boundary sections of Argyll, Scotland: Precambrian Research.

Feldmann, M., and McKenzie, J. A., 1998, Stromatolite-thrombolite associations in a modern environment, Lee Stocking Island, Bahamas: Palaios, v. 13, no. 2, p. 201-212.

Gilbert, R., 1983, Sedimentary processes of Canadian Arctic fjords: Sedimentary geology, v. 36, no. 2, p. 147-175.

Gingras, M. K., Pemberton, S. G., Muelenbachs, K., and Machel, H., 2004, Conceptual models for burrow-related, selective dolomitization with textural and isotopic evidence from the Tyndall Stone, Canada: Geobiology, v. 2, no. 1, p. 21-30.

Graham, C., and Bradbury, H., 1981, Cambrian and late Precambrian basaltic igneous activity in the Scottish Dalradian: a review: Geological Magazine, v. 118, no. 01, p. 27-37.

Halverson, G. P., Dudás, F. Ö., Maloof, A. C., and Bowring, S. A., 2007, Evolution of the 87 Sr/86 Sr composition of Neoproterozoic seawater: Palaeogeography, Palaeoclimatology, Palaeoecology, v. 256, no. 3, p. 103-129.

Hambrey, M. J., and Alean, J. C., 2016, Color Atlas of Glacial Phenomena, Crc Press.

Hambrey, M. J., and Glasser, N. F., 2012, Discriminating glacier thermal and dynamic regimes in the sedimentary record: Sedimentary Geology, v. 251, p. 1-33.

Hambrey, M. J., and Harland, W. B., 1981, Earth's pre-Pleistocene glacial record, Cambridge University Press.

Harland, W., 1964, Evidence of Late Precambrian glaciation and its significance: Problems in Palaeoclimatology, v. 705, p. 119-149.

Harris, A., and Mendum, J., 1975, The Dalradian Supergroup in Scotland, Shetland and Ireland.

Harris, C., and Murton, J. B., 2005, Interactions between glaciers and permafrost: an introduction: Geological Society, London, Special Publications, v. 242, no. 1, p. 1-9.

Hart, J. K., and Boulton, G. S., 1991, The interrelation of glaciotectonic and glaciodepositional processes within the glacial environment: Quaternary Science Reviews, v. 10, no. 4, p. 335-350.

Helwig, J., 1970, Slump folds and early structures, northeastern Newfoundland Appalachians: The Journal of Geology, v. 78, no. 2, p. 172-187.

Hoffman, P. F., Kaufman, A. J., Halverson, G. P., and Schrag, D. P., 1998, A Neoproterozoic snowball earth: Science, v. 281, no. 5381, p. 1342-1346.

Hoffman, P. F., and Schrag, D. P., 2002, The snowball Earth hypothesis: testing the limits of global change: Terra nova, v. 14, no. 3, p. 129-155.

Hsü, K. J., 1975, Catastrophic debris streams (sturzstroms) generated by rockfalls: GSA Bulletin, v. 86, no. 1, p. 129-140.

-, 2013, Physics of sedimentology: textbook and reference, Springer Science & Business Media.

Hunter, R. E., 1977, Basic types of stratification in small eolian dunes: Sedimentology, v. 24, no. 3, p. 361-387.

Ielpi, A., and Rainbird, R. H., 2016, Highly Variable Precambrian Fluvial Style Recorded In the Nelson Head Formation of Brock Inlier (Northwest Territories, Canada): Journal of Sedimentary Research, v. 86, no. 3, p. 199-216.

Ikehara, K., 1998, Sequence stratigraphy of tidal sand bodies in the Bungo Channel, southwest Japan: Sedimentary geology, v. 122, no. 1, p. 233-244.

Johnson, H., and Baldwin, C., 1996, Sedimentary environments: Processes, facies, and stratigraphy: Shallow Clastic Seas, pg, p. 232-280.

Johnson, J., and Grotzinger, J., 2006, Affect of sedimentation on stromatolite reef growth and morphology, Ediacaran Omkyk Member (Nama Group), Namibia: South African Journal of Geology, v. 109, no. 1-2, p. 87-96.

Kamp, P. J., Harmsen, F. J., Nelson, C. S., and Boyle, S. F., 1988, Barnacle-dominated limestone with giant cross-beds in a non-tropical, tide-swept, Pliocene forearc seaway, Hawke's Bay, New Zealand: Sedimentary geology, v. 60, no. 1, p. 173-195.

Kaufman, A. J., Knoll, A. H., and Narbonne, G. M., 1997, Isotopes, ice ages, and terminal Proterozoic earth history: Proceedings of the National Academy of Sciences, v. 94, no. 13, p. 6600-6605.

Kennard, J. M., and James, N. P., 1986, Thrombolites and stromatolites: two distinct types of microbial structures: Palaios, p. 492-503.

Kennedy, M. J., Runnegar, B., Prave, A. R., Hoffmann, K.-H., and Arthur, M. A., 1998, Two or four Neoproterozoic glaciations?: Geology, v. 26, no. 12, p. 1059-1063.

Kilburn, C., Shackleton, R., and Pitcher, W., 1965, The stratigraphy and origin of the Portaskaig Boulder Bed series (Dalradian): Geological Journal, v. 4, no. 2, p. 343-360.

Kirschvink, J. L., 1992, Late Proterozoic low-latitude global glaciation: the snowball Earth.

Klint, K. E. S., and Pedersen, S. A. S., 1995, The Hanklit glaciotectonic thrust fault complex, Mors, Denmark, Danmarks Geologiske Undersøgelse, v. 35.

Knight, J., 2016, Subglacial processes from drumlins in Clew Bay, western Ireland: Earth Surface Processes and Landforms, v. 41, no. 2, p. 277-288.

Kulling, O., 1934, Part XI. The» Hecla Hoek Formation» round Hinlopenstredet: NW North-East Land and NE West Spitsbergen: Geografiska Annaler, v. 16, no. 4, p. 161-254.

Lang, J., Dixon, R. J., Le Heron, D. P., and Winsemann, J., 2012, Depositional architecture and sequence stratigraphic correlation of Upper Ordovician glaciogenic deposits, Illizi Basin, Algeria: Geological Society, London, Special Publications, v. 368, no. 1, p. 293-317.

Le Ber, E., Le Heron, D. P., Winterleitner, G., Bosence, D. W., Vining, B. A., and Kamona, F., 2013, Microbialite recovery in the aftermath of the Sturtian glaciation: Insights from the Rasthof Formation, Namibia: Sedimentary Geology, v. 294, p. 1-12.

Le Heron, D., 2015, The significance of ice-rafted debris in Sturtian glacial successions: Sedimentary Geology, v. 322, p. 19-33.

Le Heron, D. P., 2012, The Cryogenian record of glaciation and deglaciation in South Australia: Sedimentary Geology, v. 243, p. 57-69.

Le Heron, D. P., and Busfield, M. E., 2016, Pulsed iceberg delivery driven by Sturtian ice sheet dynamics: an example from Death Valley, California: Sedimentology, v. 63, no. 2, p. 331-349.

Le Heron, D. P., Busfield, M. E., and Kamona, F., 2013, An interglacial on snowball Earth? Dynamic ice behaviour revealed in the Chuos Formation, Namibia: Sedimentology, v. 60, no. 2, p. 411-427.

Le Heron, D. P., Busfield, M. E., and Prave, A. R., 2014, Neoproterozoic ice sheets and olistoliths: multiple glacial cycles in the Kingston Peak Formation, California: Journal of the Geological Society, v. 171, no. 4, p. 525-538.

Lechte, M. A., and Wallace, M. W., 2015, Sedimentary and tectonic history of the Holowilena Ironstone, a Neoproterozoic iron formation in South Australia: Sedimentary Geology, v. 329, p. 211-224.

Levell, B., 1980, A late Precambrian tidal shelf deposit, the Lower Sandfjord Formation, Finnmark, north Norway: Sedimentology, v. 27, no. 5, p. 539-557.

Li, Z.-X., Bogdanova, S., Collins, A. S., Davidson, A., De Waele, B., Ernst, R., Fitzsimons, I. C., Fuck, R., Gladkochub, D., and Jacobs, J., 2008, Assembly, configuration, and break-up history of Rodinia: a synthesis: Precambrian research, v. 160, no. 1, p. 179-210.

Li, Z.-X., Evans, D. A., and Halverson, G. P., 2013, Neoproterozoic glaciations in a revised global palaeogeography from the breakup of Rodinia to the assembly of Gondwanaland: Sedimentary Geology, v. 294, p. 219-232.

Lorenz, R., Norris, J., Jackson, B., Norris, R., Chadbourne, J., and Ray, J., 2014, Trail formation by ice-shoved" sailing stones" observed at Racetrack Playa, Death Valley National Park: Earth Surface Dynamics Discussions, v. 2, no. 2, p. 1005-1022.

Macculloch, J., 1819, A description of the western islands of Scotland, including the Isle of Man comprising an account of their geological structure; with remarks on their agriculture, scenery, and antiquities. By John Macculloch, M. D. In three volumes, London :, Printed for Hurst, Robinson, and Co.; [etc., etc.].

Macdonald, F. A., Prave, A. R., Petterson, R., Smith, E. F., Pruss, S. B., Oates, K., Waechter, F., Trotzuk, D., and Fallick, A. E., 2013, The Laurentian record of Neoproterozoic glaciation, tectonism, and eukaryotic evolution in Death Valley, California: Geological Society of America Bulletin, v. 125, no. 7-8, p. 1203-1223.

Macdonald, F. A., Schmitz, M. D., Crowley, J. L., Roots, C. F., Jones, D. S., Maloof, A. C., Strauss, J. V., Cohen, P. A., Johnston, D. T., and Schrag, D. P., 2010, Calibrating the cryogenian: Science, v. 327, no. 5970, p. 1241-1243.

Mawson, D., 1949a, Sturt tillite of Mount Jacob and Mount Warren Hastings, north Flinders Ranges: Transactions of the Royal Society of South Australia, v. 72, p. 244-251.

Mawson, D., 1949b, The Elatina glaciation: Trans. R. Soc. S. Aust, v. 73, p. 117-121.

McCarroll, D., and Rijsdijk, K. F., 2003, Deformation styles as a key for interpreting glacial depositional environments: Journal of Quaternary Science, v. 18, no. 6, p. 473-489.

McCay, G., Prave, A., Alsop, G., and Fallick, A., 2006, Glacial trinity: Neoproterozoic Earth history within the British-Irish Caledonides: Geology, v. 34, no. 11, p. 909-912.

McCormick, D. S., and Grotzinger, J. P., 1993, Distinction of marine from alluvial Facies in the Paleoproterozoic (1.9 Ga) burnside formation, Kilohigok basin, NWT, Canada: Journal of Sedimentary Research, v. 63, no. 3.

Menzies, J., 2000, Micromorphological analyses of microfabrics and microstructures indicative of deformation processes in glacial sediments: Geological Society, London, Special Publications, v. 176, no. 1, p. 245-257.

-, 2002, Modern and Past Glacial Environments: Revised Student Edition, Butterworth-Heinemann.

Menzies, J., van der Meer, J., and Ravier, E., 2016, A Kinematic Unifying Theory of Microstructures in Subglacial Tills: Sedimentary Geology.

Mutti, E., Carminatti, M., Moreira, J. L., and Grassi, A. A., Chaotic deposits: examples from the Brazilian offshore and from outcrop studies in the Spanish Pyrenees and Northern Apennines, Italy, *in* Proceedings AAPG Annual Meeting, April2006, p. 9-12.

Nogueira, A. C. R., Riccomini, C., Sial, A. N., Moura, C. A. V., and Fairchild, T. R., 2003, Soft-sediment deformation at the base of the Neoproterozoic Puga cap carbonate (southwestern Amazon craton, Brazil): Confirmation of rapid icehouse to greenhouse transition in snowball Earth: Geology, v. 31, no. 7, p. 613-616.

Owen, G., and Moretti, M., 2011, Identifying triggers for liquefaction-induced soft-sediment deformation in sands: Sedimentary Geology, v. 235, no. 3, p. 141-147.

Panahi, A., and Young, G. M., 1997, A geochemical investigation into the provenance of the Neoproterozoic Port Askaig Tillite, Dalradian Supergroup, western Scotland: Precambrian Research, v. 85, no. 1, p. 81-96.

Payros, A., Pujalte, V., and Orue-Etxebarria, X., 1999, The South Pyrenean Eocene carbonate megabreccias revisited: new interpretation based on evidence from the Pamplona Basin: Sedimentary Geology, v. 125, no. 3, p. 165-194.

Pedersen, S. A. S., 2000, Superimposed deformation in glaciotectonics: Bulletin of the Geological Society of Denmark, v. 46, p. 125-144.

Pedersen, S. A. S., 2012, Glaciodynamic sequence stratigraphy: Geological Society, London, Special Publications, v. 368, no. 1, p. 29-51.

Pierrehumbert, R., Abbot, D., Voigt, A., and Koll, D., 2011, Climate of the Neoproterozoic: Annual Review of Earth and Planetary Sciences, v. 39.

Pierrehumbert, R. T., 2005, Climate dynamics of a hard snowball Earth: Journal of Geophysical Research: Atmospheres, v. 110, no. D1.

Pini, G. A., Ogata, K., Camerlenghi, A., Festa, A., Lucente, C. C., and Codegone, G., 2012, Sedimentary mélanges and fossil mass-transport complexes: a key for better understanding submarine mass movements?, Submarine Mass Movements and Their Consequences, Springer, p. 585-594.

Plaziat, J. C., Purser, B. H., and Philobbos, E., 1990, Seismic deformation structures (seismites) in the syn-rift sediments of the NW Red Sea (Egypt): Bulletin de la Société géologique de France, v. 6, no. 3, p. 419-434.

Powell, R. D., and Cooper, J. M., 2002, A glacial sequence stratigraphic model for temperate, glaciated continental shelves: Geological Society, London, Special Publications, v. 203, no. 1, p. 215-244.

Pratt, B. R., 2002, Tepees in peritidal carbonates: origin via earthquake-induced deformation, with example from the Middle Cambrian of western Canada: Sedimentary Geology, v. 153, no. 3, p. 57-64.

Prave, A., and Fallick, A., 2011, The Neoproterozoic glaciogenic deposits of Scotland and Ireland: Geological Society, London, Memoirs, v. 36, no. 1, p. 643-648.

Prave, A., Fallick, A., Thomas, C., and Graham, C., 2009, A composite C-isotope profile for the Neoproterozoic Dalradian Supergroup of Scotland and Ireland: Journal of the Geological Society, v. 166, no. 5, p. 845-857.

Rainbird, R. H., 1992, Anatomy of a large-scale braid-plain quartzarenite from the Neoproterozoic Shaler Group, Victoria Island, Northwest Territories, Canada: Canadian Journal of Earth Sciences, v. 29, no. 12, p. 2537-2550.

Ramsay, P. J., Smith, A. M., and Mason, T. R., 1996, Geostrophic sand ridge, dune fields and associated bedforms from the Northern KwaZulu-Natal shelf, south-east Africa: Sedimentology, v. 43, no. 3, p. 407-419.

Retallack, G. J., 2011, Neoproterozoic loess and limits to snowball Earth: Journal of the Geological Society, v. 168, no. 2, p. 289-308.

Rooney, A. D., Chew, D. M., and Selby, D., 2011, Re–Os geochronology of the Neoproterozoic–Cambrian Dalradian Supergroup of Scotland and Ireland: implications for Neoproterozoic stratigraphy, glaciations and Re–Os systematics: Precambrian Research, v. 185, no. 3, p. 202-214.

Rooney, A. D., Macdonald, F. A., Strauss, J. V., Dudás, F. Ö., Hallmann, C., and Selby, D., 2014, Re-Os geochronology and coupled Os-Sr isotope constraints on the Sturtian snowball Earth: Proceedings of the National Academy of Sciences, v. 111, no. 1, p. 51-56.

Rooney, A. D., Strauss, J. V., Brandon, A. D., and Macdonald, F. A., 2015, A Cryogenian chronology: Two long-lasting synchronous Neoproterozoic glaciations: Geology, v. 43, no. 5, p. 459-462.

Sawaki, Y., Kawai, T., Shibuya, T., Tahata, M., Omori, S., Komiya, T., Yoshida, N., Hirata, T., Ohno, T., and Windley, B. F., 2010, 87 Sr/86 Sr chemostratigraphy of Neoproterozoic Dalradian carbonates below the Port Askaig glaciogenic formation, Scotland: Precambrian Research, v. 179, no. 1, p. 150-164.

Schermerhorn, L., 1966, Terminology of mixed coarse-fine sediments: Journal of Sedimentary Research, v. 36, no. 3.

-, 1974, Late Precambrian mixites: Glacial and/or nonglacial?: American Journal of Science, v. 274, no. 7, p. 673-824.

Schlager, W., 2005, Carbonate sedimentology and sequence stratigraphy, SEPM Soc for Sed Geology, v. 8.

Scotese, C. R., 2009, Late Proterozoic plate tectonics and palaeogeography: a tale of two supercontinents, Rodinia and Pannotia: Geological Society, London, Special Publications, v. 326, no. 1, p. 67-83.

Selley, R., Shearman, D., Sutton, J., and Watson, J., 1963, Some underwater disturbances in the Torridonian of Skye and Raasay: Geological Magazine, v. 100, no. 03, p. 224-243.

Shanmugam, G., and Wang, Y., 2015, The landslide problem: Journal of Palaeogeography, v. 4, no. 2, p. 109-166.

Shapiro, R. S., and Awramik, S. M., 2006, Favosamaceria cooperi new group and form: a widely dispersed, time-restricted thrombolite: Journal of Paleontology, v. 80, no. 03, p. 411-422.

Smith, A., 1992, Subaqueous giant (15 m) and supergiant (40 m) dunes from the Lower Permian Vryheid Formation of the Karoo Supergroup, northern Natal, South Africa: Sedimentary geology, v. 77, no. 3, p. 215-224.

Smith, A., and Tavener-Smith, R., 1988, Early Permian giant cross-beds near Nqutu, South Africa, interpreted as part of a shoreface ridge: Sedimentary geology, v. 57, no. 1, p. 41-58.

Smith, J. V., 1974, Feldspar Minerals: 2 Chemical and Textural Properties, Springer Science & Business Media.

Spence, G. H., Le Heron, D. P., and Fairchild, I. J., 2016, Sedimentological perspectives on climatic, atmospheric and environmental change in the Neoproterozoic Era: Sedimentology, v. 63, no. 2, p. 253-306.

Spence, G. H., and Tucker, M. E., 1997, Genesis of limestone megabreccias and their significance in carbonate sequence stratigraphic models: a review: Sedimentary Geology, v. 112, no. 3-4, p. 163-193.

Spencer, A., 1985, Mechanisms and environments of deposition of late Precambrian geosynclinal tillites: Scotland and East Greenland: Palaeogeography, palaeoclimatology, palaeoecology, v. 51, no. 1, p. 143-157.

Spencer, A. M., 1966, THE SEDIMENTATION AND PETROGRAPHY OF THE PORT ASKAIG BOULDER BED (LATE PRECAMBRIAN) OF ARGYLL, WITH A DISCUSSION OF ITS ORIGIN.

-, Late pre-Cambrian glaciation in Scotland1971, Geological Society of London.

Stephenson, D., and Gould, D. E., 1995, The Grampian Highlands, Bernan Assoc.

Terry, J., and Goff, J., 2014, Megaclasts: proposed revised nomenclature at the coarse end of the Udden-Wentworth grain-size scale for sedimentary particles: Journal of Sedimentary Research, v. 84, no. 3, p. 192-197.

Thomas, G. S., and Connell, R. J., 1985, Iceberg drop, dump, and grounding structures from Pleistocene glacio-lacustrine sediments, Scotland: Journal of Sedimentary Research, v. 55, no. 2.

Thomson, J., On the occurrence of pebbles and boulders of granite in schistose rocks on Islay, Scotland, *in* Proceedings Report of the 40th Meeting of the British Association for the Advancement of Science, Liverpool1871, Volume 88.

Trewin, N. H., The geology of Scotland2002, Geological Society of London.

Van der Meer, J. J. (1993). Microscopic evidence of subglacial deformation. *Quaternary Science Reviews*, *12*, 553-553.

van der Meer, J. J., Menzies, J., and Rose, J., 2003, Subglacial till: the deforming glacier bed: Quaternary Science Reviews, v. 22, no. 15, p. 1659-1685.

van der Wateren, F. M., 1985, A model of glacial tectonics, applied to the ice-pushed ridges in the Central Netherlands, Geological Society of Denmark.

Van der Wateren, F. M., Kluiving, S. J., and Bartek, L. R., 2000, Kinematic indicators of subglacial shearing: Geological Society, London, Special Publications, v. 176, no. 1, p. 259-278.

Vandenberghe, J., 2011, Periglacial sediments: do they exist?: Geological Society, London, Special Publications, v. 354, no. 1, p. 205-212.

Williams, R., Robinson, D., Dornbusch, U., Foote, Y., Moses, C., and Saddleton, P., 2004, A sturzstrom-like cliff fall on the Chalk coast of Sussex, UK: Geological Society, London, Engineering Geology Special Publications, v. 20, no. 1, p. 89-97.

Wright, A. E., 1988, The Appin Group, *in* Winchester, J. A., ed., Later Proterozoic Stratigraphy of the Northern Atlantic Regions, Springer US, p. 177-199.

Zingg, T., 1935, Beitrag zur schotteranalyse.

Appendices

Scanning Electron Microscope (SEM)

Spencer (1966, 1971) suggested different sources supplied detrital grains to the sandstone interbeds in the PAF and the diamictite beds. One of the reasons behind this is that chess-board albite occurs in granite clasts within diamictite beds, but is missing in the sandstones, whilst microcline occurs within sandstone beds and is missing in the diamictite beds. The author found difficulties distinguishing between these two minerals by transmitted-light microscopy especially when they are altered as in the PAF. To distinguish these minerals the author chose one of the thin sections (with carbon coating) in which chess-board albite was expected, and analysed it using a scanning electron microscope (SEM) using energy dispersive X-ray spectrometry (EDS). This can distinguish chess-board albite and microcline, because it gives the correct chemical formula for each mineral. The result was helpful and the expected chess-board albite showed low peak (or none) of potassium (K) values, with a high peak in sodium (Na) (Plate 1 and 2).
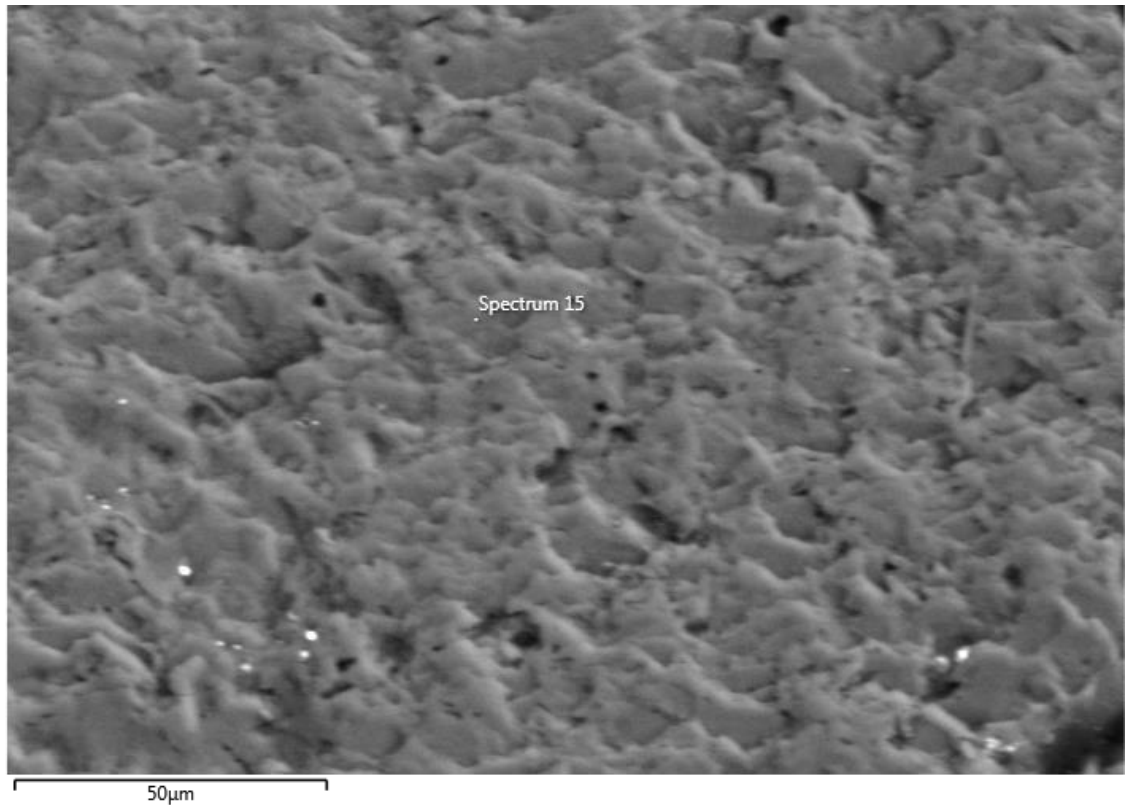

Plate 1: Electron image of the SEM using EDS, showing the location of the spectrum 15. The sample was a foliated granite in D26 on the E coast of GE.
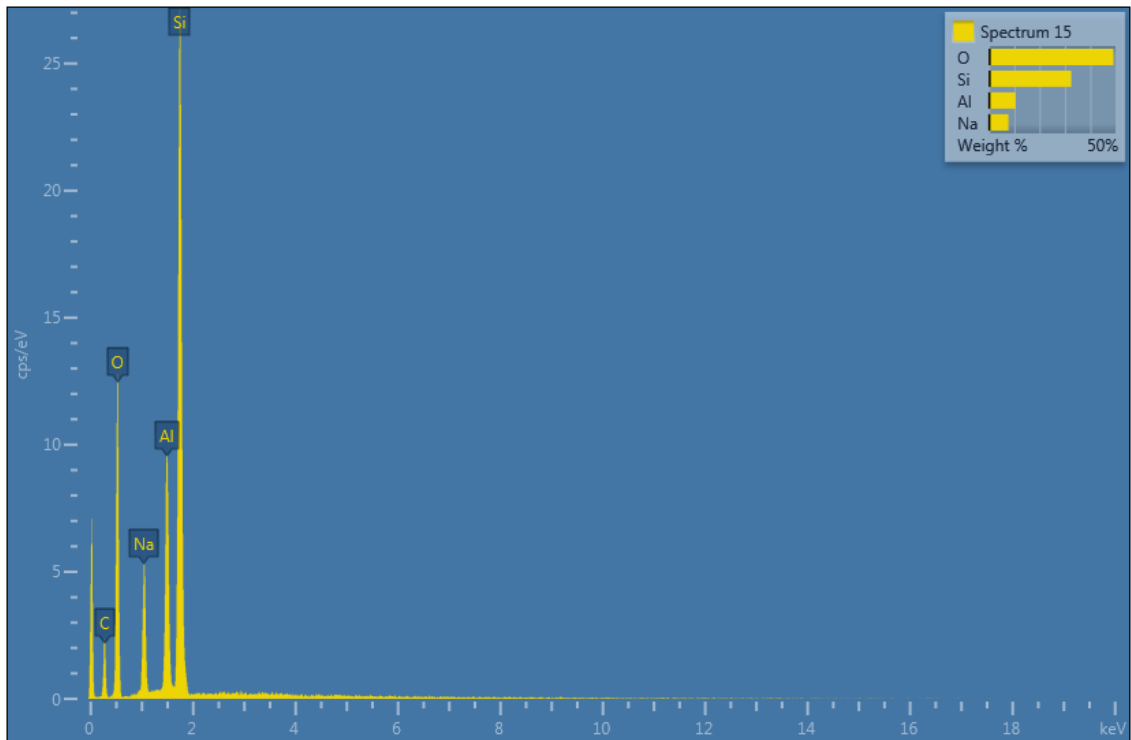
Plate 2: Spectrum 15 of the electron image (Plate 1) showing high peak of the Na and none for K, suggestive of albite rather than microcline.

However, the albite is not always pure like the example in spectrum 15 which does not show any peak of K. Sometimes there is a small peak of K with the sample. For instance, in the same thin section in spectrum 21, in addition to, the Na peak there is a low amplitude peak of K (Plate 3 and 4).
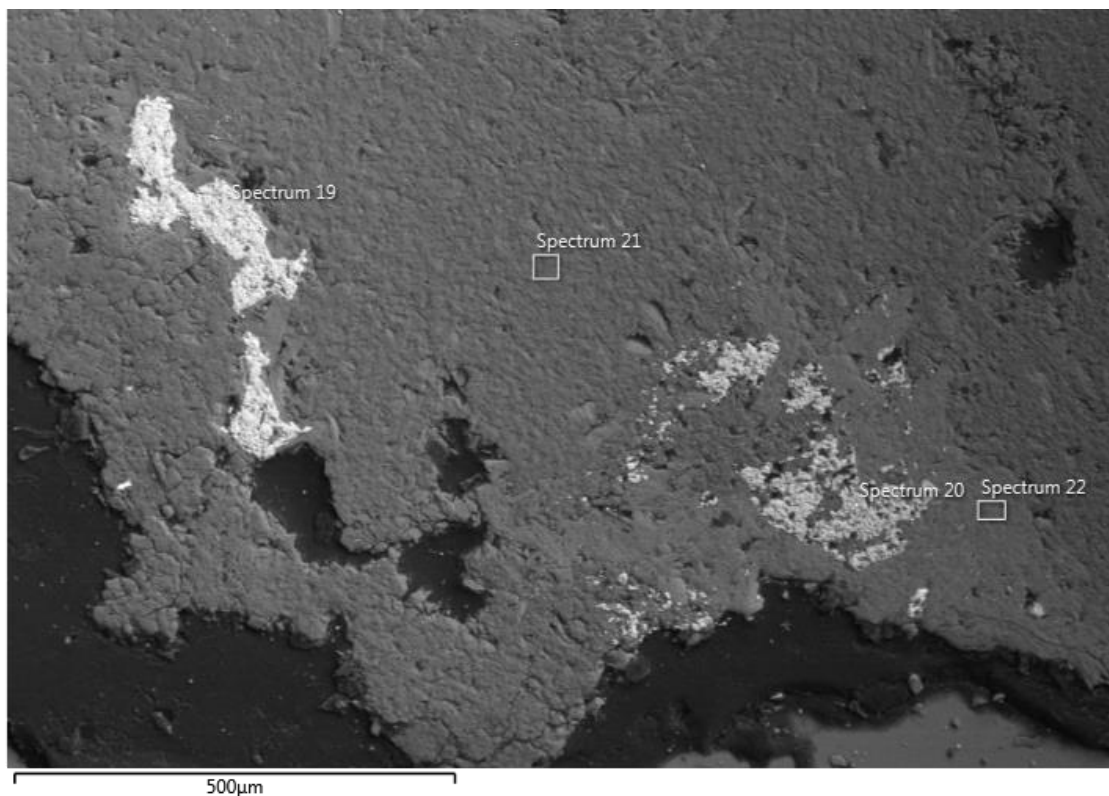

Plate 3: Electron image of the SEM using EDS, showing the location of the spectrum 21 and 22. The sample was from a foliated granite clast in D26 on the E coast of GE.
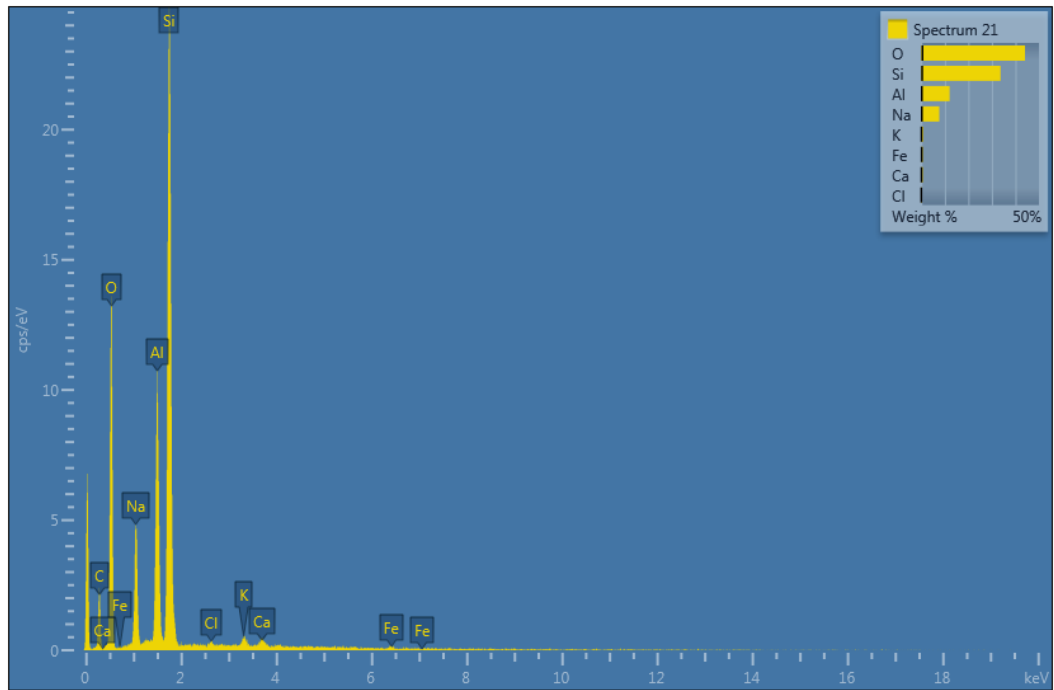
275

Plate 4: Spectrum 21 of the electron image (Fig.2.10) showing high amplitude peak of Na and low amplitude peak of K, suggesting that we have plagioclase with the albite. The Si, O, and C represent quartz grains, and the carbon coat of the thin section.

Occasionally, there is a high peak of K and a low peak of Na (Plate 5), possibly suggesting solid solution between albite and plagioclase.
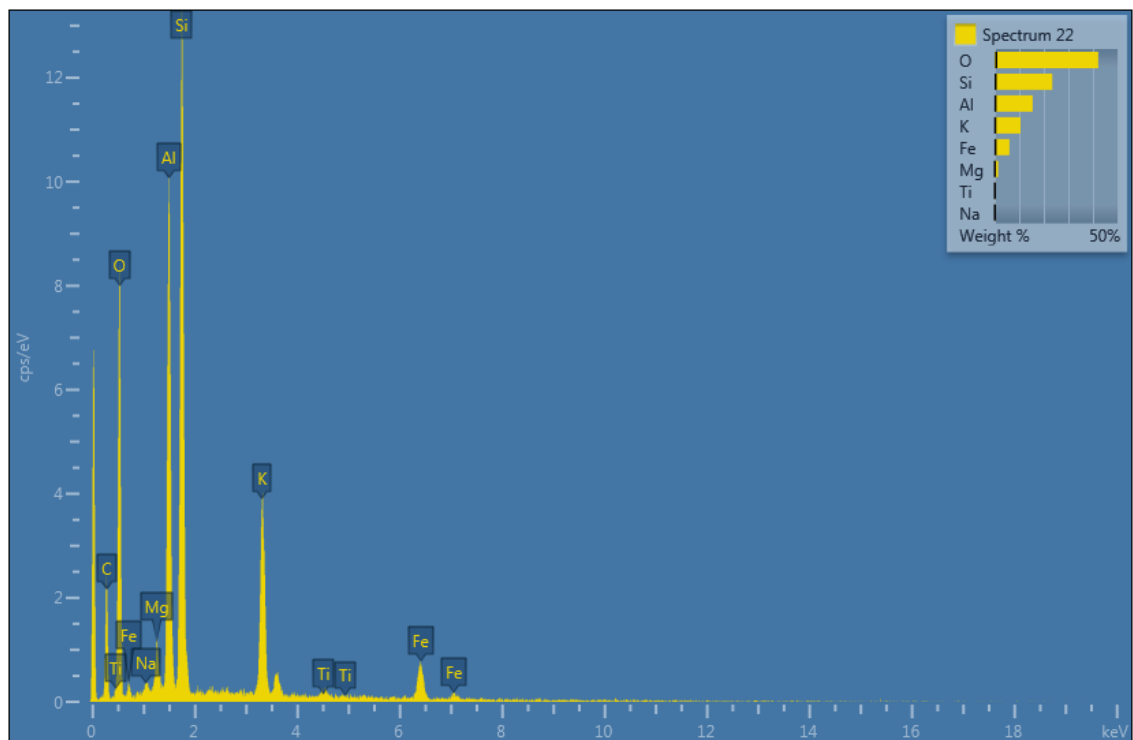

Plate 5: Spectrum 22 of the electron image (Fig.2.10) showing high amplitude peak of K and low amplitude peak of Na, suggesting there could be a solid solution between plagioclase and albite.

The feldspars are usually lath-shape (Plate 6) under the SEM and 'believed to crystallize from especially hydrous magma'(Donnelly, 1963) from amphibolite and come from an acidic magma rather than basic one (Smith, 1974).
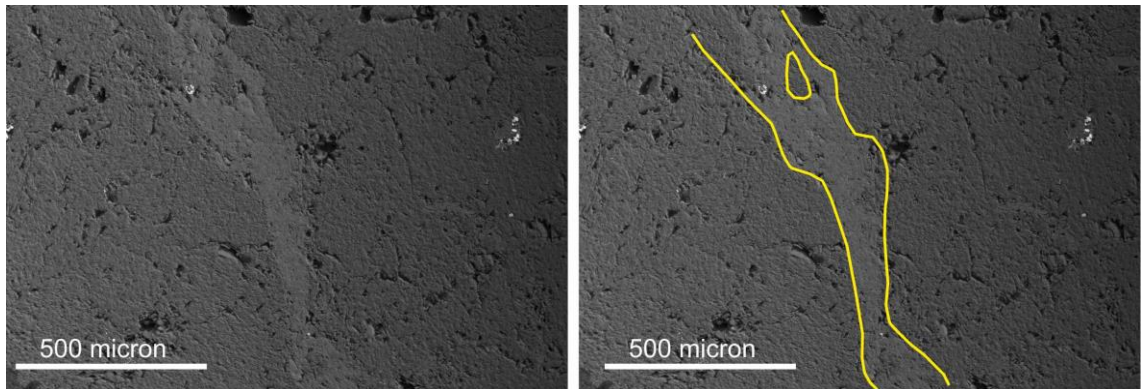

Plate 6: Lath shape of the feldspar under SEM